



The
University
Of
Sheffield.

Synthesis of unnatural amino acids for the design of multi-metal ion binding α -helical coiled coils

A Dissertation Submitted for the Degree of Doctor
of Philosophy

Liam Marshall

The University of Sheffield,

Department of Chemistry

September 2017

Preface

Declaration

This dissertation records work carried out in the Department of Chemistry at The University of Sheffield between October 2013 and June 2017 and is original except where acknowledgement by reference is made. Synthesis of the peptides discussed in this thesis was undertaken at The University of Birmingham in the group of Dr. Anna F. A. Peacock.

No portion of this work is being, nor has been, submitted for a degree, diploma, or other qualifications at any other University.

Acknowledgements

This thesis would not be possible without the contribution of countless people. I can only hope to acknowledge those who made significant contributions over these 4 years, but to anyone who has offered support over these 4 years, I will be always grateful. First, I am deeply indebted to both of my supervisors, Prof. Richard Jackson and Dr Barbara Ciani, for their support, patience, availability and advice over the course of the 4 years. I must particularly acknowledge their patience in humouring some of my more off piste ideas, and not bringing up the ones that didn't work as often as they could have. I thank all the Jackson and Ciani group members for their support and companionship in the lab, and particularly Phil Reeve for his company in all things burrito related, and Dr Chris Marklew for teaching an organic chemist how to work with proteins. I must also thank Dr Anna F. A. Peacock and her research group, without whom these peptides would never have been made, and who welcomed me into their group on my visits to Birmingham. Mehul, Akram, Nabaz, Dan and Jess, it has been a pleasure to work in the same lab groups as you all.

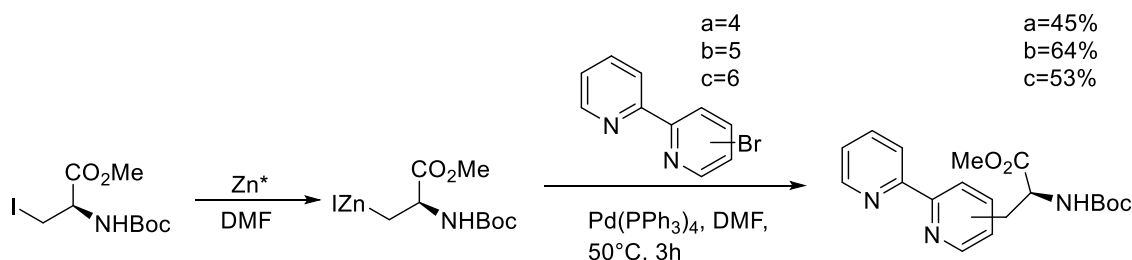
In addition, I thank all the support staff at the University of Sheffield and all the members of the Department of Chemistry for making it such a pleasant place to work.

I would also like to take this chance to acknowledge all of my friends in the University for their support and companionship throughout this PhD. Dave, Liam, Sam, Jon, Andy, Tom, and all the chemistry football crowd and those who have been to tea. Thanks to Al for getting me to go back to climbing after a poor first experience. Special thanks go to Greg, who has been a pleasure to live with over the course of our degrees. Maria, Kat, Chris and Ness, the amount of gin we consumed in the last year has I'm sure set the progress of this back by around 6 months. Steven, Kate and Niamh were great friends over this time, even if they were from York originally. Hannah and Holly were two masters students who I have remained friends with after their time here, and their electronic support was invaluable in completing this thesis. I must also thank Laura, my token non-science friend, for always being willing to listen to complaints about molecules, and for making sure this thesis isn't simply the word "so" every other word. Adham has abandoned the best city in England, but his constant optimism was a light in the dark.

Finally, I must thank my family, for their unending support. My mother, Sherrie, as well as Lucy and Chris (and now Mark!) have all be invaluable over this time, and this wouldn't have been possible without you.

Abstract

It has been established that metal binding unnatural amino acids have many applications in protein engineering. 3 isomers of bipyridylalanine have been synthesised through the Negishi cross-coupling of a serine derived zinc reagent with the corresponding bromobipyridine (Scheme 1).



Scheme 1 General synthesis of bipyridyl amino acids developed in this thesis.

A pair of bimetallic coiled coils were proposed as model systems to investigate the contribution of metal ions to the folding and stability of the peptides. Bipyridyl amino acid **c** was incorporated in the backbone of peptide sequences engineered to form parallel, trimeric α -helical coiled coils with an incorporated lanthanide binding site (Figure 1).

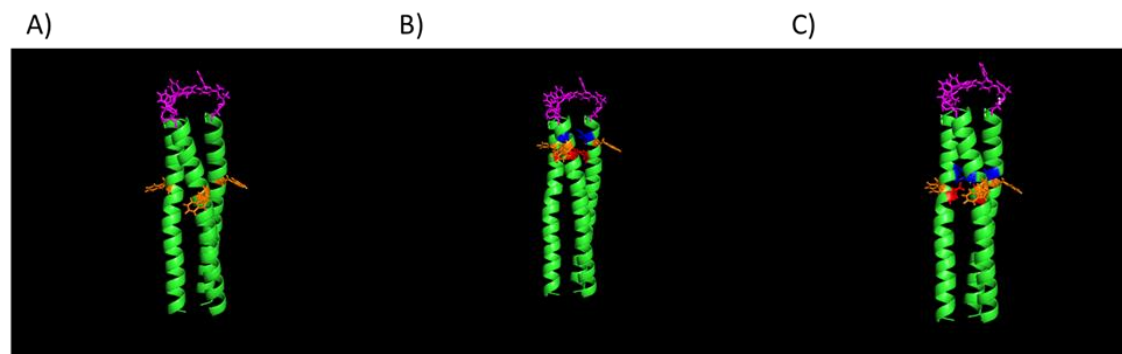


Figure 1 Peptides prepared over the course of this work. A) NB00, a model coiled coil. B) NB11, a coiled coil containing an N-terminal heptad lanthanide binding site (highlighted in red and blue) C) NB12, a coiled coil containing a central heptad lanthanide binding site. Models are derived from X-ray crystal structures of the parent MB12 peptide, with bipyridyl amino acids added to the peptide backbone. The structures are not energy minimised, not metal coordinated, and manually adjusted to represent the proposed structure of the coiled coils. Coiled coil structures derived from a crystal structure of MB12 with 3-D models of the bipyridyl amino acid added manually.

A control coiled coil structure without a lanthanide binding site was characterised to dissect the interplay between metal coordination to the bipyridyl amino acid and coiled coil folding. Concentration-dependent folding, metal coordination and thermal stability of these structures were studied using UV absorption, circular dichroism and fluorescence spectroscopy. Apparent molecular weights of the structures measured by

multi-angle laser light scattering indicated that only one sequence (NB11) is folded as trimer in the absence of metals. All coiled coils with two metal binding sites bind both transition and lanthanide metal ions, with NB11 displaying a structural distortion when bound to 1 eq. Ni^{2+} . Surprisingly, NB12 undergoes further assembly to form fibres which are disassembled by the addition of metal ions. The morphology of these was studied by electron microscopy, and the kinetics of assembly and the change in structure on metal addition were studied with circular dichroism.

Abbreviations

)))	Sonication
2D	2 dimensional
3D	3 dimensional
4Bpa	4-bipyridylalanine
5Bpa	5-bipyridylalanine
6Bpa	6-bipyridylalanine
Ac	Acetyl
Ar	Aryl
AUC	Analytical Ultra-centrifugation
Bipy	2, 2'-bipyridine
Bn	Benzyl
Boc	<i>tert</i> -butyloxycarbonyl
Cbz	Carboxybenzyl
CCC	Coiled coil concentration
CD	Circular dichroism
CoA	Co-enzyme A
Cy	Cyclohexyl
Da	Dalton
dba	Dibenzylideneacetone
deg dmol ⁻¹ cm ²	Degrees per decimole per cm squared
DIPEA	Diisopropylethylamine
DMF	Dimethyl formamide
DMA	Dimethyl acetamide
DNA	Deoxyribonucleic acid
dppf	1,1'-Bis(diphenylphosphino)ferrocene
E. coli	Escherichia coli
EDTA	Ethylenediaminetetraacetic acid
ee	Enantiomeric excess
EM	Electron microscopy
ESI	Electrospray ionisation
Et	Ethyl
Fmoc	Fluorenylmethyloxycarbonyl
FRET	Förster resonance energy transfer

ΔG	Gibbs free energy
HPLC	High performance liquid chromatography
h	hour
iPr	<i>iso</i> -Propyl
IUPAC	International Union of Pure and Applied Chemistry
K	Rate constant
L	Ligand
LC	Liquid chromatography
LG	Leaving group
M/M+	Metal/metal ion
MALDI	Matrix-assisted laser desorption ionization
MALLS	Multi-angle laser light scattering
mCPBA	meta-Chloroperoxybenzoic acid
Me	Methyl
mmol	millimole
MRI	Magnetic resonance imaging
Ms	Mesyl
MS	Mass spectrometry
nm	nanometre
NMR	Nuclear magnetic resonance
Nu	Nucleophile
PDB ID	Protein data bank identification
PG	Protecting group
Ph	Phenyl
RT	Room temperature
RuPhos	2-Dicyclohexylphosphino-2',6'-diisopropoxybiphenyl
SPhos	2-Dicyclohexylphosphino-2',6'-dimethoxybiphenyl
SPPS	Solid phase peptide synthesis
tBu	<i>tert</i> -Butyl
TEM	Transmission Electron Microscopy
Tf	Triflate
TFA	Trifluoroacetic acid
THF	Tetrahydrofuran
TLC	Thin layer chromatography
TMS	Trimethylsilyl

TOF	Time of flight
Ts	Tosyl
μM	micromolar
μm	micrometre
UV-Vis	Ultraviolet-Visible
XPhos	2-Dicyclohexylphosphino-2',4',6'-triisopropylbiphenyl
XantPhos	4,5-Bis(diphenylphosphino)-9,9-dimethylxanthene

Contents

Preface	i
Acknowledgements	ii
Abstract	iv
Abbreviations	vi
Contents	ix
Chapter 1: Introduction and Literature Review	1
1.1 <i>De novo</i> protein design and coiled coils	1
1.2 Controlling the coiled coil structure and oligomerisation state	5
1.3 The use of unnatural amino acids to influence peptide structure	9
1.4 2,2'-Bipyridine containing peptides	13
1.5 Project aims	20
1.6 References	20
Chapter 2: Synthesis of bipyridyl amino acids	23
2.1 Background	23
2.2 Previous synthesis of bipyridyl amino acids	25
2.3 Synthesis of halo-2,2'-bipyridines	28
2.3.1 Previous syntheses	28
2.3.2 2-Pyridylzinc reagents and their subsequent use in Negishi cross-coupling reactions	29
2.4 Selective cross-couplings with dihalopyridines	31
2.5 Synthesis of 4-bromo-2,2'-bipyridine from 2,2'-bipyridine	36
2.6 Aims	36
2.7 Retrosynthesis	36
2.8 Results and Discussion	39
2.8.1 Synthesis of amino acid derived iodide	39
2.8.2 Generation of 2-pyridylzinc chloride and the synthesis of 24 and 28	39
2.8.3 Synthesis of amino acids	43
2.8.4 Preparation of 2-chloropyridine 39	44
2.8.5 Synthesis of 4-bromo-2,2'-bipyridine (47)	47
2.8.6 Synthesis and Negishi cross-coupling of 2-bromo-4-iodopyridine	47

2.8.7 Synthesis of 4-bromo-2,2'-bipyridine from 2,2'-bipyridine	50
2.8.8 Protecting group exchange to generate peptide synthesis reagents	51
2.8.9 Summary of amino acid synthesis	52
2.10 References	53
 Chapter 3: Biophysical characterisation of the effect of nickel coordination to bipyridylalanine and the construction of bimetallic coiled coil systems	
3.1 Introduction	55
3.2 Design of target peptides	58
3.3 UV characterisation of the metal binding behaviour of Fmoc-6Bpa-OH (22)	60
3.4 Concentration-dependent folding of apo-peptides	64
3.5 The effect of Ni ²⁺ -6Bpa complex formation on the oligomerisation state and stability of coiled coils	65
3.5.1 The isolated contribution of Ni ²⁺ -6Bpa complex formation in a model coiled coil	65
3.5.2 Contribution of 6Bpa-Ni ²⁺ within a coiled coil with a structurally non- contributory core lanthanide binding site (NB11)	67
3.5.3 Contribution of 6Bpa-Ni ²⁺ complex formation within a coiled coil with a structurally destabilising core lanthanide binding site (NB12)	69
3.6 Mixed metal coiled coil systems	73
3.6.1 The effect of each binding site on the folding of the coiled coils	74
3.6.2 1:1 nickel: gadolinium competition in 1:3 metal: peptide systems	76
3.6.3 1:0.33 nickel: gadolinium competition in metal: peptide systems	78
3.6.4 Mixed metal behaviour of NB-12	82
3.7 Conclusions	84
 Chapter 4: Fibre formation	
4.1 Introduction and Background	87
4.1.1 Controlled disassembly of fibrous structures	88
4.2 Formation of microscale fibres of NB12	89
4.3 Metal-controlled fibre disassembly	93
4.4 Discussion	96
4.5 Conclusions	99
4.6 Future work	99

4.7 References	99
Chapter 5: Final discussion, conclusions and future work	101
5.1 Future work	106
5.1.1 New unnatural amino acids and their potential applications	106
5.1.2 Influencing coiled coil structure and oligomerisation state with bipyridine side chains	106
5.1.3 Metal-disassembled fibre systems	107
5.2 References	108
Chapter 6: Experimental	109
6.1 General Experimental	109
Synthesis of (2S)-2-([fluorenylmethoxycarbonyl]amino)-3-[5-(pyridin-2-yl)pyridin-2-yl]propanoate 19	116
Synthesis of (2S)-2-([fluorenylmethoxycarbonyl]amino)-3-[6-(pyridin-2-yl)pyridin-2-yl]propanoate 22	117
Synthesis of 6-bromo-2,2'-bipyridine (24)	118
Synthesis of 5-bromo-2,2'-bipyridine (28)	121
Synthesis of [2S]-2-([tert-butoxy]carbonyl]amino)-3-(2-chloropyridin-4-yl)propanoate (39)	122
Synthesis of methyl (2S)-2-([tert-butoxy]carbonyl]amino)-3-[5-(pyridin-2-yl)pyridin-2-yl]propanoate (44)	123
Synthesis of methyl (2S)-2-([tert-butoxy]carbonyl]amino)-3-[6-(pyridin-2-yl)pyridin-2-yl]propanoate (45)	124
Synthesis of Methyl (2S)-2-([tert-butoxy]carbonyl]amino)-3-[4-(pyridin-2-yl)pyridin-2-yl]propanoate, 46	125
Isolation of zinc-bipyridine complex 50(general procedure)	126
Synthesis of 2-bromo-4-iodopyridine 53	127
Synthesis of [2S]-2-([tert-butoxy]carbonyl]amino)-3-(2-bromopyridin-4-yl)propanoate 54	127
General procedure for peptide synthesis	129
References	131
Appendices	132

Chapter 1: Introduction and Literature Review

The development of new structures with new functions from proteins is one of the main purposes of rational peptide design. The ability to generate new functional proteins at will, drawing from rules that can be extrapolated from natural systems, is the ultimate end goal in studies of protein design and biomimetic chemistry.

This chapter briefly introduces the main secondary structures of peptides, with a focus on the design of coiled coils and their applications as model systems for investigating the controlling structural factors of proteins and the problems faced with oligomerisation state equilibria in naturally occurring coiled coil systems. The incorporation of unnatural amino acids into coiled coil species, particularly metal binding sites, has developed into a rich field with many applications in both controlling the structure and analysing the properties of coiled coils. The coordination of metal ions with a well-defined coordination number and the inclusion of appropriate ligands allows the oligomerisation state of a peptide to be fixed. Finally, the use of 2,2'-bipyridine in coiled coils has been extensively covered, with most examples involving the use of an N- or C- terminal “cap”, but the examples where bipyridylalanine has been incorporated as part of the peptide backbone have been detailed.

1.1 *De novo* protein design and coiled coils

The design of a specific protein structure from first principles has been the dream of biochemists since the first protein structure was solved. There is a wide range of structures which occur in natural proteins which all result from a fixed pool of building blocks. There are 22 naturally occurring proteinogenic amino acids (Table 1), yet the range of protein and peptide structures that can result from combinations of these is staggering in its size. Levinthal addressed this in 1969, when considering a protein containing 150 amino acids.¹ The protein possesses 450 degrees of freedom, 300 resulting from bond rotations, and 150 resulting from the bond angles of each side chain relative to each other. Even if the bond angles are known very precisely, there are still 10^{300} possible configurations, and were the protein to sequentially test each configuration for a millisecond, it would require more time than the universe has existed.

However, most proteins are much larger than 150 amino acids. Indeed, unless they display significant functionality or structure-activity relationships, any protein under 50

amino acids in size is classed as a peptide. If the process of developing and designing *de novo* (from first principles) peptides relied on understanding the relationship of each amino acid with its fellows, and the subsequent effects of these partnerships as part of a wider structure, the task would be infeasible.

Broadly speaking, the proteinogenic amino acids can be divided into three categories based on the properties of their side chain (Table 1.1). These are hydrophobic amino acids, charged amino acids, and those that have a polar side chain but no charge on the side chain at physiological pH.

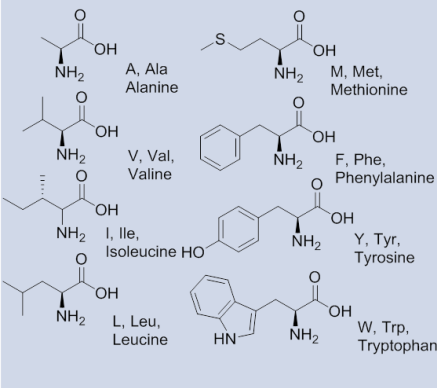
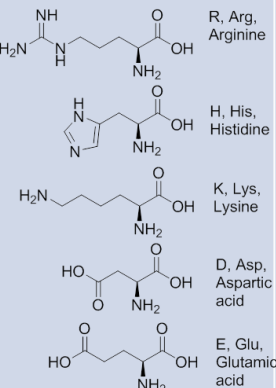
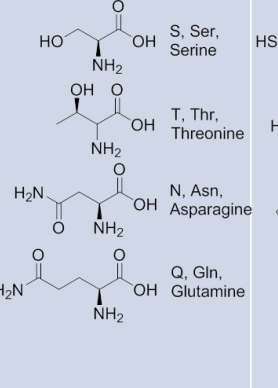
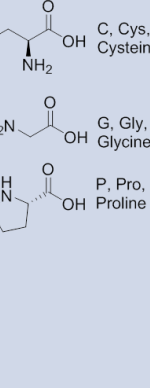
Hydrophobic	Polar	Polar, non-charged	Special cases
 <p>A, Ala, Alanine</p> <p>V, Val, Valine</p> <p>I, Ile, Isoleucine</p> <p>L, Leu, Leucine</p> <p>F, Phe, Phenylalanine</p> <p>Y, Tyr, Tyrosine</p> <p>W, Trp, Tryptophan</p>	 <p>R, Arg, Arginine</p> <p>H, His, Histidine</p> <p>K, Lys, Lysine</p> <p>D, Asp, Aspartic acid</p> <p>E, Glu, Glutamic acid</p>	 <p>S, Ser, Serine</p> <p>T, Thr, Threonine</p> <p>N, Asn, Asparagine</p> <p>Q, Gln, Glutamine</p>	 <p>C, Cys, Cysteine</p> <p>G, Gly, Glycine</p> <p>P, Pro, Proline</p>

Table 1.1 Grouping of the 20 proteinogenic amino acids based on the properties of their sidechain. Selenocysteine and pyrrolysine are omitted from this table due to their rarity in proteins, but their description and occurrence in the genetic code has been addressed by Soell and co-workers.²

Once split into these three categories (there are some exceptions to these groupings, displayed in Table 1.1), patterns of amino acids which favour the formation of a particular secondary structure begin to emerge.

The structures of proteins are controlled by weak forces working together to provide the lowest energy conformation. These include hydrophobic interactions, van der Waals and hydrogen bonding. There is not simply one conformation that the proteins can adopt, but often several tertiary structures from the same secondary structures.³⁻⁵ There are steps that can be taken to destabilise alternate conformations, but there is still not enough known about protein folding such that we can predict and design proteins with one favoured tertiary structure.

Doer and McLendon wrote in 2004 that we do not fully understand the balance of forces that control a protein folding into one specific structure.⁶ *De novo* protein design can help outline and discover these rules, and gives more information on the subject each time that a successfully folded protein is made. Their approach was to look at very short

proteins, as longer proteins have too many uncertain factors that can disrupt the formation of the folded protein. Using a shorter protein means that these factors can be limited and controlled.

Alpha helices are one of the most frequently occurring peptide secondary structures found in proteins. The structure was first described by Pauling *et. al.* after X-ray crystallography of α -keratin, α -myosin and other fibrous proteins.⁷ This has subsequently been extensively verified by X-ray crystallography of protein and peptide structures (Figure 1.2A).

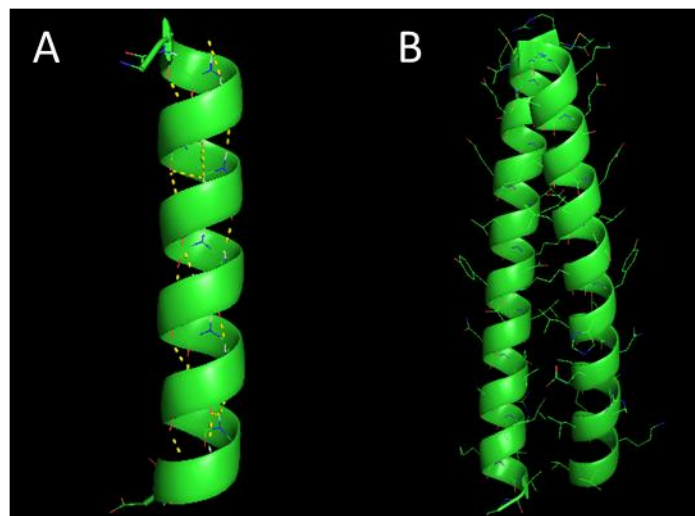


Figure 1.2 A) A protein α -helix. The arrangement of the backbone residues forming the helix is represented as a green ribbon, and the hydrogen bonds between every third amide residue have been highlighted in yellow. Figure derived from the structure of FMBP-1 Tandem repeat 3 (PDB ID 1WNK). B) A dimeric coiled coil, GCN-4. Sidechain residues are arranged with the hydrophobic residues buried within the centre of the coiled coil, with hydrophilic residues presented to the water in solution. Derived from the structure of the dimeric GCN-4 transcription factor (PDB ID 2ZTA).

Originally the paper discussed two hypotheses for the structure of the helix, but one was more fitting of the experimental data. They describe a helix with 3.5 residues per turn (or two turns per 7 amino acids). Hydrogen bonds occur within the structure between the carbonyl group of the i^{th} residue and the amide of the $(i+4)^{\text{th}}$ residue.

A coiled coil is a quaternary structure that consists of two to six amphiphilic α -helices that are wound into a left handed super-helix (Figure 1.1B).⁶ These helices require a pattern of hydrophobic and hydrophilic residues for the desired secondary structure folding (Figure 1.3). Bulky hydrophobic side chains, such as those found in valine and leucine, placed in the a and d positions of a heptad side chain, can optimise van der Waal's packing. Hydrophilic charged residues are placed in the other positions. The

largest driving force in the formation of coiled coils is the burial of the hydrophobic residues in the centre of the grouping of helices. The *e* and *g* positions of the peptide sequence can form inter-helical salt bridges, and are often designed to be complementary. These changes in hydrophobic packing or electrostatic interactions can affect the oligomerisation state, orientation and specificity of the coiled coils, as detailed in reviews by both Lupas & Gruber and Woolfson.^{8,9}

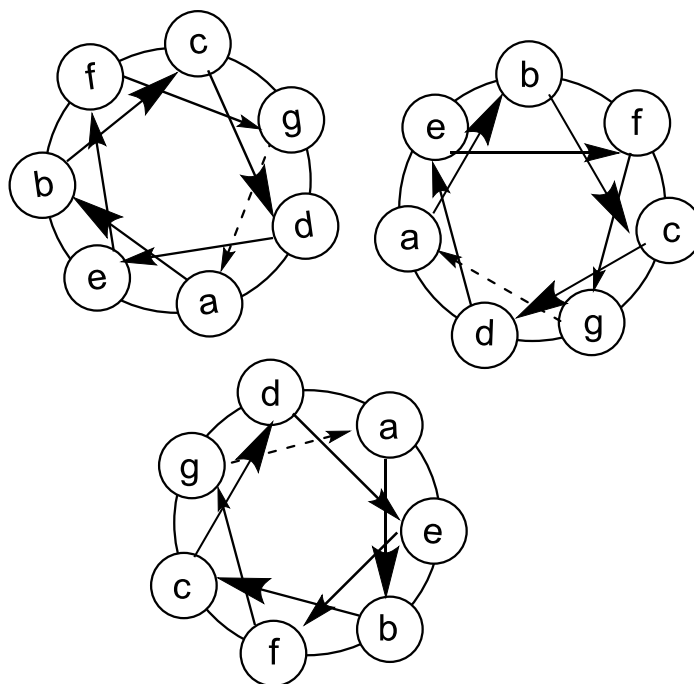


Figure 1.3 Helical wheels demonstrating the arrangement of the different amino acids in the coil. Residues *a* and *d* are hydrophobic, *b*, *c* and *f* are hydrophilic, and *e* and *g* are frequently oppositely charged. The helix is visualised along the *z*/helical axis.

The amino acids in the *b*, *c*, and *f* positions can show more variation, and are often used to install functionality or tags in the coiled coil system. Tryptophan residues can be readily incorporated into these positions, which can act as fluorescent markers to determine concentration or to monitor the environment of the coiled coil system.

Most coiled coil systems follow a pattern referred to as the 3, 4-repeat. This refers to the pattern of hydrophobic residues in the amino acid sequence of the protein. If a series of seven amino acids (a heptad) is considered, and the amino acids broadly defined as *h* (hydrophobic) or *p* (polar or charged) then a pattern of *hpphppp* will favour the formation of coiled coils. Coiled coils form when α -helices assemble to present the hydrophilic residues on the outside of the coiled coil. This allows the hydrophobic residues at the *a* and *d* positions to form a hydrophobic “stripe” within the centre of the

coiled coil, minimising the interaction with water and generating the lowest energy conformation of the peptide.

Coiled coil structures are not limited to the three-four repeat design.¹⁰ Coiled coils designed around repeating units of 11 amino acid residues can be generated, but they form a right-handed supercoil rather than the more common left-handed coil.¹¹ The two patterns can also be mixed, generating heptad-hendecad sequences which also form coiled coils.¹⁰ A coiled coil is the result of separate α -helices assembling into a quaternary structure without the formation of covalent bonds. A collection of α -helices linked by a covalent bond is referred to as a helix bundle instead of a coiled coil.¹²

Considering the aim of designing proteins and peptides with specific structures, simple secondary structures are a well-developed target for protein design. α -helices contain a repeating pattern of amino acids, and the structures can be small enough that they are readily prepared using synthetic methods and characterised more easily using techniques familiar to the chemist. With this combination of chemical accessibility and need for pattern recognition, α -helical structures and the more evolved coiled coil structure that arise from the association of α -helices have become popular targets in studying and understanding the relationship between their chemical structure and their 3D structure and function.

1.2 Controlling the coiled coil structure and oligomerisation state

The packing of sidechains in the hydrophobic core of a coiled coil can control its oligomerisation state. Harbury and co-workers found that varying the van der Waal's packing of the side chains could change the oligomeric state of the coiled coil formed.¹³ Leucine incorporation formed a dimer, but isoleucine in the same positions formed a trimer, and alternating between the two led to the formation of tetramers. However, when other combinations were investigated, a range of oligomerisation states were formed. Side chain packing around the coil controls the oligomerisation state. The van der Waal's forces of the side chains need to be packed into the optimal positions, so adopt what has been described as a "knobs into holes" structure, where only the ends of the side chains interact (Figure 1.4).

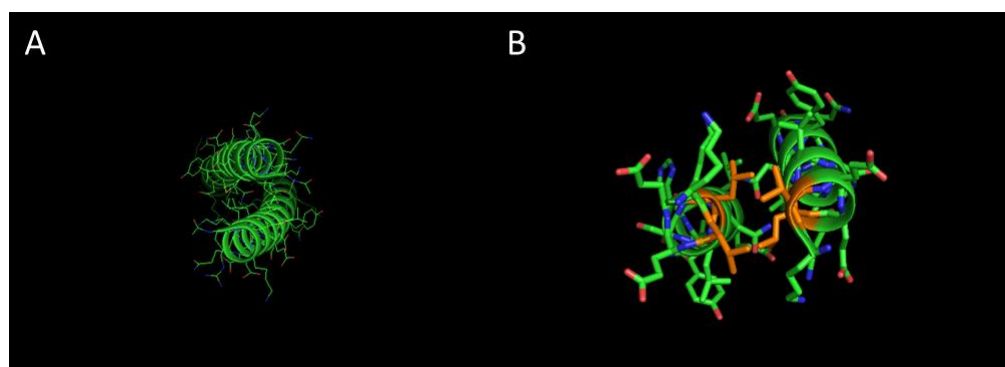


Figure 1.4 A) A z-axis view of the dimeric coiled coil of the GCN-4 transcription factor, with the winding nature of the coiled coil visualised. PDB ID 2ZTA. B) A focused view of the interior of the coiled coil, comprising of the ELLSKNYHLEN region of the protein with the remaining structure omitted for clarity. The “knobs into holes” packing of the hydrophobic amino acids is highlighted in orange.

It has been shown that, generally, coiled coil structures exist in an equilibrium of oligomerisation states.¹⁴ This makes the characterisation of one particular oligomerisation state and the effect on the equilibrium thermodynamics established in solution challenging.

The ideal system for controlled oligomerisation state while maintaining the flexibility of peptide systems would be the use of an additive that influences helix formation reversibly. One of the advantages offered by metallopeptides is the ability to “fix” structures in a specific oligomerisation state.¹⁵ Metal coordination of ligands within the system means that in the absence of metal ions the system maintains one structure or mixture of structures, and coordination of the metal ion staples the peptide in one oligomerisation state. Metalloproteins are good targets as they can be designed so that the protein will only take one conformation in the presence of the metal ion.¹⁶ It is useful to use units that are stable, only favour forming one structure, and will not interconvert into other structures.¹⁷

Metal ion complexation is proposed to create an initial metalloprotein structure, which then guides the system to form more complex structures (Figure 1.5). The coordination number of the metal ion can control the number of units participating in assembly by limiting how many chelating ligands can form the complex. This process also compensates for any loss of entropy that the system may suffer due to new organisation of the peptide subunits.

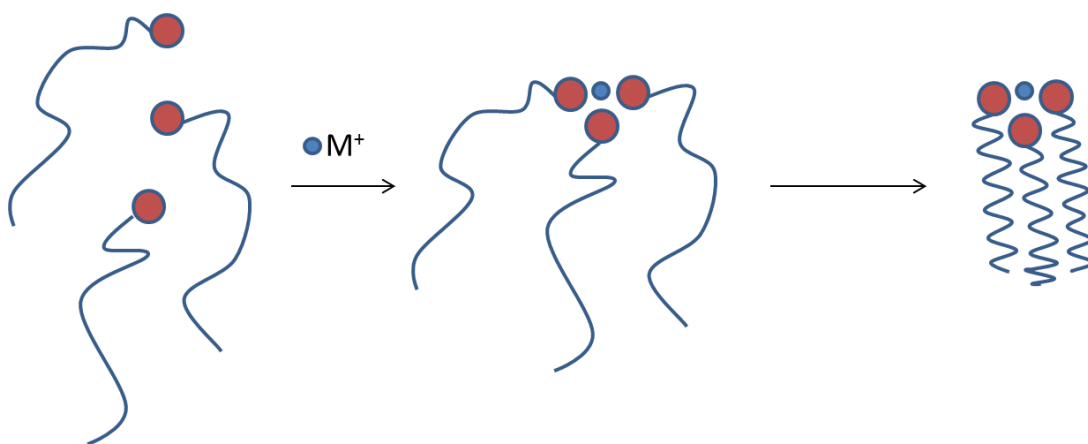


Figure 1.5 Cartoon representation of the organisation of a helix bundle on addition of metal ions. Addition of the metal ion to a solution of peptide draws the metal ligating ends of the peptide together, which encourages the system to form the final structure.¹⁵

Ghadiri and co-workers lay out some simple design principles for metalloproteins using three-stranded helical bundles as model systems.¹⁶ These are: (1) each peptide should have at least one metal binding site that binds to the metal ion, (2) any other possible tertiary structures must be disfavoured, and (3) the metal complex should have a high formation constant, so that it is thermodynamically stable. It is also favourable if the metal complex is kinetically stable, so will not unfold readily. This simplifies isolation and purification. Further elucidation of the mechanism would provide more information on what can be varied to fine tune the design of proteins that fulfil a function on demand.

In this way, through the incorporation of the correct metal binding ligand and enough knowledge about both the ligand and proteins behaviours, proteins can be designed with reasonable success to form metalloprotein structures.¹⁶

Metalloprotein design requires a properly folded protein scaffold with the appropriate number and type of ligand that will bind the metal correctly.¹⁸ The structure of many natural metalloproteins has been deduced, so we can use those and successful synthetic analogues to define principles that can be used to assemble metalloproteins and their active sites. Metal binding sites generally fulfil one of two purposes, either a structural or a functional role.¹⁹ Structural sites are due to amino acid side chains that can coordinate to metals and alter the structure of the protein, while functional units are sites that can bind and activate metal ions to give the protein its activity that are found in the pre-organised protein even without the metal ion present.

Generally, two methods of incorporation of the metal binding site are used. The overall scaffold can be designed, or specific metal binding sites can be designed for the purpose required and then attached to the protein. In their review, Pfister and co-workers covered a multitude of ways that the creation of metal binding sites in existing protein scaffolds can be achieved.²⁰ Heme, copper and non-heme iron proteins have all been successfully functionalised with additional metal binding groups.

Balaram and co-workers concentrated on the second approach, designing a new scaffold that chelates to metal ions.²¹ They looked at using templates that coordinate metal ions, so that the metal ion site that is required in the formation of the complex is still present within the protein after synthesis. Some natural amino acids can be used in this way as well, such as histidine and cysteine, to form peptide sequences only containing naturally occurring amino acids.

Metallopeptides are an excellent example of natural systems with a fixed oligomerisation state. Zinc finger peptides are a well characterised example of these types of systems.²² Zinc forms a two coordinate metal species, so coordinates to and stabilises a dimeric peptide system. The metal ions in zinc fingers are not restricted to zinc, regardless of the name, and the characterisation of the zinc binding site Cys₂His₂ has led to the design of several new metal binding coiled coil species.

Pecoraro and co-workers have found extensive success in designing new heavy metal binding species based on these design principles.²³ Designing metal binding sites within the centre of the coiled system allows for the geometry of the binding site to be controlled by the structure of the amino acids within the core, which was used to synthesise a 3-coordinate mercury binding site in a trimeric coiled coil.

This work was expanded with arsenic and cadmium as well as mercury.²⁴ The use of a peptide system that has a varying monomer: dimer: trimer equilibrium at different monomer concentrations meant that the system can be tailored with regards to the choice of metal ion, and in metal ions with variable coordination states, the conditions used define the oligomerisation state.

The metal ions used in biological systems reflect their relative abundances in the environment. Transition metals like zinc, iron, and copper are frequently encountered in biological proteins. Lanthanides and actinides are present in much lower abundances in the Earth's crust, so protein systems relying on their coordination are rarely

encountered. However, as the field of synthetic proteins develops, lanthanide binding sites have become a popular target.

Peacock and co-workers report the design of a peptide system designed from *de novo* principles that binds lanthanide ions within the centre of a coiled coil system.²⁵ The mutation of two isoleucine residues in the *a* and *d* positions of a trimeric coiled coil to an asparagine and an aspartate residue respectively generates a hard oxygen six-coordinate lanthanide binding site that can be translated throughout the coiled coil by changing the heptad which contains the mutation.²⁶ Mutation of a central heptad has a destabilising effect on the apo-peptide, but gadolinium or terbium coordination results in the increased ellipticity and stability of the peptide system. These systems have been proposed as potential MRI agents.

1.3 The use of unnatural amino acids to influence peptide structure

Point mutation of residues within peptide sequences is a well-used method in structural biology to investigate the contributions of individual amino acids to protein structure. Individual amino acids are mutated, and the change in structure and stability as a result of this is recorded.^{27,28} As protein design has become a multidisciplinary topic between biology and chemistry, the exchange of proteinogenic amino acids for unnatural amino acids has become a popular method to probe the interactions within peptides with new tools.

Most unnatural amino acids used in these studies rely on methods that change the chemical properties of the amino acid with minimal effect on the structure. While the term unnatural amino acids suggests a molecule drastically different from anything found in nature, the use of β - or γ -amino acids in place of α -amino acids can have destabilising effects on the structure of coiled coils. In a study by Koksche and co-workers, the replacement of the central heptad of a coiled coil with β - or γ -amino acids led to a significant destabilisation of the peptide species.²⁹

Fluorination of amino acids is a frequently used method in the modification of peptides. Yoder and Kumar wrote an in-depth review on the topic.³⁰ Replacing hydrogen with fluorine has a minimal effect on the structure of a chemical compound, but has a profound change on the properties. Fluorination is frequently used within medicinal chemistry to increase the lipophilicity of drugs or their membrane penetration.

Proline is the only cyclic proteinogenic amino acid. The structural inflexibility limits proline's incorporation into the main chain of peptide sequences, but it occurs at the start of helices and within the loops and turns of a protein. Marx and co-workers found that fluorination of the 4-position of proline led to the formation of two diastereoisomers of proline (Figure 1.6).³¹

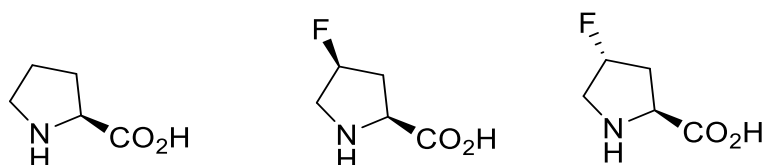


Figure 1.6 Proline, (2S, 4S)-4-fluoroproline and (2S, 4R)-4-fluoroproline.

The two isomers had opposite effects on the stability of the peptide sequence, with the (R) isomer increasing the stability and the (S) isomer decreasing the stability and generating poorly soluble unfolded peptides. This small change had a profound effect on peptide folding and stability.

Brewer and co-workers synthesised phenylalanine derivatives functionalised with alkynyl or nitrile groups resulted in unnatural amino acids with a minor increase in the steric bulk of the protein, but can now act as Förster resonance energy transfer (FRET) donor with tryptophan already present in the peptide chain (Figure 1.7).³²

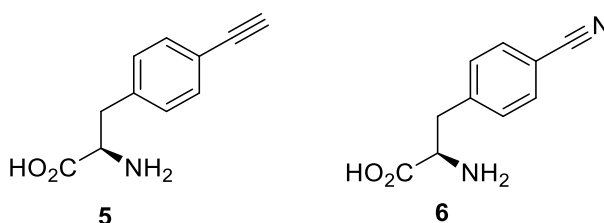


Figure 1.7 L-4-ethynylphenylalanine and L-4-cyanophenylalanine, unnatural amino acids used by Miyake-Stoner et al.³²

These unnatural amino acids were incorporated into the hydrophobic core of the peptide sequence, replacing phenylalanine. As the peptide is subject to urea denaturation, the change in environment of the FRET system reflects this, and so can be used to monitor unfolding of the protein structure.

Biphenylalanine (Figure 1.8) has found uses in the development of therapeutic peptides. Drugs containing biphenylalanine have been developed as inhibitors for histone demethylase KDM4A, or as part of tissue binding agents for cardiac tissue.^{33,34} The structural similarity of biphenylalanine to phenylalanine allowed for the modification of essential enzymes within *E. coli*. to confer dependence on a feedstock containing

unnatural amino acids, which ensures that the enzymes functioned as normal but could not exist outside of controlled environments.³⁵ This was developed as a strategy to isolate genetically modified organisms from natural ecosystems.

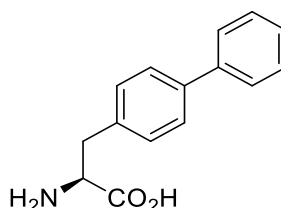


Figure 1.8 Chemical structure of 4-biphenylalanine, an unnatural amino acid derived from an extension of phenylalanine.

Biphenylalanine has also been used as a tool for protein engineering. As part of a study into the binding of peptides to collagen fibres, a peptide containing biphenylalanine displayed selective binding to collagen tissues and was investigated as part of an effort to develop collagen specific imaging.^{34,36} It can also be incorporated as part of a FRET system, similar to phenylalanine or tryptophan.³⁷

There are approaches that use covalent bonds to control the oligomerisation state of a protein structure. Goodman and co-workers synthesised a covalently capped trimeric peptide system based on a collagen model.³⁸ Tris(2-aminoethyl)amine was used as a seed in the synthesis of a trimeric helix (Figure 1.9).

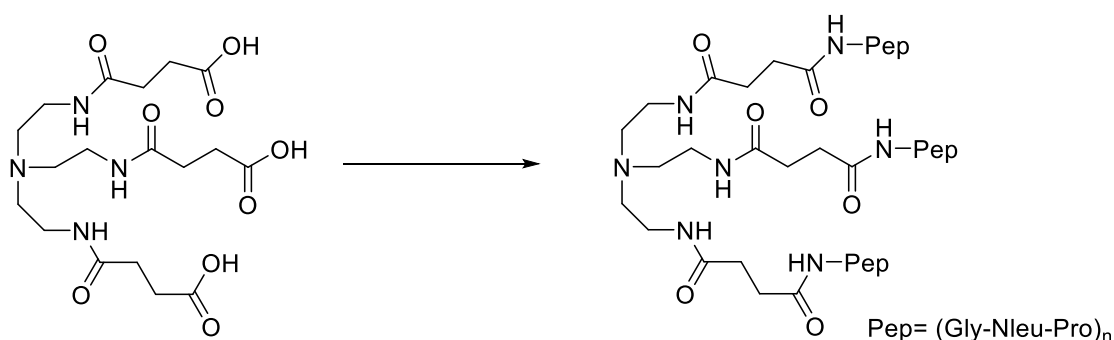


Figure 1.9 Use of tris(2-aminoethyl)amine with succinic acid spacers as the template and covalent linker of a triple helical coiled coil. Nleu represents N-isobutylglycine.³⁸

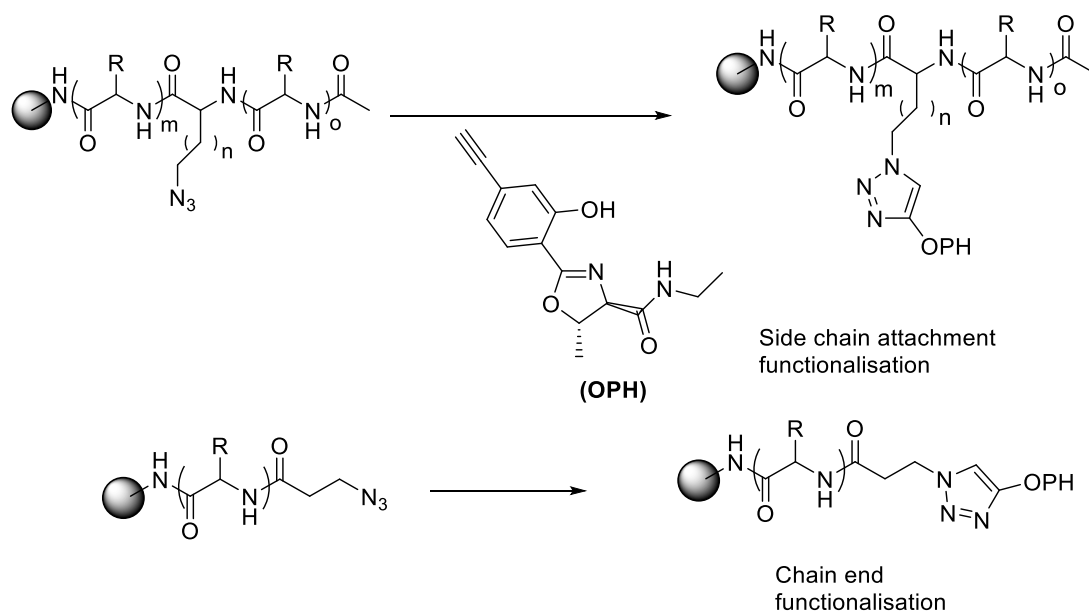
This template allows for the construction of a defined triple helical structure with an unambiguous oligomerisation state. The disadvantage of this is the lack of flexibility & modification of the structures after synthesis.

Metal ions can be used as a reversible structural trigger in proteins containing unnatural amino acids. The Ogawa group has reported extensively on the use of 4-pyridylalanine

in coiled coils, and applications stemming from the use of this bioisostere of phenylalanine. The incorporation of 4-pyridylalanine at the solvent exposed surface of a two-stranded coiled coil does not destabilise the coiled coil system.³⁹ On the addition of $\text{Pt(en)(NO}_3)_2$ the system rearranges, and forms a metal bridged 4-stranded helix bundle with pyridylalanine coordinating to platinum.

4-Pyridylalanine can also associate with the faces of a metalloporphyrin, and these units can then assemble to form further structures.⁴⁰ The structures of the assembled species were solvent dependent. The use of water led to the assembly of globular structures, while the use of phosphate buffer resulted in fibrous rods forming. The authors do not assign the formation of fibres to the protein structure, but rather hydrogen bonding between the phosphate buffer and metalloporphyrins. It is an interesting example of metal coordination not being the cause of a switch in behaviour but enabling it.

Ashkenasy and co-workers incorporated a lanthanide binding group into a coiled coil sequence (Scheme 1.1).⁴¹ In contrast to the previous examples, the unnatural amino acids incorporated within this protein sequence were larger. Rather than a small modification of the protein sequence, the properties of this unnatural amino acid can be used to determine the structure of the entire peptide sequence.



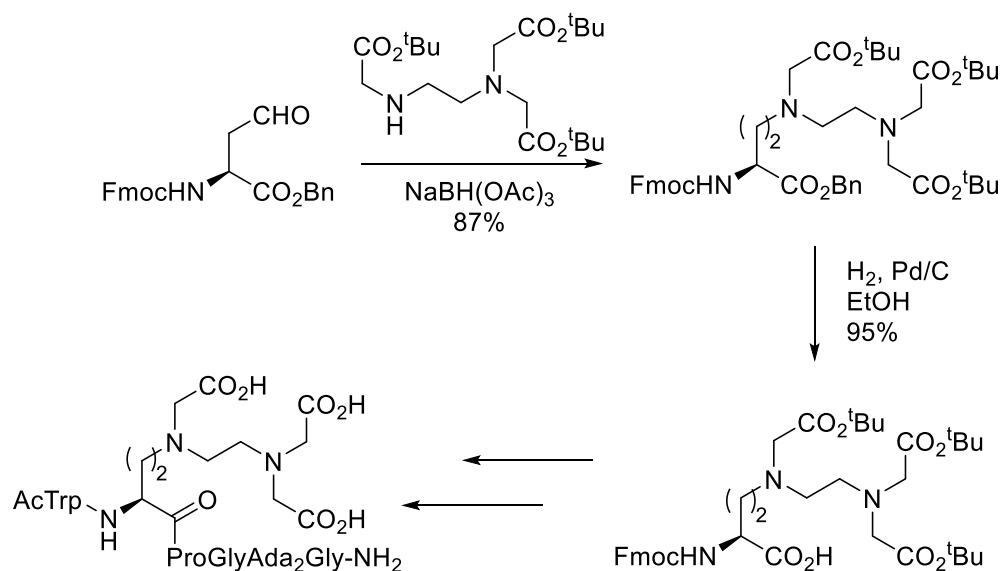
Scheme 1.1 Chain end vs side end attachment of a hydroxyl-phenyl oxazoline (HPO) group to the amino acid sequence of a coiled coil described by Ashkenasy and co-workers.⁴¹

Partial folding of the coiled coil allowed for lanthanide coordination, which then caused further folding of the coiled coil. The click chemistry used to incorporate the lanthanide

bind site allowed the lanthanide binding group to be utilised as either an N-terminal functionalisation or an attachment to the ϵ nitrogen of a lysine side chain.

The side chains used in these amino acids can even be derived from large known metal chelating agents. Delangle and co-workers demonstrated the synthesis and incorporation of EDTA derived amino acids into a short peptide system (Scheme 1.2).⁴² The Ed₃A complex provides a pentadentate binding site, while Ada₂ provides a tridentate ligand. These amino acids can be combined as necessary throughout the peptide species to generate the desired metal binding site.

The peptides reported in this paper demonstrated femtomolar affinity to terbium, detectable through the fluorescence of the terbium peak at 545 nm after sensitisation with tryptophan. The amino acids are synthesised in two steps with high yields, with high stereoselectivity. Treatment of β -serinone with protected N, N, N'-tris-(*tert*-butoxycarbonylmethyl) ethylenediamine and sodium triacetoxyborohydride provides the protected form of Ed₃A, and reduction with hydrogen over a palladium/carbon catalyst provides the amino acid prepared for solid phase peptide synthesis (SPPS). This highlights an important consideration of unnatural amino acid synthesis, where the simple preparation and incorporation of the amino acid reflects their utility in subsequent peptide systems.



Scheme 1.2 The synthesis of Ed₃A reported by Delangle and co-workers.⁴²

1.4 2,2'-Bipyridine containing peptides

Metal binding sites created from proteinogenic amino acids are advantageous as they can be easily synthesised from commonly available materials. Metal binding sites

generated through the incorporation of unnatural amino acids or chemical modification of peptide sequences is more expensive but allows for the construction of systems that do not rely on the preassembly of the peptide system in a particular oligomerisation state, and also can be used to incorporate new functionality.

Bipyridine is a well-known metal chelating ligand, and is known to form very stable metal complexes, making it desirable for this work. Hosseini and co-workers wrote a comprehensive review covering the use of the bipyridine ligand, most of which is well outside the scope of this review but serves as an example of how useful and versatile this ligand is for metal complexation.⁴³

The bipyridine system allows for independent spectroscopic study rather than depending on donor acceptor systems or interactions within the molecule. Bipyridines are also useful as their photochemical and electron transfer properties could be used in catalytically active process.⁴⁴⁻⁴⁷ There are examples of bipyridylalanine being genetically encoded and expressed in proteins through the use of microorganisms, but this thesis focuses on chemical methods of the incorporation of amino acids.⁴⁸ A semi-synthesis of bipyridylalanine functionalised cytochrome *c* mutants has also been reported, where the bipyridine residue was synthesised using solid-phase peptide synthesis and coupled to bacterially expressed proteins.⁴⁹

One of the first instances of peptide systems modified with 2,2'-bipyridine was reported by Lieberman and Sasaki.⁵⁰ A short synthetic peptide functionalised with a bipyridyl carboxylic acid was prepared using solid-state peptide synthesis techniques, and metal ion coordination resulted in a change from a random helix to an α -helical bundle. The system was stabilised by metal coordination, allowing the peptide complex to be isolated and purified (Figure 1.10).

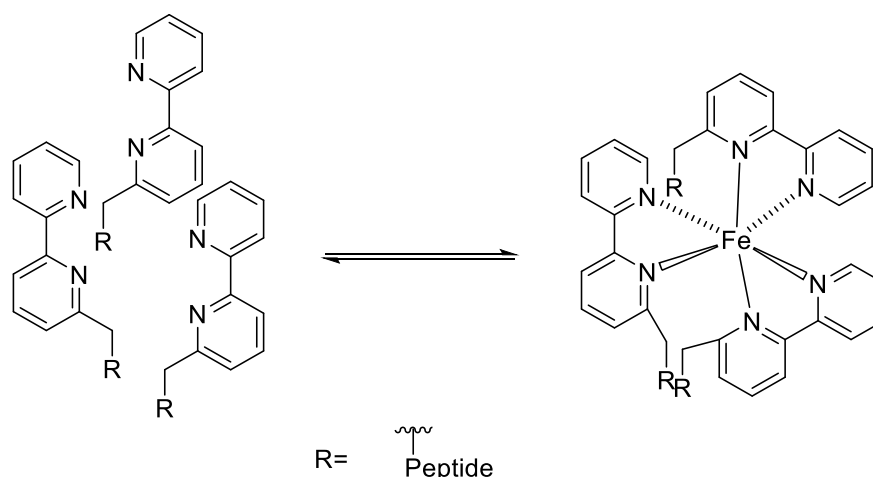


Figure 1.10 Formation of a trimeric $[\text{Fe}^{\text{II}}(\text{bipy})_3]$ complex attached to a helix bundle.

The $[\text{M}(\text{bipy-peptide})_x]^{y+}$ system has been used extensively to staple the oligomerisation state of systems studied. However, the bipyridine moiety is frequently used as a terminal modification to the peptide chain, rather than part of the amino acid backbone. A particularly good example is the system developed by Ghadiri and co-workers where 6-carboxymethylbipyridine capped the end of a short peptide sequence was designed to associate into a helix bundle structure (Figure 1.11).¹⁶

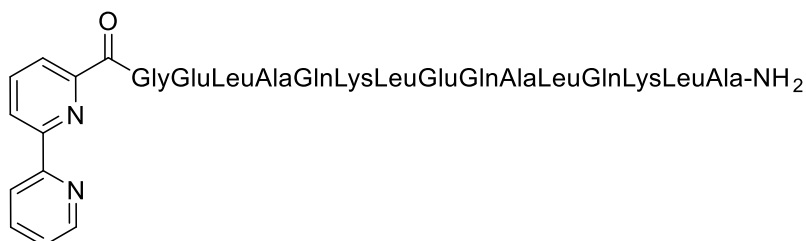


Figure 1.11 Bipyridyl capped peptide sequence used by Ghadiri to generate metal bound helix bundles.¹⁶

In the Ghadiri coiled coil, the peptide becomes more helical as a result of the titration of the metal ions into the solution. They were able to demonstrate this effect with nickel, cobalt and ruthenium ions. There are several other examples of the use of the bipyridyl cap throughout the literature for the same purpose.^{6,15,50,51} In each case, the coordination of metal ions to the peptides results in increased helicity of the peptide. Metal-binding amino acids can be incorporated into polypeptide chains, to investigate the relationship between metal binding, protein packing and increased stability.

The effect of the bipyridyl amino cap on the structure of the peptide was further investigated by Case and co-workers.¹⁵ The previous two examples used amphiphilic systems that had no controlling features to influence oligomerisation state, but when a peptide system that was purposefully designed to form a dimer was capped with the bipyridine system, it formed a trimer. Metal ion coordination had a greater influence

than the steric destabilisation caused by the clash of side chains within the peptide system. The fact that this metal ion coordination can be used to overcome destabilising interactions within the peptide provided a new system for the energetic quantification of peptide systems. The point mutation of salt bridge forming amino acids in peptide sequences containing a bipyridyl cap generated a library of sequences used to investigate the energetic contributions of different amino acid pairs, and the effect of their position in the peptide sequence.

Bipyridyl functionalisation can also be used as a bridging feature within peptide sequences, applied to form switches in peptide systems. Schneider and Kelly reported the incorporation of a bipyridine moiety into a peptide chain (Figure 1.12).⁵²

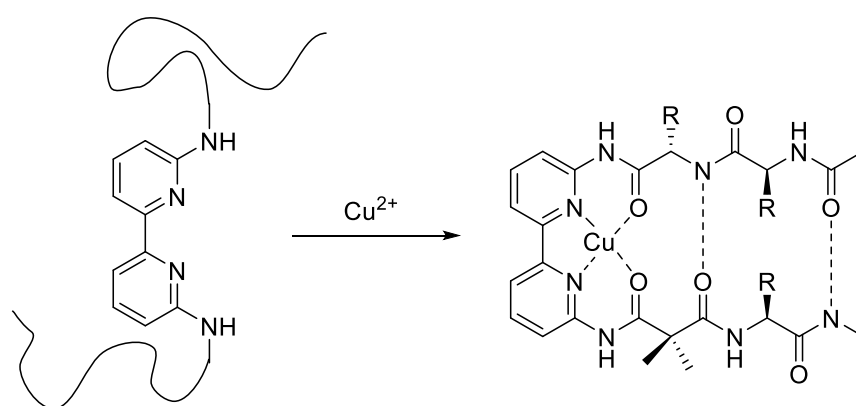


Figure 1.12 Coordination of copper ions to the bipyridine group causes the assembly of a β -sheet structure from the random coils attached to the bipyridine. Assembly is assisted by the coordination of copper to the carbonyl oxygens of the first amide bond of the peptide chain.⁵²

As a result of metal coordination, the bipyridine switches from the trans to the cis bipyridine conformation. This change in conformation causes the assembly of a β -sheet structure when copper is added to the peptide solution.

Peacock and co-workers developed this idea with tripeptide systems, linked with cysteine residues to the polypyridine binding site (Figure 1.13).⁵³ On metal coordination, these systems changed from a *transoid* to a *cisoid* conformation, bringing the peptide species together.

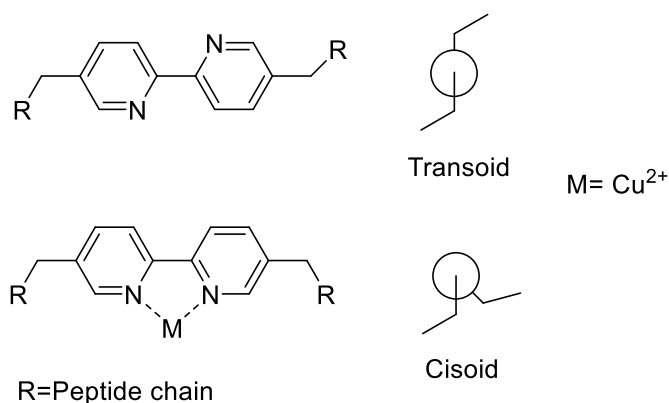


Figure 1.13 The switch between a transoid conformation, observed in the apo-peptide species, and the cisoid conformation when the bipyridine group coordinates a metal ion.⁵³

This model system was developed further as a coordination complex for DNA. The designed peptide coordinates to DNA in the absence of metal ions, but the addition of copper or zinc ions to the system resulted in an increase in peptide helicity and allowed for the selective binding of the peptide to a designed DNA sequence, demonstrating selectivity in its binding.

Torrado and Imperiali developed a similar system using a 5-amino-5'-carboxy-2,2'-bipyridine.⁵⁴ This was incorporated as a fluorescent linker in a peptide chain designed as a luminescent sensor for metal ions. The fluorescence of the bipyridine moiety is significantly increased with the addition of zinc or copper ions to a solution of the peptide.

Konno and co-workers report the use of bipyridine functionalisation in collagen triple helices.⁵⁵ Addition of Fe^{2+} ions to these species increased the thermal stability of the bipyridine-collagen species, and caused the refolding rate of the iron-collagen species to increase after thermal melts. They observed that the stereochemistry of the metal centre was shifted to form right-handed Δ -isomers rather than the expected left-handed species, dictated by the orientation of the collagen ligands.

Reymond and co-workers generated an iron-bipyridine complex where 5,5'-dimethyl-2,2'-bipyridine was linked to peptide dendrimers through sulfur bonds.⁵⁶ The stoichiometry of the species was controlled by the pH of the system. At low pH, the system formed a $[Fe^{II}(\text{bipy-peptide})_3]$ species, which was the expected coordination number. At pH 6.5, the species formed $[Fe^{II}(\text{bipy-peptide})]$. This stoichiometry was explained by the electrostatic repulsion between the anionic dendrimer branches at this pH favouring this stoichiometry. They found this monocoordinated species could act as

a catalyst for the oxidation of *o*-phenylenediamine with H₂O₂, behaviour not observed with isolated Fe²⁺ or [Fe(bipy)₃]²⁺.

Imperiali and co-workers reported both the synthesis and incorporation of bipyridyl amino acids into peptide sequences.⁵⁷⁻⁵⁹ By using the 4, 5 and 6 isomers of (S)-2-amino-3(2, 2'-bipyridyl)propanoic acids (4Bpa, 5Bpa and 6Bpa respectively), where the bipyridines vary only through which carbon atom is attached to the amino acid side chain, Imperiali found varying results in metal binding affinities, suggesting that the affinity could be tuned by changing the side chain isomer (Figure 1.14).

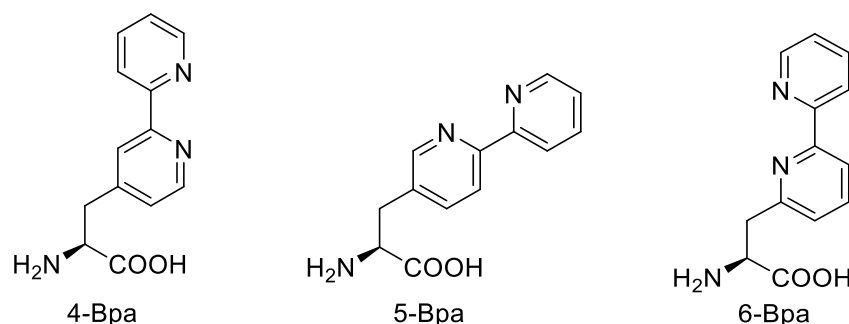


Figure 1.14 4,5 and 6Bpa⁵⁷

Imperiali and co-workers also synthesised short beta-hairpin sequences to investigate the effects of the bipyridyl backbone on their folding.⁵⁸ Their investigation concerned two different types of peptide structure, investigating the effect of metal titration into bipyridyl proteins with either a high level of pre-existing order or a more random peptide structure. It was expected that the more ordered system would see less of an increase in helicity, but more stabilisation, and the disordered system would become more organised but not reach the same levels of helicity as the more ordered system. It was observed that the pre-organised system did show stronger binding to the metal ions than the disordered system. The strength of metal binding could be modulated by varying the level of pre-organisation.

6Bpa was the weakest binding amino acid, while 4Bpa and 5Bpa were approximately the same. Imperiali suggested that this was due to the connecting alkyl chain of the amino acid being close to the metal binding site of 6Bpa and so steric hindrance was affecting the binding strength. The different isomers were also found to have different metal:protein ratios, demonstrating that choice of side chain also affects the metal-protein complex stoichiometry.

However, when two of the 6Bpa molecules were included in the chain, the metal binding affinity was greatly increased, by two orders of magnitude. This suggested that both bipyridyl side chains were acting cooperatively to bind to the same metal ion.

Erickson and co-workers demonstrate the synthesis of 4'-aminomethyl-2,2'-bipyridyl-4-carboxylic acid, and its use in a ruthenium-peptide complex (Figure 1.15).⁶⁰

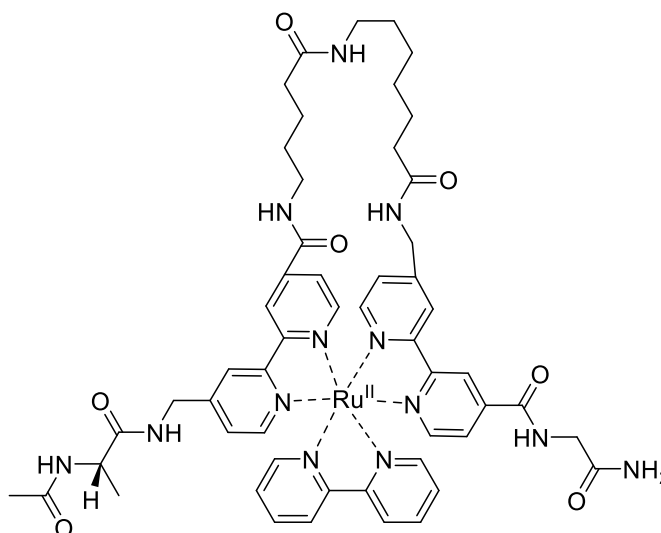


Figure 1.15 Cyclic ruthenium-peptide complex synthesised by Erickson and co-workers. The bipyridyl group acts as a linker in the linear peptide species, but coordination of ruthenium generates a cyclopeptide.⁶⁰

The similarity of this compound to those used by Kelly and co-workers (Figure 1.14) is mirrored in its application. The use of two bipyridine residues in the peptide, followed by coordination of ruthenium to the peptide caused the flexible peptide backbone to form a cage around the ruthenium ion, providing a favourable coordination geometry for the metal ion and controlling the structure of the peptide.

Bimetallic systems containing metal ions from two different areas of the periodic table are a relatively unexplored area in coiled coil research. Previous examples of systems that fall under the umbrella of bimetallic include systems that can bind zinc ions in two separate sites, used to generate a new transphosphorylation catalyst.⁶¹

However, for examples of systems that bind two different types of metal ion within the same system, i.e. both transition metal ions and lanthanide ions, a search of the literature only revealed one previous peptide example. In this example, a short peptide sequence formed a dimer with a cavity within the centre that can bind three metal ions, and was found to bind two terbium atoms and one zinc atom.⁶² These could then interact, and the proximity of the zinc ions to terbium had a measurable effect on the

electronic properties of terbium. As part of our work, we wanted to investigate how we could bind two different metal ions in the same coiled coil.

1.5 Project aims

The aims of this work are (1) to apply a novel synthetic route to the bipyridyl amino acids, and (2) to incorporate these in three-stranded coiled coil structures to modulate folding via transition metal coordination.

The trimeric coiled coil sequences used are those previously characterised by Peacock and co-workers, which also contain a lanthanide binding site.²⁵ The response of these structures to metal coordination via the bipyridine group will be characterised using circular dichroism, UV absorption and fluorescence spectroscopy.

The incorporation of two different metal binding sites into a three-stranded helical bundle might allow for selectivity in the binding of both transition and lanthanide metal ions, paving the way to the development of transition metal functionalised xenometallic peptides. For instance, the incorporation of two binding sites, one bipyridyl unit binding transition metal ions and one binding site for lanthanide ions presents the opportunity to investigate mixed metal systems with potentially interesting chemical and photophysical properties.

1.6 References

- (1) Levinthal, C. *J Chim Phys* **1968**, 65, 44.
- (2) Ambrogelly, A.; Palioura, S.; Soell, D. *Nat. Chem. Biol.* **2006**, 3, 29.
- (3) Schneider, J. P.; Kelly, J. W. *Chem. Rev.* **1995**, 95, 2169.
- (4) Cheng, R. P.; Gellman, S. H.; DeGrado, W. F. *Chem. Rev.* **2001**, 101, 3219.
- (5) Baltzer, L.; Nilsson, H.; Nilsson, J. *Chem. Rev.* **2001**, 101, 3153.
- (6) Doerr, A. J.; McLendon, G. L. *Inorg. Chem.* **2004**, 43, 7916.
- (7) Pauling, L.; Corey, R. B.; Branson, H. R. *Proc. Natl. Acad. Sci. U. S. A.* **1951**, 37, 205.
- (8) Lupas, A. N.; Gruber, M. *Adv. Protein Chem.* **2005**, 70, 37.
- (9) Woolfson, D. N. *Adv. Protein Chem.* **2005**, 70, 79.
- (10) Hicks, M. R.; Holberton, D. V.; Kowalczyk, C.; Woolfson, D. N. *Folding Des.* **1997**, 2, 149.
- (11) Harbury, P. B.; Plecs, J. J.; Tidor, B.; Alber, T.; Kimt, P. S. *Science (Washington, D. C.)* **1998**, 282, 1462.
- (12) Johansson, J. S.; Gibney, B. R.; Skalicky, J. J.; Wand, A. J.; Dutton, P. L. *J. Am. Chem. Soc.* **1998**, 120, 3881.
- (13) Harbury, P. B.; Zhang, T.; Kim, P. S.; Alber, T. *Science* **1993**, 262, 1401.
- (14) Oshaben, K. M.; Salari, R.; McCaslin, D. R.; Chong, L. T.; Horne, W. S. *Biochemistry* **2012**, 51, 9581.

- (15) Gochin, M.; Khorosheva, V.; Case, M. A. *J. Am. Chem. Soc.* **2002**, *124*, 11018.
- (16) Ghadiri, M. R.; Soares, C.; Choi, C. *J. Am. Chem. Soc.* **1992**, *114*, 825.
- (17) Zhou, T.; Ma, Y. M.; Kong, X. L.; Hider, R. C. *Dalton Trans.* **2012**, *41*, 6371.
- (18) Kennedy, M. L.; Gibney, B. R. *Current Opinion in Structural Biology* **2001**, *11*, 485.
- (19) DeGrado, W. F.; Summa, C. M.; Pavone, V.; Nastri, F.; Lombardi, A. *Annu. Rev. Biochem* **1999**, *68*, 779.
- (20) Lu, Y.; Berry, S. M.; Pfister, T. D. *Chem. Rev.* **2001**, *101*, 3047.
- (21) Venkatraman, J.; Shankaramma, S. C.; Balaram, P. *Chem. Rev.* **2001**, *101*, 3131.
- (22) Krishna, S. S.; Majumdar, I.; Grishin, N. V. *Nucleic Acids Res.* **2003**, *31*, 532.
- (23) Dieckmann, G. R.; McRorie, D. K.; Tierney, D. L.; Utschig, L. M.; Singer, C. P.; O'Halloran, T. V.; Penner-Hahn, J. E.; DeGrado, W. F.; Pecoraro, V. L. *J. Am. Chem. Soc.* **1997**, *119*, 6195.
- (24) Matzapetakis, M.; Farrer, B. T.; Weng, T.-C.; Hemmingsen, L.; Penner-Hahn, J. E.; Pecoraro, V. L. *J. Am. Chem. Soc.* **2002**, *124*, 8042.
- (25) Berwick, M. R.; Lewis, D. J.; Jones, A. W.; Parslow, R. A.; Dafforn, T. R.; Cooper, H. J.; Wilkie, J.; Pikramenou, Z.; Britton, M. M.; Peacock, A. F. A. *J. Am. Chem. Soc.* **2014**, *136*, 1166.
- (26) Berwick, M. R.; Slope, L. N.; Smith, C. F.; King, S. M.; Newton, S. L.; Gillis, R. B.; Adams, G. G.; Rowe, A. J.; Harding, S. E.; Britton, M. M.; Peacock, A. F. A. *Chem. Sci.* **2016**, *7*, 2207.
- (27) Matthews, C. R. *Methods Enzymol.* **1987**, *154*, 498.
- (28) Dutta, K.; Engler, F. A.; Cotton, L.; Alexandrov, A.; Bedi, G. S.; Colquhoun, J.; Pascal, S. M. *Protein Sci.* **2003**, *12*, 257.
- (29) Nyakatura, E. K.; Mortier, J.; Radtke, V. S.; Wieczorek, S.; Rezaei Araghi, R.; Baldauf, C.; Wolber, G.; Koksche, B. *ACS Med. Chem. Lett.* **2014**, *5*, 1300.
- (30) Yoder, N. C.; Kumar, K. *Chem. Soc. Rev.* **2002**, *31*, 335.
- (31) Holzberger, B.; Obeid, S.; Welte, W.; Diederichs, K.; Marx, A. *Chemical Science* **2012**, *3*, 2924.
- (32) Miyake-Stoner, S. J.; Miller, A. M.; Hammill, J. T.; Peeler, J. C.; Hess, K. R.; Mehl, R. A.; Brewer, S. H. *Biochemistry* **2009**, *48*, 5953.
- (33) Morera, L.; Roatsch, M.; Fuerst, M. C. D.; Hoffmann, I.; Senger, J.; Hau, M.; Franz, H.; Schuele, R.; Heinrich, M. R.; Jung, M. *ChemMedChem* **2016**, *11*, 2063.
- (34) Chen, J.; Lee, S. K.; Abd-Elgaliel, W. R.; Liang, L.; Galende, E.-Y.; Hajjar, R. J.; Tung, C.-H. *PLoS One* **2011**, *6*, e19097.
- (35) Mandell, D. J.; Lajoie, M. J.; Mee, M. T.; Takeuchi, R.; Kuznetsov, G.; Norville, J. E.; Gregg, C. J.; Stoddard, B. L.; Church, G. M. *Nature (London, U. K.)* **2015**, *518*, 55.
- (36) Abd-Elgaliel, W. R.; Tung, C.-H. *Biopolymers* **2013**, *100*, 167.
- (37) Kuragaki, M.; Sisido, M. *J. Phys. Chem.* **1996**, *100*, 16019.
- (38) Kwak, J.; De Capua, A.; Locardi, E.; Goodman, M. *J. Am. Chem. Soc.* **2002**, *124*, 14085.
- (39) Tsurkan, M. V.; Ogawa, M. Y. *Inorg. Chem.* **2007**, *46*, 6849.
- (40) Tsurkan, M. V.; Ogawa, M. Y. *Biomacromolecules* **2007**, *8*, 3908.
- (41) Samiappan, M.; Alasibi, S.; Cohen-Luria, R.; Shanzer, A.; Ashkenasy, G. *Chem. Commun.* **2012**, *48*, 9577.

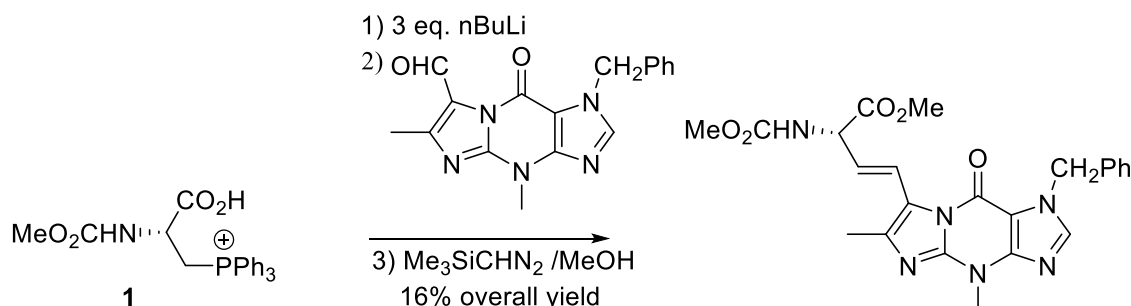
- (42) Niedzwiecka, A.; Cisnetti, F.; Lebrun, C.; Delangle, P. *Inorg. Chem.* **2012**, *51*, 5458.
- (43) Kaes, C.; Katz, A.; Hosseini, M. W. *Chem. Rev.* **2000**, *100*, 3553.
- (44) Chelucci, G.; Thummel, R. P. *Chem. Rev.* **2002**, *102*, 3129.
- (45) Ishiyama, T.; Takagi, J.; Hartwig, J. F.; Miyaura, N. *Angewandte Chemie-International Edition* **2002**, *41*, 3056.
- (46) Gilbert, J. A.; Eggleston, D. S.; Murphy, W. R.; Geselowitz, D. A.; Gersten, S. W.; Hodgson, D. J.; Meyer, T. J. *J. Am. Chem. Soc.* **1985**, *107*, 3855.
- (47) Riplinger, C.; Sampson, M. D.; Ritzmann, A. M.; Kubiak, C. P.; Carter, E. A. *J. Am. Chem. Soc.* **2014**, *136*, 13.
- (48) Luo, X.; Wang, T.-S. A.; Zhang, Y.; Wang, F.; Schultz, P. G. *Cell Chem. Biol.* **2016**, *23*, 1098.
- (49) Wuttke, D. S.; Gray, H. B.; Fisher, S. L.; Imperiali, B. *J. Am. Chem. Soc.* **1993**, *115*, 8455.
- (50) Lieberman, M.; Sasaki, T. *J. Am. Chem. Soc.* **1991**, *113*, 1470.
- (51) Ghadiri, M. R.; Case, M. A. *Angewandte Chemie-International Edition in English* **1993**, *32*, 1594.
- (52) Schneider, J. P.; Kelly, J. W. *J. Am. Chem. Soc.* **1995**, *117*, 2533.
- (53) Oheix, E.; Spencer, N.; Gethings, L. A.; Peacock, A. F. A. *Z. Anorg. Allg. Chem.* **2013**, *639*, 1370.
- (54) Torrado, A.; Imperiali, B. *J. Org. Chem.* **1996**, *61*, 8940.
- (55) Koide, T.; Yuguchi, M.; Kawakita, M.; Konno, H. *J. Am. Chem. Soc.* **2002**, *124*, 9388.
- (56) Geotti-Bianchini, P.; Darbre, T.; Reymond, J.-L. *Org. Biomol. Chem.* **2013**, *11*, 344.
- (57) Imperiali, B.; Prins, T. J.; Fisher, S. L. *J. Org. Chem.* **1993**, *58*, 1613.
- (58) Cheng, R. P.; Fisher, S. L.; Imperiali, B. *J. Am. Chem. Soc.* **1996**, *118*, 11349.
- (59) Imperiali, B.; Fisher, S. L. *J. Org. Chem.* **1992**, *57*, 757.
- (60) Bishop, B. M.; McCafferty, D. G.; Erickson, B. W. *Tetrahedron* **2000**, *56*, 4629.
- (61) Rossi, P.; Felluga, F.; Tecilla, P.; Formaggio, F.; Crisma, M.; Toniolo, C.; Scrimin, P. *J. Am. Chem. Soc.* **1999**, *121*, 6948.
- (62) Alies, B.; Wiener, J. D.; Franz, K. J. *Chemical Science* **2015**, *6*, 3606.

Chapter 2: Synthesis of bipyridyl amino acids

2.1 Background

The synthesis of new α -amino acids is of constant interest in the field of organic chemistry. Unnatural amino acids can be used in peptide and protein design, or as chiral starting materials. There are many existing methods of amino acid synthesis, the use of which have been extensively covered in articles and reviews, (see Duthaler (1994) for an overview of methods of amino acid synthesis, Ganboa (2001) for the use of β -lactams in amino acid synthesis, Ooi (2003) for the use of chiral phase transfer agents in amino acid synthesis, and Fotheringham (2001) for a general overview of unnatural amino acid synthesis).¹⁻⁴ New unnatural amino acids offer a rich source of new designs and functionalities.

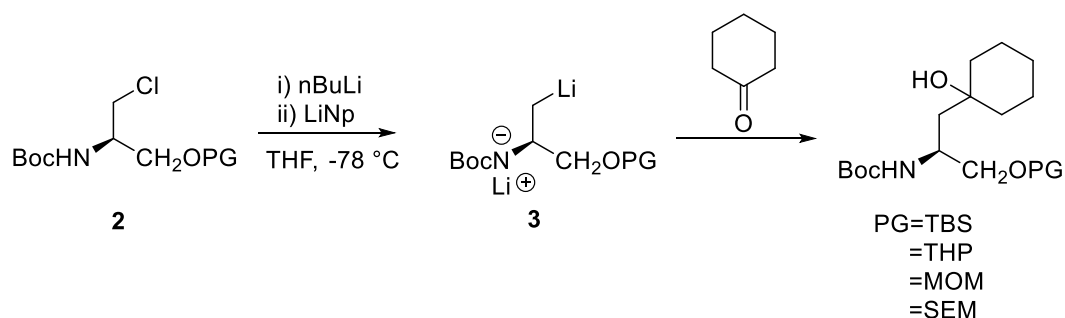
One approach to the synthesis of new α -amino acids is to use proteinogenic amino acids from the chiral pool as starting materials.¹ One application of this is the conversion of the hydroxyl side chain of serine to a range of other functional groups. For example, Tachinaka and co-workers converted the side chain of serine to phosphonium salt **1**, for use in Wittig reactions to synthesise 2-arylvinyl glycine derivatives (Scheme 2.1).⁵



Scheme 2.1 Tachinaka and co-workers synthesis of an arylvinyl glycine derivative.⁵

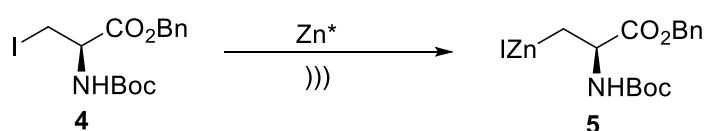
Conversion of the hydroxyl side chain to a halogen can be used to generate the starting materials required to form organometallic amino acid reagents. Metal-halogen exchange with the resulting halides yields organometallic reagents which can act as a β -anion equivalent.

A range of hydroxylated amino acids have been synthesised by the Taylor group using a lithium reagent derived from serine. Use of a combination of n-butyllithium/lithium naphthalenide impedes the β -elimination of the chloride anion and favours lithium-halogen exchange. These lithium agents acted as a hard nucleophilic reagent when reacted with ketones. (Scheme 2.2)⁶



Scheme 2.2 A lithium reagent developed by Taylor and co-workers to synthesise hydroxyl functionalised α -amino acids.⁶

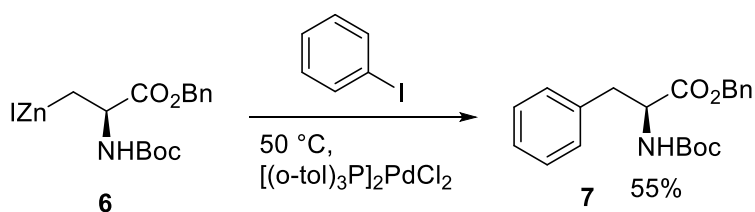
The conditions used to generate lithium reagent **3** require the use of protecting groups and reagents that prevent the decomposition of **2**. The Jackson group reported the synthesis of serine derived organozinc reagent **5**, which has the advantage that additional functional group modification after that used to synthesise iodide **4** is not required (Scheme 2.3).⁷



Scheme 2.3 Zinc insertion into the iodide generates zinc reagent **5** that can be used to synthesise unnatural amino acids.^{8,9}

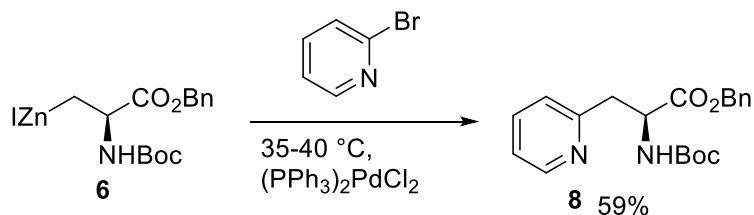
Zinc reagent **5** can undergo coupling reactions to add functional groups onto the side chain of the amino acid. This zinc reagent can be used in a range of reactions and the different uses of compound **1** have been documented by Rilatt *et. al.*, but this thesis focuses on its use in the synthesis of β -aryl amino acids.¹⁰

The first report of the methodology to synthesise β -aryl amino acids was the synthesis of protected phenylalanine derivatives, reported by Jackson *et. al.* in 1992 (Scheme 2.4).⁷ Use of a Negishi cross coupling between organozinc reagent **6** and iodobenzene yielded **7** in good yields.



Scheme 2.4 Negishi cross-coupling between zinc reagent **6** and phenyl iodide to yield **7**.⁷

This methodology was used to synthesise a range of phenylalanine derivatives, including the pyridylalanine **8** (Scheme 2.5).¹¹

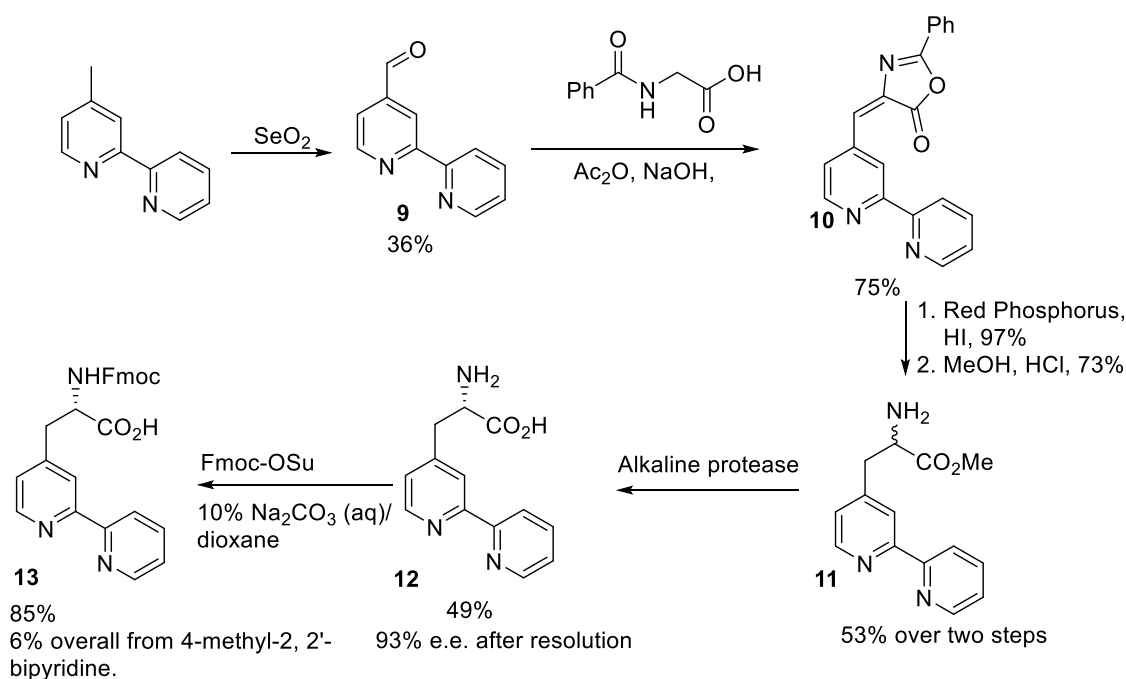


Scheme 2.5 Negishi cross-coupling between zinc reagent **2** and 2-bromopyridine.¹¹

2.2 Previous synthesis of bipyridyl amino acids

There are 3 regioisomers of 2,2'-bipyridylalanine of interest to this project, distinguished by their point of attachment to the pyridine ring. This can be attached at the 4, 5, or 6 position of the ring (referred to as 4-, 5-, and 6-Bpa). Previous synthesis of amino acids functionalised with bipyridine groups was carried out by the Imperiali group in the early 1990s.^{12,13}

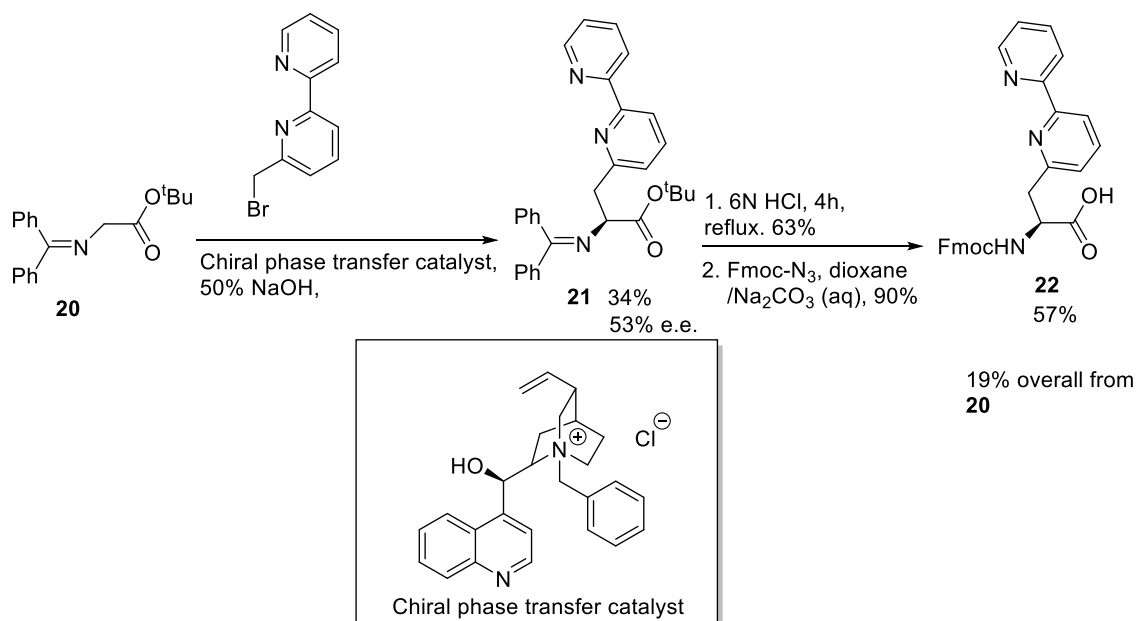
Synthesis of 4-Bpa involved the oxidation of 4-methyl-2, 2'-bipyridine with selenium dioxide to give aldehyde **9**, which was condensed with N-benzoyl glycine to yield oxazolone **10** (Scheme 2.6). Treatment with red phosphorus and HI, followed by Fischer esterification of the crude mixture gave the methyl ester **11**. Alkaline protease hydrolyses the methyl ester of the desired enantiomer, generating the unprotected amino acid of the desired isomer (**12**) and the two are then separated. Fmoc protection of compound **12** yields the Fmoc free acid **13** suitably protected for solid-phase peptide synthesis. This method relies on a synthesis of a racemic mixture of the desired compound, and then enzymatic resolution to resolve the mix of enantiomers.



Scheme 2.6 Imperiali synthesis of 4-Bpa¹³

To synthesise 5Bpa, Imperiali and co-workers treated **14** with lithium aluminium hydride followed by bromination with the Appel reaction to yield **15**. Alkylation of **15** with N-diphenylmethylene glycine yielded amino acid **16** as a product with a low enantiomeric ratio, so **16** was subject to enzymatic resolution. The cleavage of both N- and C-terminal protecting groups of amino acid **16** was followed by Fischer esterification, which yielded ester **17**. Enzymatic resolution resulted in the isolation of carboxylic acid **18**. The desired isomer was then Fmoc-protected, yielding the desired amino acid **19**.¹³

The overall yield of the synthesis of 5Bpa is higher than the synthesis of 4Bpa, a fact that can be attributed to the higher yields of the deprotection than those obtained with **11**. The phosphorus/HI method in Scheme 2.6 is lower yielding than the use of concentrated hydrochloric acid. However, the paper notes that the alkylation step becomes less selective when run at scales above 1 mmol, requiring the pooling of several reaction batches for the synthesis of large amounts.



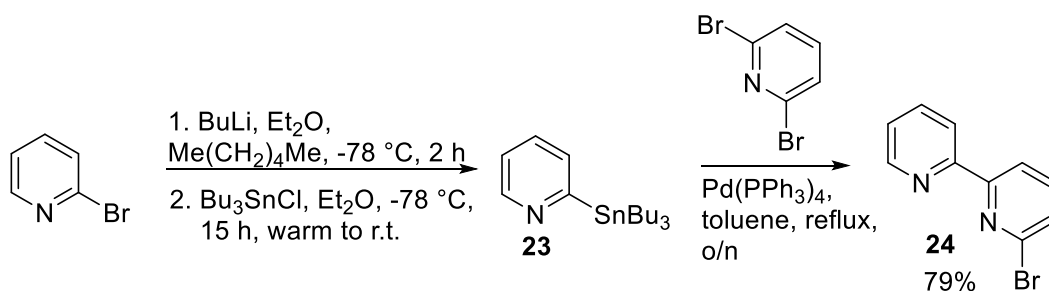
Scheme 2.8 Imperiali synthesis of 6Bpa¹²

Considering the use of zinc reagent **6** to synthesise β -aryl amino acids (Scheme 2.5), and the drawbacks encountered in Imperiali's synthesis of these bipyridyl amino acids (Schemes 2.6-2.8) namely the use of asymmetric synthesis and extensive purification of the resulting mixture of products, the use of zinc reagent **6** to synthesise compounds **13**, **19**, and **22** was considered. The use of an alanyl synthon avoids the need for stereoselective synthesis, which was the main cause for the loss of the desired material in Imperiali's synthesis. This methodology would require the synthesis of halo-2,2'-bipyridines as a coupling partner for zinc reagent **6**.

2.3 Synthesis of halo-2,2'-bipyridines

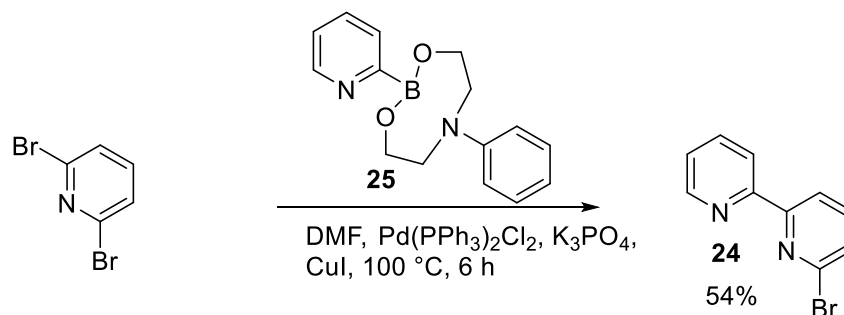
2.3.1 Previous syntheses

As 2,2'-bipyridine is one of the most frequently used ligands for metal ions, there are many methods of synthesis of the unfunctionalised ligand.¹⁵⁻¹⁷ Halogenated 2, 2'-bipyridines have been synthesised using coupling methods such as the Suzuki or Stille reactions, but each have their drawbacks. Lithium-halogen exchange of 2-bromopyridine and transmetallation with tributyltin chloride yields the Stille reagent **23**. Treatment of **23** with a palladium catalyst and 2,6-dibromopyridine in refluxing toluene yields bromobipyridine **24** in good yields (Scheme 2.9).¹⁸



Scheme 2.9 Generation of a pyridyl stannane reagent, and subsequent cross coupling with 2,6-dibromopyridine to generate 6-bromo-2,2'-bipyridine.¹⁸

Stevens and co-workers report a synthesis of 6-bromo-2,2'-bipyridine using Suzuki cross-coupling methods (Scheme 2.10).¹⁹ Suzuki reagent **25** can be selectively reacted with 2,6-dibromopyridine in a Suzuki-Miyaura reaction to generate **24**. 2-Pyridylborane reagents are now commercially available that can be used in a variety of coupling reactions.



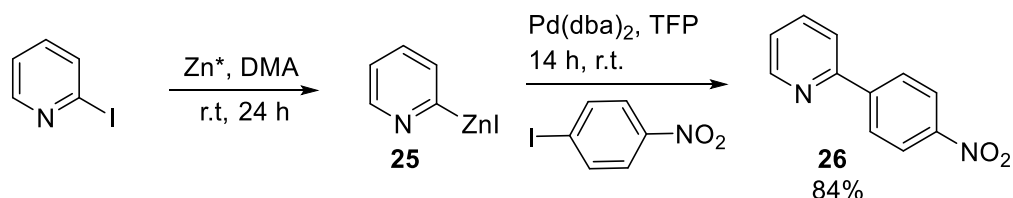
Scheme 2.10 Synthesis of 6-bromo-2,2'-bipyridine using a Suzuki-Miyaura cross coupling.¹⁹

Both Stille and Suzuki reactions have been used to synthesise halogenated bipyridines. The reactions are typically performed at high temperatures in DMF or toluene and require long reaction times. Yields using the Stille reagent are reported as variable, while the Suzuki reagent reaction is reported in high yields (Schemes 2.9 and 2.10).

2.3.2 2-Pyridylzinc reagents and their subsequent use in Negishi cross-coupling reactions.

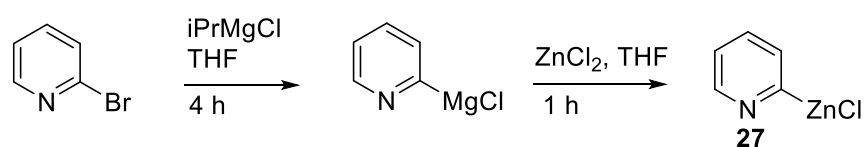
A Negishi coupling reaction is typically between an aromatic halide and an organozinc reagent. It is difficult to insert zinc metal into an sp² carbon halogen bond. Rieke and co-workers report the use of highly reactive zinc to carry out the insertion of zinc into 2-bromopyridine.²⁰ Knochel and co-workers investigated the development of direct zinc insertion into halopyridines, and discovered that optimisation of the solvent and method of zinc activation did allow for the direct insertion of elemental zinc into the halide bond of 2-iodopyridine. Initial methods reported relied on heating the insertion reaction

to 70 °C for an hour before the insertion is complete.²¹ A further publication in 2006 reported the use of zinc dust in DMA to insert zinc directly into 2-iodopyridine at 25 °C, to generate the corresponding zinc reagent after 24 hours (**25**) (Scheme 2.11).²² This zinc reagent was then used in subsequent coupling reactions. Interestingly, in the same paper 2-bromopyridine failed to undergo zinc insertion even at reflux temperatures in DMA.



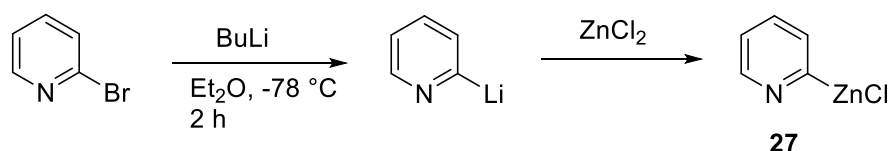
Scheme 2.11 Direct insertion of zinc into the Ar-I bond, and subsequent cross coupling to yield biaryl **26**.²²

Typically the synthesis of a pyridylzinc reagent is achieved by using a Grignard reagent to carry out metal-halogen exchange with an aryl halide, and then transmetallation through the use of a zinc halide salt to form zinc reagent **27** such as those methods described by Luzung and co-workers (Scheme 2.12).²³ The Knochel group has reported the use of the “turbo” Grignard reagent ⁱPrMgCl.LiCl and found increased rates of exchange and higher yields compared to additive-free ⁱPrMgCl in both addition and exchange reactions.²⁴ LiCl can be added to the Grignard reagent either during its synthesis or as a solution added to the commercially available Grignard reagent.



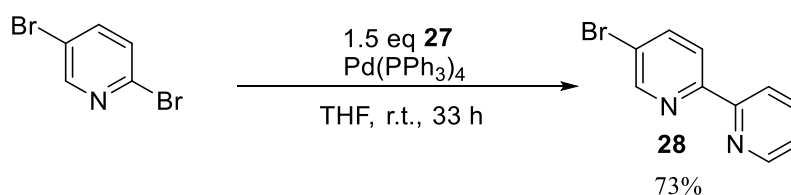
Scheme 2.12 Generation of 2-pyridylzinc reagent **27** using magnesium-halogen exchange, followed by zinc chloride transmetallation.²³

As well as magnesium, lithium has been used in the synthesis of **27**. Syntheses use lithium-halogen exchange followed by transmetallation with zinc chloride (Scheme 2.13).²⁵

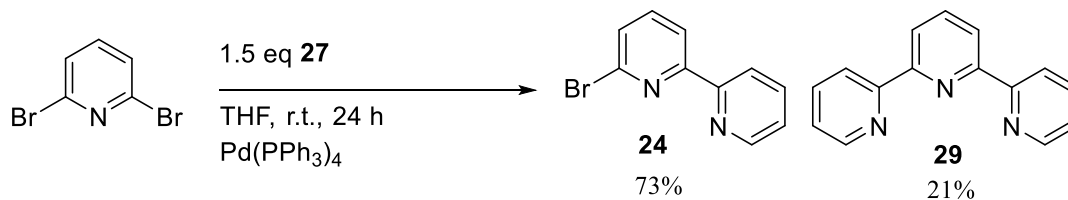


Scheme 2.13 Generating 2-pyridylzinc reagents using lithium-halogen exchange, followed by transmetalation with zinc chloride.²⁵

Pyridylzinc reagents like **27** can then be used in a variety of Negishi cross couplings with a range of halogenated heterocycles, but the one of most interest to this project is the coupling with 2,5- and 2,6-dibromopyridine to form 5- and 6-bromo-2,2'-bipyridine respectively (Schemes 2.14 & 2.15).²⁶



Scheme 2.14 Regioselective cross-coupling of zinc reagent 23 to form 5-bromo-2,2'-bipyridine²⁶



Scheme 2.15 Hanan and co-workers synthesis of 6-bromo-2,2'-bipyridine.²⁶

The presence of **29** after the synthesis of 6-bromo-2,2'-bipyridine (Scheme 15), and the absence of an analogous terpyridine in the synthesis of 5-bromo-2,2'-bipyridine (Scheme 2.14) indicates the coupling at the 2-position is faster than at the 5-position, displaying regioselectivity in the ring positions of dihalopyridines. It also suggests that the 2- and 6-positions of pyridine have similar reactivities.

2.4 Selective cross-couplings with dihalopyridines

In cross coupling reactions, the rate of oxidative addition is higher at ring positions with lower electron density. Handy and Zhang demonstrated that the ¹H NMR chemical shifts of the parent heterocycle can be used as an assignment for the electron density of the dihalogenated heterocycle.²⁷ In pyridine, this demonstrates the lowest electron density at the 2 position, then the 4, and the 3/5 positions possess the highest electron density.

Houk and co-workers performed an extensive theoretical study on the regioselectivity of haloheterocycles in palladium catalysed cross-coupling reactions.²⁸ In their set of model dichloropyridines the 2/6, 4, and 3/5 positions of pyridine demonstrated increasing bond dissociation energies respectively, consistent with experimental studies demonstrating the decreasing respective rate of oxidative addition of each of the three positions.

This difference in reactivity can be combined with carbon-halogen bond strength to control the selectivity of cross-coupling reactions further. The strength of the carbon-halogen bond also affects the rate of oxidative addition, with a lower bond dissociation energy increasing the rate of oxidative addition. In Ph-X systems, the bond dissociation energies change considerably between halogens (Figure 1).²⁹

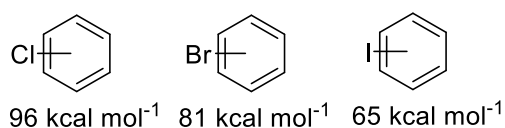
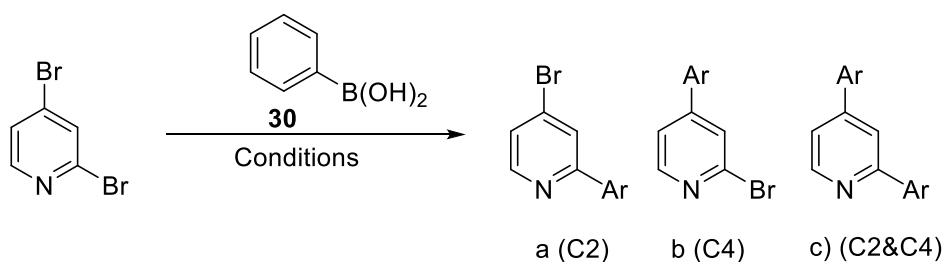


Figure 2.1 Bond dissociation energies for Ph-X at 298 K.

Two papers by Cid and co-workers are of particular interest to the project. The first describes a mechanistic study of Suzuki cross coupling reactions of 2,4-dibromopyridine with phenylboronic acid **30** in some detail.³⁰ Substitution in the 2-position was the favoured regioisomer under these conditions. In addition, 4- and di-substitution was observed in these conditions, but the formation of the disubstituted product did not correspond to the relative rates of formation of either mono-substituted product (Figure 2.2).

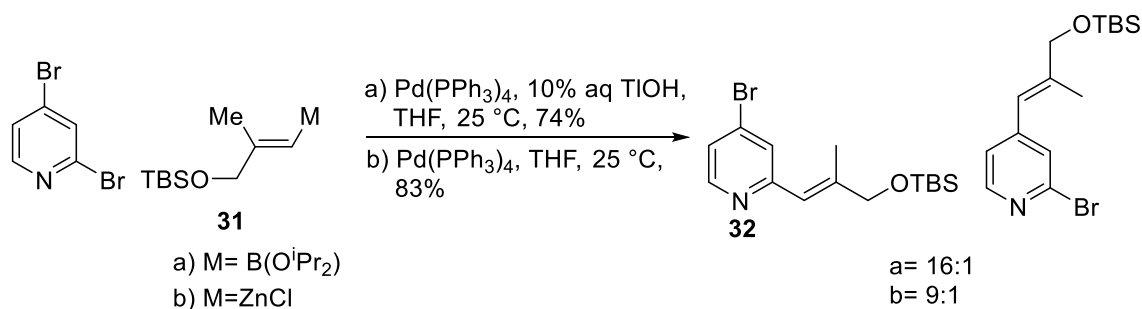
The different additives in the reaction affect the selectivity of the reaction, with the addition of aqueous thallium hydroxide yielding the highest selectivity. The mixtures of products are the result of the coupling in one position being faster. In this example, the reaction displays preferential coupling in the 2-position.



Conditions	Temperature	a:b:c	Yield (conv.)
Pd(OAc) ₂ , Cs ₂ CO ₃ , PCy ₃ , dioxane	25°C	2:1:7	- (35)
Pd ₂ dba ₃ , K ₃ PO ₄ , PCy ₃ , dioxane	25°C	11:0.3:1	43 (60)
"	25°C	7:0:1	69 (>98)
Pd ₂ (dba) ₃ , K ₃ PO ₄ , 1.5H ₂ O, 2BDBP, toluene	40°C	1:1.2:1.5	- (46)
Pd(PPh ₃) ₄ , aq K ₂ CO ₃ , toluene	50°C	6:1:0.5	31 (75)
"	50°C	6:1:1.5	40 (>98)
Pd(PPh ₃) ₄ , aq TIOH, THF	25°C	18:1:1	67 (>98)

Figure 2.2 Mechanistic study of the cross coupling between phenylboronic acid and 2,4-dibromopyridine.³⁰ BDBP= (2-biphenyl)di-*tert*-butylphosphine

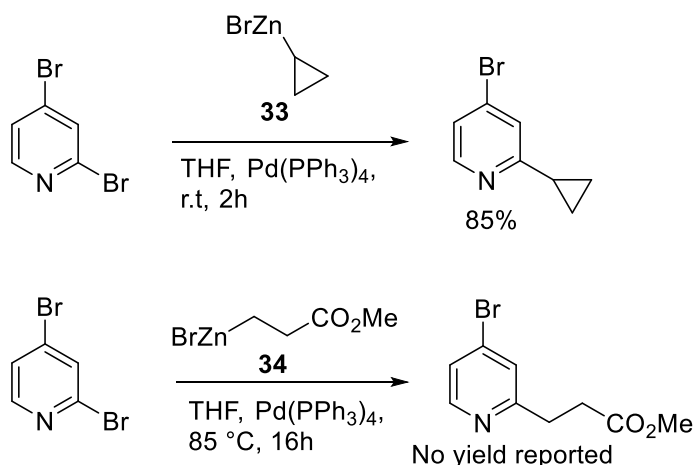
The second study of interest is one by Sicre and Cid which describes the synthesis of visual pigment A2E.³¹ The point of interest is their comparison of the key cross coupling step, which they achieved using both Suzuki-Miyaura and Negishi coupling protocols. Treatment of 2,4-dibromopyridine with the Suzuki or Negishi reagent of **31** yielded a product where substitution in the 2-position was favoured (**32**) (Scheme 2.16).



Scheme 2.16 Selectivity differences between Suzuki-Miyaura and Negishi cross coupling between 2,4-dibromopyridine and an alkenyl coupling partner.

This paper demonstrated selectivity for the 2-position in these types of cross coupling reactions. The selectivity was higher for the Suzuki cross coupling, but the selectivity of both reactions demonstrates a preference for the 2-position.

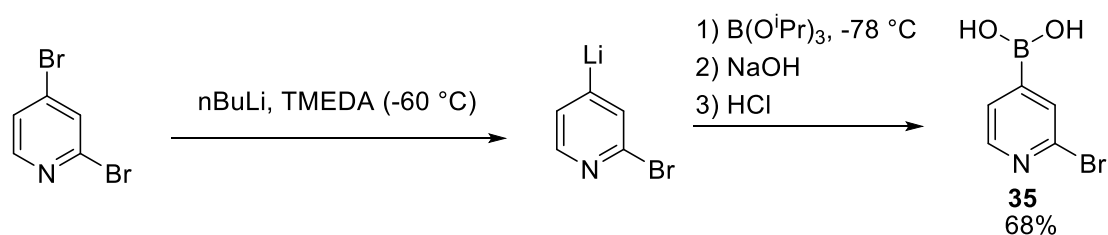
The preference for 2-substitution was also highlighted in two patents describing Negishi cross-couplings performed on 2,4-dibromopyridine (Scheme 2.18).^{32,33}



Scheme 2.18 Further examples of 2-position selectivity in Negishi reactions.

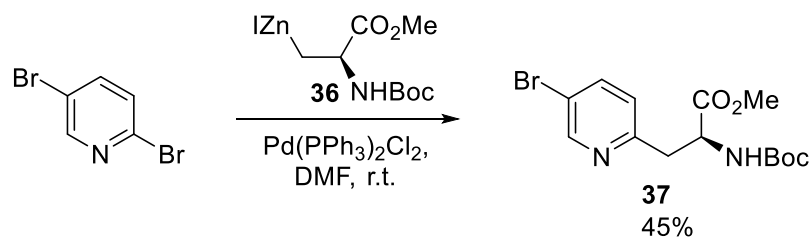
The two reactions display different rates of reactivity, with the cyclopropyl substrate **33** being much more reactive than the ester substrate **34**. These experimental sources indicate a preference for cross coupling in the 2-position of 2,4-dibromopyridine.

This selectivity for the 2-position is not applicable to metal-halogen exchange with 2,4-dibromopyridine. Treatment of 2,4-dibromopyridine with butyllithium and TMEDA led to lithium-halogen exchange in the 4-position, which was then treated with triisopropyl borate to yield boronic acid **35** (Scheme 2.19).³⁴



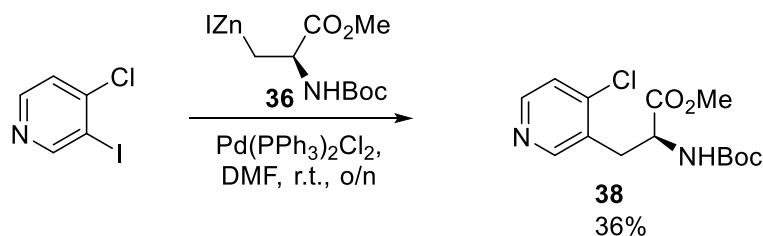
Scheme 2.19 Selective lithiation of 2,4-dibromopyridine followed by trapping as the boronic acid.

The differences in halogen reactivity and the differences in site reactivity have been used to generate selected regioisomers of halopyridylalanines by Jackson and co-workers. The synthesis of 5-bromo-2-pyridylalanine **37** has been reported by the Jackson group (Scheme 2.20), where the selectivity is consistent with that observed in Scheme 2.14.³⁵



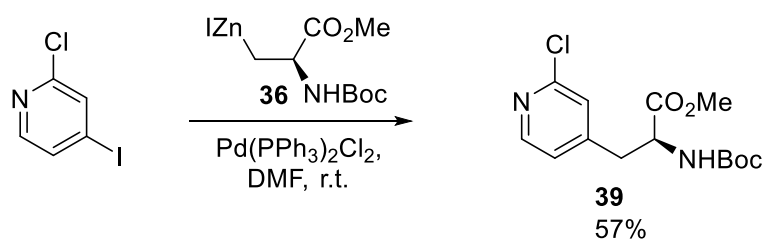
Scheme 2.20 Regioselective cross-coupling between 2,5-dibromopyridine and zinc reagent **2**.

This halogen control was demonstrated with the synthesis of chloropyridylalanine **38**, synthesised through a regioselective cross-coupling between zinc reagent **36** and 3-iodo-4-chloropyridine (Scheme 2.21).¹¹ In this case, ring position effects would favour coupling in the 4-position, but the differences in halogen reactivity generate the 3-substituted chloropyridylalanine **38**.



Scheme 2.21 Regioselective cross coupling between 3-iodo-4-chloropyridine and zinc reagent **36**.¹¹

This was further established by the synthesis of **39**. Zinc reagent **2** was selectively coupled with 2-chloro-4-iodopyridine to generate pyridylalanine **39** (Scheme 2.22).³⁶ The presence of a chloride ion in the more reactive 2-position disfavours coupling in this position, and results in coupling at the 4-position where an iodide is present.

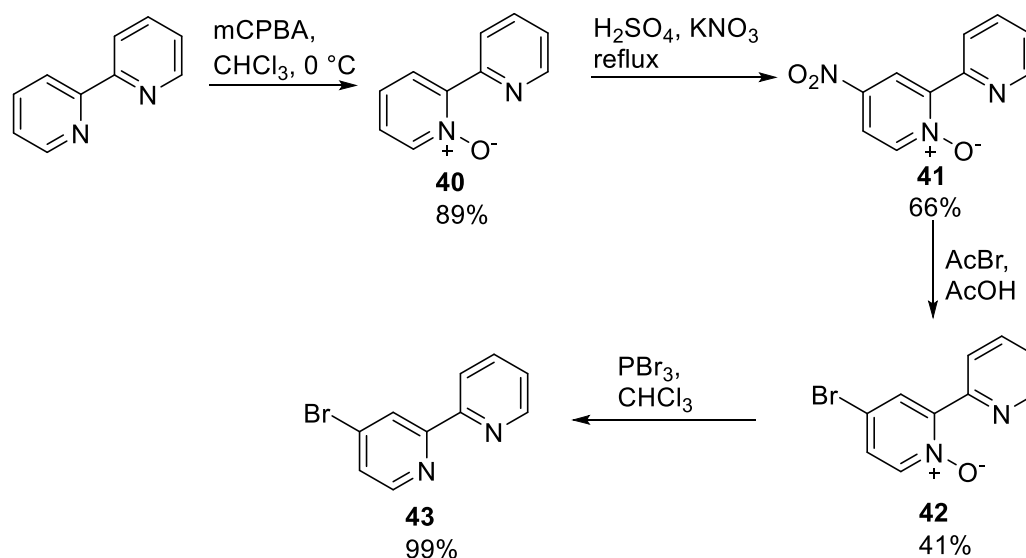


Scheme 2.22 Regioselective cross coupling between 4-iodo-2-chloropyridine and zinc reagent **36**.³⁶

The selective lithiation detailed in Scheme 2.19 could also be adapted for the synthesis of 2-bromo-4-iodopyridine, which has interesting applications in cross-couplings like those described above.

2.5 Synthesis of 4-bromo-2,2'-bipyridine from 2,2'-bipyridine

Treatment of unfunctionalised 2,2'-bipyridine can yield 4-bromo-2,2'-bipyridine without the need for selective cross-coupling reactions. The synthesis of 4-bromo-2,2'-bipyridine from 2,2'-bipyridine has been reported by Hirose and co-workers (Scheme 2.23).³⁷



Scheme 2.23 Hirose's synthesis of 4-bromo-2,2'-bipyridine from 2,2'-bipyridine.³⁷

Oxidation of the bipyridine with mCPBA yielded N-oxide **40**, which undergoes regioselective mononitration to generate **41**. N-oxide **41** is brominated using a combination of acetyl bromide and acetic acid yielding **42**. The N-oxide is then removed by treatment with phosphorous tribromide to yield bromobipyridine **43**.

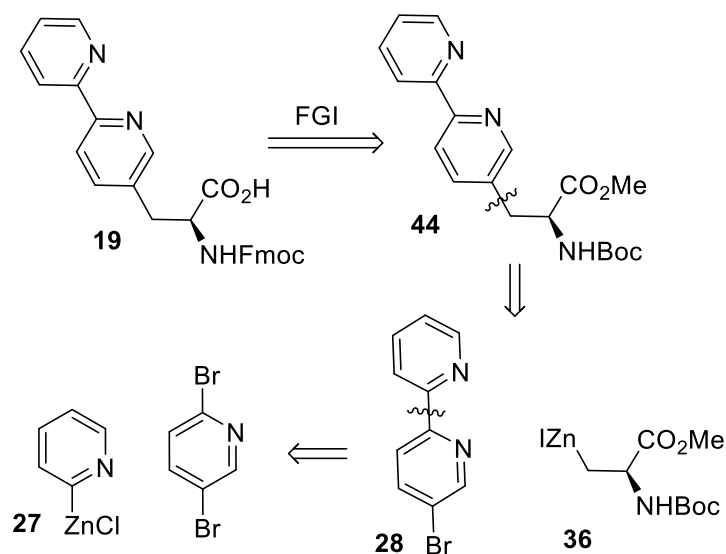
2.6 Aims

This project aims to develop effective syntheses for 4-, 5-, and 6-Bpa through the use of the Negishi cross coupling reaction so that these amino acids can be incorporated into peptide sequences and used to control their oligomerisation state.

2.7 Retrosynthesis

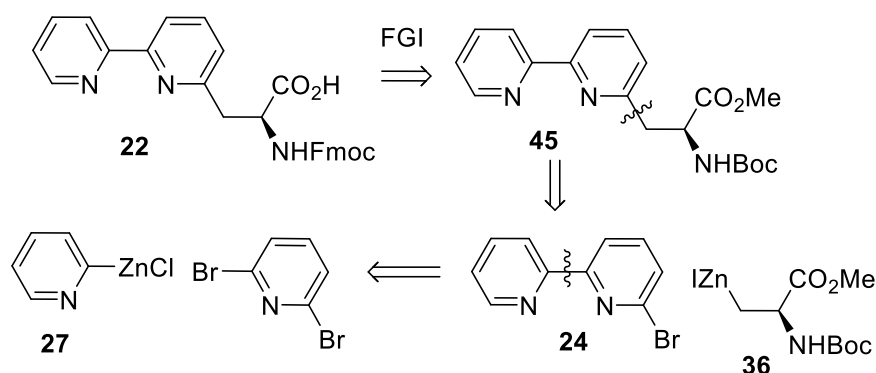
The proposed retrosynthesis of compounds **22** and **19** relies on a disconnection between the bipyridyl ring and the β -carbon of the amino acid backbone. The disconnection of **44** between the bipyridyl ring and the β -carbon of the amino acid backbone yields a synthon derived from zinc reagent **36**, and bromobipyridine **28**. Bromide **28** can be

disconnected to yield zinc reagent **27** and commercially available 2,5-dibromopyridine (Scheme 2.24).



Scheme 2.24 Proposed retrosynthesis of compound **19**.

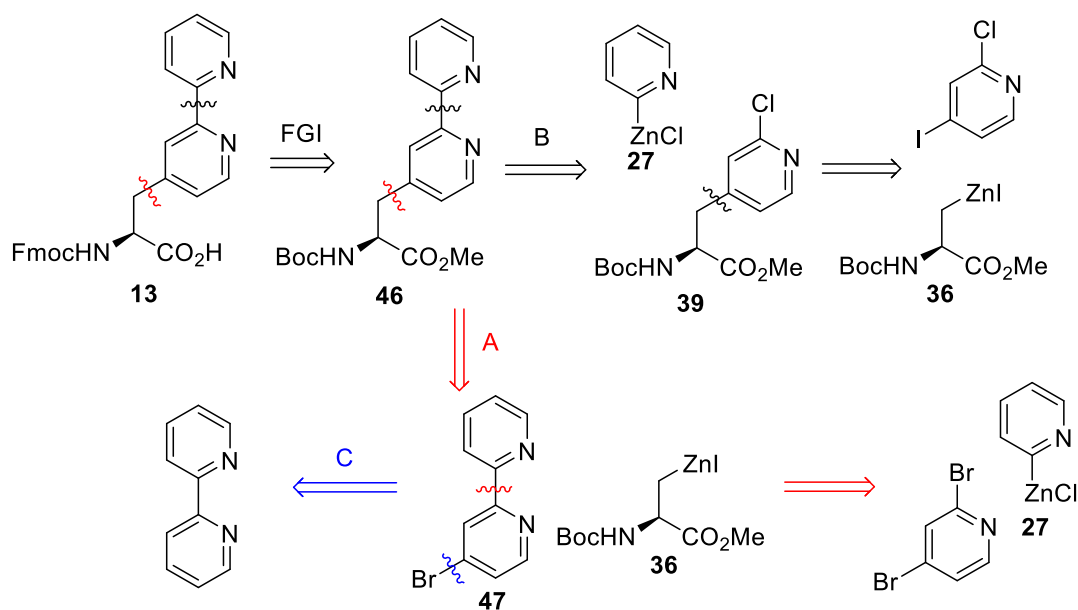
In the case of compound **45**, this disconnection yields a synthon derived from zinc reagent **36**, and bromobipyridine **24**. Bromide **24** can be disconnected at the pyridine-pyridine bond, yielding zinc reagent **27**, and commercially available 2,6-dibromopyridine (Scheme 2.25).



Scheme 2.25 Proposed retrosynthesis of compound **22**.

Some preliminary work in the group had success in this area with preliminary couplings between **36** and bromobipyridines **28** and **24**, and this encouraged this proposed route.³⁸

Compound **13** can be retrosynthesised to yield similar fragments (Scheme 2.26).



Scheme 2.26 Proposed retrosynthetic routes to **13**.

We also wished to investigate the synthesis of compound **3** through the modification of chloropyridine **39**. However, the lack of published syntheses of Negishi cross-couplings yielding 4-bromo-2,2'-bipyridine and the question of its site selectivity led to the consideration of two alternate routes in addition to the synthesis of 4-bromo-2,2'-bipyridine.

Rather than disconnecting **13** at the pyridine-alanine bond, the first disconnection between the two pyridine rings generates **27** and chloropyridine **39** (shown in disconnection route B). The second disconnection generates zinc reagent **36**, and a 4-iodo-2-chloropyridine. The synthesis of 2-chloropyridyl alanine was successfully carried out by the Jackson group previously, so the development of the chloropyridine cross coupling was the focus of this route.

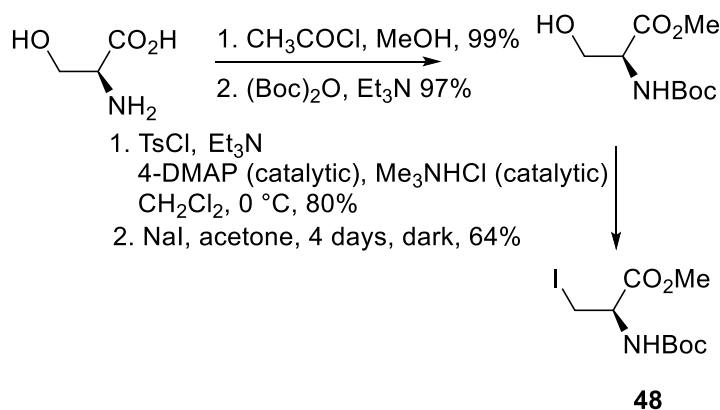
Finally, the synthesis of **47** from unfunctionalised 2,2'-bipyridine was considered (disconnection route C). 4-bromo-2,2'-bipyridine synthesised in this way has been previously reported by Hirose and co-workers, offering the possibility of synthesising the brominated bipyridine for the subsequent cross coupling.³⁷

In this chapter, the synthesis of bipyridine coupling partners **24**, **28**, and **47** and their subsequent use in Negishi cross-coupling reactions to generate amino acids **44**, **45** and **46** is discussed. Also discussed is the use of chloropyridine **39** in a Negishi cross coupling reaction to generate amino acid **46** by an alternate route.

2.8 Results and Discussion

2.8.1 Synthesis of amino acid derived iodide

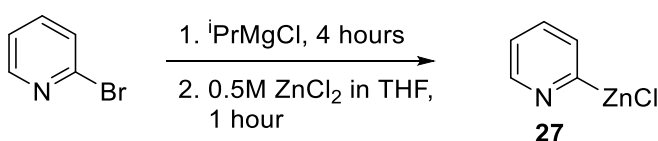
The synthesis of the serine derived iodide **48** is documented in the literature, and was carried out following these procedures.^{8,39} The iodide **48** was synthesised in 50% overall yield, consistent with the literature overall yield of 55% (Scheme 2.27).



Scheme 2.27 Esterification and Boc protection of L-serine, followed by conversion of the serine hydroxyl group to a tosyl group and the resulting pseudo-Finkelstein reaction to yield iodide **48**.⁸

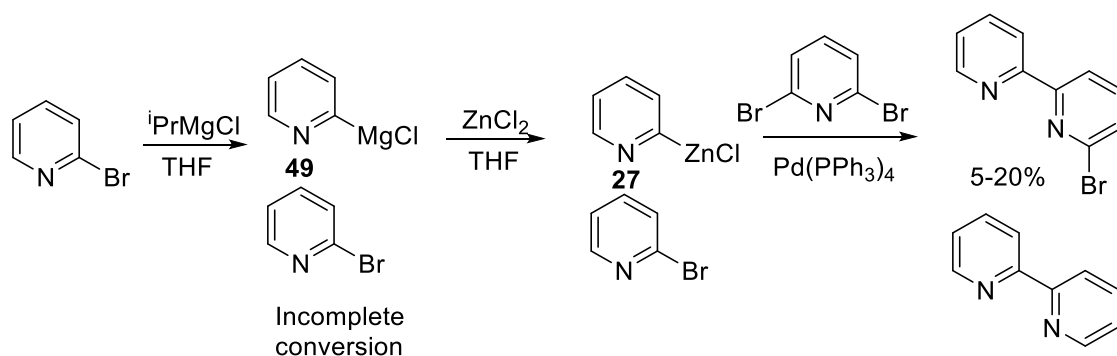
2.8.2 Generation of 2-pyridylzinc chloride and the synthesis of **24** and **28**.

The synthesis of 6-bromo-2,2'-bipyridine (**24**) was carried out through a combination of procedures. The generation of the 2-pyridylzinc halide reagent (**27**) was taken from Luzung and coworkers procedure.²³ The metal-halogen exchange between isopropylmagnesium chloride and 2-bromopyridine was followed by the transmetalation of the 2-pyridylmagnesium chloride **49** into a 2-pyridylzinc reagent with a solution of zinc chloride (Scheme 2.28).



Scheme 2.28 Conversion of 2-bromopyridine to 2-pyridylzinc chloride.

There were several problems with the synthesis of bromobipyridines **24** and **28**. Even diligently following the conditions exactly the cross-coupling reaction between 2-pyridylzinc chloride and 2,6/2,5-dibromopyridine did not go to completion, and sometimes led to 2,2'-bipyridine being observed in the crude NMR spectrum, suggesting the conversion of the 2-bromopyridine to the zinc reagent was incomplete. (Scheme 2.29)



Scheme 2.29 Incomplete conversion of 2-bromopyridine can lead to the synthesis of 2,2'-bipyridine.

To accurately monitor the formation of 2-pyridylmagnesium chloride, we found gas chromatography conditions to differentiate between bromopyridine and iodopyridine, and undertook a series of trapping experiments of the magnesiated pyridine with iodine to monitor the conversion of 2-bromopyridine to 2-iodopyridine, as a surrogate for zinc reagent formation (Table 2.1). The Grignard reagent was generated according to the exchange procedure described by Luzung and coworkers with isopropylmagnesium chloride, and then quenched with a solution of iodine to convert the magnesiated pyridine to the iodinated pyridine. Also investigated was the “turbo” Grignard developed by Knochel and co-workers.^{23,40}

Table 2.1 Relative proportions of 2-bromopyridine and 2-iodopyridine measured by gas chromatography.

Conditions	% 2-Bromopyridine	% 2-Iodopyridine
Fang & Hanan	16	84
1 eq “turbo” Grignard	13	87
2 eq “turbo” Grignard	13	87

After experimenting with the amount of Grignard reagent used we found that 2 equivalents of $i\text{PrMgCl} \cdot \text{LiCl}$ gave similar conversion of 2-bromopyridine to 2-pyridylmagnesium chloride after 4 hours when compared with 1 equivalent. We proceeded with the one equivalent conditions in the coupling reaction to generate the 2-pyridylzinc reagent. Initially, when using one equivalent of $i\text{PrMgCl} \cdot \text{LiCl}$ the bromobipyridines were successfully synthesised in yields of 10-40%. Unfunctionalised bipyridine was not detected.

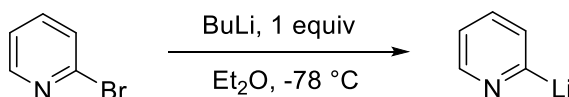
The direct insertion of zinc into 2-iodopyridine was investigated. The 2006 publication by Knochel and co-workers describes zinc activation using TMSCl /dibromoethene, but following the exchange by TLC indicated 2-iodopyridine was still present in the reaction mixture.²² Even after overnight stirring, the zinc failed to insert (Scheme 2.30). We also tried using iodine to activate the zinc dust for the insertion but this method also

failed to stimulate the reaction. Due to the expense of 2-iodopyridine compared to 2-bromopyridine we decided to continue work on generating the zinc reagent from 2-bromopyridine, due to our previous limited success with the compound.



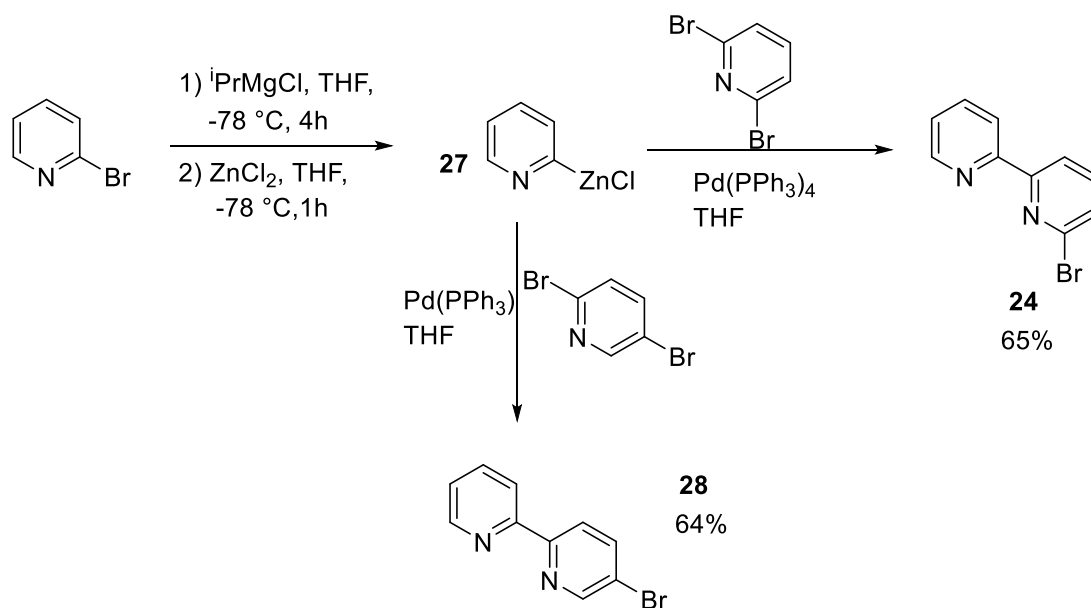
Scheme 2.30 Failed direct insertion of zinc into the Ar-I bond of 2-iodopyridine.

In addition to this work, we investigated the use of butyllithium for the metal halogen exchange reaction, due to its extensive history in both metal-halogen exchanges in general, and the more specific exchange with 2-bromopyridine documented in the literature.⁴¹ Initial metal-halogen exchanges in THF following the procedure of Wright and co-workers were unsuccessful, but using diethyl ether in place of THF yielded the successful exchange of the halogen as indicated by TLC (Scheme 2.31).⁴¹ However, the use of diethyl ether was incompatible with the zinc chloride transmetallation.



Scheme 2.31 Lithium-halogen exchange of bromine on 2-bromopyridine

After experimentation with the methods used, the synthesis of bromobipyridines **24** and **25** was performed again using a fresh bottle of isopropylmagnesium chloride, and newly purchased catalyst (Scheme 2.32). A dry ice/acetone bath was also used for the addition of both isopropylmagnesium chloride and zinc chloride addition. Coupling with 2,6-dibromopyridine proceeded in 65% yield to give **24**. The corresponding reaction with 2,5-dibromopyridine provided us with **28** in 64% yield.



Scheme 2.32 Synthesis of 6- and 5-bromo-2,2'-bipyridine.

We initially attributed the failed reactions solely to a contaminated bottle of isopropylmagnesium chloride or catalyst, until we located a paper by Busacca *et al.* describing problems in the use of isopropylmagnesium chloride, and their own methods of solving them.⁴² These methods, largely the strict use of only extremely fresh $i\text{PrMgCl}$ and the use of a dry ice/acetone bath to control the temperature of the reaction were the same as those we developed independently. The use of cryogenic temperatures, contrary to the procedures reported in the literature reports of the use of $i\text{PrMgCl}$ at room temperature for metal-halogen exchange with 2-bromopyridine suggests that lower temperatures negate any errors during addition of organometallic reagents. Ultimately, the most important result from this extended section of reaction optimisation was the importance of the use of fresh organometallic reagents.

With the new information in hand, we set out to use these conditions on all the reactions attempted previously. All magnesium-halogen exchange reactions now proceeded smoothly. In addition to this, with much better yields we were able to make use of a feature of the coupling reaction originally described by Luzung and co-workers. They noted that the complex formed by coordination of the bipyridine to zinc precipitated out of solution (Figure 2.3). Pouring the reaction mixture into a solution of disodium EDTA allowed the extraction of the desired bipyridines from the aqueous layer and purifying through the use of column chromatography.

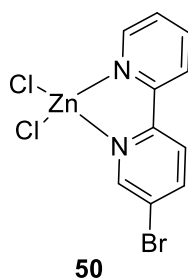


Figure 2.3 Proposed structure of Zn^{2+} -bipyridine complex

We investigated whether this chromatography step could be removed from the purification procedure. We found it was possible to isolate the zinc bipyridine complex by filtration from the reaction mixture, and wash it with further cold THF to remove the catalyst and unreacted starting material. The desired bipyridines can then be isolated by removing the coordinated zinc ions through the use of EDTA. The purity of the bipyridines by NMR spectroscopy (Figure 2.4) recovered using this method is comparable to the purity after column chromatography, and it is a much quicker and easier procedure. Although the impurity present in the filtered bipyridine was unknown, we used this material without further purification in the synthesis of the amino acid as described below.

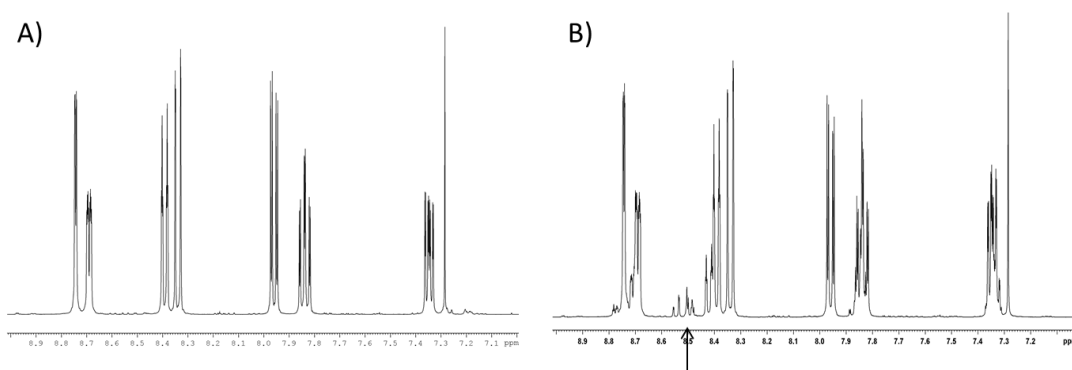
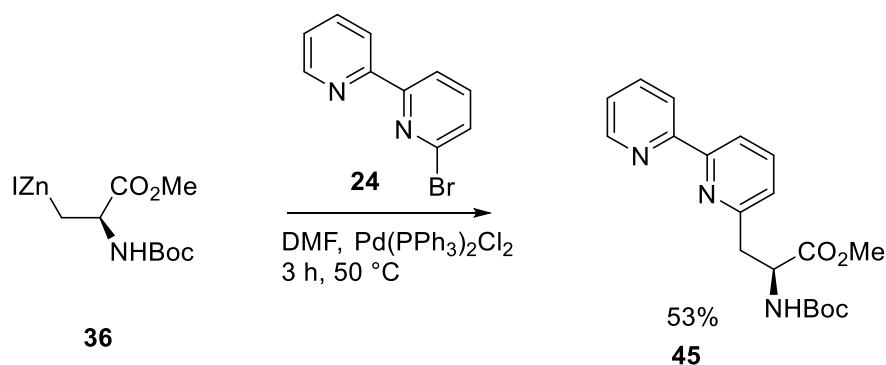


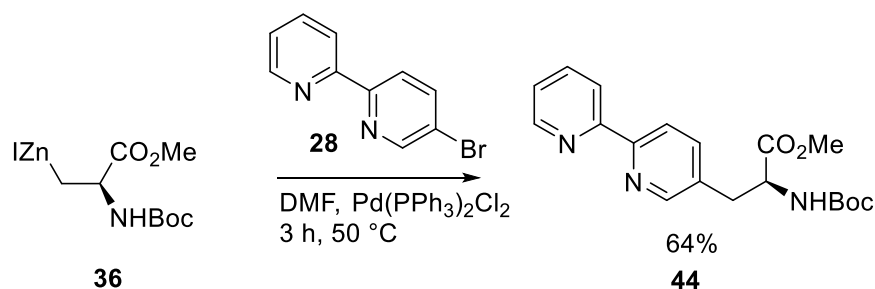
Figure 2.4 NMR spectra of 5-bromo-2, 2'-bipyridine. A) NMR spectrum of 5-bromo-2,2'-bipyridine acquired after column. B) NMR spectrum of 5-bromo-2,2'-bipyridine acquired after separation of complex from reaction mixture. Unknown impurity highlighted by arrow.

2.8.3 Synthesis of amino acids

After isolating samples of both 6-bromo-2,2'-bipyridine and 5-bromo-2,2'-bipyridine we then proceeded with the synthesis of the amino acids (Scheme 2.35 & Scheme 2.36). Treatment of **24** or **28** with zinc reagent **36** in DMF yielded the desired amino acids in good yields.



Scheme 2.35 Negishi cross coupling between zinc reagent 2 and bromobipyridine 19 to generate Boc-6Bpa-OMe



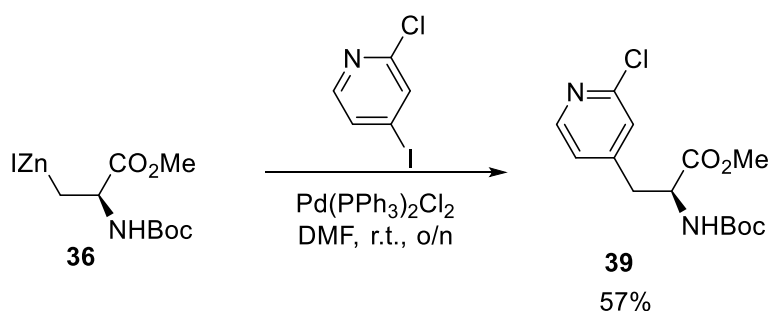
Scheme 2.36 Negishi cross coupling between zinc reagent 2 and bromobipyridine 26 to generate Boc-5Bpa-OMe

Increased reaction time results in a decreased yield of the product. After heating a synthesis of protected 5Bpa overnight, rather than for three hours, the yield of the reaction decreased from 64% to 49%, a significant decrease. No decomposition products were observed in the crude NMR spectrum, but it appeared that the longer period of heating has caused the product to degrade over this longer time.

The same methods described in Scheme 40 were used with uncolummed 5-bromo-bipyridine. The use of pure **42** proceeded in 64% yield, while the use of **42** without prior purification gave a 62% yield. This allows the scale of this reaction to be increased without the need for extensive column chromatography to yield the purified product.

2.8.4 Preparation of 2-chloropyridine **39**

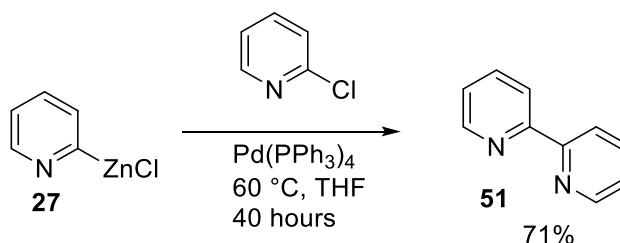
Retrosynthetic route B relies on the cross-coupling of 2-pyridylzinc chloride with chloropyridine **39**. We were able to synthesise **39** with relative ease according to the procedure developed previously.³⁶ Zinc reagent **2** was coupled to 2-chloro-4-iodopyridine in 57% yield (Scheme 2.37).



Scheme 2.37 Synthesis of 2-chloro-4-alanine-pyridine

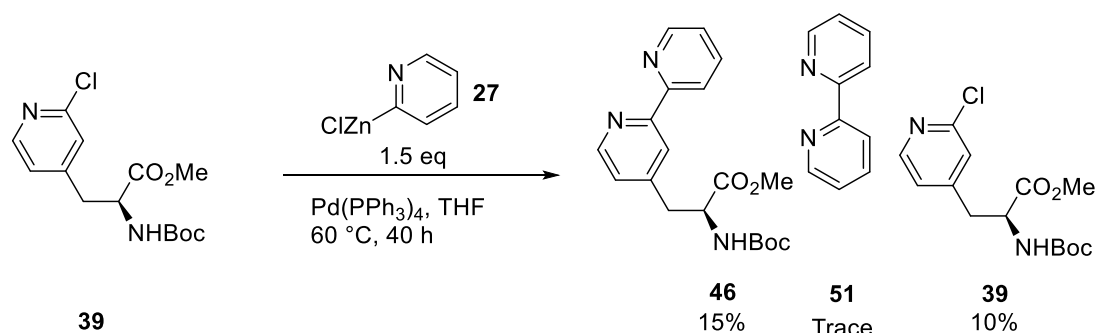
Purification of the material indicated no coupling product resulting from coupling in the 2-position. Even when the reaction was scaled up to the 10 mmol scale it proceeded in similar yields. Chloropyridine **39** was used in a series of cross-coupling reactions with 2-pyridylzinc chloride **27** to synthesise amino acid **46**. There are several methods in the literature for the coupling of 2-pyridylzinc halides with a range of aryl chlorides.^{23,26}

The first step in developing this reaction was coupling **27** to 2-chloropyridine (Scheme 2.38). This was a success, and **51** was synthesised in 71% yield.



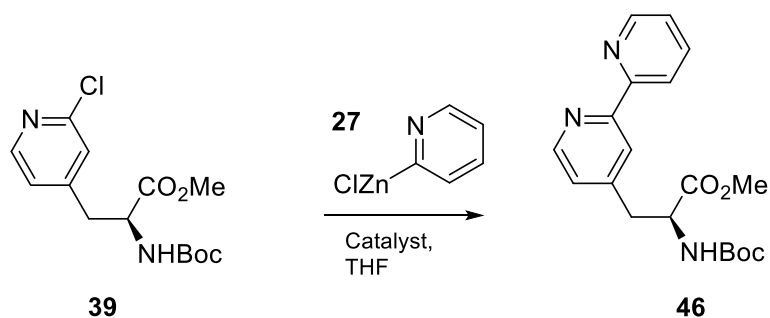
Scheme 2.38 Synthesis of 2,2'-bipyridine from 2-chloropyridine

We adapted conditions from Fang and Hanan for the synthesis of **46**, as we had previously had success in synthesising bromobipyridines **24** and **28** using their method.²⁶ The catalyst used was tetrakis(triphenylphosphine) palladium, and after heating the reaction at 60 °C for 40 hours **46** was recovered in 15% yield after purification (Scheme 2.39). This low yield proved the reaction viable, but highlighted the need to optimise the reaction conditions.



Scheme 2.39 The synthesis of 4Bpa generated a mix of products

After this preliminary experiment, different catalysts were screened (Scheme 2.40, Table 2.2). In addition to the couplings of 2-pyridylzinc chloride with aryl chlorides described by Luzung and Hanan with triphenylphosphine palladium catalysts, the Buchwald (RuPhos) and the Fu groups (P(tBu)_3) have reported alternative catalyst systems for the couplings involving aryl chlorides.^{43,44} The Knochel group published on the use of SPhos for cross-couplings containing acidic protons.⁴⁵



Scheme 2.40 The general reaction scheme for synthesis of 4Bpa

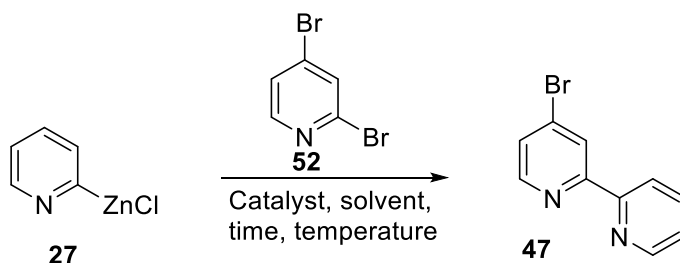
Table 2.2 Summary of the experimental conditions investigated, and the resulting yields of 62.

Catalyst	Temperature (°C)	Time	Yield of 46 (%)
$\text{Pd(PPh}_3)_4$	r.t.	40 h	0
$\text{Pd(PPh}_3)_4$	Reflux	40 h	15
$\text{Pd(PPh}_3)_2\text{Cl}_2$	r.t.	40 h	0
$\text{Pd(OAc)}_2/\text{SPhos}$	r.t.	24 h	10
$\text{Pd(OAc)}_2/\text{SPhos}$	Reflux	24 h	10
$\text{Pd(OAc)}_2/\text{RuPhos}$	Reflux	24 h	0
$\text{Pd(OAc)}_2/\text{XPhos}$	Reflux	24 h	0
$\text{Pd(OAc)}_2/\text{XantPhos}$	Reflux	24 h	0
$\text{PdCl}_2\text{dppf} \cdot \text{CH}_2\text{Cl}_2$	r.t.	24 h	10

The 2-chloro couplings were low yielding, with the reactants showing decomposition under these conditions. The reactants which did not decompose showed side product formation in the form of 2,2'-bipyridine. With this approach yielding very little of the desired product, efforts were focused on the application of retrosynthetic route A (Scheme 2.26, p 38) for compound **13**.

2.8.5 Synthesis of 4-bromo-2,2'-bipyridine (**47**)

After pursuing the synthesis of **46** through route B and this proving low yielding, the synthesis of 4-bromobipyridine was investigated. Our initial approach to the synthesis of 4-bromo-2,2'-bipyridine (**47**) involved the cross-coupling of **27** to 2,4-dibromopyridine (Figure 2.5). A control formation of **24** from the same batch of zinc reagent **27** proceeded smoothly using the same reaction conditions, but the synthesis of **47** was unsuccessful. There were very small traces of the desired product within the reaction mixture, as determined by NMR spectroscopy, but purification of these reaction mixtures failed to yield any significant amount of product. We were able to obtain a clean NMR spectrum for the product, so we had a point of reference for future reactions. The variation of reaction conditions failed to result in a higher yield (Figure 2.5), and alternate routes to the synthesis of **46** were considered.



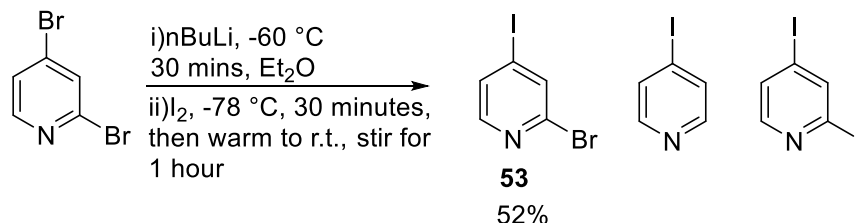
Time	Temperature (°C)	Equivalents (27)	Catalyst	Yield
18 min	r.t	1.5	Pd(PPh ₃) ₄	0
40 h	r.t.	1.5	Pd(PPh ₃) ₄	Trace (NMR)
20 min	r.t.	1.5	Pd(PPh ₃) ₄	0
40 h	r.t.	1	Pd(PPh ₃) ₄	0
24 h	r.t.	1.5	Pd(PPh ₃) ₄	0
24 h	r.t.	1.5	Pd(PPh ₃) ₄	Trace(NMR)

Figure 2.5 Negishi cross-coupling between 2-pyridylzinc chloride and 2,4-dibromopyridine. Table describes the results of each condition.

2.8.6 Synthesis and Negishi cross-coupling of 2-bromo-4-iodopyridine

The utility of 2-Cl derivative **39** was limited by the formation of side products and a low yield of 4Bpa. Our attention was focused on the substitution of the 2-chloro substituent

for a 2-bromo substituent. Bromo/iodo selectivity follows the same reasoning as chloro/iodo selectivity, but with a lesser degree of selectivity. Adapting a synthesis procedure for the synthesis of the boronic ester demonstrated by Rault and co-workers yielded the desired dihalopyridine **53** (Scheme 2.42).³⁴



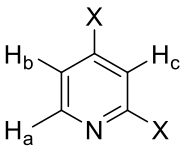
Scheme 2.42 Synthesis of 2-bromo-4-iodopyridine through selective lithiation.

Treatment of 2,4-dibromopyridine with *n*-butyllithium followed by a solution of iodine yielded **53** in good yields. Our procedure proceeded without the use of TMEDA, which explains the lower yield of the desired monolithiated product. The side products noted in the reaction scheme were indicated in the LC-MS trace of the crude reaction mixture, but were not recovered from the reaction mixture for characterisation. The product can be simply purified by recrystallization from hexane, generating a product with high purity.

To correctly analyse the outcome of cross-coupling reactions between zinc reagent **36** with dihalopyridines we required characterisation which would allow us to distinguish between the possible products of the reaction. We began by characterising our available 2,4-disubstituted halopyridines: 2,4-dibromopyridine and 2-Cl-4-I-pyridine were purchased commercially, so acted as reference and 2-chloro-4-bromopyridine was taken from the literature.⁴⁶ The synthesis of **53** has been reported in the literature through the use of the halogen-dance reaction, and the spectra were consistent with those reported.⁴⁷

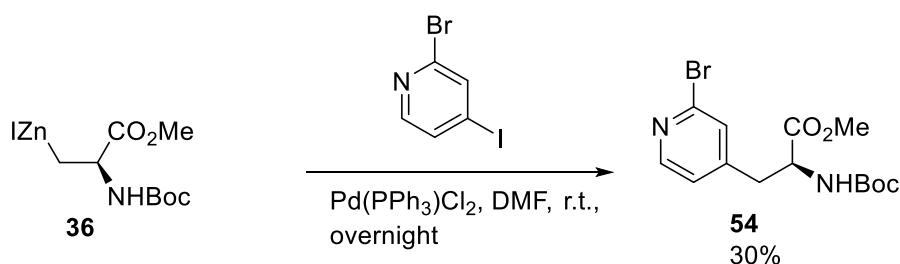
The change in the spectra on iodination was quite noticeable (Table 2.3). If we consider the spectra of 2,4-dibromopyridine and 2-bromo-4-iodopyridine, the two are clearly distinguishable.

Table 2.3 Tabulated ^1H NMR data for 2,4-dibromopyridine, 2-chloro-4-bromopyridine, 2-chloro-4-iodopyridine, and 2-bromo-4-iodopyridine.

	2,4-dibromopyridine	2-chloro-4-bromopyridine	2-chloro-4-iodopyridine	2-bromo-4-iodopyridine
H_a	8.23	8.23	8.05	8.06
H_b	7.45	7.4	7.58	7.6
H_c	7.72	7.54	7.74	7.9

The proton chemical shifts can be followed depending on the halogen in both the 2- and 4-positions of the pyridine ring. H_a is typically the most deshielded proton, so this proton can be easily assigned. A shift of -0.18 ppm is consistent with exchanging a bromide in the 4-position for an iodide. A shift of $+0.15$ ppm for H_b is consistent with exchanging a bromide in the 2-position of the pyridine ring with an iodide. A shift of $+0.2$ ppm for H_c is consistent with a bromide in the 2-position. This NMR data, combined with mass spectrometry consistent with 1 bromide and 1 iodide in the molecule, provided evidence for the product of this reaction being the proposed 2-bromo-4-iodopyridine.

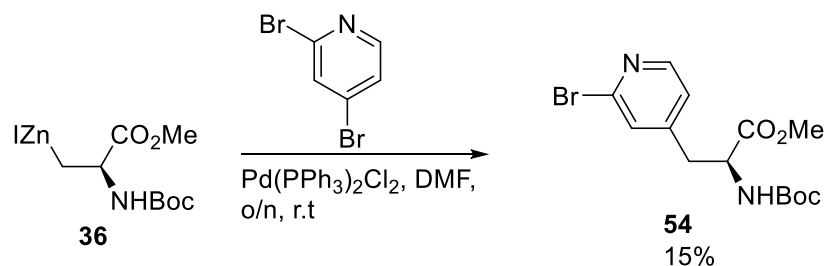
With the 2-bromo-4-iodopyridine in hand, attention was turned to the subsequent cross coupling reaction. 2-Bromo-4-iodopyridine was treated with zinc reagent **36** in the presence of bistrisphenylphosphinepalladium dichloride at room temperature overnight, which yielded **54** in 30% yield (Scheme 2.43).



Scheme 2.43 Selective cross coupling between zinc reagent **36** and 2-bromo-4-iodopyridine to generate 2-bromo-4-alanylpuridine.

A combination of ^1H and ^{13}C NMR spectroscopy indicated the formation of a monosubstituted alanylpuridine, and mass spectrometry indicated the product contained a bromide. None of the disubstituted pyridine was observed in the isolated products, but there were peaks in the crude MS which could be assigned to this product.

With these encouraging results, we investigated the cross coupling of 2,4-dibromopyridine with **36** (Scheme 2.44). The reaction was derived from the same conditions used in Scheme 37.



Scheme 2.44 The product of the reaction of 2,4-dibromopyridine with the zinc reagent

Treatment of 2,4-dibromopyridine with zinc reagent **36** resulted in the isolation of alanylpipridine **54**. Instead of the expected 2-substituted product, we observed that the majority of the coupling took place in the 4-position. From the analysis of the crude reaction mixture, we could see a range of products, but all those except **54** were only in trace amounts. On repeating the reaction, the result was consistent. In this example, none of the bis-amino acid was isolated, but there were peaks in the crude MS which confirmed its presence.

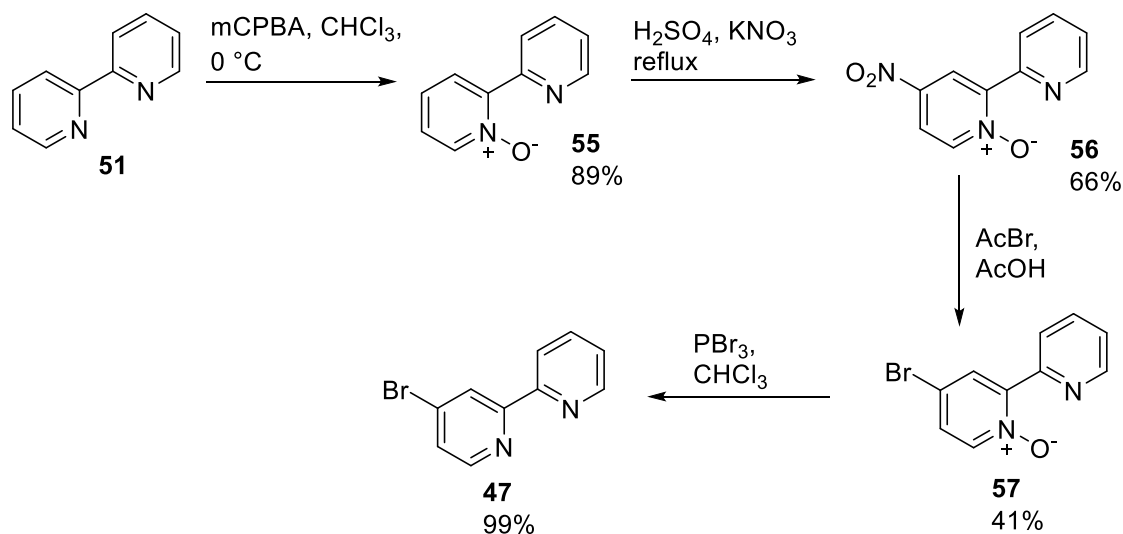
In this one very specific case, the preferred coupling position of the amino acid is suggested to be the 4-position of the 2,4-dibromopyridine. It was as efficient overall as the alternative synthesis, as it does not require the addition step of substituting the 4-bromo position with an iodide. NMR comparison of both the coupling product from 2,4-dibromopyridine and the coupling product from 2-bromo-4-iodopyridine are identical.

Time constraints in this project prevented the investigation of this compound for the synthesis of **46**, but it is interesting future work. Bromide analogues of chloropyridines typically require milder conditions, so synthesis of 4-Bpa using compound **54** may avoid the decomposition of the haloaminoacid observed in Scheme 2.39.

2.8.7 Synthesis of 4-bromo-2,2'-bipyridine from 2,2'-bipyridine

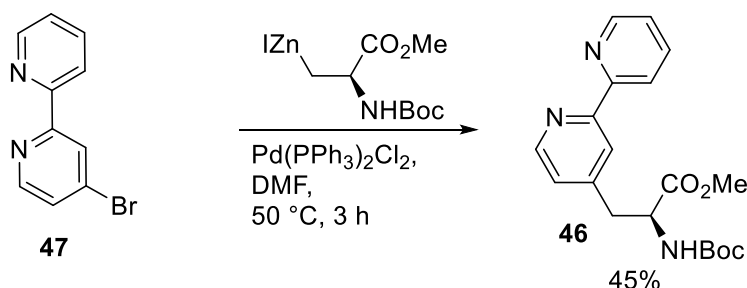
The synthesis of bromide **47** using a selective mono-coupling proved unsuccessful. Bromide **47** was successfully synthesised using methods adapted from the published procedures as part of parallel work by Maria Plunkett.⁴⁸ The oxidation of **51** with mCPBA yielded the bipyridyl N-oxide **55** in good yield. Mononitration of **55** followed by bromination yielded the bromobipyridyl N-oxide **57**, and reduction of this gave 4-

bromo-2,2'-bipyridine in excellent yield. The recorded yields were in excellent agreement with those published in the literature (Scheme 2.45).³⁷



Scheme 2.45 Synthesis of 4-bromo-2,2'-bipyridine by Maria Plunkett.

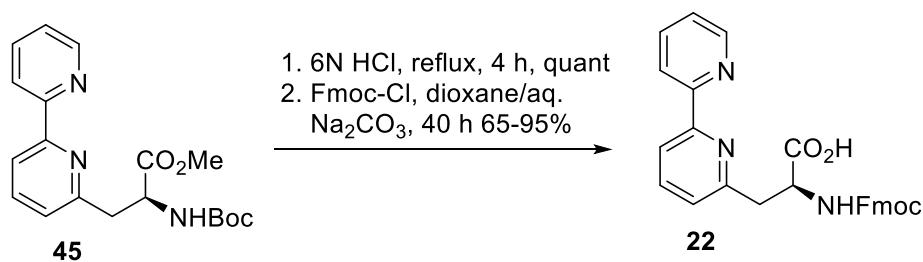
The project student reached this point, but did not have enough time to perform the final step. Negishi cross coupling of 4-bromo-2,2'-bipyridine with zinc reagent **36** in the presence of dichlorobistriphenylphosphine palladium gave protected 4-Bpa in reasonable yields (Scheme 2.46).



Scheme 2.46 Synthesis of protected 4-Bpa through a Negishi cross coupling

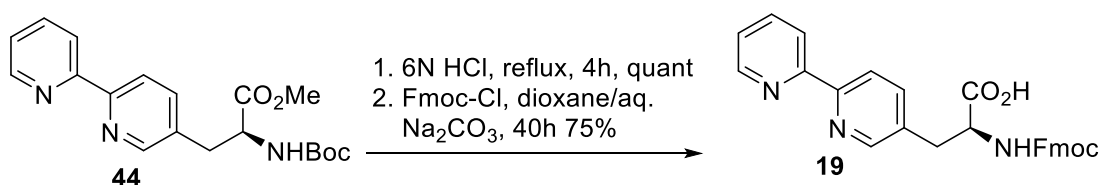
2.8.8 Protecting group exchange to generate peptide synthesis reagents

The protected amino acids were heated in refluxing 6N hydrochloric acid for 4 hours and the hydrochloride salt of the amino acid was recovered quantitatively, and in high purity. This hydrochloride salt was treated with Fmoc-Cl in a 20% solution of sodium carbonate, which yielded Fmoc-6Bpa (**22**) and Fmoc-5Bpa (**19**) in variable yields. An interesting property noted in the synthesis of Fmoc-6Bpa-OH (Scheme 2.47) was that the final product forms a gel on the addition of water, but when lyophilised reverts to a fine powder.



Scheme 2.47 Conversion of Boc-6Bpa-OMe to Fmoc-6Bpa-OH

The conversion of Boc-5Bpa-OMe to Fmoc-5Bpa-OH (Scheme 2.48) proceeded smoothly using the same methods, but without the formation of the hydrogel product. The results of the Fmoc protection are more consistent than the synthesis of the 6 isomer.



Scheme 2.48 Conversion of Boc-5Bpa-OMe to Fmoc-5Bpa-OH

2.8.9 Summary of amino acid synthesis

Each of the three amino acids has been synthesised using similar methodology. Each synthesis proceeds well, and furnishes the amino acids in 3 steps from commercially available starting materials (Figure 2.6).

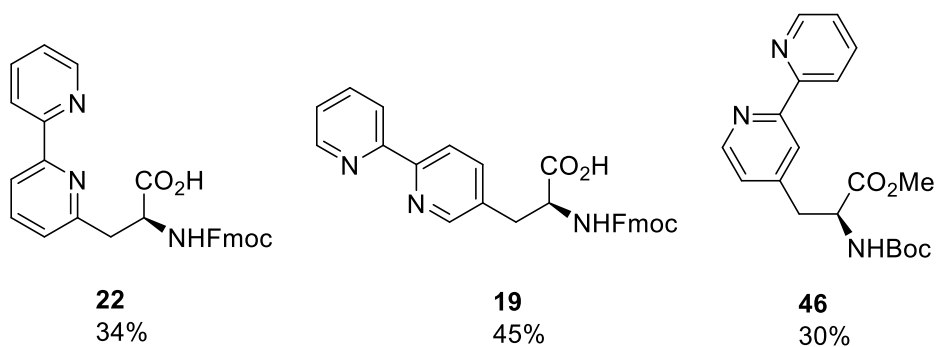


Figure 2.6 Final overall yields for the synthesis of the 3 amino acids.

2.9 Conclusions

This chapter contains details of the synthesis and properties of all three of the target molecules described in the aims section of this thesis. The 5 and 6 isomers have been synthesised in good yields and were converted to the Fmoc-protected derivatives required for peptide synthesis.

The improved purification method developed by trapping the bromobipyridines as a zinc complex allows for simpler large scale purification of the bipyridines, so they can be prepared more quickly. Trapping the bipyridines as a metal complex also allows for their recovery from reaction mixtures.

2.10 References

- (1) Duthaler, R. O. *Tetrahedron* **1994**, *50*, 1539.
- (2) Palomo, C.; Aizpurua, J. M.; Ganboa, I.; Oiarbide, M. *Synlett* **2001**, 1813.
- (3) Maruoka, K.; Ooi, T. *Chem. Rev.* **2003**, *103*, 3013.
- (4) Ager, D. J.; Fotheringham, I. G. *Curr. Opin. Drug Discovery Dev.* **2001**, *4*, 800.
- (5) Itaya, T.; Iida, T.; Shimizu, S.; Mizutani, A.; Morisue, M.; Sugimoto, Y.; Tachinaka, M. *Chemical & Pharmaceutical Bulletin* **1993**, *41*, 252.
- (6) Barfoot, C. W.; Harvey, J. E.; Kenworthy, M. N.; Kilburn, J. P.; Ahmed, M.; Taylor, R. J. K. *Tetrahedron* **2005**, *61*, 3403.
- (7) Jackson, R. F. W.; Wishart, N.; Wood, A.; James, K.; Wythes, M. J. *The Journal of Organic Chemistry* **1992**, *57*, 3397.
- (8) Jackson, R. F. W.; Perez-Gonzalez, M. *Org. Synth.* **2005**, *81*, 77.
- (9) Dunn, M. J.; Jackson, R. F. W. *Journal of the Chemical Society-Chemical Communications* **1992**, 319.
- (10) Rilatt, I.; Caggiano, L.; Jackson, R. F. W. *Synlett* **2005**, 2701.
- (11) Tabanella, S.; Valancogne, I.; Jackson, R. F. W. *Organic & Biomolecular Chemistry* **2003**, *1*, 4254.
- (12) Imperiali, B.; Fisher, S. L. *J. Org. Chem.* **1992**, *57*, 757.
- (13) Imperiali, B.; Prins, T. J.; Fisher, S. L. *J. Org. Chem.* **1993**, *58*, 1613.
- (14) O'Donnell, M. J.; Bennett, W. D.; Wu, S. *J. Am. Chem. Soc.* **1989**, *111*, 2353.
- (15) Zeng, M.; Zhang, X.; Shao, L.; Qi, C.; Zhang, X.-M. *J. Organomet. Chem.* **2012**, *704*, 29.
- (16) Shao, L.; Du, Y.; Zeng, M.; Li, X.; Shen, W.; Zuo, S.; Lu, Y.; Zhang, X.-M.; Qi, C. *Appl. Organomet. Chem.* **2010**, *24*, 421.
- (17) Qi, C.; Sun, X.; Lu, C.; Yang, J.; Du, Y.; Wu, H.; Zhang, X.-M. *J. Organomet. Chem.* **2009**, *694*, 2912.
- (18) Hanan, G. S.; Schubert, U. S.; Volkmer, D.; Riviere, E.; Lehn, J.-M.; Kyritsakas, N.; Fischer, J. *Can. J. Chem.* **1997**, *75*, 169.
- (19) Bouillon, A.; Lancelot, J.-C.; Collot, V.; Bovy, P. R.; Rault, S. *Tetrahedron* **2002**, *58*, 4369.
- (20) Kim, S.-H.; Rieke, R. D. *Tetrahedron* **2010**, *66*, 3135.
- (21) Prasad, A. S. B.; Stevenson, T. M.; Citineni, J. R.; Nyzam, V.; Knochel, P. *Tetrahedron* **1997**, *53*, 7237.
- (22) Krasovskiy, A.; Malakhov, V.; Gavryushin, A.; Knochel, P. *Angew. Chem., Int. Ed.* **2006**, *45*, 6040.
- (23) Luzung, M. R.; Patel, J. S.; Yin, J. *J. Org. Chem.* **2010**, *75*, 8330.
- (24) Krasovskiy, A.; Knochel, P. *Angew. Chem., Int. Ed.* **2004**, *43*, 3333.
- (25) Huo, J.; Hoberg, J. O. *Int. J. Org. Chem.* **2011**, *1*, 33.
- (26) Fang, Y. Q.; Hanan, G. S. *Synlett* **2003**, 852.
- (27) Handy, S. T.; Zhang, Y. *Chem. Commun. (Cambridge, U. K.)* **2006**, 299.
- (28) Garcia, Y.; Schoenebeck, F.; Legault, C. Y.; Merlic, C. A.; Houk, K. N. *J. Am. Chem. Soc.* **2009**, *131*, 6632.
- (29) Grushin, V. V.; Alper, H. *Chem. Rev. (Washington, D. C.)* **1994**, *94*, 1047.
- (30) Sicre, C.; Alonso-Gomez, J. L.; Cid, M. M. *Tetrahedron* **2006**, *62*, 11063.

- (31) Sicre, C.; Cid, M. M. *Org. Lett.* **2005**, *7*, 5737.
- (32) Holenz, J.; Karlstroem, S.; Kihlstroem, J.; Kolmodin, K.; Lindstroem, J.; Rakos, L.; Rotticci, D.; Swahn, B.-M.; Von Berg, S.; AstraZeneca AB, Swed. . 2011, p 72 pp.
- (33) Altman, M. D.; Bienstock, C. E.; Butcher, J. W.; Childers, K. K.; Di Francesco, M. E.; Donofrio, A.; Ellis, J. M.; Fischer, C.; Haidle, A. M.; Jewell, J. P.; Knowles, S. L.; Northrup, A. B.; Otte, R. D.; Peterson, S. L.; Smith, G. F.; Merck Sharp & Dohme Corp., USA . 2013, p 168pp.
- (34) Bouillon, A.; Lancelot, J.-C.; Collot, V.; Bovy, P. R.; Rault, S. *Tetrahedron* **2002**, *58*, 4369.
- (35) Tabanella, S.; Valancogne, I.; Jackson, R. F. W. *Org. Biomol. Chem.* **2003**, *1*, 4254.
- (36) Smith, T. *MChem Thesis*, University of Sheffield, **2012**.
- (37) Kodama, K.; Kobayashi, A.; Hirose, T. *Tetrahedron Lett.* **2013**, *54*, 5514.
- (38) Chilton, M. *MChem Thesis*, University of Sheffield, **2010**.
- (39) Dondoni, A.; Perrone, D. *Org. Synth.* **2000**, *77*, 64.
- (40) Krasovskiy, A.; Knochel, P. *Angewandte Chemie-International Edition* **2004**, *43*, 3333.
- (41) Garcia, F.; Hopkins, A. D.; Kowenicki, R. A.; McPartlin, M.; Rogers, M. C.; Silvia, J. S.; Wright, D. S. *Organometallics* **2006**, *25*, 2561.
- (42) Busacca, C. A.; Lorenz, J. C.; Sabila, P.; Haddad, N.; Senanayake, C. H. *Org. Synth.* **2007**, *84*, 242.
- (43) Netherton, M. R.; Dai, C.; Neuschuetz, K.; Fu, G. C. *J. Am. Chem. Soc.* **2001**, *123*, 10099.
- (44) Milne, J. E.; Buchwald, S. L. *J. Am. Chem. Soc.* **2004**, *126*, 13028.
- (45) Manolikakes, G.; Munoz Hernandez, C.; Schade, M. A.; Metzger, A.; Knochel, P. *J. Org. Chem.* **2008**, *73*, 8422.
- (46) Cvetovich, R. J.; Reamer, R. A.; DiMichele, L.; Chung, J. Y. L.; Chilenski, J. R. *J. Org. Chem.* **2006**, *71*, 8610.
- (47) Snegaroff, K.; Nguyen, T. T.; Marquise, N.; Halauko, Y. S.; Harford, P. J.; Roisnel, T.; Matulis, V. E.; Ivashkevich, O. A.; Chevallier, F.; Wheatley, A. E. H.; Gros, P. C.; Mongin, F. *Chem. - Eur. J.* **2011**, *17*, 13284.
- (48) Plunkett, M. *MChem Thesis*, University of Sheffield, **2017**.

Chapter 3: Biophysical characterisation of the effect of nickel coordination to bipyridylalanine and the construction of bimetallic coiled coil systems

3.1 Introduction

In addition to the single metal proteins discussed in Chapter 1, there are examples of proteins designed to bind multiple metal ions. One of the designs pursued in protein engineering are derived from naturally occurring diiron peptides. DeGrado and co-workers describe the design of a minimal diiron model. Through the analysis of the binding site in a zinc finger protein, the orientations of the ligating amino acids were controlled by the secondary structure of the peptide to generate a short peptide sequence that bound two iron atoms (Figure 3.1).¹

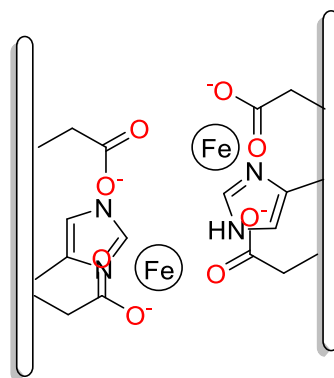


Figure 3.1 Representation of the binding of two iron atoms in the core of a 4-helix bundle. For the sake of clarity, two rods indicate the helices. Two of the carboxylates take part in bidentate binding with the iron atoms, while the other two carboxylates present act as a bridge between the iron atoms, taking part in monodentate binding to both iron atoms. The histidine coordinates to the rear face of the iron atom. The site is presented with the vacant “active site” of the protein presented to the viewer.¹

This finding marked the beginning of an extensive body of work by DeGrado and co-workers on the design of diiron peptide mimics. As an extension of the formation of a diiron model peptide, the use of mixed iron(II)/iron(III) in the system allowed for the design of a peptide which catalysed the oxidation of 4-aminophenol.² The iron(II)/iron(III) system enabled the use of oxygen to oxidise the metal ions to the reactive species, which oxidised the substrate, and could then be regenerated with the use of further oxygen.

Cytochrome *c* oxidase, a naturally occurring purple copper protein facilitates electron transfer processes, reliant on a region of the protein referred to as CuA. Tanaka and co-workers designed a four stranded coiled coil which acted as a mimic for the dinuclear CuA site.³ Following similar design principles to those used by DeGrado and co-

workers in the design of the protein featured in Figure 1, they describe the formation of a two copper protein which displayed similar electrochemical characteristics observed with the isolated native CuA site.

Lombardi and co-workers demonstrated the utility of peptide sequences which can bind multiple types of metal ion. The designed peptide was a designed diiron protein model, consisting of a helix-loop-helix hairpin, which was designed to dimerise on metal ion addition and form an anti-parallel four helix bundle. In addition to iron, this peptide was found to successfully form complexes with zinc, cobalt and manganese, expanding the range of reported dimetallic peptide sequences.⁴

Case and Ghadiri demonstrate the design of a heterometallic coiled coil containing both copper and ruthenium ions.⁵ A bipyridyl moiety is incorporated at the N-terminus of the coiled coil, and the copper binding site is comprised of histidine residues incorporated in the peptide sequence which form the composite binding site on the coordination of Ru^{2+} to the peptide. The $\text{Ru}(\text{peptide})_3$ complex is kinetically inert, and removes any issues of site selectivity within the peptide. Cu^{2+} increases the chemical stability of the peptide, as the $\Delta G_{\text{H}_2\text{O}}$ of the bimetallic coiled coil is $1.5 \text{ kcal mol}^{-1}$ greater than the coiled coil containing only ruthenium.

Other previous examples of systems that fall under the umbrella of bimetallic include systems reported by Scrimin and co-workers that can bind zinc ions in two separate sites (Figure 3.2).⁶ The dinuclear Zn^{2+} peptide catalyses the intramolecular transesterification of HPNP (2-hydroxypropyl *p*-nitrophenyl phosphate), a popular model substrate for RNA. Investigation of the activity of zinc in the catalytic cycle indicates cooperativity between the two metal sites facilitates the transesterification reaction.

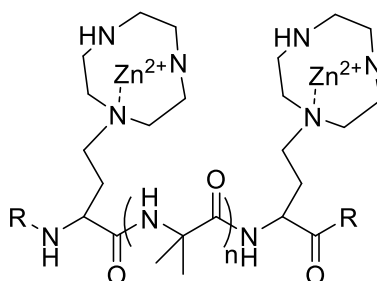


Figure 3.2 A peptide sequence containing two azacrown functionalised amino acids which can coordinate two zinc atoms. The distance between the azacrowns can be varied, and the binding constants of each zinc is independent of previous metal coordination.⁶

In their synthesis of short peptide sequences containing the Bpa moiety, Imperiali and co-workers report the successful binding of the bipyridine residue to a range of

transition metal ions, with strong binding reported for nickel, zinc, cobalt and copper.⁷ With these metal ions available to us, we were interested in designing a peptide which formed a coiled coil that could bind metal ions from two different regions of the periodic table rather than forming a species which binds a combination of transition metal ions.

Bimetallic systems containing metal ions from two different areas of the periodic table are a relatively unexplored area in coiled coil research. However, for examples of systems that bind two different types of metal ion within the same system, i.e. both transition metal ions and lanthanide ions, a search of the literature only revealed one previous peptide example. In this example, Franz and co-workers report the design of a short peptide loop which formed a dimer with a cavity within the centre that can bind three metal ions, and was found to bind two terbium atoms and one zinc atom.⁸ These could then interact, and the proximity of the zinc ions to terbium had a measurable effect on the electronic properties of terbium. As part of our work, we wanted to investigate how we could bind two different metal ions in the same coiled coil.

In this chapter, it is reported the design of new coiled coil systems containing one or two metal binding sites. The incorporation of two binding sites within these peptides, one of which binds transition metal ions and one of which binds to lanthanide ions presents the opportunity to investigate mixed metal systems. These systems have been proposed as models that could be used for electron transfer along the coiled coil, and from there the generation of new peptide-based electronics. This dual functionality also means a range of new peptide structures can be generated. The two binding sites are within different regions of the coiled coil, one placed at the N-terminus and one placed within the hydrophobic coil itself. The lanthanide binding systems themselves can be migrated within the heptads of the coiled coil, varying their position and relationship with the bipyridyl site. The two can be close enough to interact, or incorporated as two entirely separate systems. As part of our work, we wanted to investigate how we could bind two different metal ions in the same coiled coil chain.

3.2 Design of target peptides

One of the key design points for these peptides was the fact that the bipyridyl amino acids allowed us to construct peptides with two binding sites that bind different metal binding amino acids. The bipyridyl site binds transition metal ions. Generating coiled coils which can bind both transition metal and lanthanide metal ions allows for the

creation of systems which have exciting potential as catalysts and light harvesting complexes.

To this end, peptide sequences reported by Peacock and co-workers which can bind lanthanide ions, particularly gadolinium and terbium, were used as a model for the designed sequences.⁹ They are based on the sequence Ac- G (I_aA_bA_cI_dE_eQ_fK_g)_xG- NH₂, which makes use of the heptad approach to designing a coiled coil.¹⁰

Each amino acid has an assigned role:

- | | | |
|----|---|--|
| I- | Isoleucine, generates the hydrophobic core and favours the formation of 3 stranded coiled coils | |
| A- | Alanine, induces helix formation | |
| E- | Glutamate | } Both these amino acids form favourable interhelical salt bridges, encouraging formation of coiled coils. |
| K- | Lysine | |
| Q- | Glutamine, charged amino acid helps solubilise the peptide in water | |

In addition to the coiled coil forming amino acids, a designed lanthanide binding site was incorporated into the hydrophobic interior of the coiled coil. Two adjacent Ile residues were replaced with an asparagine (N) and aspartate (D) respectively, to generate a hard oxygen binding site to coordinate Gd (III) or Tb (III) ions. This site can be incorporated in each of the heptad sites with varying effects on the folding of the peptide. The lanthanide binding site has a destabilising effect on the peptide when not bound to a metal ion. Finally, a tryptophan (W) was introduced as it offers a number of advantages: it absorbs light at 280 nm ($\epsilon_{280} = 5690 \text{ M}^{-1} \text{ cm}^{-1}$), allowing the concentration of the peptide to be readily determined in solution and its emission peak is highly sensitive to its environment. The three peptide sequences are described in Table 3.1. A 3-D model of 6Bpa was manually added to X-ray crystal structure of MB-12 to generate a model of the coiled coil (Figure 3.3). The structure was manually adjusted as the apo-peptide species without energy minimisation.

Table 3.1 Peptide sequences used in this study. X indicates a bipyridyl amino acid. Mutations in the peptide sequence are highlighted in bold. Heptad repeats are shown as blocks of seven residues. Reference number NB-XX refers to the number of lanthanide binding pockets in the peptide and its heptad location respectively.

Peptide	Sequence
	abcdefg-abcdefg-abcdefg-abcdefg-abcdefg
NB00	Ac-X-G-IAAIEQK-IAAIE WK -IAAIEQK-IAAIEQK-IAAIEQK-G-NH ₂
NB11	Ac-X-G-IAA NEWK - D AAIEQK-IAAIEQK-IAAIEQK-IAAIEQK-IAAIEQK-G-NH ₂
NB12	Ac-X-G-IAAIEQK-IAA NEWK - D AAIEQK-IAAIEQK-IAAIEQK-IAAIEQK G-NH ₂

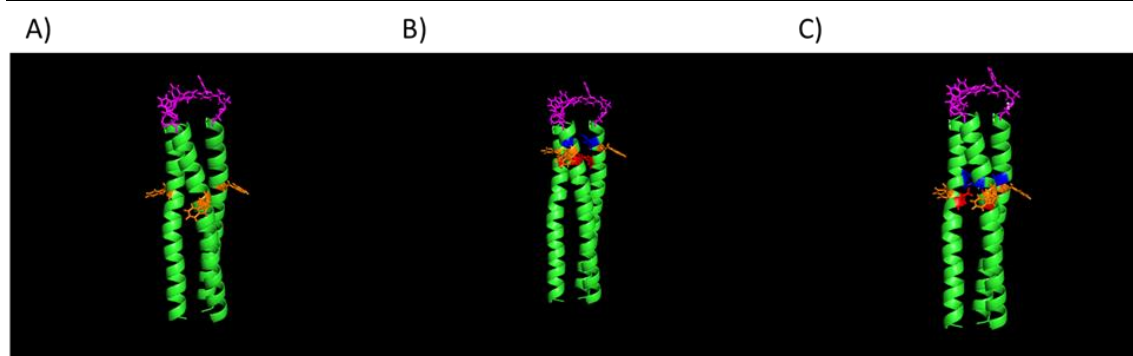


Figure 3.3 Computer generated model of A) NB00, B) NB11, and C) NB12. Bpa residues highlighted in purple, Asn in blue, Asp in red, and tryptophans in orange. The sequence is a trimeric coiled coil, with the backbone shown as a ribbon with side chains hidden. The destabilising Asp-Asn layer is shifted one heptad towards the C-terminus in NB12. The structures are not energy minimised, not metal coordinated and manually adjusted to represent the proposed structure of the coiled coils.

This site translation allows for the investigation of dual metal incorporation into a coiled coil which is already well folded, with two binding sites in close proximity. This was the proposed model electron transfer peptide, as the proximity of the metals to each other when bound is more conducive to energy transfer. It was proposed that the addition of an N-terminal bipyridyl amino acid would have minimal effect on the overall structure and stability of the peptides. With this, two peptides to investigate the effects of multiple metal ion incorporation were designed. In addition, a control peptide without the lanthanide binding group but still containing the 6-Bpa amino acid was designed to isolate the contribution and effect of 6-Bpa to the coiled coil.

3.3 UV characterisation of the metal binding behaviour of Fmoc-6Bpa-OH (22)

One of the advantages of the use of a bipyridyl side chain is the relationship between its metal binding behaviour and UV spectrum. Imperiali and co-workers determined the binding constants with transition metals for a peptide containing 6Bpa by following the

change in absorbance at 306 nm.⁷ Based on the reports of similar peptide species by Case and Ghadiri, the bipyridine complex was assumed to form a trimeric octahedral complex (Figure 3.4).^{11,12}

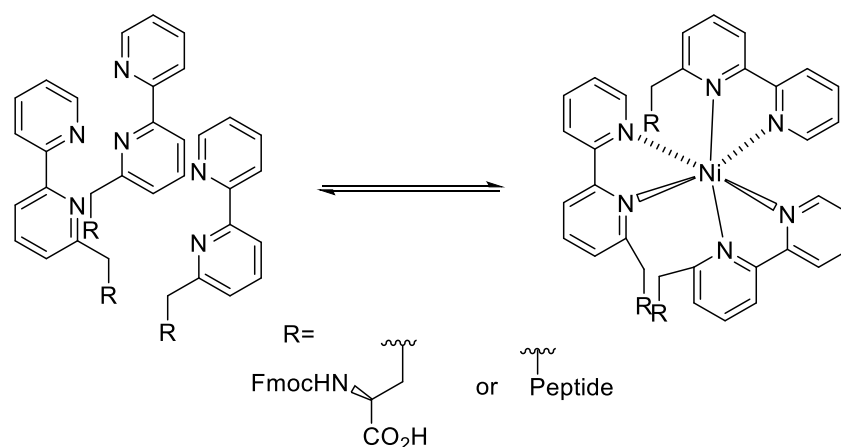


Figure 3.4 Simplified representation of metal coordination in the systems studied. Three coordinate octahedral metal binding of Ni^{2+} to three bipyridyl binding sites of bipyridylalanine.

With this proposed model, the binding of metals to Fmoc-6Bpa-OH was investigated prior to tests with the peptides. Metal binding in this thesis was monitored by following the peak at 310 nm, which forms as a result of metal coordination to the bipyridine. (Figure 3.5).

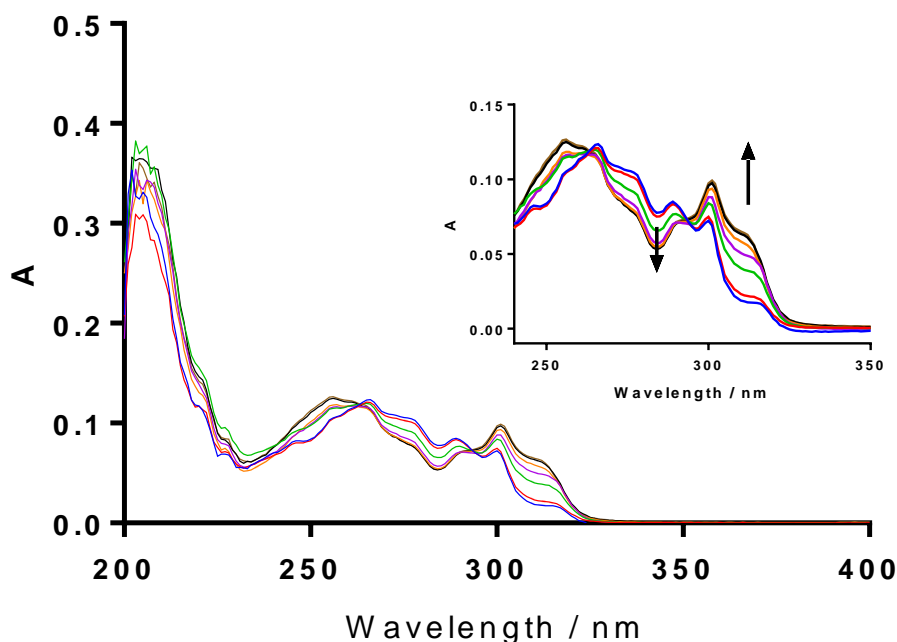


Figure 3.5 UV-Vis spectra of a titration of Fmoc-6Bpa-OH with NiCl_2 . Blue- 6 μM Fmoc-6Bpa-OH Red- 1 μM Ni^{2+} Green- 2 μM Ni^{2+} Purple- 3 μM Ni^{2+} Orange- 4 μM Ni^{2+} Brown- 5 μM Ni^{2+} Black- 6 μM Ni^{2+} . Inset is the change between 240 nm and 350 nm. Measurements carried out in a 1 cm pathlength cell. Experiments were performed in 100% v/v CH_3OH .

Dissociation constants were determined for a range of metal ions with Fmoc-6Bpa-OH (Figure 3.6). The use of methanol as a solvent in these titrations to measure the water insoluble Fmoc-6Bpa-OH species is not an accurate reflection of the properties of these species in the aqueous environment used in the protein studies. The use of H-6Bpa-OH.HCl would allow for measurements of the aqueous system, but this material proved difficult to handle and so the material was converted to the Fmoc protected compound.

This work was not intended as an exhaustive study of the metal binding study of the amino acid, but a study of its UV behaviour and identification of metal ions with strong binding to the bipyridine.

The binding isotherms display a sigmoidal curve. The lag phase at the beginning of the titration is indicative of a structural rearrangement within the system before trimer formation, indicating that the bipyridines may aggregate in solution and this structure must be disrupted before metal binding occurs.

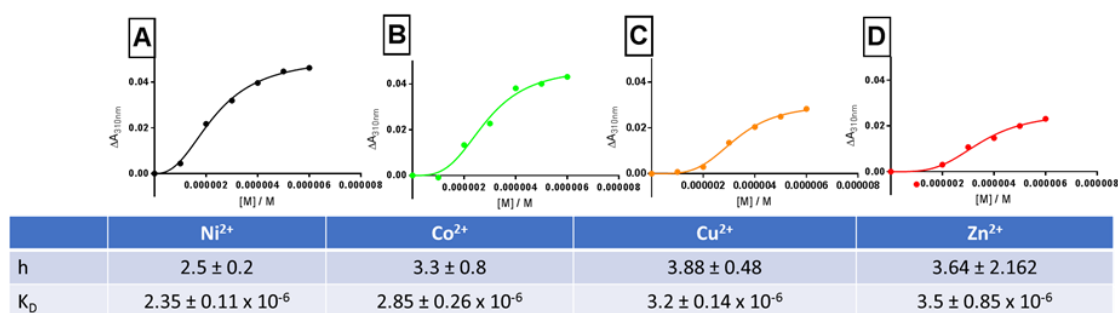


Figure 3.6 Hill plots for the determination of Fmoc-6Bpa-OH binding constants with different transition metals. A- Ni²⁺ B-Co²⁺ C-Cu²⁺ D- Zn²⁺. Table displays the h constant derived for each plot and the resulting K_D. Measurements carried out in a 1 cm pathlength cell. Experiments were performed in 100% v/v MeOH.

Plotting the change in absorbance at 310 nm against the concentration of metal ion (guest) allows us to plot the Hill curve and from this derive an apparent dissociation constant. The curve was fit to a two-state system (see Appendix, equations 5-11), as the clean isosbestic points of the spectra indicated the formation of only one metal-ligand species in this mixture. A Hill constant greater than 1 indicates cooperativity of binding in the system, so an apparent dissociation constant for the formation of the trimeric system was determined (Figure 3.7).

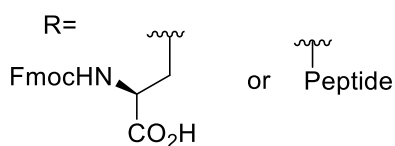
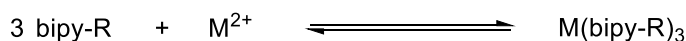


Figure 3.7 Proposed equilibrium for transition metal binding to the bipyridine ligand.

These titrations demonstrated nickel had the strongest binding affinity for the bipyridyl species. Nickel was used as the transition metal in metal binding studies of the peptides. The same changes in the UV spectrum observed in titrations of the amino acid are seen in the titration of a solution of the peptides (Figure 3.8). There is a decrease in absorbance at 285 nm and an increase at 310 nm, and the latter can be used to follow metal binding behaviour.

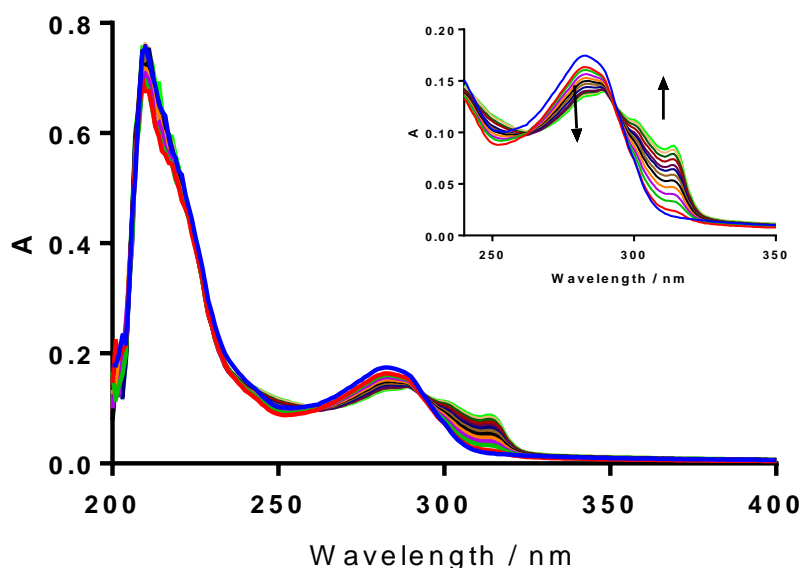


Figure 3.8 UV-Vis spectra of a titration of 10 μM NB12 with NiCl_2 . Measurements carried out in a 1 cm pathlength cell. Arrows indicated changes in absorbance with increased $[\text{Ni}^{2+}]$. Isosbestic points observed at 260 and 295 nm. Experiments were performed in 5 mM HEPES, 100 mM NaCl, pH 7.0.

The same methods used for the amino acid can be applied to the peptide species NB00, NB11, and NB12 (Figure 3.9). The data were also fit to a double reciprocal plot and a one site specific binding model, but fitting the data to the Hill equation gave the best fit.

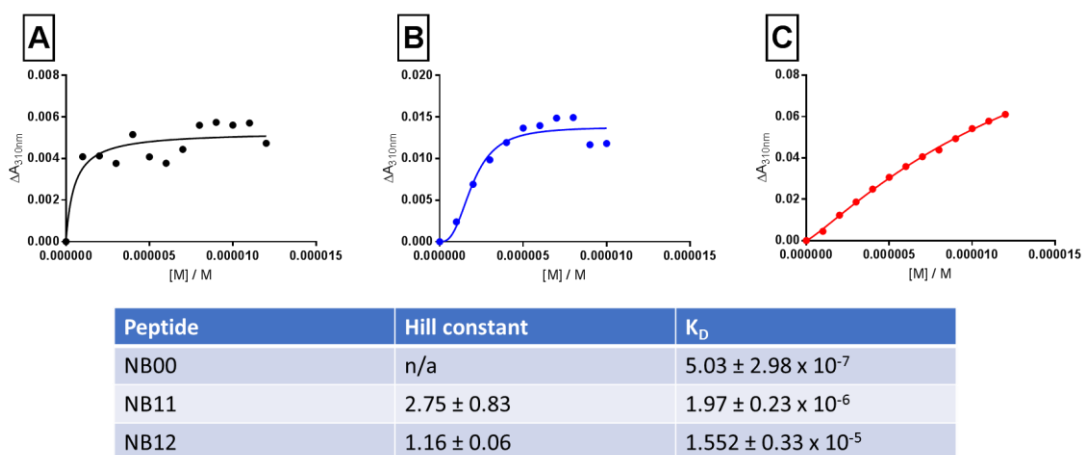


Figure 3.9 Hill plots for the determination of NB-XX binding constants with Ni²⁺. Table displays the h constant derived for each plot and the resulting K_D. A- 10 μM NB00 B- 10 μM NB11 C-10 μM NB12. Measurements carried out in a 0.1 cm pathlength cell for NB11 and NB00. Experiments were performed in 5 mM HEPES, 100 mM NaCl, pH 7.0.

NB00 displayed an immediate increase in absorbance, which then plateaued. These data could not be plotted using a Hill curve, so the binding was plotted using the specific binding curve function in GraphPad. The values derived for NB11 and NB12 also using a specific binding curve are within the same order of magnitude for those derived from the Hill plot. The binding of the peptides reflect their structural characteristics. NB00, a coiled coil species with no destabilising features binds nickel the most strongly of the three peptides. NB11 has a destabilising feature, but its effect on the peptide structure is minimal. However, this is sufficient to reduce K_D for NB11 by one order of magnitude. NB12 has a known structurally destabilising binding site, and its binding constant is two orders of magnitude less than NB00. The lag phase observed in the amino acid spectra is also observed in NB11 and NB12. Initially this was assigned to the concentration of the system studied being within the same order of magnitude as the binding constant, but the plot of the binding of NB11 at 100 μM showed the same sigmoidal binding curve as 10 μM, indicating that the lag phase is not concentration dependent.

3.4 Concentration-dependent folding of apo-peptides.

Circular dichroism was used to quantify the amount of helical structure at varying peptide concentrations (Figure 3.10). The peptide sequences are designed to form trimeric coiled coils, so if θ_{222nm} is plotted against monomer concentration we can determine the concentrations at which trimer formation is favoured .

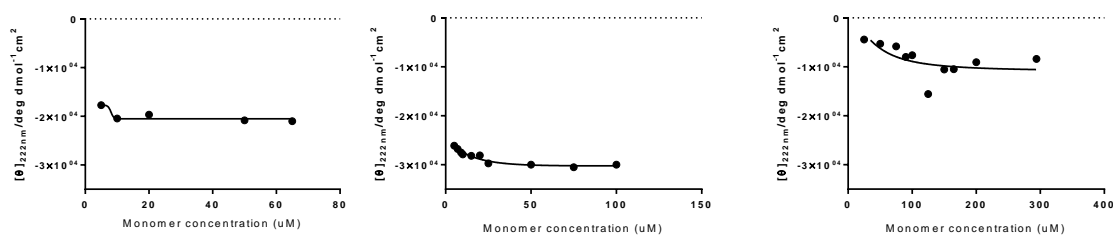


Figure 3.10 Plots of the change in $\theta_{222\text{nm}}$ for each peptide at different concentrations. A) NB00 B) NB11 C) NB12. NB00 displays a plateau after 10 μM , as does NB11 to a lesser extent. NB12 displays a plateau at concentrations above 100 μM , with an outlying point at 125 μM . These plateaus indicate the concentration at which trimer formation is favoured over existing as a monomer. Experiments were performed in 5 mM HEPES, 100 mM NaCl, pH 7.0.

NB00 shows trimer formation at very low concentrations, with no phase where the species exists as a monomer. NB11 exists primarily as a trimer at concentrations of 10 μM and above. NB12 does not favour trimer formation until relatively high concentrations above 100 μM , and also displays the broadest transition between α -helical monomer and coiled coil. There is an outlying point at 125 μM of significantly higher ellipticity than the remaining points. This data set was repeated, and the peptide does demonstrate this level of ellipticity. Increasing monomer concentration leads to the aggregation of the peptide, something also observed in NB00 at higher concentrations, which results in higher concentrations displaying lower ellipticity as a result.

The apopeptide species were subject to multiple-angle laser light scattering (MALLS) (Table 3.2).

Table 3.2 Calculated mass of each peptide species at 1 mg/mL (236 μmol) derived from MALLS. NB00 displays a weight corresponding to a dimer of NB00, NB11 a trimer, and NB12 a monomer. Monomer weight NB00: 4.226×10^{-3} , NB11/NB12: 4.228×10^{-3} Dimer weight NB00: 8.452×10^{-3} NB11/NB12: 8.456×10^{-3} Trimer weight NB00: 1.268×10^{-4} NB11/NB12: 1.268×10^{-4}

Peptide	Calculated mass (g mol^{-1})
NB00	$7.68 \times 10^3 (\pm 3.06\%)$
NB11	$1.2 \times 10^4 (\pm 1.24\%)$
NB12	$4.74 \times 10^3 (\pm 3.34\%)$

The concentrations required resulted in NB00 and NB12 being challenging to characterise by MALLS. NB11 is a trimer at these concentrations, consistent with the design of the peptide species. NB00 displays a mass value consistent with dimer formation. NB12 shows only monomer in the solution measured. Both NB00 and particularly NB12 precipitated out as gels when centrifuging the samples before injection into the system.

3.5 The effect of Ni^{2+} -6Bpa complex formation on the oligomerisation state and stability of coiled coils.

The peptide species investigated demonstrate variable folding properties over different ranges of concentrations. For NB11 and NB12, this allowed the investigation of the effect of Ni^{2+} on the peptide species at different oligomerisation states of the same peptide species. NB00 showed a plateau in its concentration dependent properties in the micromolar range studied, so acted as a control peptide for the other peptides with two binding sites.

3.5.1 The isolated contribution of Ni^{2+} -6Bpa complex formation in a model coiled coil

The titration of Ni^{2+} into a solution of 10 μM NB00 did not show a correlation between the ellipticity of the species and the proportion of Ni^{2+} added (Figure 3.11).

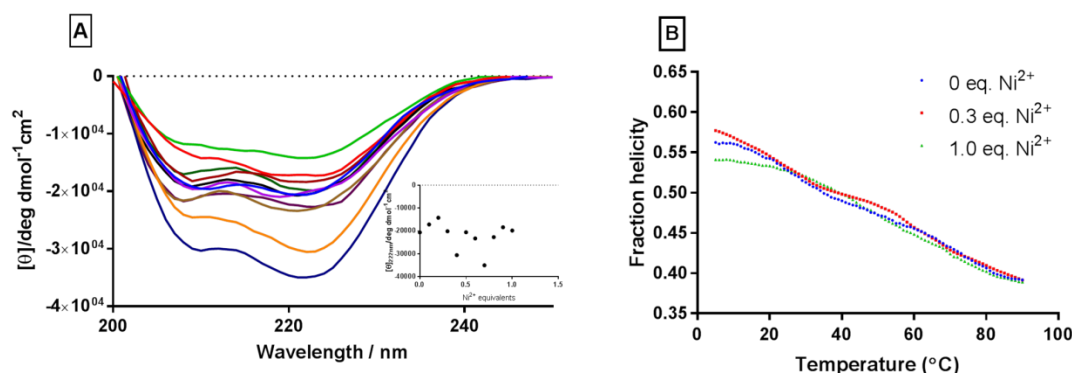


Figure 3.11 A) Titration of increasing Ni^{2+} into a solution of 10 μM NB00. Addition of Ni^{2+} is accompanied by an increase in helicity, but no $\theta_{222\text{nm}}$ displays a very small change between 0, 0.3 and 1.0 eq Ni^{2+} . Plot of $\theta_{222\text{nm}}$ against eq Ni^{2+} inset. The two outlying points at 0.4 and 0.7 eq. correspond to the dark blue and orange plots shown in the titration. The plot does not show a decrease between 0 and 1.0 eq. Ni^{2+} . B) Thermal melts of 10 μM NB00 coordinated to 0 (blue), 0.3 (red) and 1.0 (green) eq Ni^{2+} . The addition of Ni^{2+} to the system does not affect the broad melt curve or final helicity of the peptide. Experiments were performed in 5 mM HEPES, 100 mM NaCl, pH 7.0.

The change in ellipticity with temperature can be used to determine the enthalpy of unfolding. The melt data displays a very broad sigmoidal curve. The successful determination of an enthalpy changes using van't Hoff analysis relies on sigmoidal data, and can be calculated by plotting $\ln K$ against $1/T$ results in a graph where the gradient of the steepest portion of the graph gives the enthalpy change (Figure 3.12).

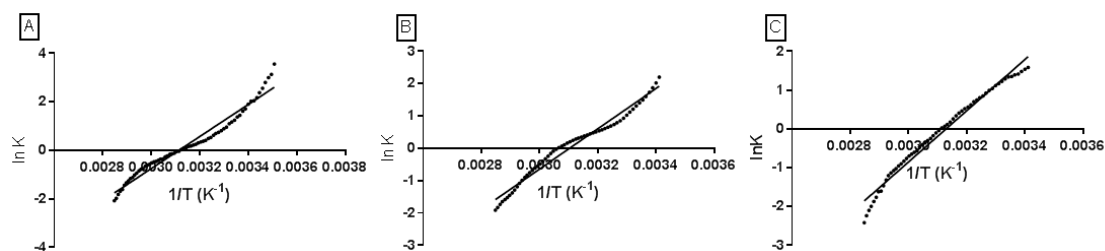


Figure 3.12 Van't Hoff plots for the NB00 melts shown in Figure 3.11B. A- 0 eq Ni^{2+} B- 0.3 eq Ni^{2+} C- 1.0 eq Ni^{2+} . Data is truncated to show the area of steepest incline within the plot. 1/slope of the fit gives the change in enthalpy for the system. Experiments were performed in 5 mM HEPES, 100 mM NaCl, pH 7.0.

Table 3.3 Tabulated values for the enthalpies derived for 11 A, B and C.

Eq. Ni^{2+}	ΔH (kcal mol $^{-1}$)
0	13.1 ± 0.3
0.3	12.4 ± 0.3
1.0	13.1 ± 0.3

The enthalpy values (Table 3.3) determined show metal ion concentration has a minimal effect on the enthalpy of unfolding. This suggests that the coordination of Ni^{2+} does not influence the structure or stability of the already folded coiled coil.

3.5.2 Contribution of 6Bpa- Ni^{2+} within a coiled coil with a structurally non-contributory core lanthanide binding site (NB11)

The mutation of two isoleucine residues in the first and second heptads to Asn and Asp residues has a minimal destabilising effect on NB11. The coiled coil forms above 10 μM monomer concentration, consistent with the behaviour of NB00. At 3 μM monomer concentration, at which the peptide exists as an isolated α -helix, the CD signal is consistent with the presence of α -helices, with dual minima at 208 and 222 nm. This profile changes, and the minima at 222 nm becomes more negative than the minima at 208 nm as the nickel concentration is increased (Figure 3.13).

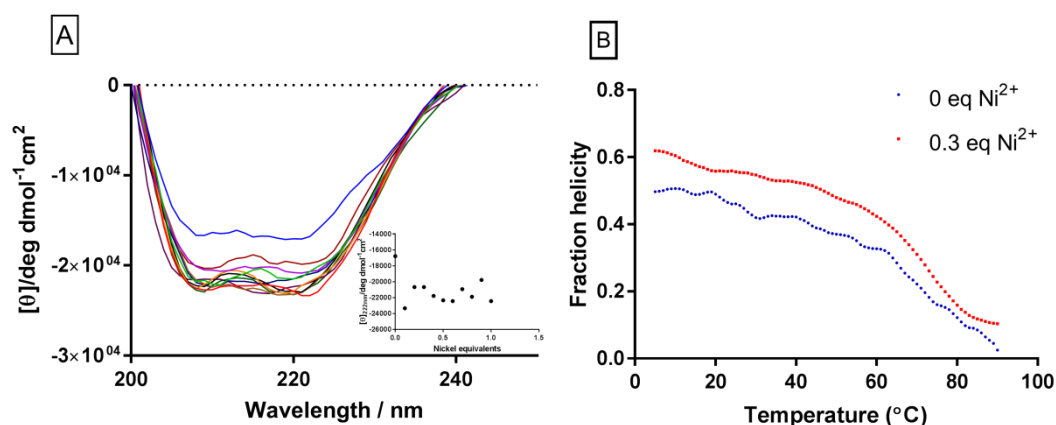


Figure 3.13 A) Titration of increasing Ni^{2+} into a solution of 3 μM NB11. Addition of Ni^{2+} up to 0.3 eq. is accompanied by an increase in helicity, and $\theta_{222\text{nm}}$ is unchanged between 0.3 and 1.0 eq Ni^{2+} . Plot of $\theta_{222\text{nm}}$ against eq Ni^{2+} inset. The plot shows an increase between 0 and 0.3 eq. Ni^{2+} , and from 0.3 to 1.0 eq Ni^{2+} $\theta_{222\text{nm}}$ remains unchanged. B) Thermal melts of 3 μM NB11 coordinated to 0 (blue) and 0.3 (red) eq Ni^{2+} . The addition of Ni^{2+} to the system results in a sharper change in the melt transition between 60 and 80 $^{\circ}\text{C}$, as well as a higher fraction ellipticity at 90 $^{\circ}\text{C}$. Experiments were performed in 5 mM HEPES, 100 mM NaCl, pH 7.0.

After 0.3 equivalents of nickel the change in helicity becomes minimal as the value plateaus. This is consistent with the formation of a trimeric $[\text{Ni}(\text{NB11})_3]^{2+}$ system, and indicates the formation of an octahedral configuration around the coordinated metal ion. The melt profiles of both the apo- and metallopeptide species demonstrate the stabilising effect of nickel coordination. The enthalpies of unfolding for the 3 μM NB11 system demonstrate the effect of the coordination of metal ions. An increase of 3.4 kcal mol^{-1} demonstrates the metal ion has a considerable stabilising effect (Table 3.4) on the peptide system.

Table 3.4 Tabulated enthalpies of unfolding for the melts shown in Figure 3.13B.

Eq. Ni^{2+}	ΔH (kcal mol^{-1})
0	8.1 ± 0.2
0.3	11.5 ± 0.4

The 3 μM system demonstrates the formation of a three-coordinate peptide species, but the CD characterisation data for the species is not consistent with the formation of a coiled coil. Coiled coil formation for the NB11 species is represented by a system with an ellipticity of $-30,000 \text{ deg dmol}^{-1} \text{cm}^2$ or higher, as shown in the concentration curve demonstrated above, while this system plateaus at $20\text{--}22,000 \text{ deg dmol}^{-1} \text{cm}^2$. The system may be forming an associated bundle in this case, which justifies a 3:1 stoichiometry with a much lower ellipticity, due to association of three alpha-helices rather than the formation of coiled coil.

The behaviour of these peptides at 10 μM was also investigated. At concentrations of 10 μM and above, the ellipticity of the NB11 does not change significantly with higher monomer concentration, so this point can be used as the maximum folding of the apo-peptide (Figure 3.14).

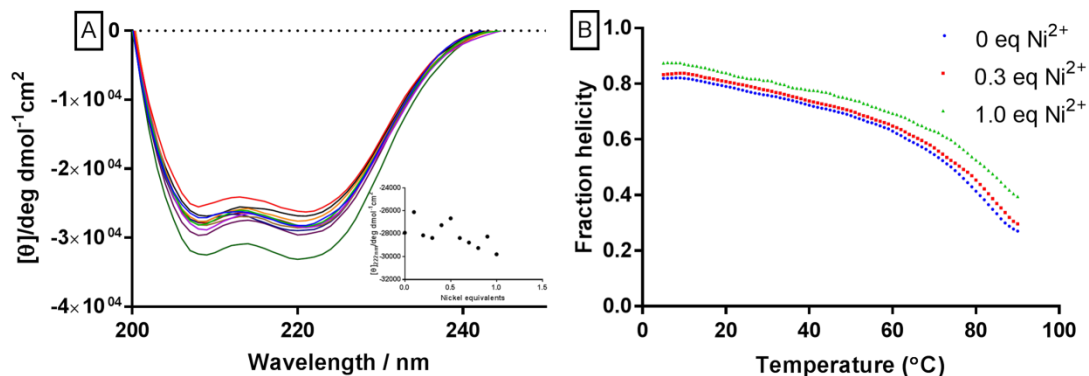


Figure 3.14 A) Titration of increasing Ni^{2+} into a solution of 10 μM NB11. Addition of Ni^{2+} up to 1.0 eq. is accompanied by an increase in helicity, and $\theta_{222\text{nm}}$ continually increases between 0.1 and 1.0 eq Ni^{2+} . Plot of $\theta_{222\text{nm}}$ against eq Ni^{2+} inset. The plot shows an increase between 0 and 1.0 eq. Ni^{2+} . B) Thermal melts of 10 μM NB11 coordinated to 0 (blue), 0.3 (red) and 1.0 (green) eq Ni^{2+} . The addition of Ni^{2+} to the system does not affect the melt profile of the species, but the value of $\theta_{222\text{nm}}$ at 90 $^{\circ}\text{C}$ increases corresponding to the amount of Ni^{2+} titrated into the peptide solution. Experiments were performed in 5 mM HEPES, 100 mM NaCl, pH 7.0.

This titration pattern is consistent with an already folded system that is not affected structurally by the addition of Ni^{2+} . There is a fluctuation within them of $-2000 \text{ deg dmol}^{-1} \text{cm}^2$, which is a fluctuation of 5% ellipticity. The apo-peptide has a value of $-27,916 \text{ deg dmol}^{-1} \text{cm}^2$, the 0.3 metallated version $-28,368 \text{ deg dmol}^{-1} \text{cm}^2$, and at 1:1 metal to peptide the system only decreases to $-29,795 \text{ deg dmol}^{-1} \text{cm}^2$ (79.6%, 79.7% and 83.6% respectively).

The UV binding isotherm supports this (Figure 3.9). When considering both the UV and CD spectra, both figures show the system is binding each successive metal ion equivalent, but this is not significantly affecting the coiled coil structure.

However, as discussed previously in this thesis, metal ions do not simply influence structure formation. In this system, the addition of increased nickel to the peptide system increases the stability of the coiled coil system without corresponding to a resultant increase in ellipticity (Table 3.5).

Table 3.5 Tabulated enthalpies of the melts shown in Figure 3.14B.

Eq. Ni ²⁺	ΔH (kcal mol ⁻¹)
0	10.4 ± 0.2
0.3	10.5 ± 0.2
1.0	9.3 ± 0.1

The enthalpies of unfolding indicated a further effect within the system. The enthalpy values for 0 and 0.3 equivalents of nickel show no change. On addition of 1.0 equivalents of nickel however, the value decreases by 1 kcal mol⁻¹. This decrease was unexpected.

3.5.3 Contribution of 6Bpa-Ni²⁺ complex formation within a coiled coil with a structurally destabilising core lanthanide binding site (NB12)

The mutation of two isoleucine residues of the second and third heptads to Asp and Asn respectively has a minimal destabilising effect on NB11. The NB12 peptide displays folding behaviour consistent with a very poorly folded coiled coil. The concentration curve demonstrated above (Figure 3.10) shows the peptide sequence to require much higher monomer concentrations to assemble into a coiled coil sequence, concentrations above 100 μ M compared to the 10 μ M concentration required to assemble NB00 and NB11. The ellipticity of this coiled coil remains much lower than the coiled coils formed by NB00 and NB11. At a monomer concentration of 50 μ M, the behaviour of the α -helices can be observed. The profile of the spectra is distinct from the previous species. The expected minima at 208 nm has shifted towards 201 nm, a feature observed in other species that exist as a mixture of random coils and α -helices (Figure 3.15).

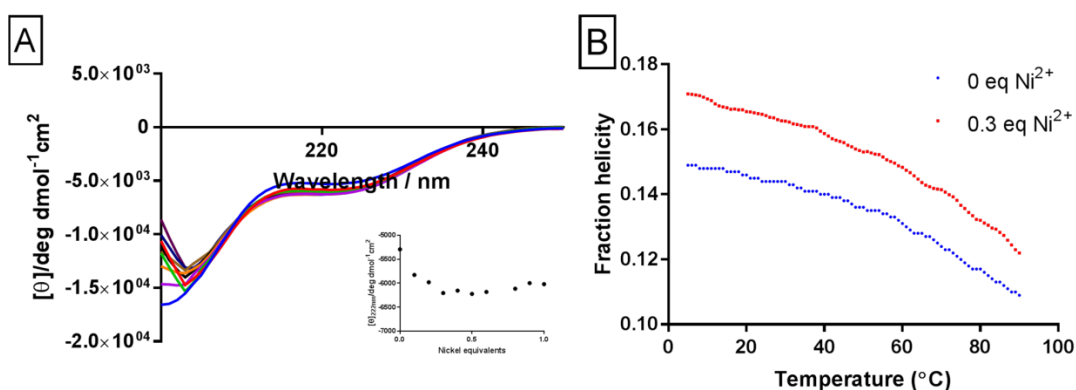


Figure 3.15 A) Titration of increasing Ni²⁺ into a solution of 50 μ M NB12. Addition of Ni²⁺ up to 0.3 eq. is accompanied by an increase in helicity, and $\theta_{222\text{nm}}$ is unchanged between 0.3 and 1.0 eq Ni²⁺. Plot of $\theta_{222\text{nm}}$ against eq Ni²⁺ inset. The plot shows an increase between 0 and 0.3 eq. Ni²⁺, and from 0.3 to 1.0 eq Ni²⁺ $\theta_{222\text{nm}}$ remains unchanged. Data at 0.7 eq. Ni²⁺ omitted as an outlier. B) Thermal melts of 50 μ M NB12 coordinated to 0 (blue) and 0.3 (red) eq Ni²⁺. The addition of Ni²⁺ to the system results in a sharper change in the melt transition between 60 and 80°C, as well as a higher fraction ellipticity at 90°C. Experiments were performed in 5 mM HEPES, 100 mM NaCl, pH 7.0.

The increase in the helicity of NB12 plateaus at 0.3 equivalents of nickel, indicating the bipyridyl species has become saturated and further coordination is not having an effect on the structure of the species. The melt profile of 50 μM NB12 changes appropriately, demonstrating the titration of nickel into the system increases the thermal stability of the peptide (Figure 3.15B).

The increase in ellipticity with metal titrations is expected to be indicative of an increase in the enthalpy of unfolding of the system, as the system should become more stable due to the metal coordination. This is supported by an enthalpy change of $1.9 \text{ kcal mol}^{-1}$ with the addition of 0.3 eq Ni^{2+} (Table 3.6).

Table 3.6 Tabulated enthalpies of the melts shown in Figure 3.15B.

Eq. Ni^{2+}	$\Delta H \text{ (kcal mol}^{-1}\text{)}$
0	9.6 ± 0.1
0.3	11.5 ± 0.2

At a monomer concentration of 90 μM , the ellipticity of the system has increased but it does not yet pass the concentration at which trimer formation is favoured. It occupies a useful intermediary stage for any structural intermediates that may be observed (Figure 3.16). The profile of the 90 μM spectra is very similar to that of the 50 μM titrations. The minima at 222 and 201 nm are still consistent with a mix of oligomerisation states.

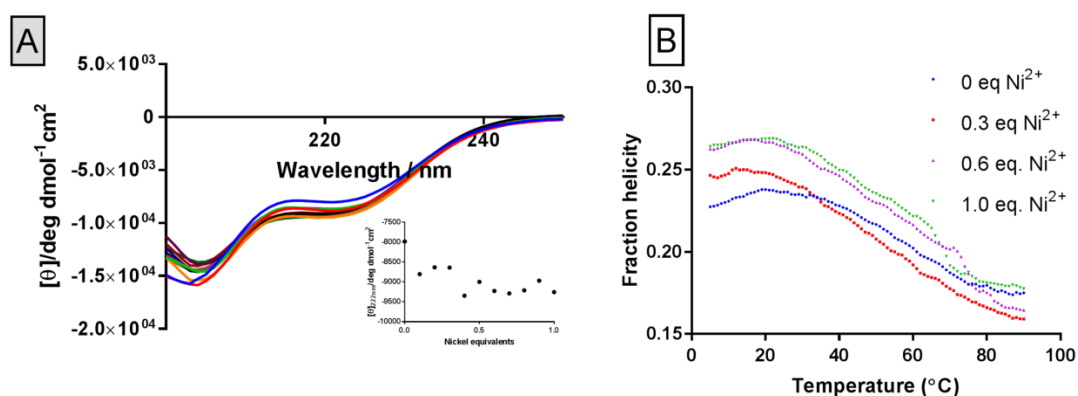


Figure 3.16 A) Titration of increasing Ni^{2+} into a solution of 90 μM NB12. Addition of Ni^{2+} up to 0.6 eq. is accompanied by an increase in helicity. Plot of $\theta_{222\text{nm}}$ against eq Ni^{2+} inset. The plot shows an increase between 0 and 0.1 eq. Ni^{2+} , and from 0.3 to 0.4 eq Ni^{2+} . B) Thermal melts of 90 μM NB11 coordinated to 0 (blue), 0.3 (red), 0.6 (purple) and 1.0 (green) eq Ni^{2+} . The addition of Ni^{2+} to the system results in a sharper change in the melt transition between 60 and 80 $^{\circ}\text{C}$. The endpoints of the melts for 0.3 and 0.6 eq Ni^{2+} show a lower $\theta_{222\text{nm}}$ at 90 $^{\circ}\text{C}$ than the apo-peptide, but 1.0 eq Ni^{2+} results in a higher endpoint. Experiments were performed in 5 mM HEPES, 100 mM NaCl, pH 7.0.

Within the titration, the system displays two plateaus in its titration behaviour. The first is between 0.1 equivalents and 0.3, indicating the formation of the $\text{M}[\text{NB12}]_3$ species,

but on addition of further metal ions the system displays a second folding shift. The second increase between 0.3 and 0.4 equivalents is smaller than the first plateau, a change of $-700 \text{ deg dmol}^{-1} \text{ cm}^2$ rather than $-1700 \text{ deg dmol}^{-1} \text{ cm}^2$, or 2% and 5% helicity respectively. If the change is real, this indicates that it is a very small change in the peptide structure with the second shift, where the first shift is a larger change in the system. Comparatively, the change in the 50 μM with nickel coordination is only 2%, so the second plateau is comparable, indicating that the first change in ellipticity at 90 μM may be due to the arrangement of the species into a helix bundle, organised by the coordination of nickel to the bipyridine system.

The melts demonstrate this shift in behaviour well (Figure 3.16B). All of the melt profiles show similar behaviour. There is no clear demonstration of cooperative unfolding behaviour, but a steady unfolding of the peptide sequence from the levels observed in the 90 μM titrations to the levels of ellipticity recorded in the 50 μM titrations. The endpoints of the melts for 0.3 and 0.6 eq Ni^{2+} show a lower $\theta_{222\text{nm}}$ at 90°C than the apo peptide, but 1.0 eq Ni^{2+} results in a higher endpoint of the melt.

The enthalpy of unfolding for the apo 90 μM species is much higher than for the 50 μM species, consistent with its greater helicity and indicative of changing the balance of the equilibrium further in favour of coiled coil formation (Table 3.7). With the titration of metal ions into the system, increasing the amount of nickel in the system destabilises the system considerably.

Table 3.7 Tabulated values of the enthalpies derived from the melts shown in Figure 3.16B.

Eq. Ni^{2+}	$\Delta H \text{ (kcal mol}^{-1}\text{)}$
0	22.5 ± 0.4
0.3	18.5 ± 0.3
0.6	14.7 ± 0.3
1.0	19.4 ± 0.6

The full characterisation of NB12 was completed with the analysis of the fully folded system. This required a monomer concentration of 125 μM , far in excess of any of the other systems measured. Even without plotting $[\text{Ni}^{2+}]$ vs $\theta_{222\text{nm}}$, inspection of the spectra shows clear changes in the behaviour of the system grouped into concentration bands (Figure 3.17).

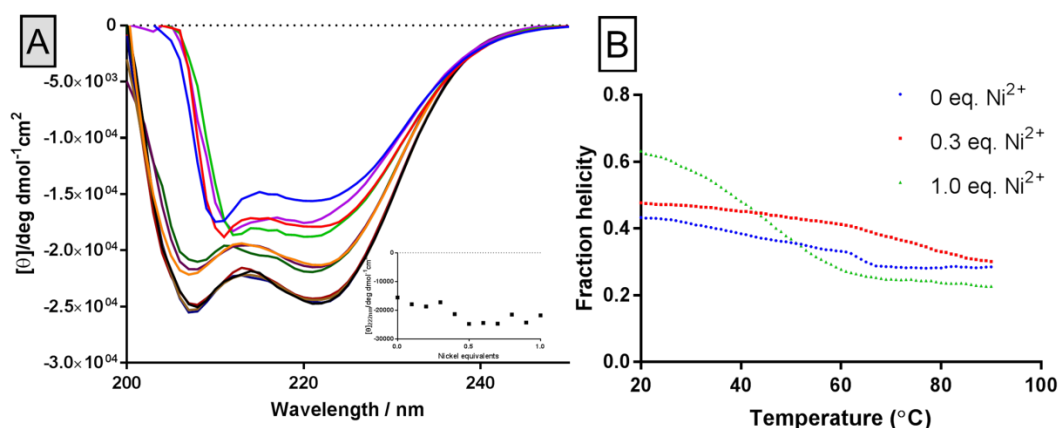


Figure 3.17 A) Titration of increasing Ni^{2+} into a solution of 125 μM NB12. Addition of Ni^{2+} up to 0.5 eq. is accompanied by an increase in helicity. Plot of $\theta_{222\text{nm}}$ against eq Ni^{2+} inset. The plot shows an increase between 0 and 0.1 eq. Ni^{2+} , and from 0.3 to 0.5 eq Ni^{2+} . B) Thermal melts of 125 μM NB12 coordinated to 0 (blue), 0.3 (red), and 1.0 (green) eq Ni^{2+} . The addition of Ni^{2+} to the system results in a sharper change in the melt transition between 60 and 80 $^{\circ}\text{C}$. The endpoint for the melt of 1.0 eq Ni^{2+} peptide shows a lower $\theta_{222\text{nm}}$ at 90 $^{\circ}\text{C}$. Experiments were performed in 5 mM HEPES, 100 mM NaCl, pH 7.0.

The apo-peptide stands alone, and then there are two plateaus again within this system. Similar to the 90 μM system, there seems to be more than one binding event taking place. The melts offer the same insight into the protein. The apo and 3:1 metal : peptide species follow the same trend observed before, where the titration of the metal follows the decrease in ΔH , indicating the metal is decreasing the energetic barrier to unfolding. However, the 1:1 titration completely disobeys this trend, demonstrating a clear and obvious sigmoidal unfolding curve, and a huge increase in ΔH of almost 10 kcal mol^{-1} (Table 3.8).

Table 3.8 Tabulated values of the enthalpies derived from the 125 μM NB12 melts shown in Figure 3.17B.

Eq. Ni^{2+}	ΔH (kcal mol^{-1})
0	17.2 ± 0.4
0.3	15.14 ± 0.2
1.0	24.74 ± 0.2

The observation of this two-state behaviour in the NB12 system but not in the NB11 is a reflection on the effect of the binding site and its shift in heptad position. NB11 becomes very well folded and stable with the addition of metal ions, there are minimal disruptions to the system, and the most stable species is rapidly generated, even when the apo-peptide is below the coiled coil concentration (CCC). NB12 has a very destabilising second heptad lanthanide group, which prevents it from readily assembling into its most folded state. Though this sequence is disadvantaged when trying to

assemble stable well folded structures, it is proposed that this instability promotes the generation of intermediate states within the peptide sequence.

From this previous data it is clear that the effect of the metal ion is stabilising, but not sufficiently to cause a coiled coil to form far away from the critical concentration demonstrated in Figure 1 for NB12.

3.6 Mixed metal coiled coil systems

NB11 was the target peptide for the formation of a mixed metal coiled coil. Its folding behaviour was more reliable than NB12, and the proximity of the bipyridine group to the lanthanide binding group could have interesting applications for functional mixed metal species coiled coils. Ni(II) and Gd(III) ions were chosen as the metal species for this work, as nickel was previously shown to have the strongest binding constant with the bipyridine group, and gadolinium has been shown to bind strongly to the lanthanide binding site in the parent peptides.^{9,10}

To ensure that the results were correctly interpreted, the two metal ions need to bind exclusively to one binding site. To ensure that there was no binding of the Bpa side chain to the gadolinium ions, gadolinium chloride was titrated into a solution of Fmoc-6Bpa-OH to demonstrate its lack of binding (Figure 3.18). Unpublished work from the Peacock group has shown that the lanthanide binding site binds very poorly if at all to transition metal ions. This eliminates this possibility of nickel coordinating to both sites. The titration of Gd³⁺ into a methanolic solution of Fmoc-6Bpa-OH showed no change in the UV-Vis spectra of the amino acid, consistent with a lack of binding to the bipyridine group. Titration into an aqueous solution of NB11 monitored by CD shows an increase in the ellipticity of the peptide, with a plateau at 0.4 eq. of Gd³⁺ (Figure 3.18B).

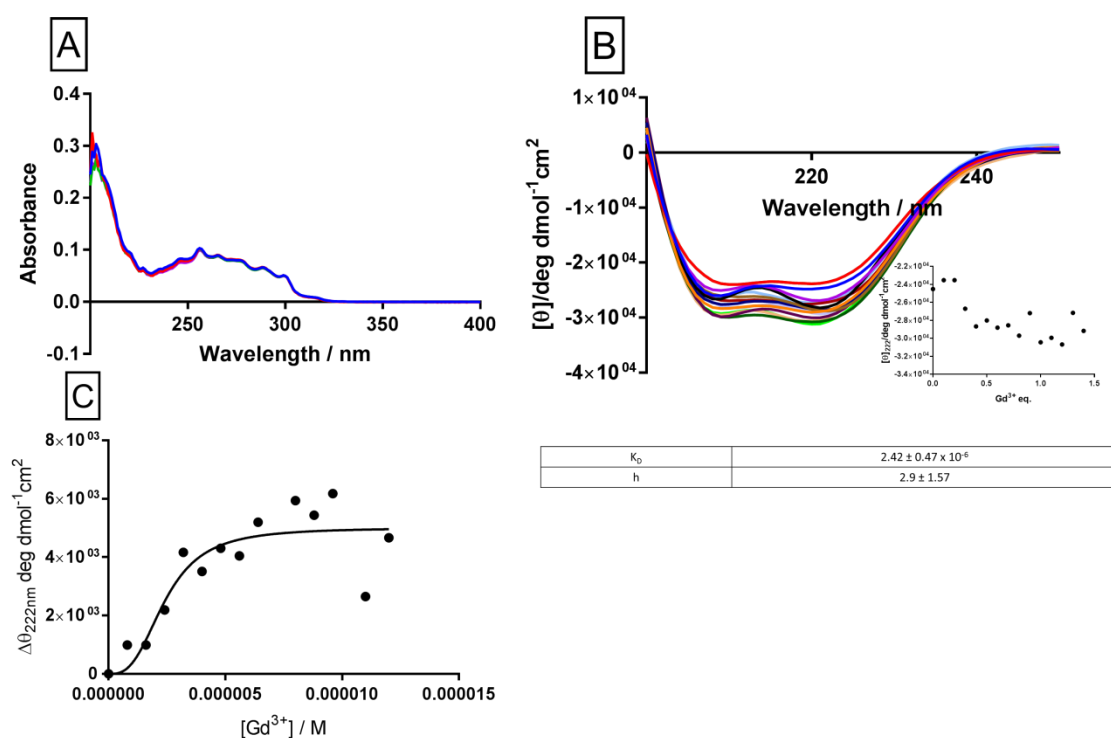


Figure 3.18 Characterisation of the behaviour of NB11 in response to Gd³⁺ addition. A) UV-Vis spectra of a 10 μM solution of Fmoc-6Bpa-OH titrated with increasing concentrations of GdCl₃. The spectra shows no change on addition of Gd³⁺. Spectra recorded at 25°C, in 100% v/v MeOH. B) CD spectra of the titration of GdCl₃ into an 8 μM solution of NB11. Inset- Plot of Δθ_{222nm} vs eq Gd³⁺. After 0.4 eq of GdCl₃ has been added, the value plateaus, but shows a scattered distribution at high concentrations of Gd³⁺. C) A Hill plot of Δθ_{222nm} against [Gd³⁺], used to determine a dissociation constant for NB11 with Gd³⁺. All samples recorded in 5mM HEPES buffer, 100mM NaCl, pH 7.0.

This is consistent with the formation of a 1:3 metal:peptide complex, as observed by Peacock and co-workers in their studies of the unmodified MB1-1 peptide.

The selectivity of both metal ions was then accounted for. With this information in hand, experiments to determine the mixed metal behaviour of the peptides were performed.

3.6.1 The effect of each binding site on the folding of the coiled coils

From the recorded literature behaviour of the MB peptides and the behaviour observed in the metal binding studies performed before, it was expected that the coordination of the different metal ion species would have different magnitudes of effect on the folding of the peptide (Figure 3.19).

This demonstrates the different effects of gadolinium and nickel ions on the peptide species. As demonstrated in the nickel characterisation section, nickel has little effect on already folded peptide species other than a small increase in the stability of the peptide in the melt.

The titration of gadolinium into the system increases the ellipticity by 15%, approaching the theoretical maximum helicity. The difference in coordination effects is explained by the location of each metal binding site. The coordination of the nickel ion is proposed to draw together the ends of the coiled coil with the N-terminal bipyridyl group. The lanthanide binding site, being in the hydrophobic core of the coiled coil, has a more substantial effect upon the peptide.

Changing the nickel:peptide ratio to 1:1 only increases the ellipticity to a very small degree. It is conceivable that the proximity of the lanthanide binding group to the bipyridine site in the peptide sequence (less than one heptad away) means the unfavourable clash of the lanthanide binding amino acids without the presence of a lanthanide ion discourages the formation of Ni[MB11]₃, while the addition of the lanthanide ion overcomes this destabilisation.

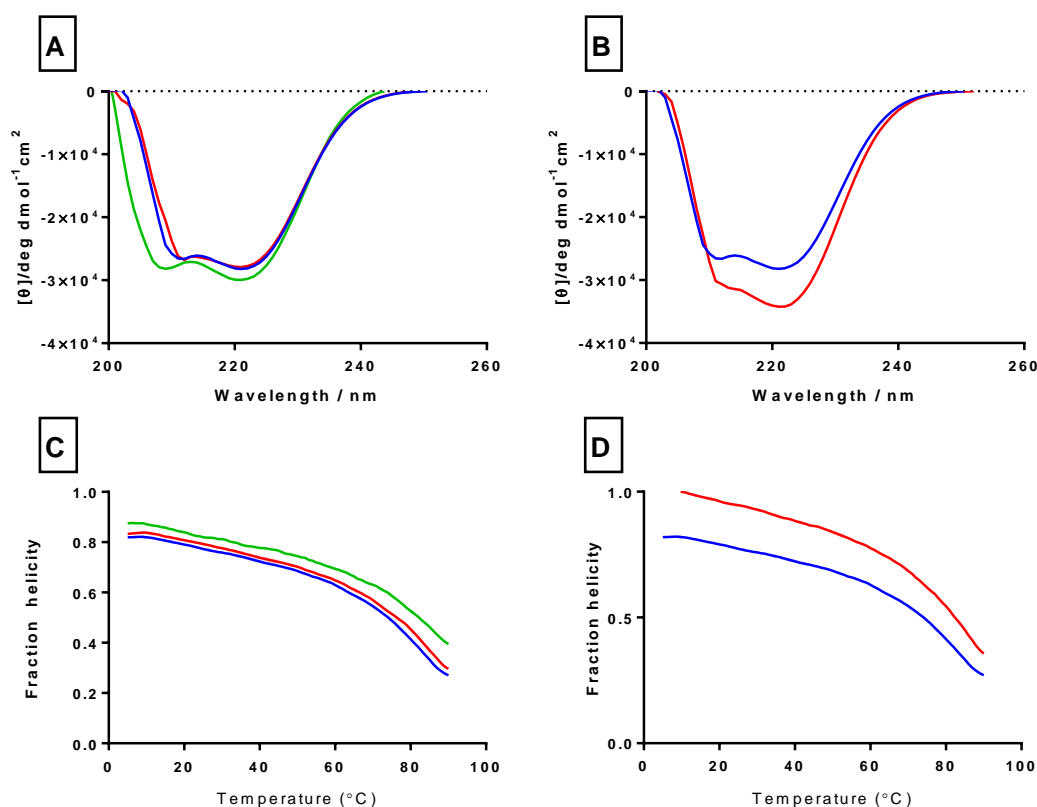


Figure 3.19 A & C)- Titrations & melts of 10 μM NB11 with NiCl₂ Blue- 10 μM NB11 Red- 0.3 eq NiCl₂ Green- 1.0 eq NiCl₂. 1 equivalent of nickel is required to fully stabilise the coiled coil system. The addition of Ni²⁺ to the system does not affect the melt profile of the species, but the value of θ_{222nm} at 90°C increases corresponding to the amount of Ni²⁺ titrated into the peptide solution. B&D)- Titrations & melts of 10 μM NB11 with GdCl₃ Blue- 10 μM NB11, Red- 0.3 eq GdCl₃. Gd³⁺ requires only 0.3 equivalents to stabilise coiled coil formation. All samples recorded in 5mM HEPES buffer, 100mM NaCl, pH 7.0.

It is interesting to note that the addition of 1 equivalent of nickel leads to a higher fraction folded at the melt end point than the 0.3 equivalents of gadolinium chloride.

The bipyridine coordination appears to have a stronger stabilising effect on the peptide that is formed, even if the peptide is more folded in the presence of gadolinium chloride initially.

The binding constant for Ni(II) is slightly higher than that determined for Tb (III), a lanthanide ion that displayed almost identical binding behaviour to gadolinium chloride in the work by the Peacock group (Table 3.9).

Table 3.9 Tabulated binding constants of NB11 with both Gd^{3+} and Ni^{2+} .

$K_{D_{Ni}}$	$1.97 \pm 0.23 \times 10^{-6}$
$K_{D_{Gd}}$	$2.42 \pm 0.47 \times 10^{-6}$

Metal-bipyridine coordination is stronger than the lanthanide-Asp/Asn coordination, which is to be expected. The Asp/Asn binding is strong due to the stabilising effects that lanthanide coordination has on the peptide sequences, and the system is set up to strongly favour the interaction, but the nickel-bipyridine coordination has these advantages as well as a contribution from the chelate effect.

3.6.2 1:1 nickel: gadolinium competition in 1:3 metal: peptide systems

The first set of experiments established the behaviour of the two metal ions in direct competition with each other at the same concentration. Attention was then turned to their behaviour in mixtures with each other. These data immediately show two clear distributions in the folding and stability of the peptide species (Figure 3.20).

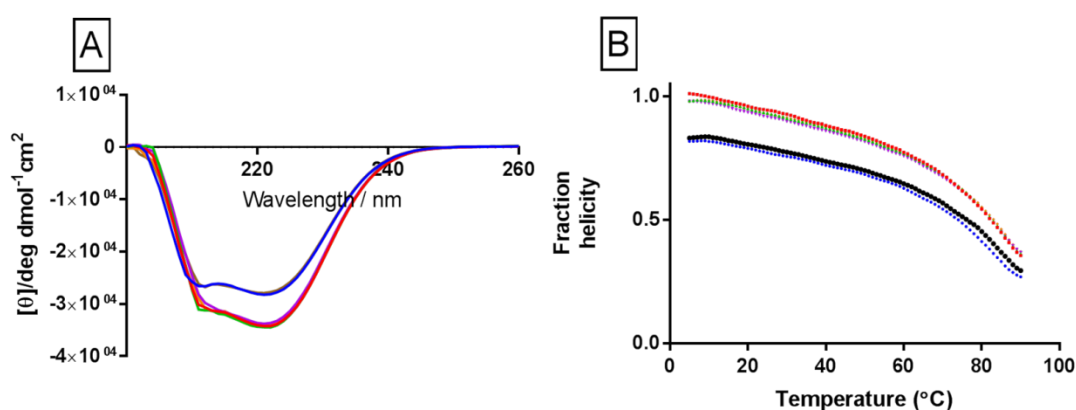


Figure 3.20 A) CD spectra of the 1:1 competition experiments with nickel and gadolinium. Blue -10 μM NB11, Red- 0.3 eq $GdCl_3$ Purple- 0.3 eq $NiCl_2$, equil., then 0.3 eq $GdCl_3$ Green- 0.3 eq $GdCl_3$, equil., then 0.3 eq $NiCl_2$ Brown- 0.3 eq $NiCl_2$, Orange- 0.3 eq $NiCl_2$ and $GdCl_3$ simultaneously. All samples recorded in 5mM HEPES buffer, 100mM NaCl, pH 7.0. All samples containing 0.3 eq Gd^{3+} demonstrate identical ellipticity. B) Thermal melts of the 1:1 competition experiments with nickel and gadolinium. Blue -10 μM NB11, Red- 0.3 eq $GdCl_3$ Purple- 0.3 eq $NiCl_2$, equil., then 0.3 eq $GdCl_3$ Green- 0.3 eq $GdCl_3$, equil., then 0.3 eq $NiCl_2$ Brown- 0.3 eq $NiCl_2$, Orange- 0.3 eq $NiCl_2$ and $GdCl_3$ simultaneously. All samples recorded in 5mM HEPES buffer, 100mM NaCl, pH 7.0. All of the samples containing 0.3 eq of Gd^{3+} maintain a higher level of helicity over the temperature ranges shown, with a shallower melt profile.

The apo-peptide, and 0.3 eq Ni^{2+} peptide display very similar behaviour, while the addition of 0.3 equivalents of Gd^{3+} in all experiments means the peptide becomes almost completely folded, with the appropriate melt traces and absorption spectra to demonstrate this. The melt profiles for any of the experiments containing 0.3 equivalents of Gd^{3+} are all very close to identical, indicating that the dominant species in any of these experiments is $\text{Gd}(\text{MB11})_3$, with no mixed metal coordination. The UV spectra for the folded peptide species shows:

At equivalent concentrations, the gadolinium binding dominates the structure of the peptide species. The staggered additions were intended to demonstrate whether the addition of one metal type could prevent the binding of the second metal species, and in this case it appears the peptide has simply formed the most stable $(\text{M})[\text{peptide}]_3$ species possible. The addition of 0.3 equivalents of Ni^{2+} has not prevented the binding of the lanthanide ions after this, something that is clearly indicated by the molar ellipticity of the sample.

When titrated by itself, 0.3 equivalents of Ni^{2+} has very little effect on the folding or stability of the peptide, so the next step is to increase the equivalents of Ni^{2+} to the point where it has a significant positive effect on the peptide, as we have seen before at 1 equivalent.

3.6.3 1:0.33 nickel: gadolinium competition in metal: peptide systems

After the direct competition experiments, investigations turned to the effect on the system if the equivalents of nickel were increased. Two questions were the main source of interest:

- 1- Can the peptide become more folded than the values obtained with 0.3 eq Gd^{3+} ?
- 2- Can the gadolinium effects be blocked by Ni^{2+} ?

The addition of 1 equivalent of NiCl_2 has a more pronounced effect on the folding of the peptide in the mixed systems (Figure 3.21). The folding of the system increases, and the melt profile is less shallow. The mixed metal experiments show the formation of a system that is less folded than the $\text{Gd}(\text{NB11})_3$ species. At 90 °C it maintains a higher helicity than the gadolinium species. This indicates the 1.0 equivalent of NiCl_2 is substantially increasing the stability of the peptide, even beyond that caused by the binding of 0.3 equivalents of GdCl_3 .

In experiments where 1.0 eq of Ni^{2+} is added, $\theta_{222\text{nm}}$ remains level at 83% helicity. This illustrates the dominant structural effect on the peptide in these conditions is the

contribution of metal binding to the bipyridine. The simultaneous addition of both 1.0 eq. Ni^{2+} and 0.3 eq Gd^{3+} results in a spectra resembling the pure gadolinium coordinated peptide.

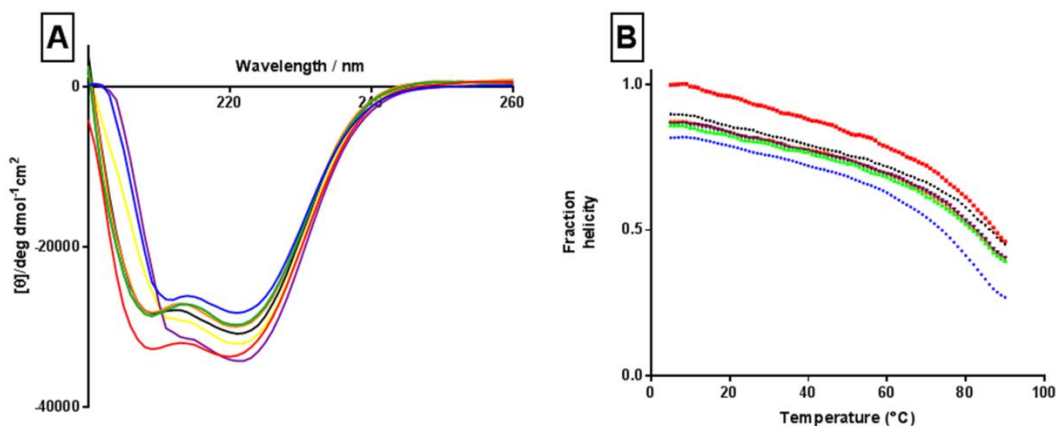


Figure 3.21 CD titrations (A) and melts (B) from the competitive binding experiments between 1.0 eq NiCl_2 and 0.3 eq GdCl_3 . All samples measured in 5mM HEPES buffer, 100mM NaCl, pH 7.0. Blue- 10 μM NB11, Green-1.0 eq NiCl_2 , equil., 0.3 eq GdCl_3 Orange- 1.0 eq NiCl_2 , Purple-0.3 eq GdCl_3 , Black- 1.0 eq NiCl_2 & 0.3 eq GdCl_3 simultaneously Red- 1.0 eq NiCl_2 and GdCl_3 simultaneously Yellow- combined average of the 1.0 eq NiCl_2 and 0.3 eq GdCl_3 . The addition of 1.0 eq Ni^{2+} stabilises the formation of the coiled coil system, and decreases the effect of 0.3 eq Gd^{3+} in these systems.

The addition of Gd^{3+} to peptide solutions containing 1.0 eq Ni^{2+} increases the helicity of the peptide at 90 $^{\circ}\text{C}$ to greater than that observed for peptides coordinated to each metal ion independently. These two combined observations suggest a system where the structure of the peptide is dictated by Ni^{2+} , but the presence of Gd^{3+} increases the stability of the coiled coil.

The cooled system after a melt was carried out shows no change in ellipticity or the profile of the spectra. It was possible that unfolding the peptide would lead to an increase in the ellipticity after melting, as the degradation of the coil structure might mean that the lanthanide binding site was no longer blocked off from binding the lanthanide ions in the solution. This would mean the peptide refolds to the higher ellipticity observed with experiments when 0.3 equivalents of GdCl_3 can bind freely. The structure formed in this mixture is not the kinetic product resulting from the rate of nickel ion binding being higher than the rate of gadolinium binding.

Fluorescence experiments can be used to determine the dual metal binding of the system. When terbium is titrated into the peptide system, the coordination of the peptide sensitises the terbium and generates characteristic emission spectra with peaks at 490, 545, 585, 620, and 650 nm. Nickel binding can be monitored with the change in the

bipyridine UV spectra, where the presence of a peak at 310 nm indicates the nickel is still bound to the peptide.

As the system in question was the mixed 1.0 eq Ni^{2+} /0.3 Gd^{3+} species, this was subject to a titration experiment to determine the effect of terbium on the system (Figure 3.22).

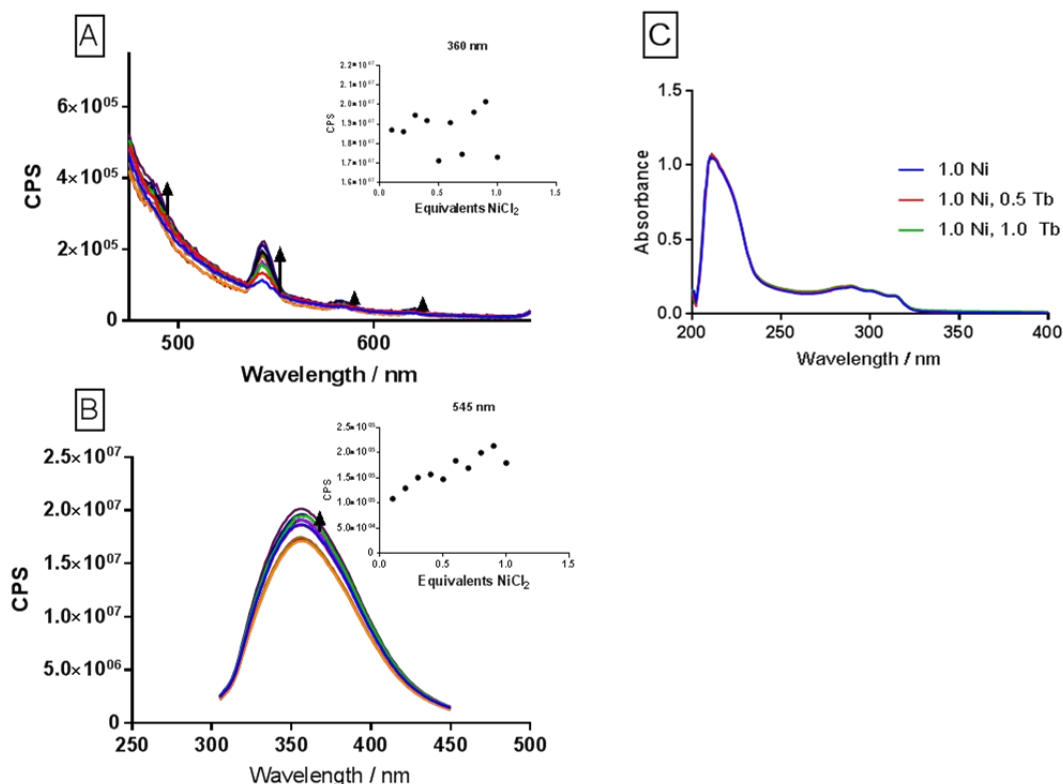


Figure 3.22 A) Terbium emission spectra and plot (inset) upon titration of TbCl_3 into 30 μM peptide monomer/1.0 eq Ni^{2+} for NB1-1. All spectra recorded at 293 K in 5mM HEPES buffer pH 7.0. $\lambda_{\text{exc}} = 280$ nm. Spectra recorded with a 350 nm cut off filter. B) Tryptophan emission spectra and plot (inset) upon titration of Tb(III) into 30 μM peptide monomer for NB1-1. $\lambda_{\text{exc}} = 280$ nm. Each system shows increased fluorescence with increasing terbium concentration. C) UV spectrum of 30 μM 1.0 eq Ni species titration with Tb^{3+} . The spectrum remains unchanged even at 1.0 eq Tb, indicating the terbium is not disrupting nickel binding in this system. All samples recorded at 293 K in the presence of 5 mM HEPES buffer, 100mM NaCl, pH 7.0.

This increase in fluorescence indicates terbium binding to the peptide system. The UV spectra of the system at 0, 0.5 and 1.0 eq Tb^{3+} shows no change in the bipyridine system, and the expected nickel-bipy peaks are present, indicating that both metals are coordinated to the system. The tryptophan emission increases with increasing terbium addition, but there are several outlying points past 0.5 equivalents of terbium. Peacock and co-workers note that the addition of Tb^{3+} to their MB11 peptide results in decreasing terbium fluorescence.

These combined data provide evidence for the presence of both metals in the peptide system. The CD data of the mixed metal system indicates a distortion in the peptide

system, as the ellipticity of the system is the same as 1.0 eq Ni^{2+} itself. There is spectroscopic evidence to show the presence of both metals in the peptide system.

The titration curve of the terbium fluorescence shows a diffuse binding curve, consistent with poor terbium binding, but the fluorescence increases as expected. The lower than expected ellipticity can be assigned to 1.0 equivalent of nickel fixing the distorted structure of the peptide species in place, and the terbium site is less defined and so shows a broader binding curve.

Having established this behaviour in the 1.0 equivalent Ni^{2+} system, a very brief experiment with the apo and 0.3 eq Ni^{2+} system was conducted (Figure 3.23).

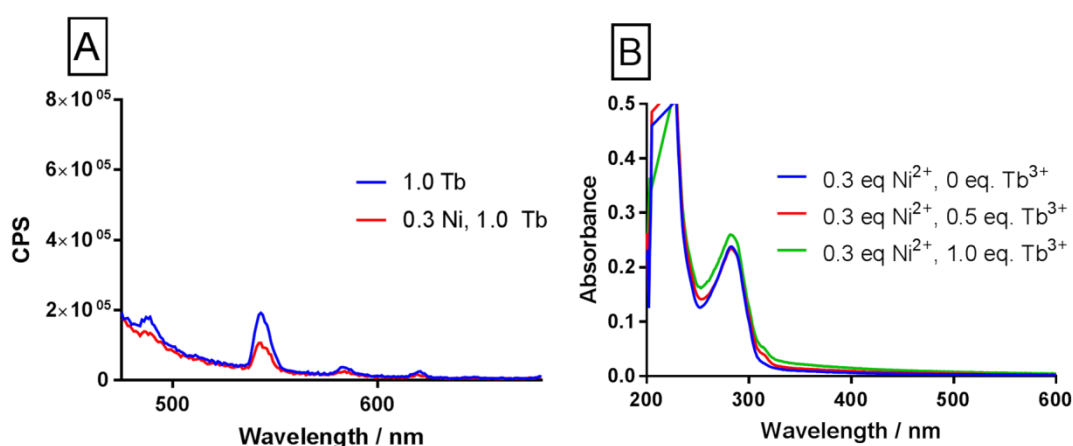


Figure 3.23 A) Fluorescence spectra of 30 μM NB11 in the presence of terbium, with emission peaks at 490, 545, 585, and 620 nm. Both species demonstrate terbium binding, although this is diminished in the presence of 0.3 equivalents of nickel. B) UV spectra of the 0.3 eq Ni species. The absorbance increases very slightly in the presence of increasing terbium, but the weak peak at 310 nm shows nickel is still binding to the system. All samples recorded at 293 K in the presence of 5 mM HEPES buffer, 100mM NaCl, pH 7.0.

Both systems display fluorescence, and the 0.3 eq Ni^{2+} system shows metal binding with the UV spectrum of the peptide system. Time constraints prevented further investigation of the NB11 mixed metal system, but it is an interesting system for further investigation without the need for the distorted 1.0 eq Ni^{2+} system.

To ensure the validity of our results, the oligomerisation state of the mixed metal species was investigated using Ultra-Analytical centrifugation (AUC) (Table 11). The peptide species are on the limit of detection for the system available to us.

Table 3.10 Tabulated AUC data for the metallated species of NB11. Samples recorded at 60 μM monomer concentration at 60k RPM. The addition of any metallated system results in an increase in the proportion of trimer observed.

Species	Weight average molar mass/kDa	Theoretical maximum weight average molar mass / kDa	Proportion trimer complex (%)
NB11 Apo	9.8	12.7	77
0.3 Ni	12.2	12.76	95
1.0 Ni	14.1	12.89	109
0.3 Ni / 0.3 Gd	14.5	12.92	112
1.0 Ni / 0.3 Gd	11.3	13.05	86.6

These results show that the coordination of 0.3 eq Ni^{2+} , and the 1.0/0.3 eq $\text{Ni}^{2+}/\text{Gd}^{3+}$ system increased the proportion of trimer complex present in solution. 1.0 eq Ni^{2+} and 0.3 eq $\text{Ni}^{2+}/0.3$ eq Gd^{3+} gave results reporting a higher than maximum trimer formation, so represents a mixture with trimer formation present as well as other possible oligomers. The results are consistent with this metal coordination controlling the oligomerisation state of the complex, but were not useful in discriminating between the different metallated peptide systems.

3.6.4 Mixed metal behaviour of NB-12

The NB-12 peptide is an isomer of the NB-11 peptide, with a one heptad translation of the lanthanide binding site towards the C-terminus of the peptide. In an uncoordinated peptide, this leads to a less folded peptide, due to the unfavorable interactions between the Asp and Asn side chains. This is clearly reflected by the ellipticity of the two peptides at the same concentrations (Table 3.11).

Table 3.11 Tabulated data for the change in $\theta_{222\text{nm}}$ with concentration for the NB11, NB12 and NB00 at three different concentrations.

Peptide	10 μM	50 μM	100 μM
NB00	-20,474	-20,837	-23,324
NB11	-27,894	-30,000	-30,000
NB12	-5502	-5293	-3503

NB12 is a very poorly folded peptide when compared to NB-11 and NB-00. Coiled coil formation is not favoured, and it is necessary to reach very high concentrations before we see the shift to a coiled coil. It is clear at 125 μM , the peptide takes a more typical coiled coil profile, but even at this concentration it is only 43% folded (Figure 3.24).

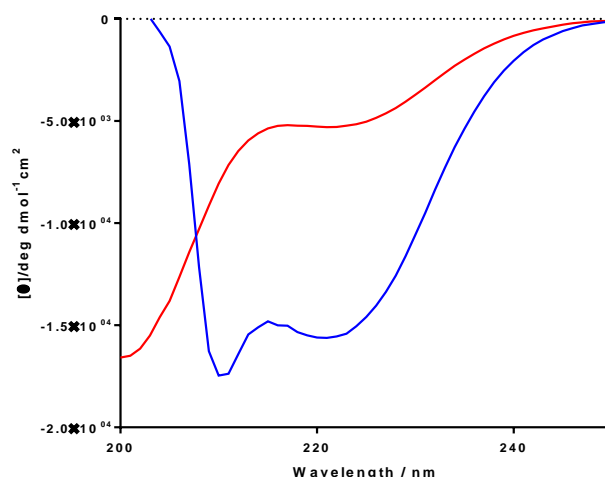


Figure 3.24 Concentration dependent effects on the folding of NB12, at 50 μM (red) and 125 μM (blue). The high ellipticity at 125 μM is consistent with the anomalous result observed in the concentration depended effects observed in Figure 9C. All samples recorded in 5 mM HEPES buffer, 100 mM NaCl, pH 7.0.

This reluctance to forming a coiled coil presented interesting possibilities for the formation of the mixed metal coiled coil. If we compare the same conditions demonstrated in the competitive binding experiments above, the immediate differences in the way the system behaves are clear (Figure 3.25).

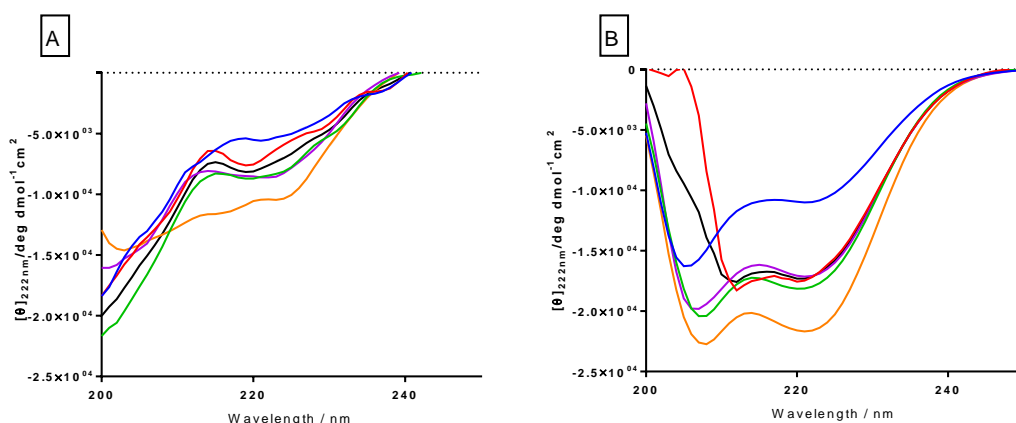


Figure 3.25 A) Titrations of 10 μM NB12 with 0 equiv metal ions (blue), 0.3 equiv NiCl_2 (red), 0.3 eq GdCl_3 (green), 1.0 equiv NiCl_2 (purple), 0.3 eq GdCl_3 and NiCl_2 (orange) simultaneously and a combined average of 0.3 Ni and 0.3 Gd separately (black). B) Cooperative binding of NB12 to gadolinium and nickel ions. All samples recorded in 5 mM HEPES buffer, 100 mM NaCl, pH 7.0. Blue- 125 μM NB12 Red- 0.3 eq NiCl_2 Green- 1.0 eq Ni Purple- 0.3 eq GdCl_3 Orange- 0.3 eq Gd & 1.0 eq Ni simultaneously Black- average spectra for 0.3 Ni & 0.3 Gd separately. All samples recorded in 5 mM HEPES buffer, 100 mM NaCl, pH 7.0.

The NB12 species becomes as folded in the presence of 1.0 equivalent of Ni^{2+} as it does in the presence of 0.3 equivalents of Gd^{3+} . This suggests that the pinching together of the three coil ends has more of a stabilizing effect on the peptide than the balancing of the repulsive Asp-Asn charges within the core of the peptide.

The simultaneous addition of 0.3 equivalents Gd^{3+} and Ni^{2+} cause the peptide to become well folded. The contribution of the two metals simultaneously is greater than the combined increase on the addition of each separately. It becomes clear that these effects are not concentration dependent, but reflect the design and properties of the peptide itself. The melt profiles of the 10 μM mixed species (not shown, appendix figure x) showed limited change between the different metallopeptides and the apo-peptide. Characterisation of NB12 was halted after evidence of its further assembly into higher order structures, which was pursued to characterise the actual species present in these samples.

3.7 Conclusions

The behaviour of three new peptide systems with 6Bpa included at the N-terminus have been investigated at different concentrations, comprising of one control peptide (NB00), one peptide containing a destabilising lanthanide binding group (NB11), and one peptide containing a lanthanide binding group (NB12) that does not affect the folding of the peptide.

The behaviour of the peptides studied was far more consistent when the CCC had been passed, and below this concentration the peptide systems tend to behave unpredictably. The results indicate that the metal binding site in this system is predominantly pre-assembled, both in the case of the known Ln binding site as demonstrated by Peacock and coworkers, and in the new bipyridyl binding site engineered at the N-terminus of the peptide. Any metal binding behaviour here can be used to impart functionality rather than structural control. The titration of metal ions into the system does have a clear stabilising effect on the peptide however (Figure 3.26).

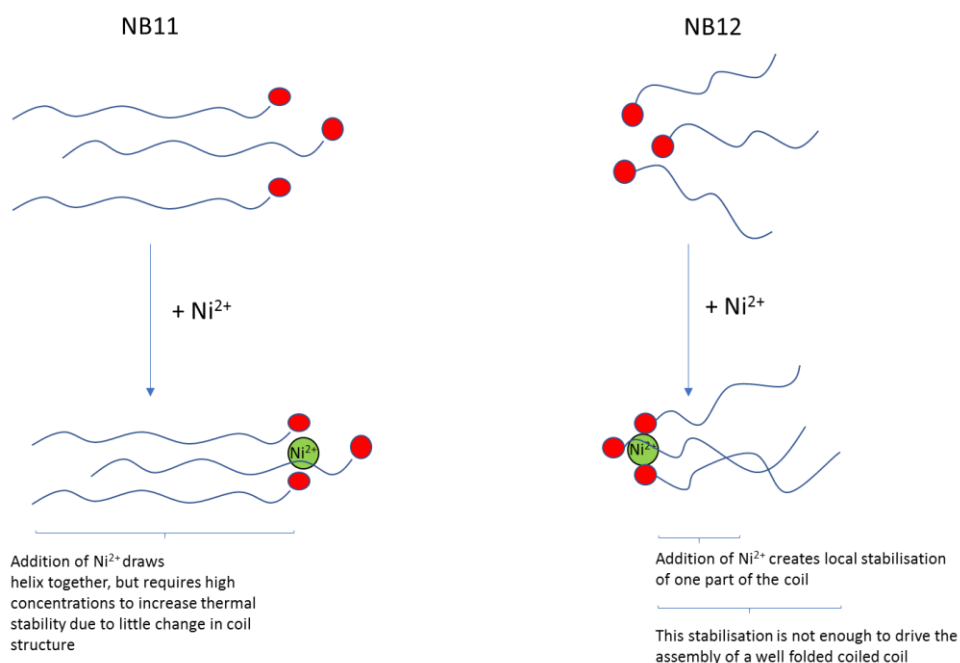


Figure 3.26 Cartoon representation of the different behaviours of NB11 (left) and NB12 (right) on the addition of Ni^{2+} ions.

NB12 was found to increase its folding and thermal melt stability as metal ions which coordinate to the N-terminal bipyridine residue are titrated in. The ellipticity does not increase to the levels demonstrated by other isomeric systems with higher folding, which indicates the local stabilisation of one segment of the peptide is not sufficient to overcome the destabilisation of another segment, although the overall organisation of the peptide is increased.

NB11 can still respond to the metal binding event at the N-terminus, increasing the folding of the peptide to higher levels than the apo-peptide. The melt behaviour increases fractionally with the titration of metal ions into the system, but it requires extremely high equivalents of metal ions to have a significant effect on the melt profile.

The incorporation of a metal binding group into a coiled coil system and the subsequent binding of metal to it is insufficient to guarantee the increased folding and stability of this family of coiled coils, but they remain a useful way to incorporate functionality into the peptide system.

As a conclusion to these studies, we demonstrate the effect that a shift of one heptad can have on the metal binding properties of a peptide system. NB11, the most helical coiled coil of the series synthesised, can bind both lanthanide and transition metal ions. The ratio of these metal ions used controls the structure of the peptide species formed but

does not exclude both metal ions from binding. NB12, the least helical coiled coil of the series, can bind two different types of metal ion cooperatively, where the combined increase in helicity is greater than the combined separate contributions of the different metal ions. This metal binding behaviour is observed to be the same at different concentrations of peptide, demonstrating it is affected by the ligands available to bind the metal ions more than the folded state of the peptide systems in question. However, NB12 proceeds to assemble into higher order fibrous structures, so it was discounted as a useful mixed metal species.

3.8 References

- (1) Lombardi, A.; Summa, C. M.; Geremia, S.; Randaccio, L.; Pavone, V.; DeGrado, W. F. *Proc. Natl. Acad. Sci. U. S. A.* **2000**, *97*, 6298.
- (2) Kaplan, J.; DeGrado, W. F. *Proc. Natl. Acad. Sci. U. S. A.* **2004**, *101*, 11566.
- (3) Shiga, D.; Funahashi, Y.; Masuda, H.; Kikuchi, A.; Noda, M.; Uchiyama, S.; Fukui, K.; Kanaori, K.; Tajima, K.; Takano, Y.; Nakamura, H.; Kamei, M.; Tanaka, T. *Biochemistry* **2012**, *51*, 7901.
- (4) Martin de Rosales, R. T.; Faiella, M.; Farquhar, E.; Que, L., Jr.; Andreozzi, C.; Pavone, V.; Maglio, O.; Nastri, F.; Lombardi, A. *JBIC, J. Biol. Inorg. Chem.* **2010**, *15*, 717.
- (5) Ghadiri, M. R.; Case, M. A. *Angewandte Chemie-International Edition in English* **1993**, *32*, 1594.
- (6) Rossi, P.; Felluga, F.; Tecilla, P.; Formaggio, F.; Crisma, M.; Toniolo, C.; Scrimin, P. *J. Am. Chem. Soc.* **1999**, *121*, 6948.
- (7) Cheng, R. P.; Fisher, S. L.; Imperiali, B. *J. Am. Chem. Soc.* **1996**, *118*, 11349.
- (8) Alies, B.; Wiener, J. D.; Franz, K. J. *Chemical Science* **2015**, *6*, 3606.
- (9) Berwick, M. R.; Slope, L. N.; Smith, C. F.; King, S. M.; Newton, S. L.; Gillis, R. B.; Adams, G. G.; Rowe, A. J.; Harding, S. E.; Britton, M. M.; Peacock, A. F. A. *Chem. Sci.* **2016**, *7*, 2207.
- (10) Berwick, M. R.; Lewis, D. J.; Jones, A. W.; Parslow, R. A.; Dafforn, T. R.; Cooper, H. J.; Wilkie, J.; Pikramenou, Z.; Britton, M. M.; Peacock, A. F. A. *J. Am. Chem. Soc.* **2014**, *136*, 1166.
- (11) Gochin, M.; Khorosheva, V.; Case, M. A. *J. Am. Chem. Soc.* **2002**, *124*, 11018.
- (12) Ghadiri, M. R.; Soares, C.; Choi, C. *J. Am. Chem. Soc.* **1992**, *114*, 825.

Chapter 4: Fibre formation

4.1 Introduction and Background

The ability to construct larger assemblies from coiled coil subunits finds applications in both fundamental science as a natural extension of investigating the design rules for protein assembly, and it is of interest in the development of new nanomaterials.

α -helical coiled coils are highly represented in natural fibrous protein structures. Coiled coil proteins found in muscle fibres (tropomyosin) and those used to form intermediate filaments in cytoskeletal structures both exist as fibres.^{1,2}

Using these systems as inspiration designed coiled coil systems have been shown to assemble into more ordered fibres.^{3,4} The first report of a fully assembled designed coiled coil fibre was from Woolfson and coworkers in 2000.⁵ A dimeric coiled coil that forms a staggered sticky-ended heterodimer was used to generate fibres (Figure 4.1).



Figure 4.1 Cartoon representation of the assembly of sticky ended coiled coils to form fibres. Complementary charges on the coiled coils cause the fibres to align longitudinally. Derived from a diagram displayed in Woolfson and co-workers.⁵

Several groups successfully reported the formation of coiled coil fibres, and design rules for these fibres began to emerge, similar to the rules defined for the coiled coils themselves after the first successful example.⁶ Eisenberg and co-workers particularly demonstrated it was possible to generate domain swapped fibres using principles from protein design.⁷ The properties of peptide fibres can be controlled by varying the electrostatic properties of coiled coil side chains, leading to fibres of varying stiffness and thickness.⁸ Woolfson wrote an in depth review, discussing the generation of fibrous biomaterials from collagen –like and α -helical peptides that covered the state of the field in 2009.⁹ Since then, coiled-coil fibrous systems have been used to assemble a range of higher order structures, such as hydrogels or even cage structures (See Woolfson 2009 for hydrogels, 2013 for cages formed from coiled coils, and 2015 for peptide nanotubes).¹⁰⁻¹²

The common driving force of fibre assembly from coiled coil peptides is the complementary nature of charges incorporated in the peptide backbone, which causes them to assemble end to end with other subunits. The formation of fibres occurs because the assembled structure being more stable than the discrete coiled coil oligomers.⁵

The formation of salt bridges from charged amino acids together with the burial of hydrophobic residues are the controlling forces in the formation of higher order assemblies. If hydrophobic residues cannot be buried in the coiled coil core, aggregation occurs since the hydrophobic regions assemble to reduce their exposure to water molecules.

Hartgerink and co-workers reported a fibre system that relies on the formation of an aromatic core, based on tryptophan, phenylalanine and tyrosine residues, which they found also assembled into hydrogels on the introduction of phosphate counter-ions in the buffer solution.¹³ The burial of the hydrophobic residues in the core of the fibrous structure resulted in more uniform fibres, straight and unbranched, but the introduction of the polar hydroxyl group of tyrosine disrupted the core, leading to fibres which display branching and breakages.

Synthetic fibrous structures are composed of smaller repeating units, rather than existing as a single unbroken chain. One aspect of this regular repeating unit is that the assembled coiled coils themselves can be treated as one repeating unit.

4.1.1 Controlled disassembly of fibrous structures

The formation of protein fibres in natural systems requires corresponding mechanisms for their disassembly. The aggregation of protein systems in the brain is one of the most popular hypotheses for Alzheimer disease, so investigating mechanisms for disassembly of higher order structures is of clear interest. The control of the fibrous nature of systems is desirable, as this allows for the generation of fibre-based switches and “smart” systems.

van Hest and co-workers reported a peptide fibre system into which they incorporated p-nitrophenylchloroformate as a photolabile linker into amphiphilic peptide fibres. The fibre systems assemble with no interference from the linker, but on UV irradiation the fibres disassemble completely. The disassembly is irreversible, but it presents a possible mechanism for the control over the presence of fibres.^{14,15}

Chmielewski and co-workers functionalised a model collagen fibre with bipyridine groups.¹⁶ They found this system formed fibres on the addition of Fe^{2+} , as the fibres arranged radially around the metal-bipyridine complex. Further study of these systems revealed that a change in the order of addition affected the morphology of the supramolecular peptide structures. If the fibres self-assemble on the presence of metals, the system forms linear aggregations of fibres. On assembly of the apo-peptide, the

peptide forms curved disks, and the addition of Fe^{2+} changes the morphology and forms hollowed spheres. Addition of EDTA to the metal-peptide spheres resulted in the formation of disks which resemble those formed by the apo-peptide.¹⁷

During the development of the hetero-metallic coiled coils, we studied how the position of the gadolinium binding site affected the stability of the coiled coil trimer. Interestingly, the NB12 sequence resulted in a particularly destabilised coiled coil structure. It was proposed that if fibres could be formed from the apo-peptides, the addition of Ni^{2+} , Gd^{3+} and combinations thereof would have different effects on the fibres formed.

This chapter presents circular dichroism and electron microscopy data supporting the formation of blunt ended coiled coil fibres from the NB12 sequence. Interestingly, these fibres seem to respond to metal ion coordination by apparently reverting to a soluble state, implying the existence of a dynamic equilibrium between coiled coil oligomer and fibre that can be controlled by metal chelation.

4.2 Formation of microscale fibres of NB12

Circular dichroism characterisation of the NB12 coiled coil indicates that a folded structure is formed at 125 μM and above. A 125 μM solution of NB12 was left to self-assemble over a week, and the change in circular dichroism spectra was monitored (Figure 4.2).

The solution showed signs of fibre formation at 24 hours after mixing. There was an immediate reduction of 15,000 $\text{deg dmol}^{-1} \text{cm}^2$ in the 208 nm signal at 24 hours, and the 222 nm signal continued to decrease in intensity after 48 hours.

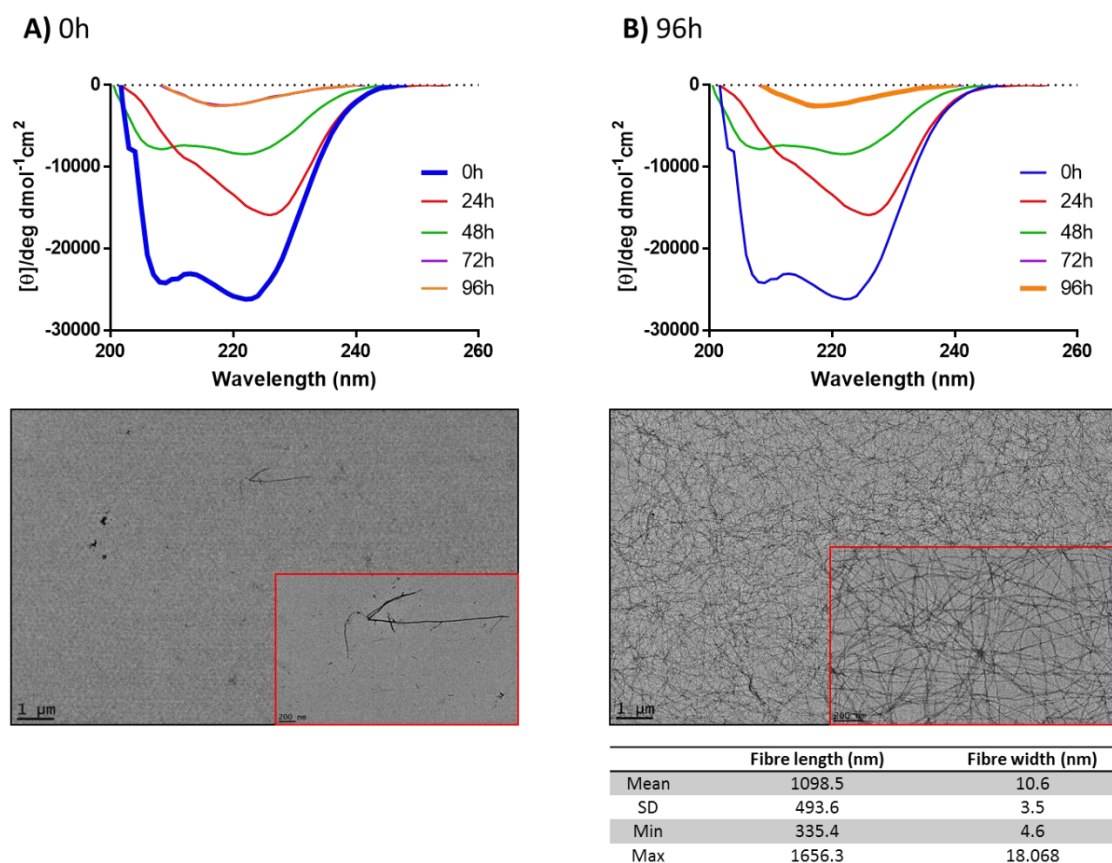


Figure 4.2 Rates of fibre formation and characterisation of NB12 at 125 μ M with circular dichroism and electron microscopy. A) A 125 μ M solution of the NB12 peptide and EM image of the peptide solution. The CD spectrum of the peptide shows the characteristic coiled coil structure. Transmission electron micrographs of 125 μ M NB12 stained with 1% uranyl acetate. Low-magnification image (scale bars: 1 μ m); (inset): high-magnification images (scale bar: 200 nm). A solitary fibre can be observed, indicating fibre formation on solution mixing. B) 125 μ M solution of NB12 after 96 hours. Signal intensity has dropped significantly and the 222 nm minima has almost completely disappeared, indicative of aggregation and more specifically fibre formation. Transmission electron micrographs of matured 125 μ M NB12 stained with 1% uranyl acetate. Low-magnification image (scale bars: 1 μ m); (inset): high-magnification images (scale bar: 200 nm). The peptide has assembled into a large fibrous network of single fibres which display no branching or breaks. All CD spectra recorded in 5 mM HEPES, 100 mM NaCl, pH 7.0. All spectra recorded at 25°C. For all fibre measurements, n=30 where possible. Length of fibres measured from visible fibre termini and tracked along the resulting fibre with use of the freehand tool in ImageJ.

This can be interpreted as the removal of peptide from the solution during assembly into larger structures, reducing the concentration of coiled coils in solution. Interestingly, these results agree with the MALLS data where after centrifugation before measurement, the NB12 peptide precipitated out from solution leaving only a very small amount of monomer. Dilution of the starting 125 μ M NB12 solution to 10 μ M, resulted in the retention of fibre structures. Thinning of the fibres after dilution suggests the

existence of an equilibrium that is concentration dependent (Figure 4.3).

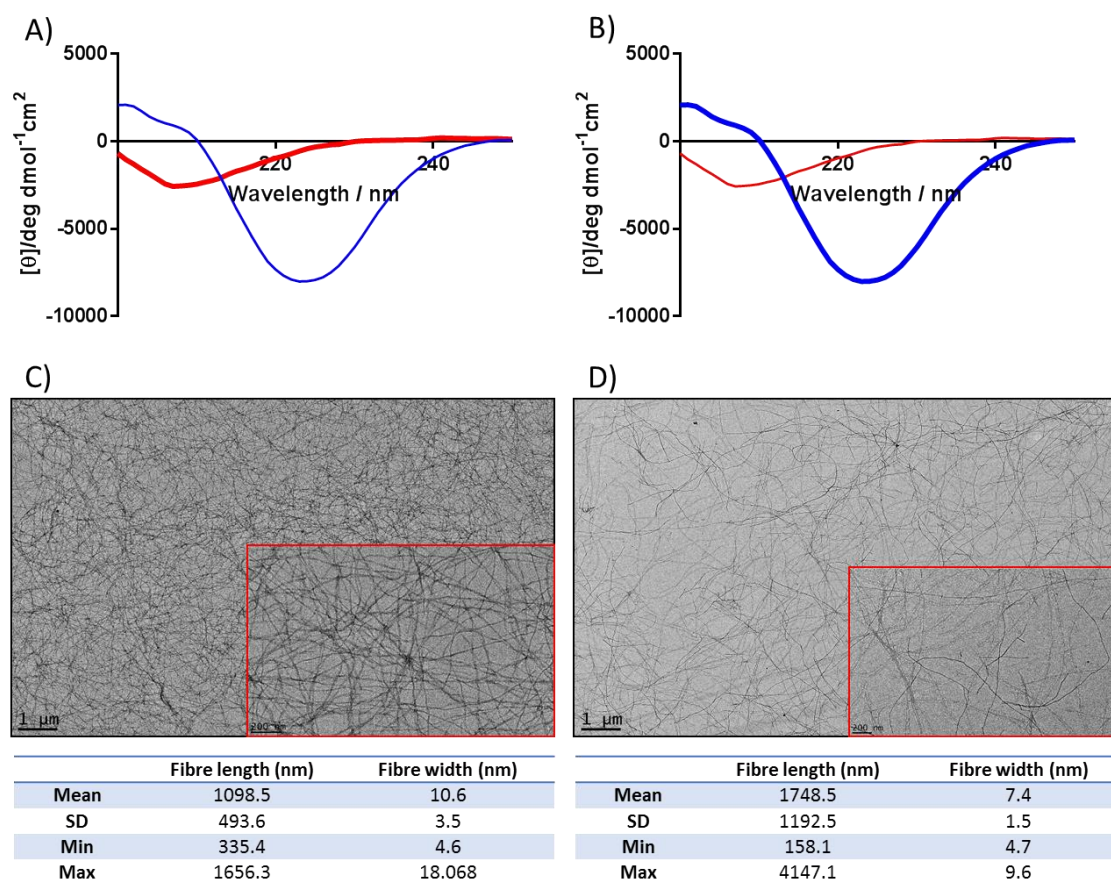


Figure 4.3 Dilution of 125 μM fibrous solution to 10 μM , monitored by circular dichroism and electron microscopy. A) 125 μM solution of NB12 after 96 hours. Signal intensity has dropped significantly and the 208 nm minima has almost completely disappeared, indicative of aggregation and more specifically fibre formation. Transmission electron micrographs of matured 125 μM NB12 stained with 1% uranyl acetate. Low-magnification image (scale bars: 1 μm); (inset): high-magnification images (scale bar: 200 nm). The peptide has assembled into a large fibrous network of single fibres which display no branching or breaks. All CD spectra recorded in 5 mM HEPES, 100 mM NaCl, pH 7.0. All spectra recorded at 25°C. B) 10 μM solution of NB12 fibres after dilution from A. The signal intensity has increased compared to the 125 μM sample, and redshifted to 222 nm rather than 208. Transmission electron micrographs the diluted species stained with 1% uranyl acetate. Low-magnification image (scale bars: 1 μm); (inset): high-magnification images (scale bar: 200 nm). The fibrous network has become less dense compared to A but is still present. Some fibres show breaks or bent sections, but this may be due to mechanical stress from transfer between solutions and mixing. All CD spectra recorded in 5 mM HEPES, 100 mM NaCl, pH 7.0. All spectra recorded at 25°C. For all fibre measurements, $n=30$ where possible. Length of fibres measured from visible fibre termini and tracked along the resulting fibre with use of the freehand tool in ImageJ.

Having assembled fibres from coiled coil samples of the peptide and having matured a sample of 10 μM NB12 with no fibre formation observed, we were interested to investigate fibre formation at an intermediate concentration between where the peptide exists as monomers (10 μM), and one where trimer formation is favoured (125 μM). A 100 μM sample of NB12 was assembled over the course of a week and monitored by circular dichroism (Figure 4.4).

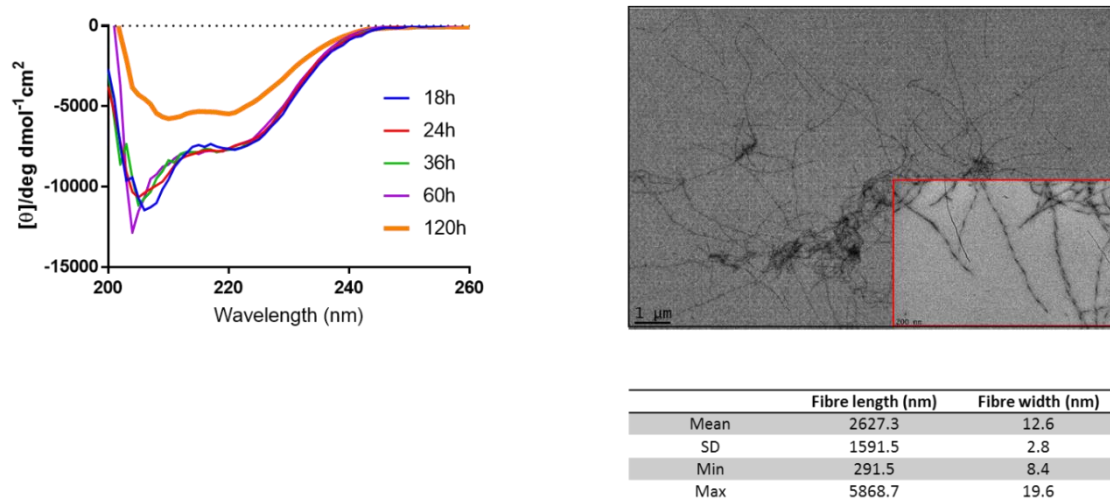


Figure 4.4 Rates of fibre formation and characterisation of NB12 at 100 μ M with circular dichroism and electron microscopy. CD spectrum of a 100 μ M solution of NB12 after 120 hours. Signal intensity has dropped significantly but the characteristic double minima of the system is still present. Transmission electron micrographs of matured 125 μ M NB12 stained with 1% uranyl acetate. Low-magnification image (scale bars: 1 μ m); (inset): high-magnification images (scale bar: 200 nm). The peptide has assembled into a large fibrous network of single fibres which display no bends or breaks but have aggregated into clumps. Striations within the peptide fibres can be observed, with the dark patches having a mean length of 48.1 ± 17.9 nm and the light patches a mean length of 98.9 ± 28.6 nm. All CD spectra recorded in 5 mM HEPES, 100 mM NaCl, pH 7.0. All spectra recorded at 25°C. For all fibre measurements, $n=30$ where possible. Length of fibres measured from visible fibre termini and tracked along the resulting fibre with use of the freehand tool in ImageJ.

This assembly reaction displayed a lag phase suggesting the peptide system assembles into seed structures before the longitudinal growth of fibres commences. In a solution of 125 μ M, the sample demonstrated a change in the spectra at 24 hours, but the spectra for the 100 μ M system remained largely unchanged until 120 hours had passed, and fibres were present (Figure 4.4).

The 100 μ M sample assembles to form thicker fibres than both the 125 μ M and 10 μ M solutions of fibres. In this sample, striations within the sample can also be observed. Regular alternating light and dark patches within the peptide can be seen, particularly in the highlighted high magnification image.

To establish if the propensity to form fibres correlated with coiled coil stability, NB11 was used as a control. A 500 μ M sample of NB11 assembled for 1 week displayed formation of very few and small fibres (Figure 4.5) supporting the idea that the destabilised nature of NB12 is necessary for the formation of fibres from this family of peptides. NB11 forms a well folded coiled coil, so there is no energetic stabilisation derived from the assembly of fibres.

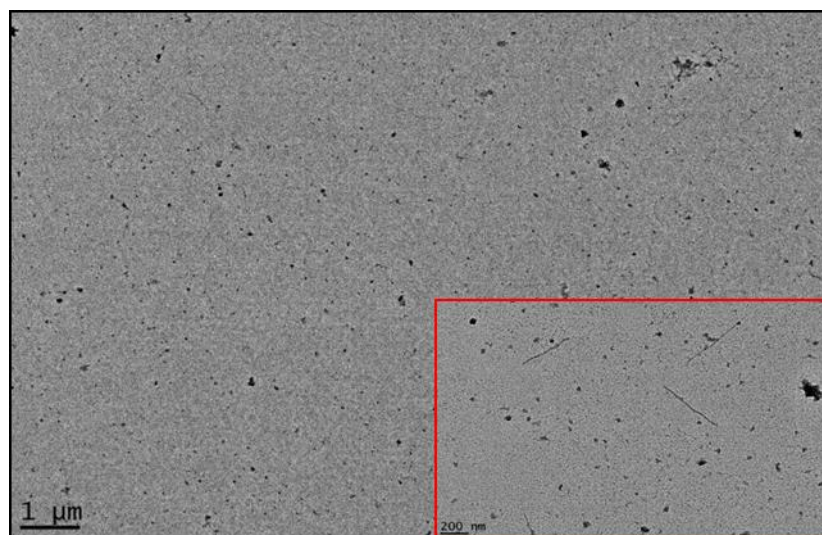


Figure 4.5 Limited fibre formation of NB11. Transmission electron micrographs of 500 μ M NB11 fibers, stained with 1% uranyl acetate. Low-magnification image (scale bars: 1 μ m); (inset): high-magnification images (scale bar: 200 nm). After 120 h, the systems begin to show the formation of small fibres. CD spectra omitted due to concentration of NB11 oversaturating the detector.

4.3 Metal-controlled fibre disassembly

A driving force behind fibre assembly by NB12 could be the bipyridyl moiety at the N-terminus of the peptide chain. The bipyridine unit could take part in stabilising π -stacking interactions which encourage fibre formation, as the hydrophobic residues associate to minimise their interaction with water. The poorly folded nature of the peptide allows for the freedom of movement in the bipyridyl chains to associate into an ordered structure, something not possible in the more ordered NB11 species.

This hypothesis could be easily tested by attempting fibre formation with the original MB12 sequence from Peacock and co-workers.¹⁸ Alternatively, solutions of metal ions shown to bind well to the peptides were titrated into a solution of the fibres to remove the hydrophobic/ π -stacking effect (Figure 4.6). Titration of metals in samples of assembled fibres resulted in disassembly of the fibre structures.

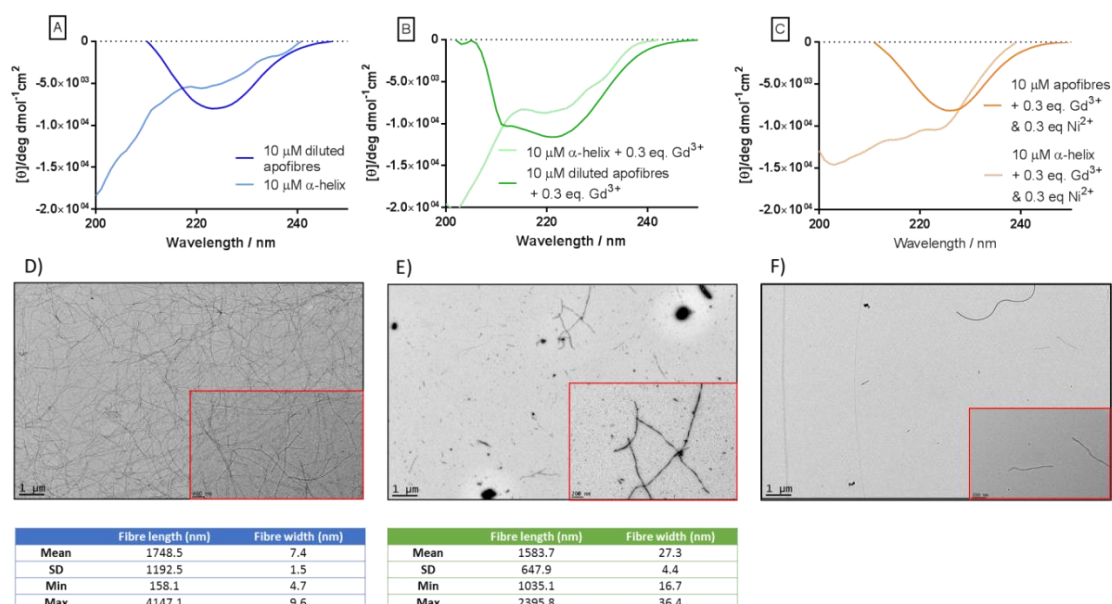


Figure 4.6. 10 μM fibre solutions treated with metal ions, monitored by circular dichroism and electron microscopy. A) Light blue- An unmaturred 10 μM sample of NB12 Dark blue- A 10 μM solution of NB12 fibres after dilution from a 125 μM solution of peptide fibres. The signal intensity has increased compared to the fresh 10 μM sample, and redshifted to 222nm rather than 208. Transmission electron micrographs the diluted species stained with 1% uranyl acetate. Low-magnification image (scale bars: 1 μm); (inset): high-magnification images (scale bar: 200 nm). The fibrous network is not as dense as that shown in Figure 3A. Some fibres show breaks or bent sections, but this may be due to mechanical stress from transfer between solutions and mixing. B) 10 μM solution of NB12 fibres after treatment with 0.3 eq GdCl_3 . Light green- a 10 μM fresh sample of NB12 treated with 0.3 eq GdCl_3 . Dark green- A 10 μM solution of NB12 fibres after dilution from a 125 μM solution of peptide fibres treated with 0.3 eq GdCl_3 . The signal intensity has increased compared to the fresh sample, and the characteristic double minima of a coiled coil is still present. Transmission electron micrographs the diluted species stained with 1% uranyl acetate. Low-magnification image (scale bars: 1 μm); (inset): high-magnification images (scale bar: 200 nm). The fibrous network has become less dense compared to A but is still present. Fibres have become shorter and thicker. Striations observed in the apo-peptide are still present, with the length of the dark regions increased to 89.2 ± 26.3 nm and the light patches remaining a similar length of 105.6 ± 27.2 nm. $N=17$ for these measurements due to the lack of fibres. C) 10 μM solution of NB12 fibres after treatment with 0.3 eq GdCl_3 and 0.3 eq NiCl_2 . Light orange- a 10 μM fresh sample of NB12 treated with 0.3 eq GdCl_3 and 0.3 eq NiCl_2 . Dark orange- A 10 μM solution of NB12 fibres after dilution from a 125 μM solution of peptide fibres treated with 0.3 eq GdCl_3 and 0.3 eq NiCl_2 . The signal intensity has decreased compared to the fresh sample, and the characteristic double minima of a coiled coil is absent. Transmission electron micrographs the diluted species stained with 1% uranyl acetate. Low-magnification image (scale bars: 1 μm); (inset): high-magnification images (scale bar: 200 nm). The fibrous network has completely disassembled. All CD spectra recorded in 5 mM HEPES, 100 mM NaCl, pH 7.0. All spectra recorded at 25°C. For all fibre measurements, $n=30$ where possible. Length of fibres measured from visible fibre termini and tracked along the resulting fibre with use of the freehand tool in ImageJ.

The addition of 0.3 eq. of Gd^{3+} resulted in the reduction of fibre density in the sample, and the fibres that remain are thicker and more truncated than the apofibres. The same set of striations observed in Figure 4.4 are observed here, but the dark patches have almost doubled in length while the light patches remain a similar length to those observed in the apo-peptide. This set of titrations was intended to investigate the effect of coordinating metal ions to the central lanthanide binding site, and this leads to shorter, thicker fibres, with greatly reduced density of fibres.

The addition of a supplemental 0.3 eq. Ni^{2+} results in an almost complete lack of fibrous structures, with occasional fibres observed throughout the sample.

We also investigated the propensity of NB12 to form fibres when it is pre-coordinated to metal. Metal coordination stabilises the coiled coils and should shift the equilibrium towards coiled coil formation rather than fibre assembly. The NB12 coiled coil is mostly folded coordinated to 1.0 eq. Ni^{2+} /0.3 eq. Gd^{3+} so the sample was assembled for 1 week (Figure 4.7).

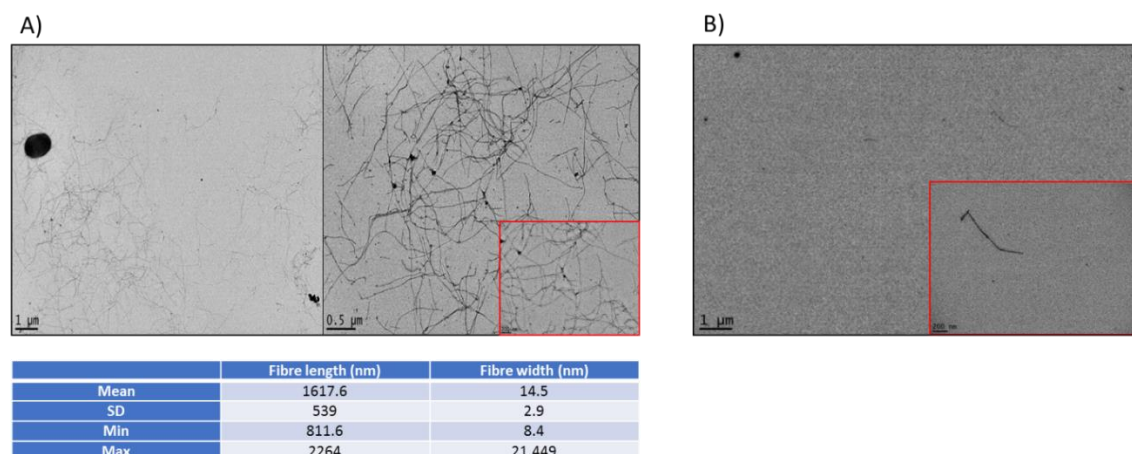


Figure 4.7 Fibre formation of 125 μM NB12 with 1.0 eq Ni^{2+} and 0.3 eq Gd^{3+} and dilution of resulting fibres. A) A 125 μM solution of NB12 matured with 1.0 eq NiCl_2 and 0.3 eq GdCl_3 . Transmission electron micrographs of the species stained with 1% uranyl acetate. Low-magnification image (scale bars: 1 μm); (inset): high-magnification images (scale bar: 200 nm). A fibrous network has formed, with aggregation of the peptide species and breaks in the fibres. B) A 10 μM solution of A prepared by dilution from the 125 μM sample. Transmission electron micrographs of the species stained with 1% uranyl acetate. Low-magnification image (scale bars: 1 μm); (inset): high-magnification images (scale bar: 200 nm). Dilution of the fibre network has led to the complete disassembly of the fibres save for one observable fibre. For all fibre measurements, $n=30$ where possible. Length of fibres measured from visible fibre termini and tracked along the resulting fibre with use of the freehand tool in ImageJ.

Interestingly, and in contrast to predictions, fibre formation is observed in a sample of 125 μM NB12 pre-coordinated to 1.0 eq. Ni^{2+} and 0.3 eq Gd^{3+} . Nonetheless, these fibres are wider than those formed by the apo-peptide, but of similar width of those formed by NB12 when it is pre-coordinated to 0.3 eq Gd^{3+} (Figure 4.7).

Strikingly, when these fibre solutions are diluted 10 times (to 10 μM), only a solitary fibre is left on the EM grid, suggesting that the fibre network has almost completely disassembled and that metal pre-coordination affects the equilibrium between fibrous assembly and coiled coil structure by shifting it towards the most stable specie, i.e. the coiled coil (Figure 4.8).

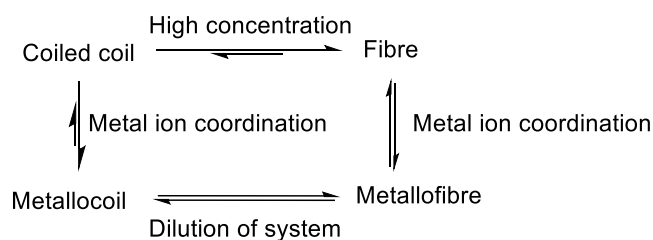


Figure 4.8 Equilibrium dictating the structures formed under different conditions.

4.4 Discussion

Apo-NB12 forms fibre networks at concentrations where trimer concentration is heavily favoured. Apo-NB11 also forms fibres, but these fibres are much smaller and less prevalent than NB12 fibres. This suggests the destabilised NB12 peptide is more driven to form fibres due to stabilisation as part of a higher order structure, a driving force not present in NB11. In the 100 μM fibrous system, the fibres display regular striations that suggest the top-down representation of a helix, with those aspects closest to the microscope being presented as light patches, and the gaps as dark voids where the stain has filled the gaps (Figure 4.9).

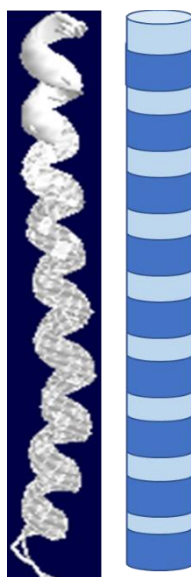


Figure 4.9 Graphical explanation for the striations observed in some of the fibres imaged.

The NB12 apofibres are stable to dilution, and the 10 μM fibres studied at these concentrations disassemble on the addition of metal ions to the system. The addition of nickel ions to the peptide system has a greater effect on fibre disassembly than the addition of gadolinium ions. Any system with nickel ions added to the system shows a lower density of fibrous species than any system with gadolinium ions added. The addition of gadolinium results in thicker, shorter fibres, while nickel discourages fibre formation at all.

The addition of metal ions to a system does not preclude fibre formation if the sample is matured at high concentrations of peptide. These fibrous networks are more branching and thicker than the apo-peptide systems and indicate a less stable fibre network. On dilution, the fibre network completely disassembles. These results suggest interplay between two key features of NB12 that result in fibre formation. The first feature concerns the stability of the peptide. Destabilisation by the central lanthanide binding group influences the structure to assemble into higher order structures, as the resulting assembly is less exposed to water molecules than existing as a discrete coiled coil. Gadolinium coordination, which has been shown to increase the folding and stability of the peptide species disassembles fibres.

The second feature is the unnatural amino acid substitution in the N-terminus heptad. The bipyridine amino acid present at the N-terminus of the coiled coil must influence the formation of fibres, as any metal binding to this site disassembles the peptide species. To account for both features, the following assembly pathway is proposed (Figure 4.10).

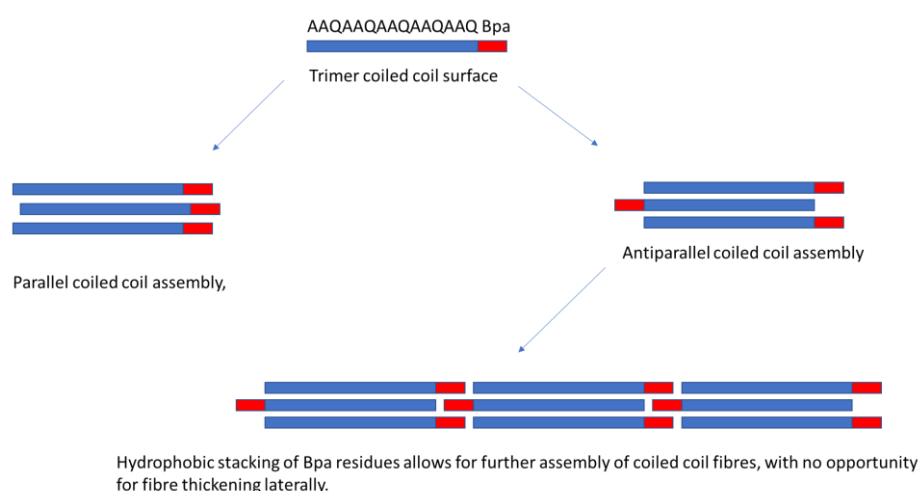


Figure 4.10 Coiled coil sizing and potential fibre assembly mechanisms of NB12. A) Computer generated model of NB12. The backbone and terminal bipyridyl amino acids are shown, all other features hidden. Measurement of this model generates a width of 12.156 nm and a length of 55.37 nm. B) Cartoon representation of the assembly of the trimeric coiled coil into trimeric fibre species. End to end association is enabled by π -stacking of the bipyridyl N-terminal amino acids to assemble longitudinally into fibres. The mixture of lengths observed in the EM images is accounted for by the lack of a mechanism to inhibit end to end assembly other than the exhaustion of all available material. Bpa residues at the N-terminus of the peptide highlighted in red.

The homogenous nature of the amino acids presented on the outside of the coiled coil does not negatively influence the assembly of the peptide species. The peptide is poorly folded, and the N-terminal end of the peptide chains are spaced apart to minimise interactions between the negatively charged Asp-Asn residues present in the lanthanide

binding site. Assembly of the bipyridine groups through a combination of hydrophobic burial and π -stacking generates fibre formation.

In a fibre assembled from a dimeric coiled-coil, a mean width of 2 nm is expected.⁸ If we assume that a dimeric fibre has a mean width of 2 nanometres, we can assume that a trimeric coiled coil has a width of three nanometres. A trimer of trimers would yield a width of 9 nanometres, and a tetramer of trimers corresponds to 12 nanometres. A width of 9 nanometres is observed for apofibres (Figure 4.11). The addition of metal ions to the peptide species causes the fibres which remain in solution to thicken considerably.

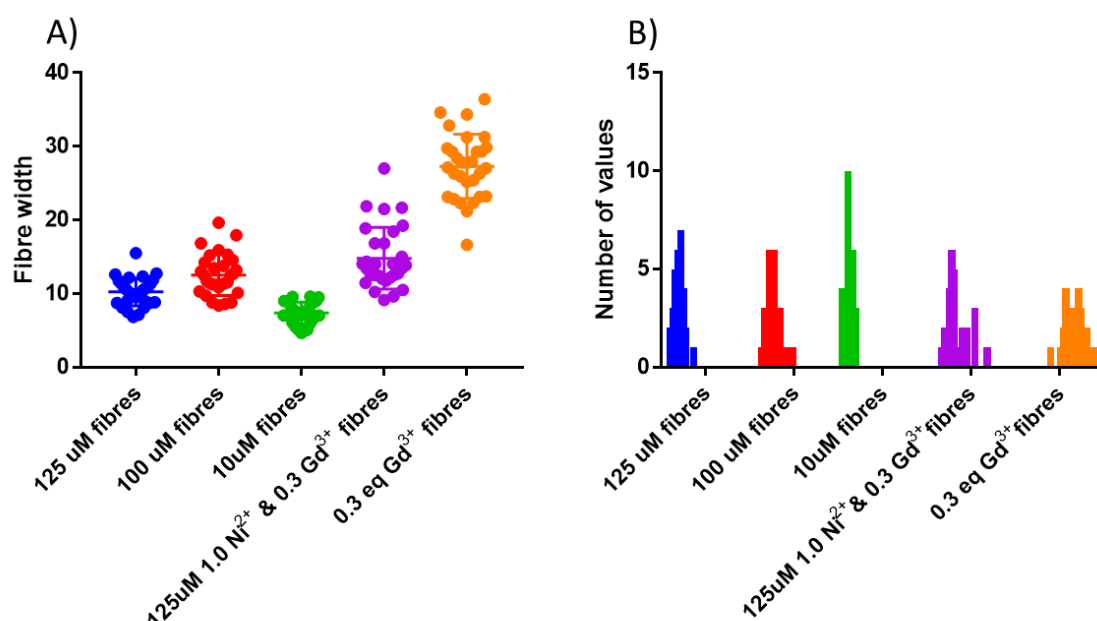


Figure 4.11 Distributions in the width of fibres formed. A) Plot of the measured fibre widths. Widths and error values were determined using the measurement function of ImageJ, and $N=30$ was used for each measurement. The apo-peptide fibres display small changes in the widths of the system, from a mean of 10 to a mean of 7 on dilution to 10 μ M. The fibres are within the same error range until the coordination of gadolinium into the system, at which point the thickness of the fibres approximately triples. B) Frequency distribution of the different widths of observed fibres, with a bin size of 4 and a range of 0-35 nm. Apo-peptide fibres display a narrow distribution, with most fibres grouped around the mean. The addition of metal ions to the system results in a broadening of the distribution of fibre widths.

The formation of fibres from coiled coils is not an irreversible process. Fibres and coiled coils of NB12 exist as an equilibrium between the fibres and the coiled coils. Addition of metal ions to the fibres is proposed to push the equilibrium in favour of the formation of coiled coils, so when metal ions are added to the system, it causes the fibres to disassemble. In the case of the metallated fibre network these show a greater distribution of fibres with widths consistent with the apo system, but the distribution begins to skew towards thicker fibres. The 0.3 eq Gd^{3+} 10 μ M system displays the thickest fibres formed, but those present are short and density of fibres is low.

4.5 Conclusions

In this chapter, new fibrous assemblies of a blunt ended bipyridyl functionalised coiled coil have been demonstrated. The apo-peptide systems are stable to dilution and maintain their fibrous form at concentrations as low as 10 μ M. These systems are disassembled with the addition of metal ions to the peptide system, with coordination of nickel to the terminal bipyridine site having a greater effect than coordination of gadolinium to the central lanthanide binding site.

An assembly mechanism has been proposed for this novel fibrous system, accounting for the properties observed. With fibre thickness for the apo-peptide systems of between 7 and 12 nm, this is consistent with a trimeric or tetrameric coil of coiled coils. The fibres are also blunt ended homotrimers, an exception to most of systems reported in the literature, which are heterodimeric sticky ended coiled coil systems. This is the first example of complete disassembly of fibre systems with metal ions.

4.6 Future work

These fibres are potentially interesting for the generation of recyclable peptide systems. The fact that they are disassembled by metal ion coordination is a novel control feature, and the use of hydrophobic metal binding groups to generate coiled coil fibres could have applications in the generation of new biomaterials. The simple nature of these systems means that modifications would be straightforward, and the substitution of the bipyridyl amino acid in different positions of the peptide structure could be used to generate fibre structures with a range of morphologies.

4.7 References

- (1) Perry, S. V. *J. Muscle Res. Cell Motil.* **2001**, 22, 5.
- (2) Steinert, P. M.; Marekov, L. N.; Fraser, R. D. B.; Parry, D. A. D. *J. Mol. Biol.* **1993**, 230, 436.
- (3) Prive, G. G.; Anderson, D. H.; Wesson, L.; Cascio, D.; Eisenberg, D. *Protein Sci.* **1999**, 8, 1400.
- (4) Ogihara, N. L.; Weiss, M. S.; Degrado, W. F.; Eisenberg, D. *Protein Sci.* **1997**, 6, 80.
- (5) Pandya, M. J.; Spooner, G. M.; Sunde, M.; Thorpe, J. R.; Rodger, A.; Woolfson, D. N. *Biochemistry* **2000**, 39, 8728.
- (6) Potekhin, S. A.; Melnik, T. N.; Popov, V.; Lanina, N. F.; Vazina, A. A.; Rigler, P.; Verdini, A. S.; Corradin, G.; Kajava, A. V. *Chemistry & Biology* **2001**, 8, 1025.
- (7) Ogihara, N. L.; Ghirlanda, G.; Bryson, J. W.; Gingery, M.; DeGrado, W. F.; Eisenberg, D. *Proc. Natl. Acad. Sci. U. S. A.* **2001**, 98, 1404.

- (8) Papapostolou, D.; Bromley, E. H. C.; Bano, C.; Woolfson, D. N. *J. Am. Chem. Soc.* **2008**, *130*, 5124.
- (9) Woolfson, D. N. *Biopolymers* **2010**, *94*, 118.
- (10) Banwell, E. F.; Abelardo, E. S.; Adams, D. J.; Birchall, M. A.; Corrigan, A.; Donald, A. M.; Kirkland, M.; Serpell, L. C.; Butler, M. F.; Woolfson, D. N. *Nat. Mater.* **2009**, *8*, 596.
- (11) Fletcher, J. M.; Harniman, R. L.; Barnes, F. R. H.; Boyle, A. L.; Collins, A.; Mantell, J.; Sharp, T. H.; Antognozzi, M.; Booth, P. J.; Linden, N.; Miles, M. J.; Sessions, R. B.; Verkade, P.; Woolfson, D. N. *Science (Washington, DC, U. S.)* **2013**, *340*, 595.
- (12) Burgess, N. C.; Sharp, T. H.; Thomas, F.; Wood, C. W.; Thomson, A. R.; Zaccai, N. R.; Brady, R. L.; Serpell, L. C.; Woolfson, D. N. *J. Am. Chem. Soc.* **2015**, *137*, 10554.
- (13) Bakota, E. L.; Sensoy, O.; Ozgur, B.; Sayar, M.; Hartgerink, J. D. *Biomacromolecules* **2013**, *14*, 1370.
- (14) Loewik, D. W. P. M.; Meijer, J. T.; Minten, I. J.; Van Kalker, H.; Heckenmueller, L.; Schulten, I.; Sliepen, K.; Smittenaar, P.; Van Hest, J. C. M. *J. Pept. Sci.* **2008**, *14*, 127.
- (15) Meijer, J. T.; Henckens, M. J. A. G.; Minten, I. J.; Loewik, D. W. P. M.; van Hest, J. C. M. *Soft Matter* **2007**, *3*, 1135.
- (16) Przybyla, D. E.; Chmielewski, J. *J. Am. Chem. Soc.* **2008**, *130*, 12610.
- (17) Przybyla, D. E.; Rubert Perez, C. M.; Gleaton, J.; Nandwana, V.; Chmielewski, J. *J. Am. Chem. Soc.* **2013**, *135*, 3418.
- (18) Berwick, M. R.; Lewis, D. J.; Jones, A. W.; Parslow, R. A.; Dafforn, T. R.; Cooper, H. J.; Wilkie, J.; Pikramenou, Z.; Britton, M. M.; Peacock, A. F. A. *J. Am. Chem. Soc.* **2014**, *136*, 1166.

Chapter 5: Final discussion, conclusions and future work

This thesis describes the synthesis of 3 isomers of bipyridylalanine, and the subsequent incorporation of bipyridylalanine into three-stranded coiled coils. Two coiled coil trimers were engineered to contain one lanthanide binding site each in the hydrophobic core of different heptad repeats to bind mixtures of lanthanide and transition metal ions. The serendipitous discovery that the most unstable of the two coiled coils, NB12, also formed fibrous structures was also investigated, and a dynamic equilibrium between metal coordinated trimer and fibrous structure unveiled.

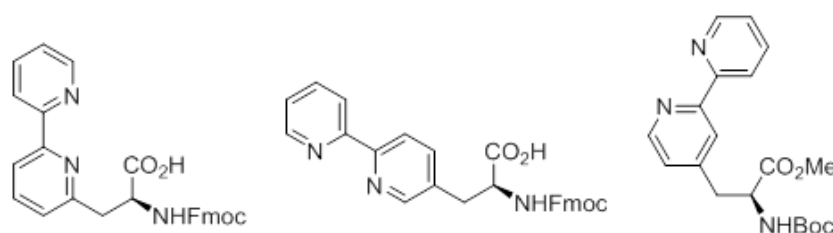


Figure 5.1 Amino acids synthesised in this thesis.

The first part of the thesis describes the synthesis of the bipyridyl amino acids 4-, 5- and 6-Bpa (Figure 5.1) using Negishi cross-coupling reactions. The initial concerns over the use of a metal-catalysed cross-coupling reaction for the synthesis of metal binding amino acids, did not hinder the synthesis and the three isomers were made successfully in moderate yields. The use of the appropriate bromobipyridine in the synthesis of the amino acids was the highest yielding method of synthesis, and given the commercial availability of the three isomers of bromo-2,2'-bipyridine, this route is viable for future use of the bipyridyl amino acids in protein engineering. Alternate routes to the synthesis of 4-Bpa were investigated, but the use of 2-pyridylzinc chloride with 2-chloro-4-alanylpipridine led to low yields of the desired product, side products in the form of 2,2'-bipyridine, and the decomposition of the starting material. Conversion of the Boc/methyl ester derivatives to the Fmoc/carboxylic acid compounds required for peptide synthesis was straightforward, and can be carried out at the gram scale.

The second part of the thesis describes the investigation of the properties of the 2,2'-6-bipyridylalanine containing peptides NB00, NB11, and NB12. The effect of monomer concentration on coiled coil formation was investigated, and the effects of metal addition to the peptide at different ratios of the structure were investigated.

The control peptide lacking the lanthanide binding site (NB00) demonstrated no appreciable change in folding with the addition of Ni^{2+} (Figure 5.2). Its helical content was consistent with a fully-folded coiled coil, showing a cooperative melt profile. The resulting enthalpy of unfolding for the apo- and metallopeptide showing also little change. UV spectroscopy of the peptide on metal coordination indicates strong binding of nickel to the bipyridine group.

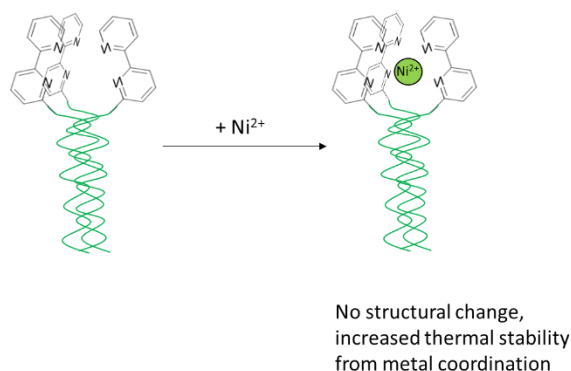


Figure 5.2 Cartoon representation of the behaviour observed in NB00

When a lanthanide binding site is introduced between the first and second heptads of the coiled coil (NB11), the structure still binds strongly to Ni^{2+} , as monitored through UV and CD spectroscopy. At concentrations where the coiled coil is fully formed, the effect of metal addition on folding of the peptide are minimal. Increasing Ni^{2+} concentration results in a small increase in the helical content and thermal stability of the coiled coil. At concentrations where the coiled coil is not fully formed, the addition of Ni^{2+} results in a much larger increase in the helical content of the peptide, as the Ni^{2+} ion draws the bipyridine sidechains at the end of the peptide together. Increasing Ni^{2+} concentration increases the enthalpy of unfolding, suggesting the formation of a better packed structure. NB11 was also used as a model peptide for the mixed lanthanide/transition metal peptide (Figure 5.3). NB11 appears to bind Tb^{3+} also in the presence of Ni^{2+} , suggesting that nickel coordination does not prevent lanthanide ions from binding. Nonetheless, the lower intensity of the Tb^{3+} signal, in the presence of Ni^{2+} coordinated peptide suggests the possibility of a higher hydration state of the lanthanide. Competition experiments binding transition and lanthanide metal ions were carried out to elucidate the effects of mixed metal binding. The individual addition of lanthanide ions to the coiled coil increases the folding to a greater extent than coordination of transition metal ions to the N-terminal bipyridylalanines. Upon addition of equal amounts of lanthanide and Ni^{2+} (ratio of 3:1 peptide monomer to metals), the peptide structures mirrors that of the pure gadolinium peptide. Interestingly, the CD spectra of

the peptide does not increase with the addition of gadolinium to the species when 1.0 equivalent of nickel has been bound. This indicates the nickel is fixing the structure of the peptide in place, preventing the core lanthanide binding site from dictating the structure of the peptide as it does in the equal metal concentration experiments.

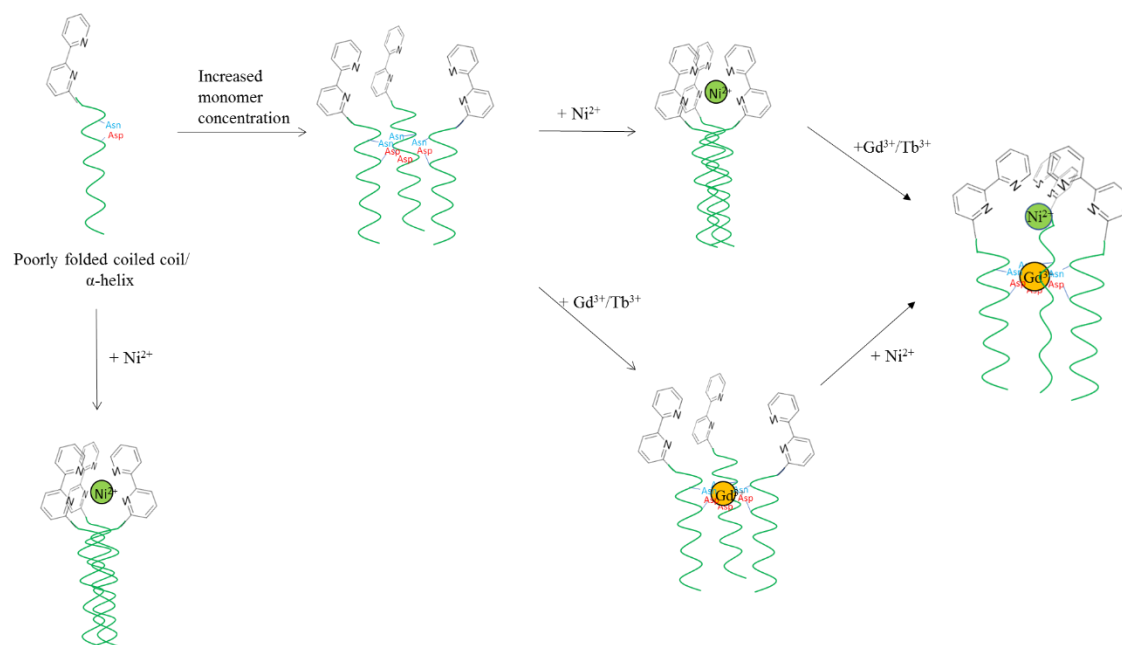


Figure 5.3 Cartoon representation of the behaviour observed in NB11 when titrated with both nickel and lanthanide ions

When the lanthanide binding site is introduced between the second and third heptad of the coiled coil (NB12) it displays the weakest metal binding of each of the three peptides, a full two orders of magnitude lower than that shown by NB00 and NB11. The poor folding of the peptide, and the resultant high monomer concentration required for the peptide to form a coiled coil reflect the effect of the destabilising lanthanide binding site. This allowed for the study of the peptide over a range of concentrations, from the poorly folded peptide at 50 μM monomer concentration to the more folded 125 μM monomer concentration. At 50 μM , the increase in helicity plateaus at a ratio of 3:1 of Ni^{2+} (peptide monomer to metal), accompanied by an increase in the enthalpy of unfolding of the metallopeptide that reflects the stabilising effect of the nickel on the helical bundle. At 90 μM , the helical content of NB12 reaches two different plateaus over the course of a titration of Ni^{2+} , one at a ratio of 2.5:1 (0.4 equivalents), and one at a ratio of 5:1 (0.6 equivalents of metal added). Again, these transitions are accompanied by an increase in the enthalpy of unfolding suggesting the formation of compact structures. There is no empirical evidence for the binding of two metal ions to the peptide, but we considered the possibility that the lanthanide binding site could bind a second nickel ion. Unpublished work by the Peacock group has investigated the titration

of transition metal ions into the parent MB-XX peptides and found no binding. This was explained by the size of the coordination site for lanthanides being too large for the smaller nickel ions, disfavoured binding. However, we proposed that due to the increased folding resulting from nickel coordination to the bipyridine groups drawing the ends of the peptides together, the asparagine and aspartic acid groups of the lanthanide binding site are forced closer together. This reduces the size of the binding site, making nickel binding more favourable. However, this disagrees with the results found in the fluorescence studies of NB11, as it is clearly demonstrated that even in the presence of 1 equivalent of nickel, the peptide species can still bind terbium in the lanthanide binding site.

The discovery of fibre formation by the destabilised apo-coiled coil NB12 was serendipitous, resulting from the investigation of aggregated samples of NB12. The rate of fibre formation was concentration dependent and showed fibre formation after 24 hours. Peptide samples below the coiled coil concentration displayed a lag phase in fibre formation, indicating that there is a structural rearrangement that takes place within the peptides that must occur before fibre formation can occur. This was assigned to the need for the peptides to form seed structures, from which the fibres can grow. The structural features of NB12 are distinct from other fibre forming peptides, as it was designed to exist as discrete parallel coiled coil trimers, and its sequence is capped at the N- and C-termini. This structure does not follow the 'sticky'-ended arrangement of other designed coiled coil fibres, therefore we concluded fibre formation must follow different mechanisms relying on the destabilised coiled coil structure and the hydrophobic nature of the bipyridine side chain incorporated in the peptide.¹ The destabilised nature of NB12 clearly plays a major role in its ability to assemble into fibres, as the self-assembly of the peptides into fibres is more favourable than existing as the α -helical coiled coil. We proposed a novel assembly mechanism for these fibres, which relies on the π -stacking of the bipyridine units to form interactions between antiparallel bundles of coiled coils. These fibres are fairly kinetically stable, displaying thinning of the fibres upon 15x dilution of the fibre sample.

Additionally, the equilibrium of fibre formation can be also affected by the addition of metal ions. The circular dichroism spectrum of the solutions shows partial reversal of the fibres into helical structures, and TEM indicates that the fibres are not present. Ni²⁺ coordination has a greater destabilising effect on the fibres than lanthanide binding, as judged from the density and width of the fibres present in EM images. However, the

presence of metal does not preclude metal formation. Fibres are formed in the presence of a mixed metal solution, which dissipate on dilution of the peptide samples. This suggests the existence of a 4-component equilibrium within the species between coiled coil, metallo-coiled coil, metallofibre and fibres (Figure 5.4).

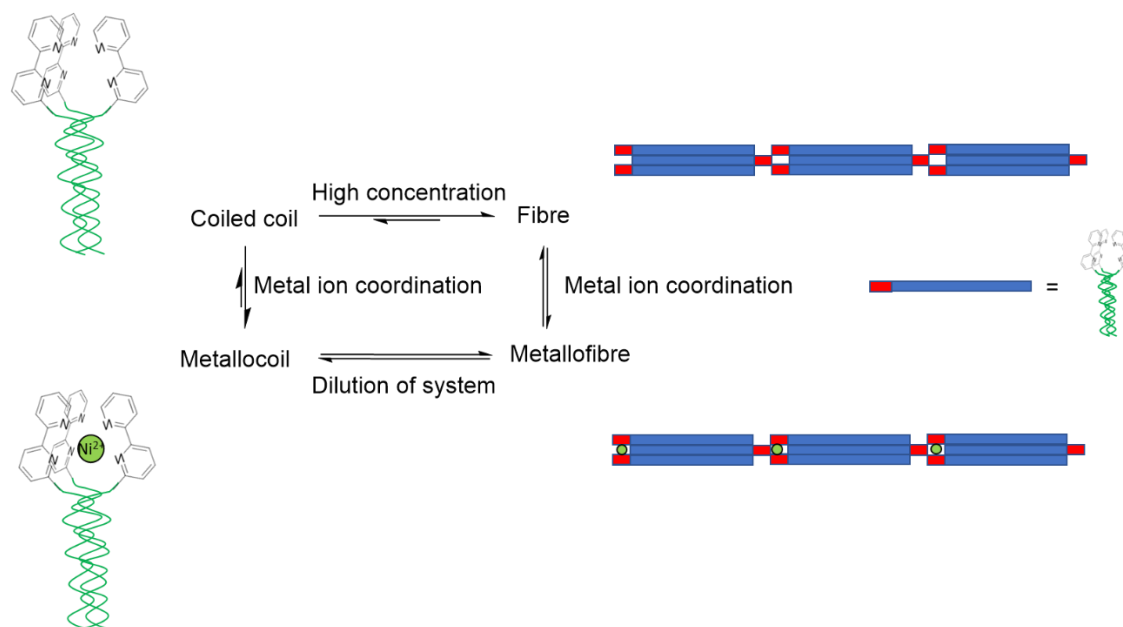


Figure 5.4 Cartoon representations of the different behaviours observed in NB12 and the proposed equilibrium of the mixed-metal fibre solution.

The rate of metallofibre formation was not investigated due to time constraints but indicates that metal coordination disassembles the fibres predominantly at dilute fibre concentrations.

Taken together, these results indicate the functionalisation of coiled coil peptides with bipyridine side chains offers a rich source of functionality and structural control not present in coiled coils lacking unnatural amino acids.

The synthesis route utilised in generation of the amino acids offers a straightforward method of the synthesis of unnatural amino acids with an aromatic side chain, available from commercially available materials. Potential applications of the peptides include the synthesis of further mixed metal species, where the structural perturbations in the presence of high nickel concentrations might allow for the control of the hydration state of lanthanide ions within the coiled coil, which is of interest in the field of MRI imaging agents. Bipyridine incorporation in the core of the coiled coil, or the use of multiple bipyridine sites in conjunction with the lanthanide binding site offers the generation of more complex mixed metal species, where electron transfer systems might be derived that rely on transition metal interactions that can influence any lanthanide ions bound.

Finally, the fibres offer the potential for new morphologies of coiled coil fibres, with the novel assembly mechanism proposed indicating the use of aromatic sidechains for longitudinal fibre assembly as a previously unexplored area.

5.1 Future work

5.1.1 New unnatural amino acids and their potential applications

The synthesis method applied to these amino acids makes use of the coupling of an aromatic halide to an amino acid zinc reagent. This approach is only limited by the availability of the aromatic coupling partners available. Imperiali and co-workers report the synthesis of phenathroline amino acids, and previous reports by Delangle and Ashkenasy have proved that amino acids with large sidechains can be incorporated into helical peptides with the correct design.²⁻⁴ Montenegro and co-workers have reported the synthesis of cyclopeptide nanotubes functionalised with pyrene sidechains which can associate with carbon nanotubes through interactions with the π -surface of the carbon tubes.⁵ It would be interesting to synthesise coiled coils functionalised with similar side-chains for the same purpose. To use the examples used in this thesis, the substitution of the solvent exposed hydrophobic tryptophan with a pyrene or a larger aromatic system might allow their conjugation to carbon nanotubes.

5.1.2 Influencing coiled coil structure and oligomerisation state with bipyridine side chains

The peptides described in this thesis have interesting applications in biotechnology. Only the 6-isomer of bipyridylalanine was incorporated into peptides, but the use of 4- or 5-Bpa and the resulting change in the orientation of the coordination site would allow for metal binding to be tailored. The studies of the well folded NB11 peptide above agree with previous findings that metals bind strongly to prearranged binding sites, so the use of these bipyridine ligands arranged correctly could be used to generate metal binding sites within protein structures.

The use of bipyridyl amino acids could be applied to studies on the effects of point mutations within peptide systems. The use of bipyridyl-metal ion systems to fix proteins into a defined oligomerisation state as the individual features of the peptide are varied could allow for the extensive study of the changes in thermodynamic properties of the peptide caused by the point mutations.

Extending the investigation of the NB-XX family of peptides also has interesting possibilities. The two peptides used in this study concern modification of the heptads of

the coiled coil closest to the N-terminal bipyridylalanine, but it would be of interest to investigate the distance dependent effects between nickel coordination to the bipyridine side chain and the lanthanide binding site as it is translated along the peptide further towards the C-terminus. Influencing the behaviour of the lanthanide binding site with a controlled bipyridine “switch” offers the potential to access new chemistry within the lanthanide binding site. As the MB-XX coiled coils were originally designed as MRI imaging agents, if the coordination of metals to the bipyridine can affect the behaviour of gadolinium, then this can be applied to *in vivo* systems. One of the issues in the use of dyes or imaging agents in biological systems is the localisation of the dye in the appropriate region. Systems have been developed which rely on specific conditions to trigger the signal. The difference in oxygen levels between cancer tumours and healthy biological tissue have been used as triggers, but if the relaxivity of gadolinium can be controlled with transition metals, then this could be tailored to specific regions. If a system can be developed which bind to specific metal ions (for the sake of this example, iron) whose concentration varies within the body, then a stronger or weaker MRI signal would result, allowing for the visualisation of specific areas (such as the liver or the blood). Such a system would rely on coordination in levels which do not cause damage to the biological system, or a reversible trigger to return the metal ions from the bipyridine system.

5.1.3 Metal-disassembled fibre systems

The development of fibrous systems derived from coiled coils is a popular target in the field of biotechnology. After the first successful report, systems have been developed with variable thickness and morphology, with several different designs being successfully developed.^{1,6} Woolfson and co-workers developed the principle of “sticky-ended” peptide fibres, taking inspiration from the assembly of strands of DNA. Blunt-ended or capped coiled coils typically do not form fibres, as the methods for their longitudinal association are limited. The development of systems which form due to π -interactions would allow for the expansion of fibre morphologies available. Particularly interesting would be the design of heteromeric fibre systems, where the assembling coiled coils are formed from a mix of non-fibre forming peptides, or fibres which rely on sticky ended assembly instead.

Recyclable coiled coils are a popular target, as the reversibility of fibre assembly might allow for the development of fibre “machinery”. Dissassembly of naturally occurring fibrous structures like the ESCRT family of proteins relies on the action of enzymes.

This metal controlled disassembly offers a novel mechanism of disassembly, which does not denature the peptide used in the samples irreversibly. The action of EDTA was not investigated in either the metallofibre or diluted metallofibre samples, but the effect of this on the fibre mixtures would be of interest. Przybyla and coworkers showed the effect of repeated metal coordination and EDTA chelation cycles and their effect on the morphology of the structures formed.⁷ The CD spectrum of the metal disassembled fibres indicates it is not a reversal of the process, so the reassembly of fibre systems after metal ion extraction requires investigation. Fibre assembly does not occur at concentrations of 10 μ M, but the fibres can exist at these concentrations. If the fibres are being disassembled into smaller bundles, then they may reassemble into fibres at lower concentrations, shifting the concentrations required for fibre formation.

5.2 References

- (1) Pandya, M. J.; Spooner, G. M.; Sunde, M.; Thorpe, J. R.; Rodger, A.; Woolfson, D. N. *Biochemistry* **2000**, *39*, 8728.
- (2) Niedzwiecka, A.; Cisnetti, F.; Lebrun, C.; Delangle, P. *Inorg. Chem.* **2012**, *51*, 5458.
- (3) Samiappan, M.; Alasibi, S.; Cohen-Luria, R.; Shanzer, A.; Ashkenasy, G. *Chem. Commun.* **2012**, *48*, 9577.
- (4) Cheng, R. P.; Fisher, S. L.; Imperiali, B. *J. Am. Chem. Soc.* **1996**, *118*, 11349.
- (5) Montenegro, J.; Vazquez-Vazquez, C.; Kalinin, A.; Geckeler, K. E.; Granja, J. R. *J. Am. Chem. Soc.* **2014**, *136*, 2484.
- (6) Papapostolou, D.; Bromley, E. H. C.; Bano, C.; Woolfson, D. N. *J. Am. Chem. Soc.* **2008**, *130*, 5124.
- (7) Przybyla, D. E.; Rubert Perez, C. M.; Gleaton, J.; Nandwana, V.; Chmielewski, J. *J. Am. Chem. Soc.* **2013**, *135*, 3418.

Chapter 6: Experimental

6.1 General Experimental

Dihalopyridines 2,6-dibromopyridine, 2,5-dibromopyridine, 2,4-dibromopyridine, and 2-chloro-4-iodopyridine were purchased from Manchester Organics[®]. All other reagents used in the synthesis of amino acids were purchased from Sigma-Aldrich[®]. All reagents used in peptide synthesis were purchased from AGTC Biotechnology[®]. DMF and NMP used in peptide synthesis were listed as peptide synthesis grade. All metal salts used in metal binding studies were purchased from Fisher Scientific[®]. All reagents used as supplied without further purification.

All reactions were performed with stirring using a magnetic stirrer bar, and all reactions that required dry solvents were performed in flame dried glassware under an atmosphere of nitrogen. All solvents used were of HPLC quality and were purchased from Fisher Scientific[®]. All dry solvents were obtained from the in house Grubbs dry solvent system (model: SPS-200-6). All other reagents and solvents were used as received from suppliers without further purification, unless otherwise stated. Petroleum ether refers to the fraction that boils between 40-60 °C.

Flash column chromatography was performed under pressure on silica gel 60 purchased from Davisil[®] Fluorochem. All columns were monitored by TLC using pre coated silica plates. TLC plates were visualised with UV irradiation at 254 nm and/or ninhydrin dissolved in MeOH. Gas chromatography was carried out on a Perkin Elmer[®] Autosystem XL Gas Chromatograph.

Melting points were measured on a Linkam[®] HFS91 heating stage, with a TC92 controller, and are uncorrected. Infrared spectra were measured on a Perkin Elmer[®] Paragon 1000 FT-IR spectrometer. Only selected peaks were reported, and the absorption maxima are given to the nearest cm^{-1} . ^1H and ^{13}C NMR spectra were recorded on a Bruker AV-400 spectrometer at room temperature. Chemical shifts are assigned relative to the residual solvent peaks and are quoted in parts per million with respect to the residual solvent peaks, and are given to the nearest 0.01 ppm for ^1H spectra and the nearest 0.1 ppm for ^{13}C spectra. The multiplicities are defined as s = singlet, d = doublet, t = triplet, q = quartet, m = multiplet, br. = broad. Coupling constants are quoted in Hertz to the nearest 0.5 Hz, and have been rationalised. High resolution mass spectra were recorded on a MicroMass[®] LCT Premier XE spectrometer

operating in electrospray mode. Optical rotations were recorded on a Perkin Elmer[®] 241 automatic polarimeter at λ 589 nm (Na, D-line).

Peptide Synthesis

Peptides were synthesized on a CEM[®] Liberty 1 automated peptide synthesizer on Rink amide MBHA resin (0.25 mmol scale), using standard microwave Fmoc-amino acid solid-phase peptide synthesis protocols. Fmoc-6Bpa was synthesised as described in the amino acid synthesis section of this thesis, and coupling of its HBTU activated ester was performed in NMP instead of the standard DMF. This coupling step was performed manually with an orbital shaker at room temperature.

All peptides were N-terminally acetylated and C-terminally amidated. The peptides were cleaved from the resin using a mixture of triisopropylsilane, tri-fluoroacetic acid and water (95:5:5) and precipitated into cold diethyl ether. This mixture was centrifuged at 4000rpm for 10 minutes, washed with further cold ether, and centrifuged once more. The peptides were then dissolved in water and freeze-dried. Peptides were purified by HPLC on an X-Bridge[®] Prep C18 5uM column (19 mm x 250 mm) using a water–acetonitrile gradient and trifluoroacetic acid as the ion-pairing agent. Fractions were analysed by HPLC using an X-Bridge C18 5uM analytical column (6 mm x 250 mm), and peptides were identified by electrospray mass spectrometry. The concentrations of pure peptide solutions were determined from the tryptophan and 6Bpa absorbance at 285 nm in water.

Crude peptides were purified by reversed-phase high-performance liquid chromatography (RP-HPLC) using a X-Bridge[®] Prep C18 5uM column (19 mm x 250 mm) attached to a Perkin Elmer[®] Series 200 LC Pump and 785A UV/Vis Detector. For preparative runs, concentrations up to 50 mg/mL (0.5 mL) were injected and peak fractions of interest pooled and lyophilized. All peptide sequences synthesized in this thesis were water soluble, so all samples were prepared by dissolving the peptide powder in H₂O and the solution centrifuged before injection to remove undissolved material. A flow rate of 17 mL/min was used for all separations. The aqueous phase (solvent A) consisted of a mixture (v/v) 99.9% H₂O with 0.1% TFA while the organic phase (solvent B) consisted of 100% CH₃CN.

Initial HPLC injections of each peptide sample were set to 30 min for linear gradients of 0-100% of solvent B to detect different compound peaks, and either shorter times (15

min) or shorter gradients (from solvent A to B) applied for subsequent injections depending on each peptide sequence. Analytical runs of the purified peptides after ES-MS analysis were used to confirm the presence of a single peptide within the pure fraction. These were small-scale runs (1 mg/mL loading) in a 30 minutes linear gradient of 0-100% of solvent B. A UV-Vis lamp was used as detector and 285 nm was the wavelength selected in all cases to monitor and detect the chromophore of the Trp and 6Bpa amino acids – which were part of all the peptide sequences.

Desalting and preparation of peptide solutions

After lyophilisation, all peptides were obtained as a white powder. These samples were dissolved in Millipore H₂O and centrifuged in Amicon Ultra 0.5 mL centrifugal filters with a molecular weight cut-off of 3 kDa. Samples were centrifuged at 13000 rpm for 15 minutes. This was repeated with Millipore H₂O 4 times, and then the desired experimental buffer 4 times. After this, the solution concentration was measured using the UV absorbance of the peptides at 285 nm, as described below.

Preparation of amino acid and peptide samples for UV-Vis spectroscopy

The Fmoc protected amino acid Fmoc-6Bpa-OH was prepared in a 6 uM methanolic solution, prepared from dilution of a 60uM methanolic solution. Solution concentrations were taken from the determined concentration after serial dilution. This was then titrated with 1mM aqueous solutions of ZnCl₂, CuCl₂, FeCl₂, MnCl₂, CoCl₂ and NiCl₂. Each sample was mixed from their stock solutions and allowed 20 minutes of equilibration time. After this, the UV-Vis spectrum was recorded at 25°C. From this, the behaviour with different metal ions was determined.

The UV-Vis behaviour for the Bpa-containing peptides was recorded in the same manner. A stock solution of the peptide in HEPES buffer was prepared, and diluted to a 10uM concentration, and titrated with increments of NiCl₂ solution. The samples were allowed to equilibrate for 20 minutes and then the UV-Vis behaviour was recorded.

Ultraviolet-visible spectroscopy (UV-Vis)

UV/Vis absorbance spectra were measured with a Cary 50 Bio UV-Visible spectrophotometer using quartz cuvettes of 10 mm pathlength. All peptides were

dissolved and measured in HEPES for peptide-concentration determination, and were dissolved within the buffer solution when HEPES or acetate were used as solvent/buffer of the samples.

Peptide samples were prepared from 1-5 mg of peptide powder dissolved in 1-2 mL of solvent (Millipore H₂O or HEPES) and the absorbance recorded maximums at 285 nm corresponding to the absorption of Trp and 6Bpa, which is the chromophore for all the peptide sequences and shows a combined molar extinction coefficient of $\epsilon = 17344 \text{ cm}^2 \text{ mol}^{-1}$ at 285 nm at neutral pH. An extinction coefficient for 6Bpa at 285 nm was obtained from Imperiali and co-workers, and an extinction coefficient for tryptophan at 285 nm was obtained from the PhotoCAD database.^{1,2}

The Beer-Lambert law (Equation 1) was used to calculate the concentration of each peptide sample:

$$\text{Equation 1: } A = \epsilon \times c \times l$$

A being the absorbance, c being the concentration of the peptide sample (mol/L), l being the path length of the beam of light throughout the cuvette that contains the sample (1 cm in our case), and ϵ the molar extinction coefficient ($\text{cm}^2 \text{ mol}^{-1}$).

Since the absorbance was determined by the spectrometer and we knew the values of $l = 1$ and the molar extinction coefficient (ϵ), the concentration was calculated with Equation 2:

$$\text{Equation 2: } c = A / \epsilon$$

Circular dichroism spectroscopy (CD)

Materials which display dichroism absorb light in ratios dependent on the polarity. Circular dichroism (CD) is the difference of absorptivity between left-handed and right-handed circularly polarised light, expressed as molar ellipticity. Molar ellipticity is derived from the difference in absorption of left-handed and right-handed polarised light, treated with a conversion value to remove concentration dependence from the measured ellipticity.

CD spectra displaying two negative minima around 208 and 222 nm and a positive maximum around 190 nm are associated with a high degree of α -helical content. The ratio of the minima at these wavelengths has been used as an approximation for the differentiation between an α -helical structure and a coiled coil structure.

$$\alpha\text{-helix } \theta_{222\text{nm}}/\theta_{208\text{nm}} = <1.0$$

$$\text{Coiled coil } \theta_{222\text{nm}}/\theta_{208\text{nm}} = \geq 1.0$$

In contrast, unstructured (random coil) peptide strands display intense negative minima around 200 nm, and small positive maxima around 210 nm.

CD measurements are usually reported in degrees of ellipticity (θ) or molar ellipticity (or mean residue ellipticity, MRE), which is circular dichroism corrected for concentration and it is calculated as shown:

$$MRE = \theta_{222}(c \times N)$$

Where $\theta_{222\text{nm}}$ is the ellipticity at 222 nm, c is the molar concentration, and N is the number of amino acids involved in the peptide or peptide mixture being measured.

Thermal denaturation curves were measured by monitoring the $\theta_{222\text{nm}}$ (mean residue ellipticity at 222 nm) at various temperatures ranging from 5 °C to 90 °C with a temperature gradient of 2 °C/min and equilibrating each reached temperature for 10 seconds prior to next measurement.

The α -helical content can be approximated from the minima where α -helices contribute the most to ellipticity. The % helicity was calculated based on the theoretical maximum ellipticity value -35789 deg dmol⁻¹ cm² res⁻¹ for our coiled coils, based on reports by Scholtz and co-workers.³ This is based on the equation

$$\theta_{\text{max}} = -40,000 * [(n-4)/n]$$

Where -40,000 is the maximum ellipticity value, and n is the number of amino acid residues in the peptide sequence. Our determination of peptide folding assumes that all other non-alpha helical species in the peptide solution are treated as unfolded random coils.

Van't Hoff analysis of the temperature-controlled melts was carried out according to the methods of

Circular dichroism (CD) spectroscopy was carried out using a Jasco J-810 spectrophotometer fitted with a Jasco PTC-423-5 temperature controller and Julabo circulatory water bath. Cuvettes of 0.1- and 1.0-cm path length were used (Hellma GmbH & Co. and Starna Ltd.). Spectra were collected in continuous mode with a resolution of 1.0 nm, averaging data for 10s at each point depending on sample concentration. The buffer system used was 5 mM HEPES, 100 mM sodium chloride. Temperature dependencies of the CD signals and spectra were measured using a ramping rate of 2°C/min. In all experiments baseline signals for buffer alone were measured and subtracted from the raw peptide data.

Fluorescence Spectroscopy

All fluorescence spectra were taken on a Fluoromax-4 spectrofluorometer, equipped with a 150W continuous output xenon lamp. Spectrofluorometer was equipped with single-grating excitation and emission spectrometers, blazed at 330 nm (excitation) and 500 nm (emission). All spectra recorded with a 350 nm cut on filter. All spectra are reported baseline subtracted.

MALLS and AUC

UC was carried out on an Optima XLA analytical ultracentrifuge (Beckman) equipped with an adsorption optical system and an An-60Ti (GCN4-p1, ATF-p) or an An-50Ti (Cort-Ir) rotor. Sedimentation equilibrium data were collected at rotor speeds of 28,000, 35,000, and 41,000 rpm. The *MW* reported in [Table 1](#) is calculated at the highest sample concentration. Sedimentation equilibrium data of Cort-Ir were recorded at three different protein concentrations (0.25, 0.5, and 1.0 mg/mL) and at rotor speeds of 27,000, 31,000, and 35,000 rpm. The sedimentation profiles were monitored at two wavelengths (275 nm for tyrosine and 235 nm for peptide backbone absorption). The data were fitted globally using a single ideal species model. Solvent density for PBS was taken as 1.004 g/mL.

Size exclusion chromatography coupled to MALS was performed on a DAWN EOS 18-angle detector connected to an Optilab Rex refractometer (Wyatt). Peptide solutions (100 μ L of 3–5 mg/mL) were injected on a Superdex 75 10/30 size exclusion chromatography column equilibrated with PBS. Molecular weights were calculated by using the Wyatt ASTRA version 4.90.08 software package.

All AUC and MALLS experiments were carried out by Dr Thomas Jowitt of The University of Manchester.

Transmission Electron Microscopy (TEM)

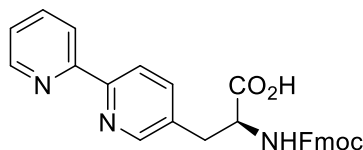
Fixation and embedding of the samples is carried out on the dark side of a carbon-coated 400-mesh copper grid (Agar Scientific). Carbon film grids are subject to glow discharge under partial vacuum for 30 seconds before sample loading. A droplet of the sample of appropriate concentration and buffer is added onto the grid and left for 30 seconds before sucking off the excess of liquid with filter paper. A droplet of double distilled water is added to the grid and after 20 seconds is blotted with filter paper. This washing step is repeated once more before negative staining. A droplet of uranyl acetate solution (used as negative staining) is added onto the grid and dried with filter paper after 30 seconds. The sample is then ready to be inserted into the microscope and be analysed.

Electron microscopy was carried out on a FEI Tecnai G2 Spirit Transmission Electron Microscope.

Protein Models

Models of the peptides used in this thesis were created through the addition of a 3-D representation of the amino acid to the crystal structure of MB12 and mutating the residues as appropriate. Structure manipulation was carried out in PyMol (The PyMol Molecular Graphics System, Version 2.0 Schrödinger, LLC)⁴. 3-D representations of the amino acid were created in ProDrug.⁵

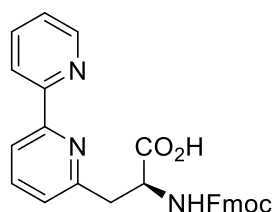
Synthesis of (2S)-2-([fluorenylmethyloxycarbonyl]amino)-3-[5-(pyridin-2-yl)pyridin-2-yl]propanoate **19**



Methyl (2S)-2-([(tert-butoxy)carbonyl]amino)-3-[5-(pyridin-2-yl)pyridin-2-yl]propanoate (1.8 g, 5 mmol) was added neat to a 100 mL round bottom flask containing 6 N hydrochloric acid (50 mL). This was heated to 100°C for 4 hours, until no starting material remained by TLC. After this time, the reaction was cooled to room temperature and extracted with ether (3 x 50 mL). The aqueous layer was reduced by azeotropic distillation with toluene. The resulting white powder was lyophilised to yield (S)- α -amino-(2,2'-bipyridine)-5-propanoic acid hydrochloride as a white crystalline solid. This was used without further purification. NMR characterisation was consistent with the literature.⁶ This was immediately taken on to the next stage. The hydrochloride salt (1.3 g, 5 mmol) was dissolved in 20% aqueous sodium carbonate solution (10 mL) in a 100 mL round bottom flask and cooled in an icebath to 0°C. Fluorenylmethyloxycarbonyl chloride (1.6 g, 6 mmol) dissolved in dioxane (20 mL) was added dropwise over two hours. After two hours, the icebath was removed, and the solution was stirred for 36 hours. The solution is diluted with water (100 mL) and extracted with ether (3 x 50 mL). The aqueous phase is cooled in an ice bath, and the pH is adjusted to pH 2.0 using 6N hydrochloric acid. After 15 minutes, a precipitate forms. The resulting suspension was centrifuged at 4000 rpm for 10 minutes. The supernatant is removed, and fresh water (50 mL) is added to the pellet. The mixture is vortexed for 5 minutes, and then subject to centrifugation at 4000 rpm for five minutes. The supernatant is decanted and the pellet is taken up into the minimum amount of methanol and precipitated into water (50 mL). This suspension is shell frozen and lyophilised. This yields the product as a pale pink powder (1.74 g, 3.75 mmol, 75% yield). m.p. 114-116°C (lit. 117°C) δ_{H} (400 MHz, d_6 -DMSO) 8.66 (d, J = 5.0 Hz, 1H), 8.33 – 8.21 (m, 1H), 8.17 – 8.09 (m, 1H), 7.91 (dd, J = 15.0, 7.5 Hz, 2H), 7.81 (t, J = 7.5 Hz, 1H), 7.75 – 7.70 (m, 1H), 7.61 (ddd, J = 7.0, 4.5, 3.0 Hz, 1H), 7.59 – 7.53 (m, 2H), 7.48 – 7.36 (m, 2H), 7.34 (dt, J = 7.5, 4.0 Hz, 2H), 7.26 (dd, J = 13.0, 6.0 Hz, 1H), 5.11 – 5.04 (m, 1H), 4.31 – 4.18 (m, 2H), 4.12 (t, J = 6.0 Hz, 1H), 3.67 – 3.60 (m, 1H), 3.15 (dt, J = 14.5, 7.0 Hz, 1H). δ_{C} (100 MHz, d_6 -DMSO) 170.2, 157.8, 152.7, 149.7, 148.9, 146.4, 143.9, 143.2, 140.7, 135.4, 129.5, 129.0, 127.7, 127.1, 124.9, 123.9, 121.2, 120.0, 68.2,

59.1, 46.1, 31.8 m/z ES found MH⁺ 466.1762, C₂₈H₂₄N₃O₄ requires 466.1761 [α]_D²⁵ - 157.1, (*c* 0.7, DMSO). Characterisation data largely in agreement with literature, some discrepancies in chemical shifts of ¹³C NMR, but ¹H NMR, [α]_D²⁵ and m/z in agreement with assigned product.

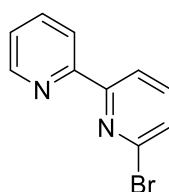
Synthesis of (2S)-2-([fluorenylmethyloxycarbonyl]amino)-3-[6-(pyridin-2-yl)pyridin-2-yl]propanoate **22**



Methyl (2S)-2-([(tert-butoxy)carbonyl]amino)-3-[6-(pyridin-2-yl)pyridin-2-yl]propanoate (1.8 g, 5 mmol) was added neat to a 100 mL round bottom flask containing 6 N hydrochloric acid (50 mL). This was heated to 100°C for 4 hours, until no starting material remained by TLC. After this time, the reaction was cooled to room temperature and extracted with ether (3 x 50 mL). The aqueous layer was reduced by azeotropic distillation with toluene. The resulting gum was lyophilised to yield (S)- α -amino-(2,2'-bipyridine)-6-propanoic acid hydrochloride salt as a white crystalline solid. NMR data was consistent with the literature.⁷ This was immediately taken on to the next stage. The hydrochloride salt (1.4 g, 5 mmol) was dissolved in 20% aqueous sodium carbonate solution (10 mL) in a 100 mL round bottom flask and cooled in an icebath to 0°C. Fluorenylmethyloxycarbonyl chloride (1.6 g, 6 mmol) dissolved in dioxane (20 mL) was added dropwise over two hours. After two hours, the icebath was removed, and the solution was stirred for 36 hours. At this time, the solution becomes a viscous gel. The solution is diluted with water (100 mL) and extracted with ether (3 x 50 mL). The aqueous phase is cooled in an ice bath, and the pH is adjusted to pH 2.0 using 6N hydrochloric acid. After 10 minutes, a precipitate forms. The resulting suspension was centrifuged at 4000 rpm for 10 minutes. The supernatant is removed, and fresh water (50 mL) is added to the pellet. The mixture is vortexed for 5 minutes, and then subject to centrifugation at 4000 rpm for five minutes. The supernatant is decanted again, the pellet is taken up into the minimum amount of methanol and precipitated into water (50 mL). This suspension is shell frozen and lyophilised. This yields the product as a pale orange powder (2.3 g, 5 mmol, 99% yield). m.p. 142-145°C (lit. not reported) δ _H (400 MHz, MeOD) 8.80 (dd, *J* = 6.0, 1.5 Hz, 1H), 8.74 – 8.62 (m, 2H), 8.30 (d, *J* = 8.0 Hz,

1H), 8.08 (t, $J = 8.0$ Hz, 1H), 8.02 (ddd, $J = 7.5, 6.0, 1.5$ Hz, 1H), 7.70 (dd, $J = 15.0, 7.5$ Hz, 2H), 7.63 (d, $J = 7.5$ Hz, 1H), 7.47 (dd, $J = 11.0, 7.5$ Hz, 2H), 7.24 – 7.03 (m, 1H), 5.12 (dd, $J = 10.0, 4.0$ Hz, 1H), 4.27 (d, $J = 7.0$ Hz, 2H), 4.05 (t, $J = 7.0$ Hz, 1H), 3.65 (dd, $J = 15.5, 4.5$ Hz, 1H), 3.43 – 3.37 (m, 1H); δ_C (100 MHz, MeOD) 176.5, 159.9, 148.9, 146.0, 143.3, 140.6, 137.5, 136.0, 131.4, 129.8, 129.1, 127.4, 127.2, 127.0, 126.1, 124.8, 122.8, 121.8, 68.9, 55.6, 54.1, 40.8; m/z ES found MH^+ 466.1761, $C_{28}H_{24}N_3O_4$ requires 466.1761; $[\alpha]_D^{25}$ -63.1 (c 1.0, MeOH). Characterization data largely in agreement with literature, some discrepancies in chemical shifts of ^{13}C NMR, but 1H NMR, $[\alpha]_D^{25}$ and m/z in agreement with assigned product.

Synthesis of 6-bromo-2,2'-bipyridine (**24**)



Method 1

2.0M Isopropylmagnesium chloride in THF (1.6 mL, 3.2 mmol) was added drop wise to 2-bromopyridine (0.29 mL, 3 mmol) at -78 °C, being careful not to generate an exotherm. This light brown solution was allowed to warm to room temperature and stirred for 4 hours at room temperature. After this time, a 0.5M solution of zinc chloride in THF (7.2 mL, 3.6 mmol) was added to mixture drop wise at -78 °C, being careful not to generate a significant exotherm. This was allowed to stir for 1 hour at room temperature. After this time, tetrakis(triphenylphosphine) palladium (47 mg, 0.04 mmol, 2 mol %) and 2,6-dibromopyridine (0.477g, 2.01 mmol) were added and the mixture was allowed to stir for 24 hours at room temperature.

After this time, the mixture was poured into an aqueous solution (300 mL H_2O) of EDTA (1.5 g, 5.13 mmol) and sodium carbonate (2.4g, 22.6 mmol) and stirred for 1 hour. This mixture was extracted with diethyl ether (3x 50mL). The organic layers were dried with magnesium sulfate and the solvent was then removed under reduced pressure to yield the crude mixture of 6-bromo-2,2'-bipyridine. This mixture was purified using an alumina (Brockman I, neutral) column to yield 6-bromo-2,2'-bipyridine (0.31g, 1.32 mmol, 66%) as a white solid. m.p. $73-75$ °C (lit $70-71$ °C)⁸; R_f 0.36 (10:90 EtOAc: petroleum ether); δ_H (400 MHz, $CDCl_3$) 8.69 (m, 1H), 8.43 (dt, $J = 8.0, 1.0$ Hz, 1H),

8.40 (dd, $J = 8.0, 1.0$ Hz, 1H), 7.85 (td, $J = 7.5, 2.0$ Hz, 1H), 7.70 (t, $J = 8.0$ Hz, 1H), 7.52 (dd, $J = 8.0, 0.9$ Hz, 1H), 7.36 (m, 1H). δ_C (100 MHz, $CDCl_3$) 157.4, 154.5, 149.3, 141.7, 139.3, 137.0, 128.0, 124.3, 121.6, 119.8 m/z (ES+) Found: MH^+ 234.9882, $C_{10}H_7N_2^{79}Br$ requires MH^+ 234.9871. Characterisation data consistent with that reported in the literature.⁸

Method 2

2.0M Isopropylmagnesium chloride in THF (3.2 mL, 6.4 mmol) was added drop wise to a 0.5M solution of lithium chloride (14.4 mL, 7.2 mmol) and allowed to stir at room temperature for 1 hour. 2-bromopyridine (0.29 mL, 3 mmol) was added to this mixture drop wise. This light brown solution was stirred for 4 hours at room temperature. After this time, a 0.5M solution of zinc chloride in THF (7.2 mL, 3.6 mmol) was added to the mixture, being careful not to generate a significant exotherm. This was allowed to stir for 1 hour at room temperature. After this time, tetrakis(triphenylphosphine) palladium (47 mg, 0.04 mmol, 2 mol%) and 2,6-dibromopyridine (0.477g, 2.01 mmol) were added and the mixture was allowed to stir for 24 hours at room temperature.

After this time, the mixture was poured into an aqueous solution (300 mL H_2O) of EDTA (1.5 g, 5.13 mmol) and sodium carbonate (2.4g, 22.6 mmol) and stirred for 1 hour. This mixture was extracted with diethyl ether (3x 50mL). The organic layers were dried with magnesium sulfate and the solvent was then removed under reduced pressure to yield the crude mixture of 6-bromo-2,2'-bipyridine. This mixture was purified using an alumina (Brockman I, neutral) column to yield 6-bromo-2,2'-bipyridine (0.18 g, 0.8mmol). Yield: 0.18 g, 40%. Characterisation consistent with that above.

Method 3

Following the procedure of Knochel and coworkers, Zinc dust (0.325 g, 4.9mmol) was added to a 25 mL side-arm round bottom flask that was dried under vacuum. The zinc was then flame dried, before adding dry DMA (2 mL). 1,2-dibromoethane (0.075g, 0.4 mmol) in DMA (2 mL) was added. The flask was heated with a heat gun until ethylene began to evolve, at which point it was allowed to cool. Heating was repeated until no further ethylene was evolved. Trimethylsilyl chloride (0.08 mL, 0.6 mmol) was added neat, and the mixture was stirred for 5 minutes.

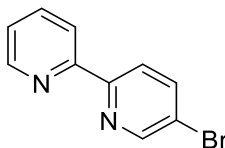
After activation of the zinc, 2-iodopyridine (0.213 mL, 2mmol) in DMA (2 mL) was added drop wise. An exotherm was observed, and the mixture was monitored by TLC.

Method 4

A solution of 2.5 M n-butyllithium (1.2 mL, 3 mmol) was added to THF (13 mL) and the mixture was cooled to -78 °C. 2-bromopyridine (0.29 mL, 3 mmol) was added drop wise to this mixture, and the mixture was allowed to stir at -78 °C for 2 hours. Zinc chloride (0.5M in THF) was added (7.2 mL, 3.6 mmol) and the mixture was allowed to warm to room temperature and stir for 1 hour. After this time tetrakis(triphenyl)phosphine palladium (47 mg, 0.04 mmol, 2 mol%) and 2,6-dibromopyridine (0.477g, 2.01 mmol) were added and the mixture was allowed to stir for 24 hours at room temperature.

After this time, the mixture was poured into an aqueous solution (300 mL H₂O) of EDTA (1.5 g, 5.13 mmol) and sodium carbonate (2.4g, 22.6 mmol) and stirred for 1 hour. This mixture was extracted with diethyl ether (3x 50mL). The organic layers were dried with magnesium sulfate and the solvent was then removed under reduced pressure to yield the crude mixture of 6-bromo-2,2'-bipyridine. This mixture was purified by trapping the bipyridine with 0.5M zinc chloride in THF (8 mL, 4mmol). The beige solid was isolated using a Buchner funnel, and washed with cold THF. This was then dissolved in a solution of EDTA (1.5 g, 5.13 mmol) and sodium carbonate (2.4g, 22.6 mmol) and stirred for 1 hour. This mixture was extracted with diethyl ether (3x 50mL). The organic layers were dried with magnesium sulfate and the solvent was then removed under reduced pressure to yield 6-bromo-2,2'-bipyridine as a white solid. (0.014 g, 0.06 mmol). Yield: 0.014g, 3%. Characterisation data consistent with above.

Synthesis of 5-bromo-2,2'-bipyridine (28)

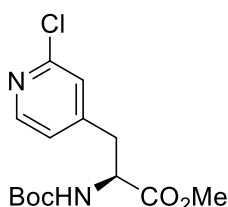


2.0M Isopropylmagnesium chloride in THF (1.6 mL, 3.2 mmol) was added drop wise to 2-bromopyridine (0.29 mL, 3 mmol) at -78 °C, being careful not to generate an exotherm. This light brown solution was allowed to warm to room temperature and stirred for 4 hours at room temperature. After this time, a 0.5M solution of zinc chloride in THF (7.2 mL, 3.6 mmol) was added to mixture drop wise at -78 °C, being careful not to generate a significant exotherm. This was allowed to stir for 1 hour at room

temperature.. This was allowed to stir for 1 hour at room temperature. After this time, tetrakis(triphenylphosphine) palladium (47 mg, 0.04 mmol, 2 mol %) and 2,5-dibromopyridine (0.476 g, 2.01 mmol) were added and the mixture was allowed to stir for 40 hours at room temperature.

After this time, the mixture was poured into an aqueous solution (300 mL H₂O) of EDTA (1.5 g, 5.13 mmol) and sodium carbonate (2.4g, 22.6 mmol) and stirred for 1 hour. This mixture was extracted with diethyl ether (3x 50mL). The organic layers were dried with magnesium sulfate and the solvent was then removed under reduced pressure to yield the crude mixture of 5-bromo-2,2'-bipyridine. This mixture was purified using 10:90 EtOAc:Petrol over an alumina (Brockman I, neutral) column to yield 5-bromo-2,2'-bipyridine as a white solid (0.3 g, 1.28 mmol, 64%). m.p 76-77 °C (lit. 74-75 °C) R_f (10:90 EtOAc:Petrol); δ_H (400 MHz, CDCl₃) 8.74 (dd, *J* = 2.0, 1.0 Hz, 1H), 8.69 (ddd, *J* = 5.0, 2.0, 1.0 Hz, 1H), 8.39 (dt, *J* = 8.0, 1.0 Hz, 1H), 8.34 (dd, *J* = 8.5, 1.0 Hz, 1H), 7.96 (dd, *J* = 8.5, 2.5 Hz, 1H), 7.84 (td, *J* = 8.0, 2.0 Hz, 1H), 7.35 (ddd, *J* = 7.5, 5.0, 1.0 Hz, 1H). δ_C (100 MHz, CDCl₃) 154.5, 151.2, 149.2, 141.6, 139.3, 137.0, 124.3, 121.5, 119.8 m/z (ES⁺) Found MH⁺ 237.01, C₁₀H₇N₂⁷⁹Br requires MH⁺ 236.98. Characterisation data consistent with the literature values.⁸

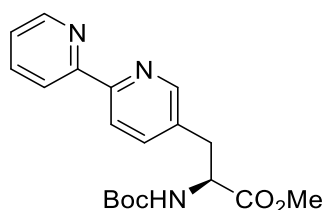
Synthesis of [2S]-2-([(tert-butoxy)carbonyl]amino)-3-(2-chloropyridin-4-yl) propanoate (**39**)



Zinc dust (0.588 g, 9 mmol) was flame dried in a 25 mL side-arm round bottomed flask. To this was added dry DMF (3 mL) and iodine (0.06 g, 0.24 mmol). The mixture was stirred until the brown colour dissipated. After this time N-(tert-butoxycarbonyl)-β-iodoalanine methyl ester (0.988 g, 3.00 mmol) and iodine (0.03 g, 0.12 mmol) were added. The insertion was monitored by TLC (40:60 petroleum ether: ethyl acetate) until insertion was complete. The solution of the zinc reagent was then transferred away from the zinc into a new 10 mL side arm flask. The remaining zinc was washed with dry DMF (3 mL) and this was also added.

To the solution of the zinc reagent was added 2-chloro-4-iodopyridine (0.934 g, 3.9 mmol) and $\text{Pd}(\text{PPh}_3)_2\text{Cl}_2$ (0.1 g, 0.3 mmol, 5 mol%). The mixture was then stirred overnight at room temperature (16 hours). After this time, the mixture was poured into an aqueous solution (300 mL H_2O) of EDTA (0.97 g, 3.3 mmol) and sodium carbonate (1.4 g, 13.2 mmol). The mixture was extracted with ethyl acetate (3 x 100 mL), and the organic layers were dried over magnesium sulfate and the solvent removed under reduced pressure to yield a red oil. The crude product was purified via column chromatography, using a mixture of 30:70 ethyl acetate/petroleum ether on silica, to yield methyl [2S]-2-([(tert-butoxy)carbonyl]amino)-3-(2-chloropyridin-4-yl) propanoate as a beige solid. (0.541 g, 1.71 mmol, 15%). m.p 73-74°C R_f 0.1 (70:30 petrol:EtOAc) δ_{H} (400 MHz, CDCl_3) 8.29 (d, $J = 5.0$ Hz, 1H), 7.13 (s, 1H), 7.02 (dd, $J = 5.0, 1.5$ Hz, 1H), 5.07 (d, $J = 8.0$ Hz, 1H), 4.60 (q, $J = 6.5$ Hz, 1H), 3.75 (s, 3H), 3.17 (dd, $J = 14.0, 6.0$ Hz, 1H), 2.99 (dd, $J = 14.0, 6.5$ Hz, 1H), 1.42 (s, 9H). δ_{C} (100 MHz, CDCl_3) 171.5, 151.7, 149.6, 148.9, 125.2, 123.3, 80.5, 53.6, 52.6, 37.3, 28.3 The expected quaternary carbon at 156 ppm was not observed. m/z (ES+) Found MH^+ 315.1122, $\text{C}_{14}\text{H}_{20}\text{ClN}_2\text{O}_4$ MH^+ requires 315.1112. $[\alpha]_{\text{D}}^{25} +106.4$, c 0.94, CHCl_3

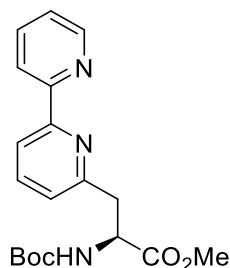
Synthesis of methyl (2S)-2-([(tert-butoxy)carbonyl]amino)-3-[5-(pyridin-2-yl)pyridin-2-yl]propanoate (**44**)



Zinc dust (0.235g, 3.6 mmol) was flame dried in a 10 mL side-arm round bottomed flask. To this was added dry DMF (0.75 mL) and iodine (0.06 g, 0.24 mmol). The mixture was stirred until the brown colour dissipated. After this time N-(tert-butoxycarbonyl)- β -iodoalanine methyl ester (0.3987 g, 1.21 mmol) and iodine (0.03 g, mmol) were added. The insertion was monitored by TLC (40:60 petroleum ether: ethyl acetate) until insertion was complete. The solution of the zinc reagent was then transferred away from the zinc into a new 10 mL side arm flask. The remaining zinc was washed with dry DMF (0.75 mL) and this was also added. 5-bromo-2,2'-bipyridine (0.1865 g, 0.79 mmol) and $\text{Pd}(\text{PPh}_3)_2\text{Cl}_2$ (0.029 g, 0.04 mmol, 5 mol%) were added to the solution of the zinc reagent. The mixture was heated at 50 °C for 3 hours.

After this time, the mixture was allowed to cool and was poured into an aqueous solution (300 mL H₂O) of EDTA (1.5 g, 5.13 mmol) and sodium carbonate (2.4g, 22.6 mmol). The mixture was stirred for an hour before being extracted with ethyl acetate (3 x 50 mL). The organic layer was dried with magnesium sulfate, and the solvent removed under reduced pressure to yield the crude product. This was purified using column chromatography (silica, 60:40 petrol : ethyl acetate) to yield methyl (2S)-2-([(tert-butoxy)carbonyl]amino)-3-[5-(pyridin-2-yl)pyridin-2-yl]propanoate as a yellow oil (0.183 g, 0.51 mmol, 64%). R_f: 0.15 (40:60 ethyl acetate/petroleum ether) δ_H (400 MHz, CDCl₃) 8.67 (ddd, *J* = 5.0, 2.0, 1.0 Hz, 1H), 8.45 (d, *J* = 2.0 Hz, 1H), 8.41 – 8.30 (m, 2H), 7.82 (td, *J* = 7.5, 2.0 Hz, 1H), 7.61 (dd, *J* = 8.0, 2.0 Hz, 1H), 7.31 (ddd, *J* = 7.5, 5.0, 1.0 Hz, 1H), 5.15 (d, *J* = 8.0 Hz, 1H), 4.65 (dt, *J* = 8.0, 6.0 Hz, 1H), 3.74 (s, 3H), 3.23 (dd, *J* = 14.0, 6.0 Hz, 1H), 3.12 (dd, *J* = 14.0, 6.0 Hz, 1H), 1.43 (s, 9H). δ_C (100 MHz, CDCl₃) 171.8, 156.1, 155.8, 155.6, 150.1, 149.2, 137.7, 137.0, 132.2, 123.7, 121.1, 120.9, 80.2, 54.2, 52.5, 35.5, 28.3; *m/z* Found 358.1764 (MH⁺) C₁₉H₂₄N₃O₄ requires 358.1767 [α]_D²⁵ +75.0 (*c* 1.0, CHCl₃)

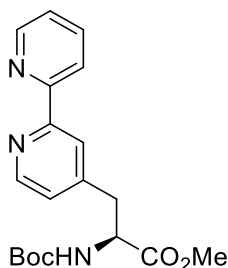
Synthesis of methyl (2S)-2-([(tert-butoxy)carbonyl]amino)-3-[6-(pyridin-2-yl)pyridin-2-yl]propanoate (**45**)



Zinc dust (0.295 g, 4.5 mmol) was flame dried under vacuum in a 10 mL side-arm round bottomed flask. To this was added dry DMF (0.75 mL) and iodine (0.06 g, mmol). The mixture was stirred until the brown colour dissipated. After this time N-(tert-butoxycarbonyl)- β -iodoalanine methyl ester (0.497 g, 1.5 mmol, 1.5 equiv.) and iodine (0.03 g, 0.12 mmol) were added. The insertion was monitored by TLC (40:60 petroleum ether : ethyl acetate) until insertion was complete. The solution of the zinc reagent was then transferred away from the zinc into a new 10 mL side arm flask. The remaining zinc was washed with dry DMF (0.75 mL) and this was also added. 6-bromo-2,2'-bipyridine (0.206 g, 0.877 mmol) and Pd(PPh₃)₂Cl₂ (0.054 g, 0.08 mmol, 9 mol %) were added to the solution of the zinc reagent. The mixture was heated at 50 °C for 3 hours.

After this time, the mixture was allowed to cool and was poured into an aqueous solution (300 mL H₂O) of EDTA (1.5 g, 5.13 mmol) and sodium carbonate (2.4 g, 22.6 mmol). The mixture was stirred for an hour before being extracted with ethyl acetate (3 x 50 mL). The organic layer was dried with magnesium sulfate, and the solvent removed under reduced pressure to yield the crude product. This was purified using column chromatography (silica, gradient column of 70:30 petrol:ethyl acetate to 40:60 petrol : ethyl acetate) to yield methyl (2S)-2-([(tert-butoxy)carbonyl]amino)-3-[6-(pyridin-2-yl)pyridin-2-yl]propanoate as a brown gum (0.164 g, 0.46 mmol, 53%). m.p 97-99 °C R_f 0.2 (40:60 EtOAc: petroleum ether) δ_H (400 MHz, CDCl₃) 8.68 (d, *J* = 4.5 Hz, 1H), 8.38 (d, *J* = 8.0 Hz, 1H), 8.31 (d, *J* = 8.0 Hz, 1H), 7.85 (td, *J* = 8.0, 2.0 Hz, 1H), 7.77 (t, *J* = 8.0 Hz, 1H), 7.37 – 7.29 (m, 1H), 7.18 (d, *J* = 7.5 Hz, 1H), 5.98 (d, *J* = 8.5 Hz, 1H), 4.79 (dt, *J* = 9.0, 5.0 Hz, 1H), 3.72 (s, 3H), 3.51 (dd, *J* = 15.5, 5.0 Hz, 1H), 3.38 (dd, *J* = 15.5, 5.0 Hz, 1H), 1.44 (s, 9H). δ_C 172.0, 156.3, 156.0, 155.6, 155.5, 149.1, 137.6, 137.0, 131.9, 123.8, 121.2, 119.0, 79.7, 54.1, 52.6, 39.0, 28.5; *m/z* (ES+) Found 358.1783 (MH⁺) C₁₉H₂₄N₃O₄ requires 358.1767 [α]_D²⁵ +85.4 (*c* 0.97, CHCl₃)

Synthesis of Methyl (2S)-2-([(tert-butoxy)carbonyl]amino)-3-[4-(pyridin-2-yl)pyridin-2-yl]propanoate, **46**



A)

2.0M Isopropylmagnesium chloride in THF (1.1 mL, 2.2 mmol) was added drop wise to 2-bromopyridine (0.19 mL, 2 mmol) at -78 °C, being careful not to generate an exotherm. This light brown solution was allowed to warm to room temperature and stirred for 4 hours at room temperature. After this time, a 0.5M solution of zinc chloride in THF (4.6 mL, 2.3 mmol) was added to mixture drop wise at -78 °C, being careful not to generate a significant exotherm. This was allowed to stir for 1 hour at room temperature.

To this mixture was added methyl (2S)-2-([(tert-butoxy) carbonyl] amino)-3-(2-chloropyridin-4-yl) propanoate (0.417 g, 1.3 mmol) and Pd(PPh₃)₄ (0.0271 g, 0.02

mmol, 3 mol%). The mixture was heated to 50 °C for 40 hours. The mixture was allowed to cool, and the solution was poured into an aqueous solution (300 mL H₂O) of EDTA (1.5 g, 5.13 mmol) and sodium carbonate (2.4g, 22.6 mmol). This mixture was stirred overnight, and then extracted with ethyl acetate (3 x 50 mL). The organic layers were dried over magnesium sulfate, and the solvent was removed under reduced pressure to yield the crude product. The product was purified using column chromatography (silica, gradient column from 100 % petrol to 50:50 petrol:ethyl acetate, with increments of 5%). This provided methyl (2S)-2-([(tert-butoxy) carbonyl] amino)-3-[2-(pyridin-2-yl)pyridin-4-yl]propanoate as a yellow oil (74 mg, 0.2 mmol). Yield (74 mg, 15%). R_f 0.2 (40:60 EtOAc:Petrol) δ_H (400 MHz, CDCl₃) 8.66 (ddd, *J* = 5.0, 2.0, 1.0 Hz, 1H), 8.59 (d, *J* = 5.0 Hz, 1H), 8.38 (dd, *J* = 8.0, 1.0 Hz, 1H), 8.22 (s, 1H), 7.81 (td, *J* = 7.5, 2.0 Hz, 1H), 7.30 (ddd, *J* = 7.5, 5.0, 1.5 Hz, 1H), 7.12 (dd, *J* = 5.0, 2.0 Hz, 1H), 5.10 (d, *J* = 8.5 Hz, 1H), 4.67 (q, *J* = 7.0 Hz, 1H), 3.75 (s, 3H), 3.25 (dd, *J* = 14.0, 5.5 Hz, 1H), 3.10 (dd, *J* = 14.0, 7.0 Hz, 1H), 1.39 (s, 9H). δ_C (100 MHz, CDCl₃) 171.86, 155.84, 149.12, 146.39, 136.97, 124.49, 123.83, 122.05, 121.23, 60.40, 53.84, 52.52, 38.01, 29.71, 28.23, 21.06, 14.20. m/z (ES+) Found MH⁺ 358.1770 C₁₉H₂₄N₃O₄ MH⁺ requires 358.1767. [α]_D²⁵ +4.2 (*c* 1.42, CHCl₃)

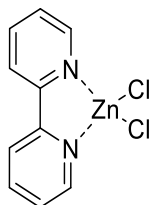
B)

A flask containing Zn (0.1 g, 1.5 mmol, 4.4 equiv.) was briefly flame dried under vacuum, before dry DMF (0.35 mL) and I₂ (0.03 g, 0.12 mmol, 12.5 mol%) were added. The brown solution quickly became colourless. Iodoalanine (0.171 g, 0.52 mmol, 2 equiv.) and I₂ (0.013 g, 0.06 mmol, 7 mol%) were added, with the resulting brown solution again becoming colourless. The zinc insertion was monitored by TLC, and when complete (~20 min) the suspension was allowed to settle. The supernatant was transferred *via* syringe to another flask. The remaining zinc was washed with dry DMF (0.35 mL), which was also transferred to the new flask. To this solution of organozinc reagent was added (Ph₃P)₂PdCl₂ (0.013 g, 0.02 mmol, 10 mol%) and 4-bromo-2,2'-bipyridine (0.06 g, 0.25 mmol, 1.0 equiv.).

The resulting solution was heated to 50 °C for 3 h, before being cooled to r.t. and poured onto a solution of EDTA (0.37 g, 1.26 mmol, 1.6 equiv.) and Na₂CO₃ (0.54 g, 5.06 mmol, 6.2 equiv.) in H₂O (80 mL). The aqueous solution was extracted with EtOAc (3 x 40 mL), and the organic extracts were dried over Na₂SO₄ and concentrated under reduced pressure to yield a yellow oily solid. The crude product was purified by

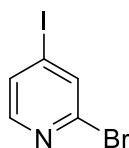
column chromatography (silica, gradient column from 100 % petrol to 50:50 petrol:ethyl acetate, with increments of 5%). This provided methyl (2S)-2-([(tert-butoxy) carbonyl] amino)-3-[2-(pyridin-2-yl)pyridin-4-yl]propanoate as a yellow oil (40 mg, 0.112 mmol, 45%).

Isolation of zinc-bipyridine complex **50**(general procedure)



Synthesis of 5-bromo-2,2'-bipyridine was carried out in the same way as described in Method 1 for the synthesis of the bromobipyridines. After the reaction was complete the reaction mixture was then applied directly to a sinter funnel. This yields a beige solid that is washed with further cold THF until the solvent runs colourless. This solid (the proposed zinc-bipyridine species) can be air dried and stored in this manner for some time, with no apparent loss of product. The beige solid is then added to an aqueous solution (300 mL H₂O) of EDTA(1.5 g, 5.13 mmol) and sodium carbonate (2.4g, 22.6 mmol) and stirred for 1 hour. The solution is then extracted with diethyl ether (3x 50 mL), dried and the solvent is then removed under reduced pressure to yield 5-bromo-2,2'-bipyridine as an off white solid (0.3 g, 1.3 mmol, 65%). Characterisation data was consistent with that recorded for 5-bromo-2,2'-bipyridine above, aside from the discrepancy recorded in the NMR, discussed above.

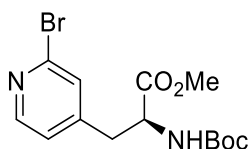
Synthesis of 2-bromo-4-iodopyridine **53**



A solution of 2.0 M n-butyllithium in ether (0.5 mL, 1 mmol) was cooled to -60 °C in a flame dried 10 mL round bottom flask. To this a solution of 2,4-dibromopyridine (0.24 g, 1 mmol) in ether (2.5 mL) was added dropwise, maintaining a temperature of -60 °C. The dark orange mixture was allowed to react at this temperature over 30 minutes, after which the solution was cooled to -78 °C. A solution of iodine (0.15 g, 1.2 mmol) in anhydrous ether (2.5 mL) was added dropwise to the solution over 10 minutes. After 10 minutes further stirring at -78 °C after the addition was complete, the solution was

allowed to warm to room temperature and stirred for 30 minutes. The resulting brown mixture was diluted with diethyl ether (20 mL), and washed with 1M sodium thiosulfate (2 x 50 mL) and brine (2 x 50 mL). The organic layer was dried with magnesium sulfate and the solvent removed under reduced pressure to yield the crude product. This was recrystallized from hexane to yield 2-bromo-4-iodopyridine as a pale brown solid (0.15 g, 0.52 mmol, 52%). m.p. 52-55 °C (lit. not reported), δ_{H} (400 MHz, CDCl_3) 8.04 (d, $J = 5.0$, 1H), 7.90 (dd, $J = 1.5$, 0.5 Hz, 1H), 7.62 (dd, $J = 5.0$, 1.5 Hz, 1H). δ_{C} (100 MHz, CDCl_3) 150.1, 142.5, 136.8, 132.2, 106.6; m/z (ES+) Found MH^+ 282.8498 $\text{C}_5\text{H}_3^{79}\text{BrIN}$ requires MH^+ 282.8488. Characterisation data consistent with literature.⁹

Synthesis of [2S]-2-([(tert-butoxy)carbonyl]amino)-3-(2-bromopyridin-4-yl) propanoate **54**



A) Synthesis from 2,4-dibromopyridine

Zinc dust (0.588 g, 9 mmol) was flame dried in a 5 mL side-arm round bottomed flask. To this was added dry DMF (3 mL) and iodine (0.06 g, 0.24 mmol). The mixture was stirred until the brown colour dissipated. After this time N-(tert-butoxycarbonyl)- β -iodoalanine methyl ester (0.988 g, 3.00 mmol) and iodine (0.03 g, 0.12 mmol) were added. The insertion was monitored by TLC (40:60 petroleum ether: ethyl acetate) until insertion was complete. The solution of the zinc reagent was then transferred away from the zinc into a new 10 mL side arm flask. The remaining zinc was washed with dry DMF (3 mL) and this was also added.

To the solution of the zinc reagent was added 2,4-dibromopyridine (0.85 g, 3.6 mmol) and $\text{Pd}(\text{PPh}_3)_2\text{Cl}_2$ (0.035 g, 0.15 mmol, 5 mol%). The mixture was then stirred overnight at room temperature (16 hours). After this time, the mixture was poured into an aqueous solution (300 mL H_2O) of EDTA (0.99 g, 3.3 mmol) and sodium carbonate (1.4 g, 13.2 mmol). The mixture was extracted with ethyl acetate (3 x 100 mL), and the organic layers were dried over magnesium sulfate and the solvent removed under reduced pressure to yield the crude product. This was purified using column chromatography (silica, 70:30 petroleum ether: ethyl acetate) to yield [2S]-2-([(tert-butoxy)carbonyl]amino)-3-(2-bromopyridin-4-yl) propanoate as a dark brown oil (0.19 g, 0.54 mmol, 15 %). R_f 0.15 (70:30 petroleum ether: ethyl acetate) δ_{H} (400 MHz,

CDCl₃) 8.28 (d, *J* = 5.0 Hz, 1H), 7.29 (s, 1H), 7.05 (dd, *J* = 5.0, 1.5 Hz, 1H), 5.06 (d, *J* = 8.0 Hz, 1H), 4.60 (d, *J* = 7.0 Hz, 1H), 3.75 (s, 3H), 3.15 (dd, *J* = 14.0, 6.0 Hz, 1H), 2.97 (dd, *J* = 14.0, 6.5 Hz, 1H), 1.42 (s, 9H). δ_C (100 MHz, CDCl₃) 176.7, 149.8, 148.6, 147.7, 132.7, 129.3, 123.3, (Signal at 80.0 ppm corresponding to OC^tBu not observed) 53.8, 52.3, 37.6, 28.3 m/z (ES+) Found MH⁺ 359.0605, C₁₄H₁₉⁷⁹BrN₂O₄ requires M 359.0601, [α]_D²⁵ +70.0 (c = 1.0, CHCl₃)

B) Synthesis from 2-bromo-4-iodopyridine

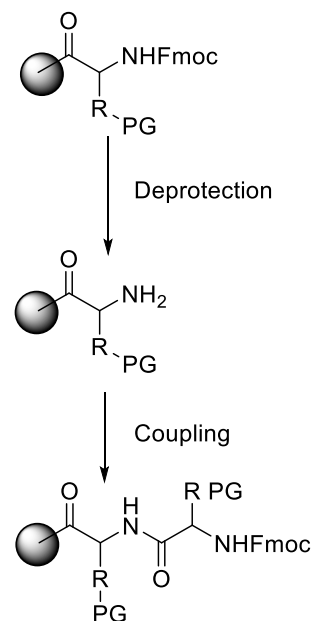
Zinc dust (0.588 g, 9 mmol) was flame dried in a 5 mL side-arm round bottomed flask. To this was added dry DMF (3 mL) and iodine (0.06 g, 0.24 mmol). The mixture was stirred until the brown colour dissipated. After this time N-(tert-butoxycarbonyl)-β-iodoalanine methyl ester (0.988 g, 3.00 mmol) and iodine (0.03 g, 0.12 mmol) were added. The insertion was monitored by TLC (40:60 petroleum ether: ethyl acetate) until insertion was complete. The solution of the zinc reagent was then transferred away from the zinc into a new 10 mL side arm flask. The remaining zinc was washed with dry DMF (3 mL) and this was also added. To the solution of the zinc reagent was added 2-bromo-4-iodopyridine (0.92 g, 3.6 mmol) and Pd(PPh₃)₂Cl₂ (0.035 g, 0.15 mmol, 5 mol%). The mixture was then stirred overnight at room temperature (16 hours).

After this time, the mixture was poured into an aqueous solution (300 mL H₂O) of EDTA (0.99 g, 3.3 mmol) and sodium carbonate (1.4 g, 13.2 mmol). The mixture was extracted with ethyl acetate (3 x 100 mL), and the organic layers were dried over magnesium sulfate and the solvent removed under reduced pressure to yield the crude product. This was purified using column chromatography (silica, 70:30 petroleum ether: ethyl acetate) to yield [2S]-2-([(tert-butoxy)carbonyl]amino)-3-(2-bromopyridin-4-yl) propanoate as a dark brown oil (0.4 g, 1.1 mmol, 30 % yield).

General procedure for peptide synthesis

Peptides were synthesized on a CEM Liberty Blue automated peptide synthesizer on rink amide MBHA resin (0.25 mmol scale, 0.65 mmol g⁻¹). Synthesis was halted after addition of the N-terminal glycine, and addition of Fmoc-6Bpa-OH was carried out manually. All amino acid residues were added following the same general procedure. Most of the procedure was carried out with the following procedure:

1. Shake resin in DMF for 30 minutes to swell.
2. Drain DMF from resin
3. Suspend resin in 10 mL deprotection solution (20% piperidine in DMF, 0.1 M HOBT).
4. Shake for 30 minutes.
5. Drain deprotection solution
6. Resuspend in 10 mL fresh deprotection solution. Shake for 30 minutes.
7. Drain deprotection solution.
8. Wash with DMF (3x 10 mL)
9. Add Fmoc-amino acid (0.2 M in NMP), activator (0.5 M in DMF) and activator base (2M DIPEA in NMP). Shake for 3h.
10. Drain solution.
11. Wash with DMF (3 x 10 mL)



Capping of peptide sequences

After the final Fmoc deprotection step, the DMF/piperidine deprotection media was filtered from the resin, and the beads were washed with DMF (3 x 10 mL). 20 mL of capping mixture (20% acetic anhydride, 20% DIPEA in DMF) was added to the resin. This was shaken for 25 minutes. The capping mixture was filtered off, and the resin was washed with ether (3 x 10 mL) and DCM (3 x 10 mL). Resin was allowed to dry fully before cleavage

Cleavage

Four 50 mL falcon tubes filled with 40 mL ether were chilled in a -20°C or below freezer for 2 hours. Capped resin was added to a clean falcon tube, and a solution of 98:1:1 TFA:TIPS:H₂O. (20mL) was added. This was shaken for 2.5-3 hours, and then

filtered to remove the TFA solution. Air was passed over the TFA solution until the solution volume is reduced by 3 or 4 times. This was precipitated into the chilled ether and left to settle overnight in the freezer.

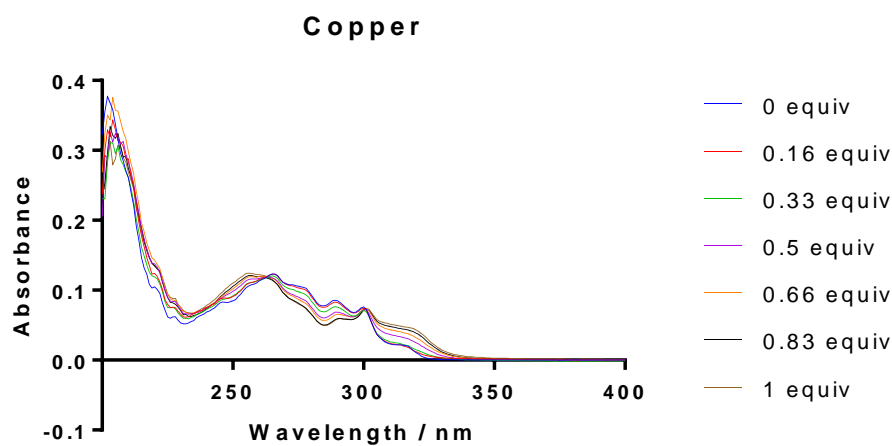
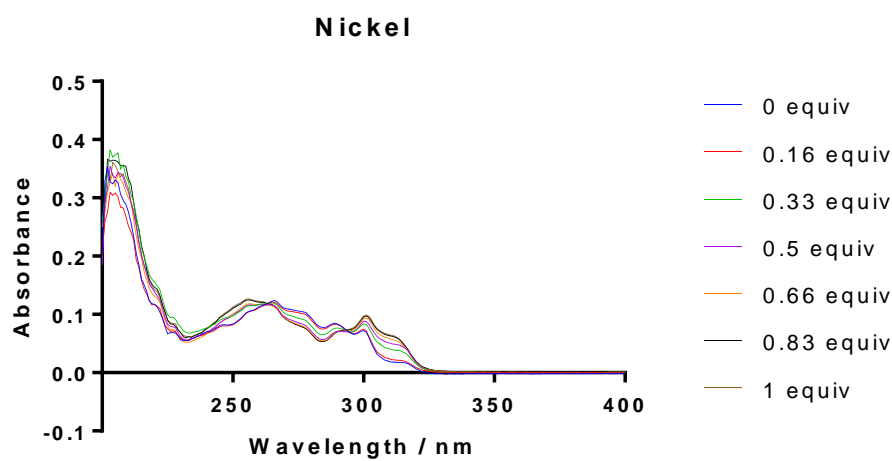
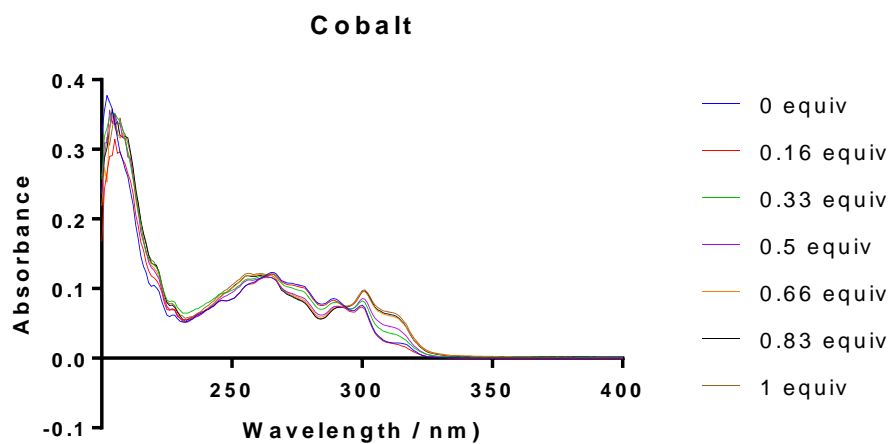
The falcon tubes were centrifuged at 4000 rpm for 30 minutes. The supernatant was decanted, and the tubes refilled with cold ether (50 mL). Samples were vortexed and then centrifuged again. This yielded the crude peptide. Crude peptides were purified by HPLC.

After HPLC is complete, acetonitrile was removed under reduced pressure, and the aqueous solutions were lyophilised to yield the purified peptide.

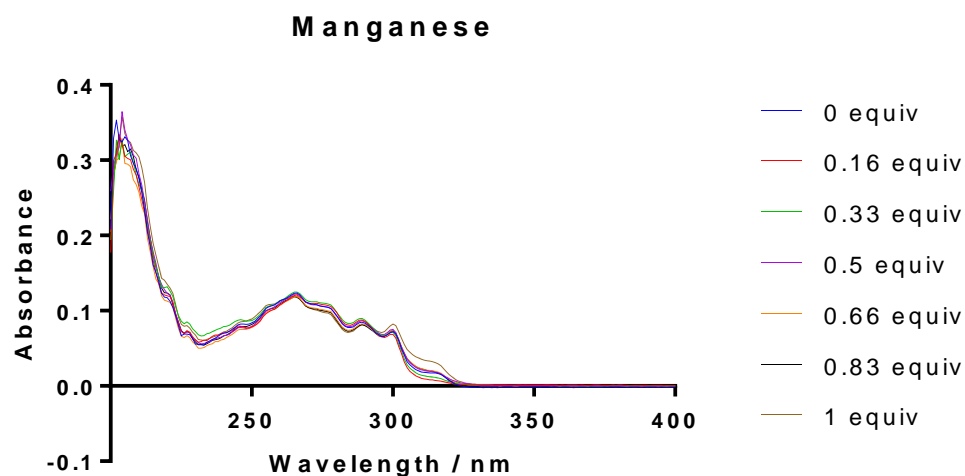
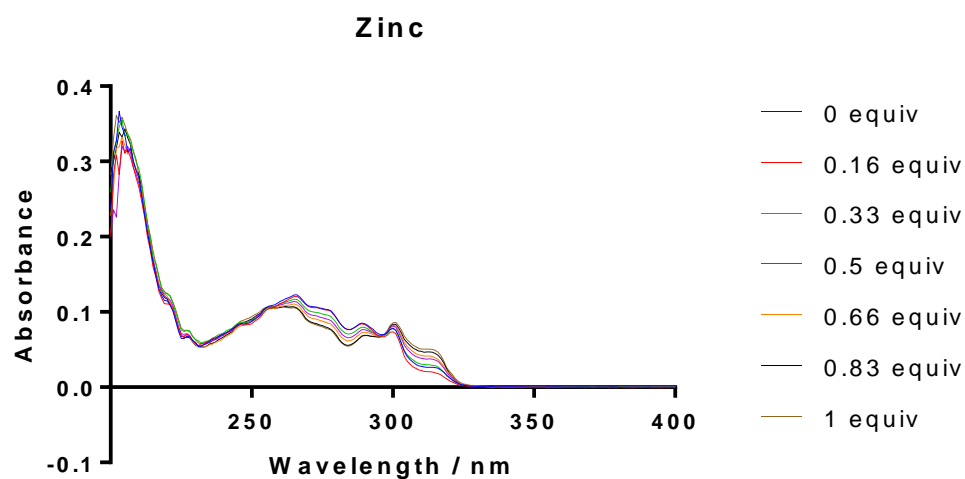
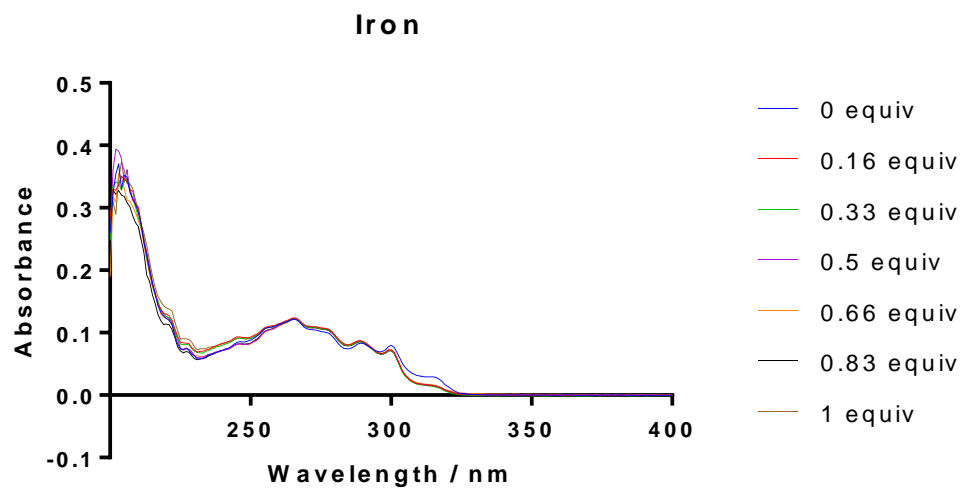
References

- (1) Cheng, R. P.; Fisher, S. L.; Imperiali, B. *J. Am. Chem. Soc.* **1996**, *118*, 11349.
- (2) Dixon, J. M.; Taniguchi, M.; Lindsey, J. S. *Photochem. Photobiol.* **2005**, *81*, 212.
- (3) Myers, J. K.; Pace, C. N.; Scholtz, J. M. *Proceedings of the National Academy of Sciences* **1997**, *94*, 2833.
- (4) The PyMOL Molecular Graphics System, Version 1.8 Schrödinger, LLC.
- (5) Schuettelkopf, A. W.; van Aalten, D. M. F. *Acta Crystallogr., Sect. D: Biol. Crystallogr.* **2004**, *D60*, 1355.
- (6) Imperiali, B.; Prins, T. J.; Fisher, S. L. *J. Org. Chem.* **1993**, *58*, 1613.
- (7) Imperiali, B.; Fisher, S. L. *J. Org. Chem.* **1992**, *57*, 757.
- (8) Fang, Y. Q.; Hanan, G. S. *Synlett* **2003**, 852.
- (9) Bouillon, A.; Lancelot, J.-C.; Collot, V.; Bovy, P. R.; Rault, S. *Tetrahedron* **2002**, *58*, 4369.

Appendices

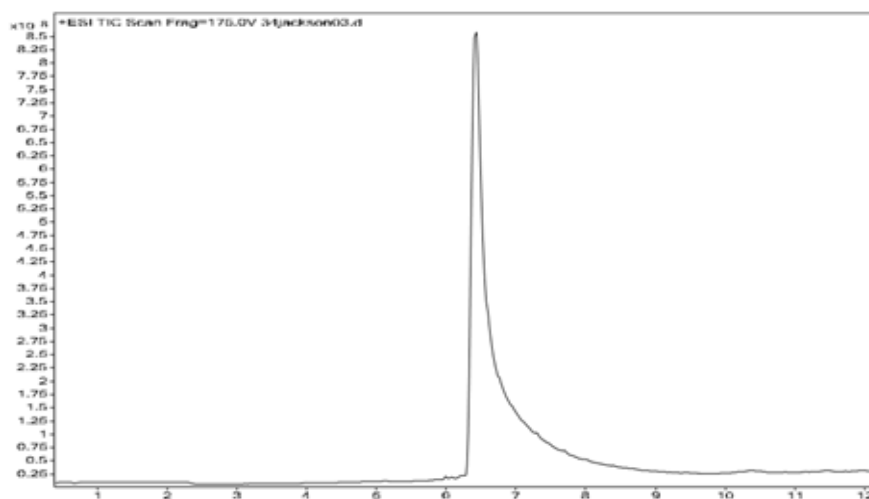


Supplementary Figure 1 UV absorption spectra for the titration of 6 μ M Fmoc-6Bpa-OH with cobalt (II), nickel (II) and copper (II) metal ion solutions. Experiments were performed in 100% v/v CH₃OH.

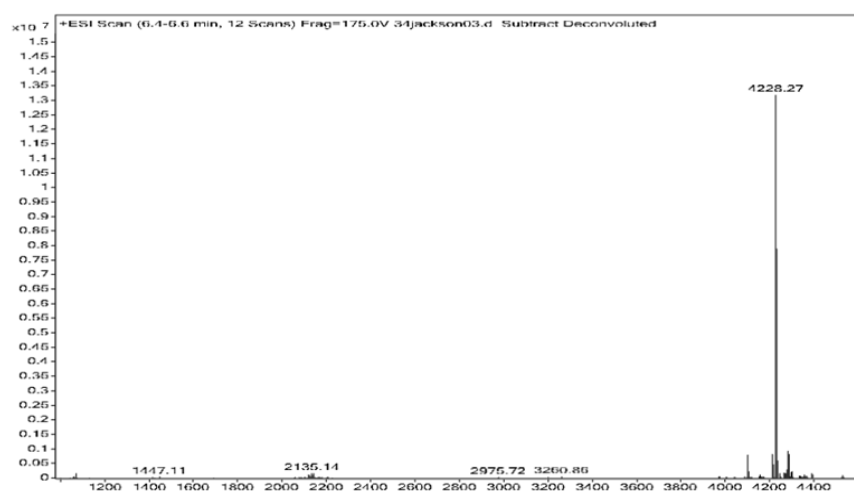


Supplementary Figure 2 UV absorption spectra for the titration of 6uM Fmoc-6Bpa-OH with iron (II), zinc (II) and manganese (II) metal ion solutions. Experiments were performed in 100% v/v CH₃OH

Δ

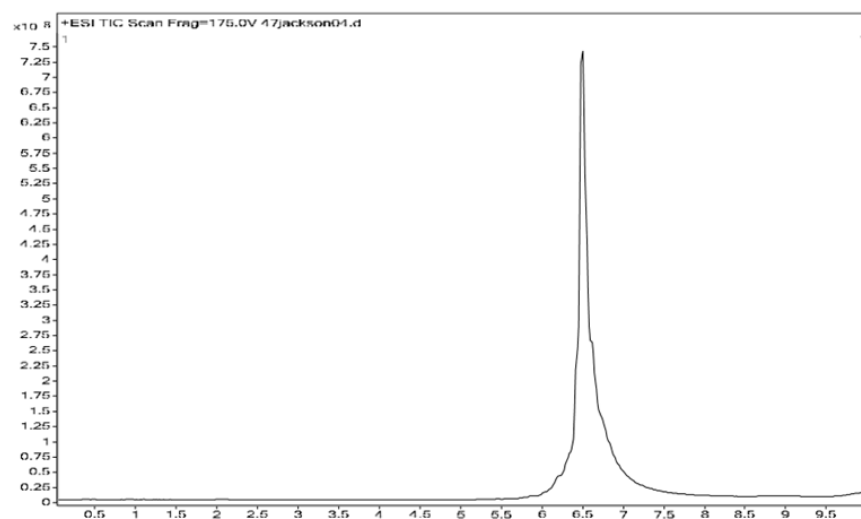


R

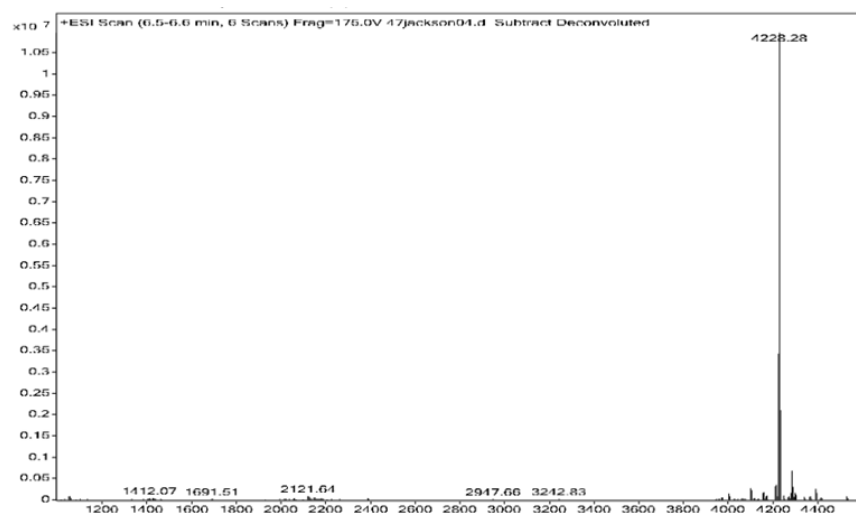


Supplementary Figure 1 (A) C18-analytical HPLC trace of pure NB1-1 using a linear 0 to 100% MeCN + 0.05% TFA gradient in H₂O + 0.05% TFA over 10 minutes. (B) Electrospray mass spectrum of pure NB1-1

A



B



Supplementary Figure 4 (A) C18-analytical HPLC trace of pure NB1-1 using a linear 0 to 100% MeCN + 0.05% TFA gradient in H₂O + 0.05% TFA over 10 minutes. (B) Electrospray mass spectrum of pure NB1-1

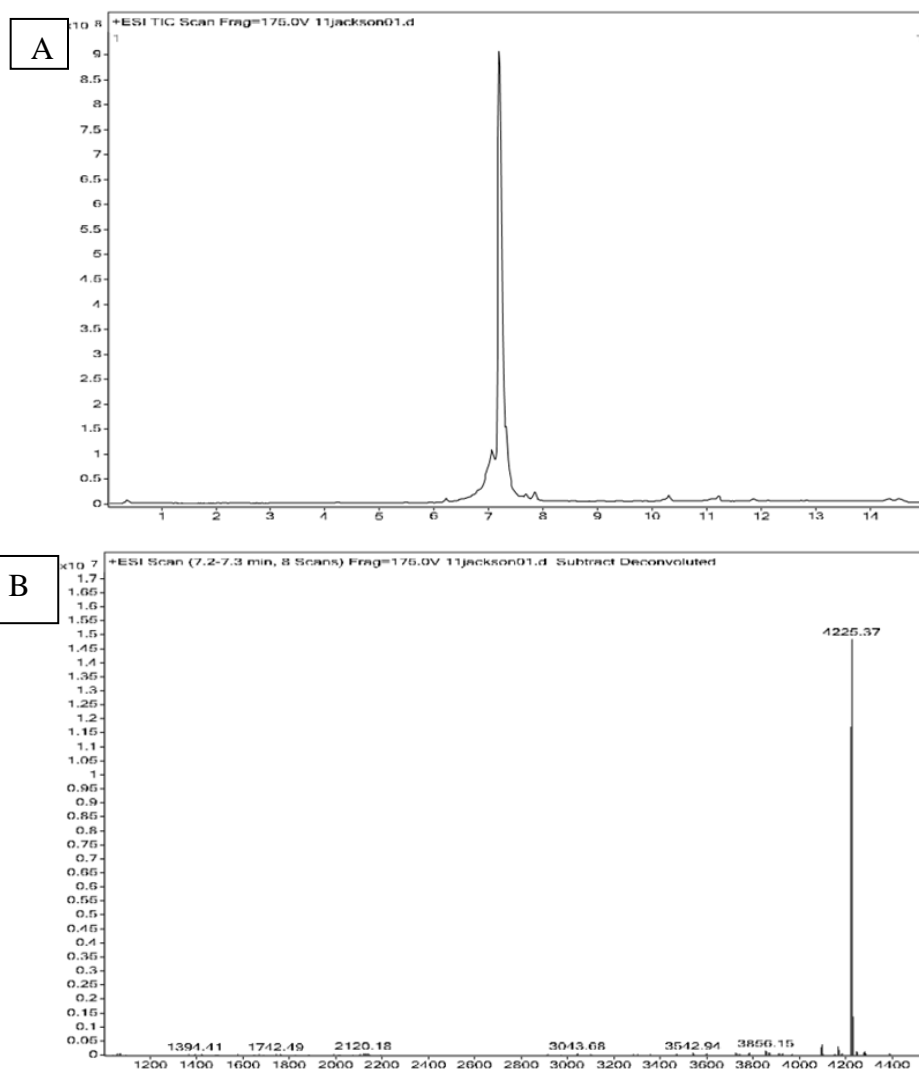
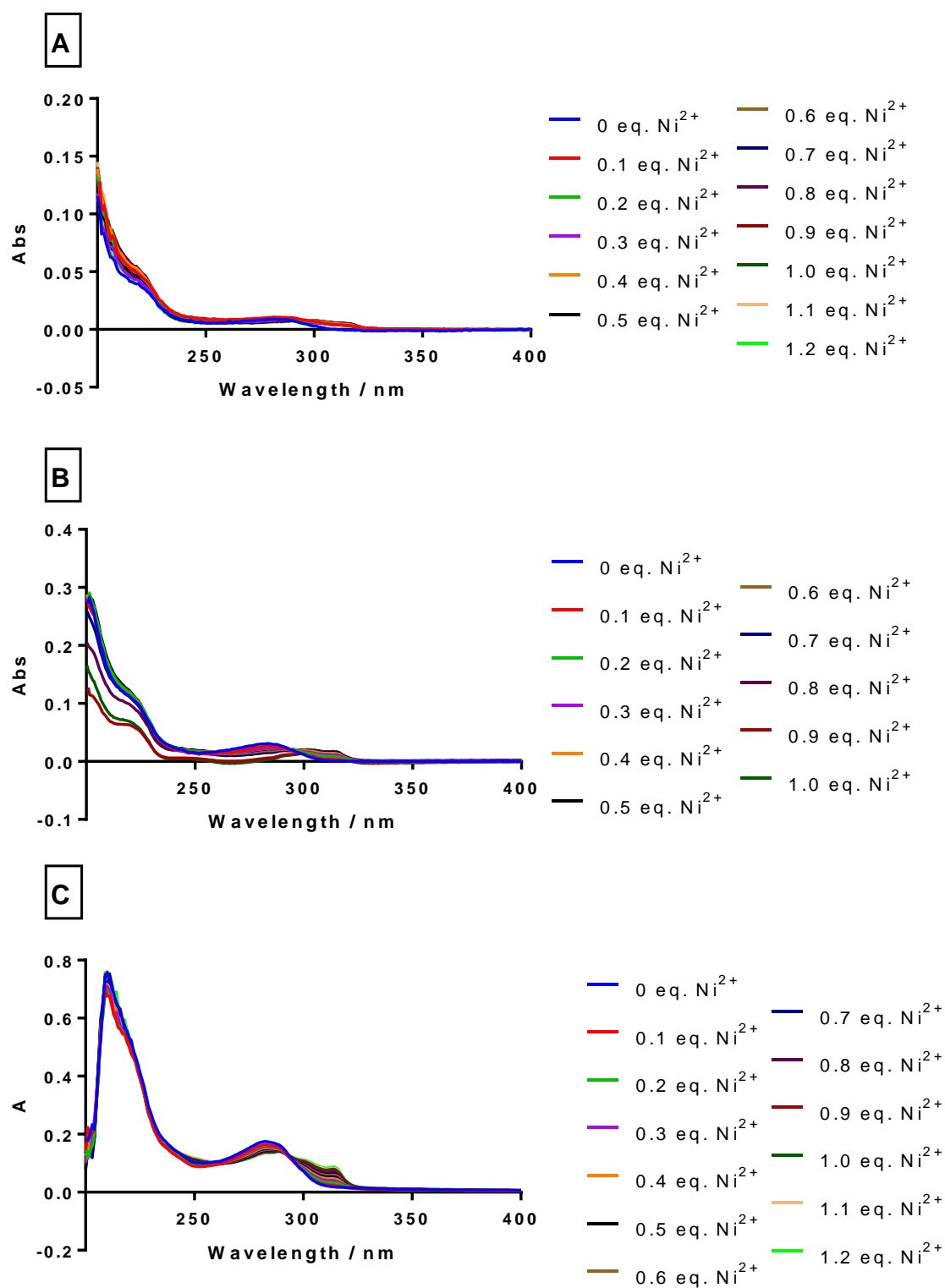
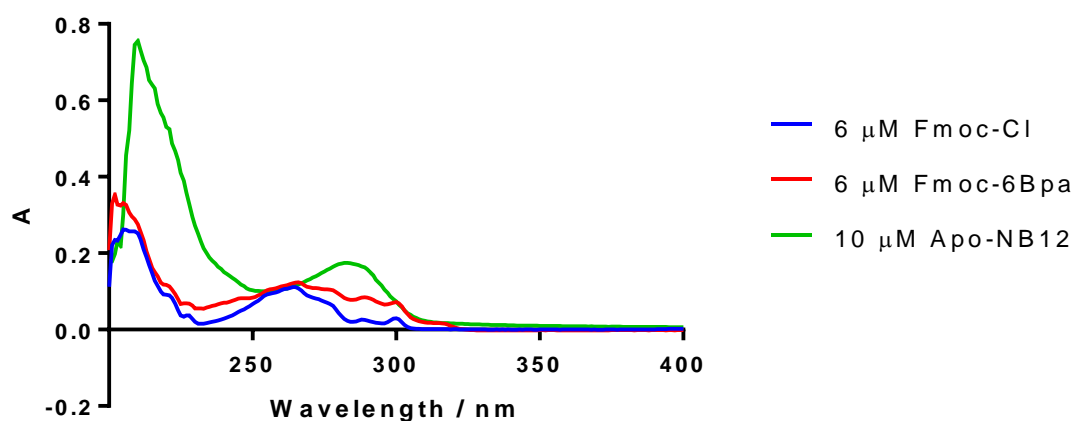


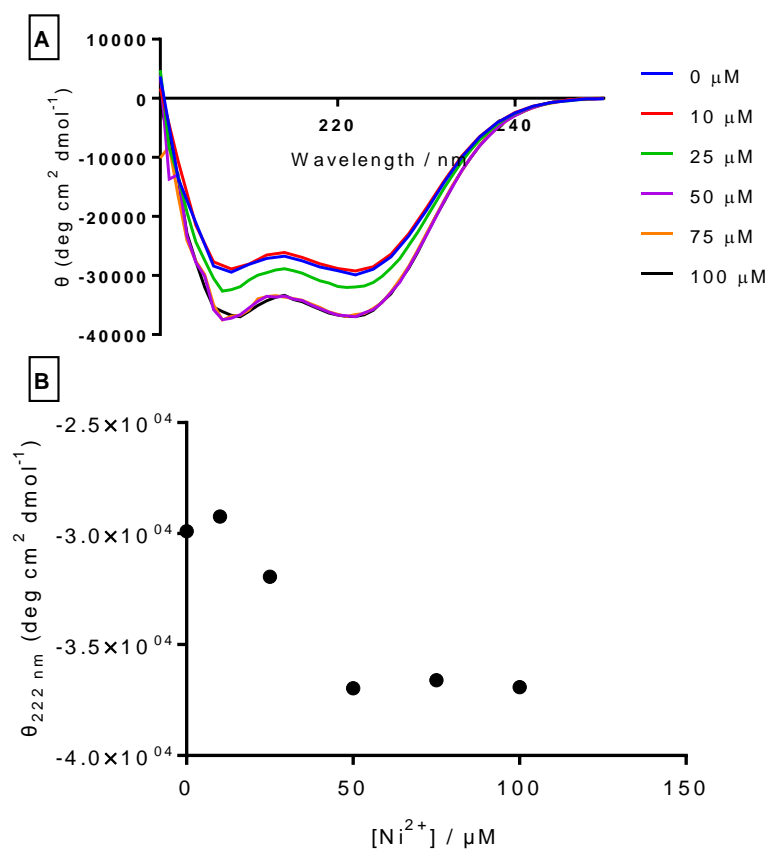
Figure 5 (A) C18-analytical HPLC trace of pure NB00 using a linear 0 to 100% MeCN + 0.05% TFA gradient in H₂O + 0.05% TFA over 10 minutes. (B) Electrospray mass spectrum of pure NB00



Supplementary Figure 6 UV-Vis titrations of A) NB00 B) NB11 C) NB12 with Ni^{2+} . All samples recorded in 25°C, 5 mM HEPES, 100 mM NaCl, pH 7.0. A & B recorded in a 1 mm pathlength cell, C recorded in a 10 mm pathlength cell.



Supplementary Figure 7 Comparative UV-Spectra of Fmoc chloride, Fmoc-6Bpa-OH, and apo-NB12. Indicates lack of Fmoc contribution to the UV spectra observed in 6-Bpa titrations. Fmoc-Cl and Fmoc-6Bpa recorded in 100% v/v MeOH, with NB12 recorded in All samples recorded in 25°C, 5 mM HEPES, 100 mM NaCl, pH 7.0. All samples recorded in a 10 mm pathlength cell.



Supplementary Figure 8 Far-UV CD spectra of 100 μM NB11. A) CD spectra of the change in the CD spectra when Ni^{2+} is added to a concentrated sample of NB11. Both $\theta_{222\text{ nm}}$ and $\theta_{208\text{ nm}}$ show an increase, with the peptide displaying an increase in helicity and becoming more folded as metal is titrated in. B) Plot of $\theta_{222\text{ nm}}$ against concentration of Ni^{2+} . A lag phase is observed, with the increase in ellipticity plateauing at 50 μM Ni^{2+} , or 2:1 peptide: metal ratio. All samples recorded in 25°C, 5 mM HEPES, 100 mM NaCl, pH 7.0. A & B recorded in a 1 mm pathlength cell, C recorded in a 10 mm pathlength cell.

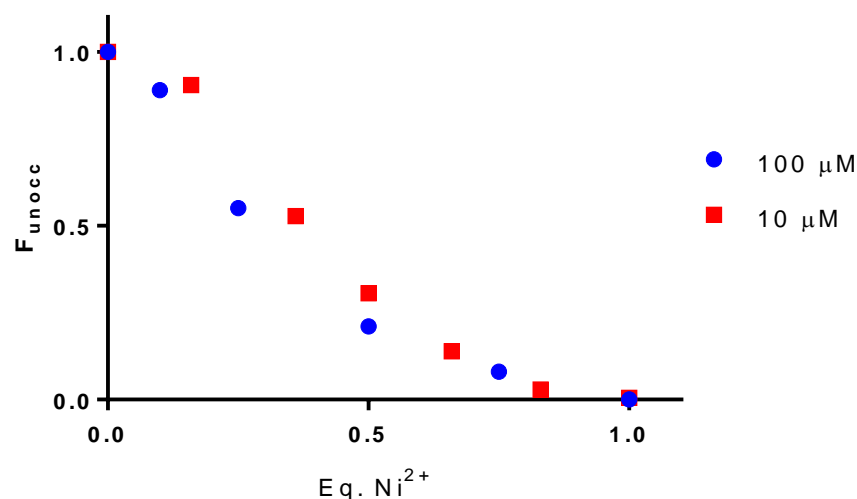
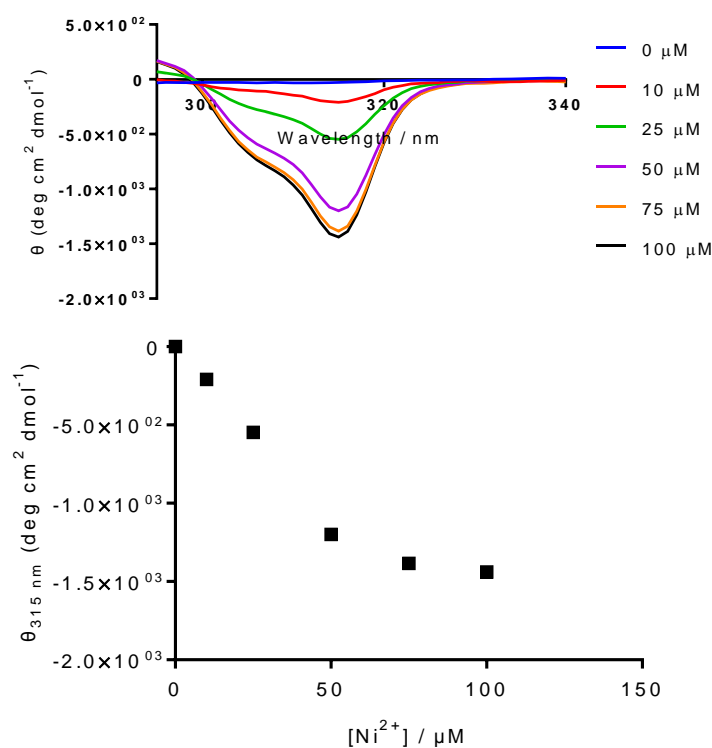
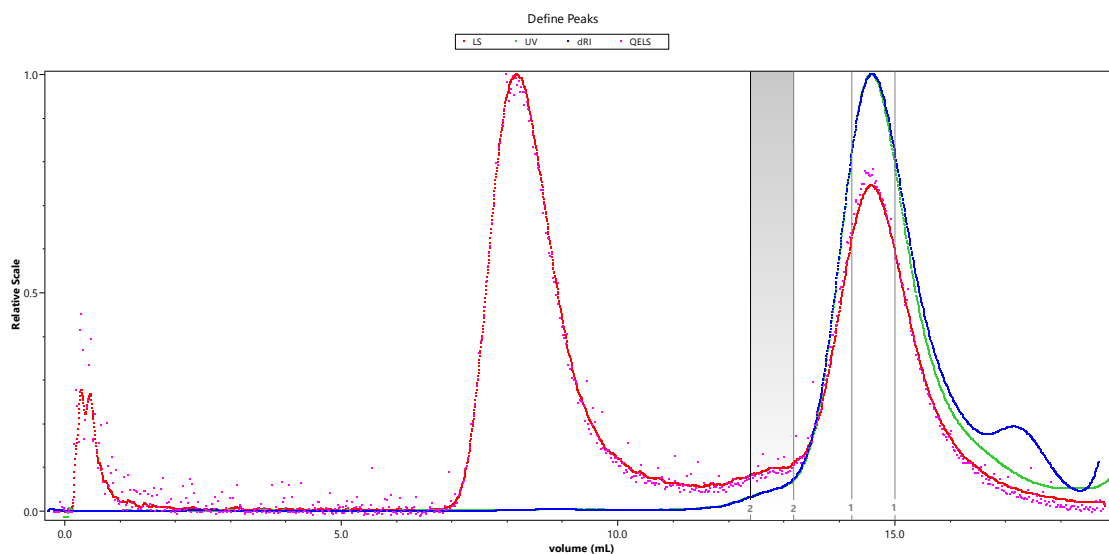


Figure 9 Comparative plot of the fraction of unoccupied sites at both 100 and 10 μM , and the change on addition of Ni^{2+} . At both concentrations the plots follow the same pattern, and display an initial lag phase indicative of a structural rearrangement before trimer formation occurs. All samples recorded in 25°C, 5 mM HEPES, 100 mM NaCl, pH 7.0. A & B recorded in a 1 mm pathlength cell, C recorded in a 10 mm pathlength cell.



Supplementary Figure 10 Aromatic region CD spectra of 100 μM NB11. A) CD spectra of the change in the CD spectra when Ni^{2+} is added to a concentrated sample of NB11. A peak appears at 315 nm, indicative of the formation of a nickel-bipyridine complex. B) Plot of $\theta_{315 \text{ nm}}$ against concentration of Ni^{2+} . No lag phase is observed, with the increase in ellipticity plateauing at 50 μM Ni^{2+} , or 2:1 peptide: metal ratio. All samples recorded in 25°C, 5 mM HEPES, 100 mM NaCl, pH 7.0. A & B recorded in a 1 mm pathlength cell, C recorded in a 10 mm pathlength cell.

NB11 MALLS Data

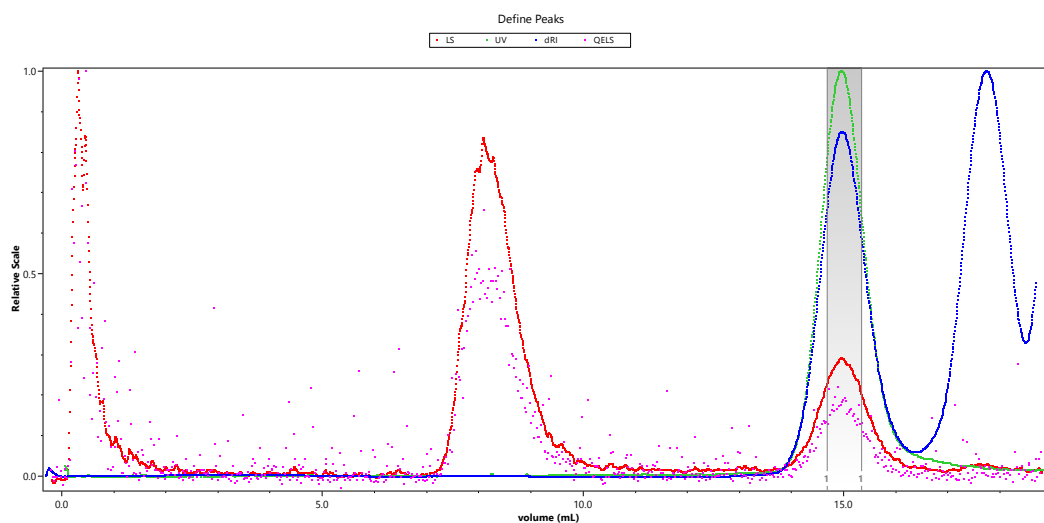


Supplementary Figure 11 MALLS trace for 236 μ M NB11, with light scattering marked in red, UV monitoring at 285 nm in green, differential refractometry in blue, and quasi-elastic light scattering traces marked in purple.

Peak Results

	Peak 1	Peak 2
Hydrodynamic radius (Q) moments (nm)		
Rh(Q)n	20.884 ($\pm 9.196\%$)	169.277 ($\pm 24.317\%$)
Rh(Q)w	21.021 ($\pm 9.200\%$)	172.741 ($\pm 24.514\%$)
Rh(Q)z	21.159 ($\pm 9.205\%$)	176.794 ($\pm 24.605\%$)
Rh(Q)(avg)	2.409 ($\pm 1.711\%$)	21.252 ($\pm 10.067\%$)
Masses		
Calculated Mass		
(μg)	287.77	14.76
Mass Fraction		
(%)	95.1	4.9
Molar mass moments (g/mol)		
Mn	1.201×10^4 ($\pm 1.240\%$)	3.436×10^4 ($\pm 8.339\%$)
Mp	1.209×10^4 ($\pm 1.019\%$)	2.706×10^4 ($\pm 8.072\%$)
Mw	1.201×10^4 ($\pm 1.243\%$)	3.538×10^4 ($\pm 8.566\%$)
Mz	1.202×10^4 ($\pm 2.781\%$)	3.641×10^4 ($\pm 19.393\%$)
Mz+1	1.202×10^4 ($\pm 4.488\%$)	3.741×10^4 ($\pm 30.870\%$)
M(avg)	1.199×10^4 ($\pm 0.107\%$)	3.386×10^4 ($\pm 0.759\%$)
Polydispersity		
Mw/Mn	1.000 ($\pm 1.755\%$)	1.030 ($\pm 11.955\%$)
Mz/Mn	1.000 ($\pm 3.045\%$)	1.060 ($\pm 21.110\%$)
rms radius moments (nm)		
Rn	n/a	23.4 ($\pm 54.2\%$)
Rw	n/a	23.9 ($\pm 52.7\%$)
Rz	n/a	24.4 ($\pm 51.6\%$)
R(avg)	n/a	24.3 ($\pm 4.6\%$)

NB12 MALLS Data



Supplementary Figure 12 MALLS trace for 236 μ M NB12, with light scattering marked in red, UV monitoring at 285 nm in green, differential refractometry in blue, and quasi-elastic light scattering traces marked in purple.

Peak Results

Peak 1

Hydrodynamic radius (Q) moments (nm)

Rh(Q)n	162.173 ($\pm 39.783\%$)
Rh(Q)w	162.917 ($\pm 39.760\%$)
Rh(Q)z	163.789 ($\pm 39.699\%$)
Rh(Q)(avg)	2.566 ($\pm 21.930\%$)

Masses

Calculated Mass (μg)	45.61
Mass Fraction (%)	100.0

Molar mass moments (g/mol)

Mn	4.740×10^3 ($\pm 3.336\%$)
Mp	4.843×10^3 ($\pm 2.735\%$)
Mw	4.749×10^3 ($\pm 3.398\%$)
Mz	4.757×10^3 ($\pm 7.661\%$)
Mz+1	4.767×10^3 ($\pm 12.448\%$)
M(avg)	4.694×10^3 ($\pm 0.310\%$)

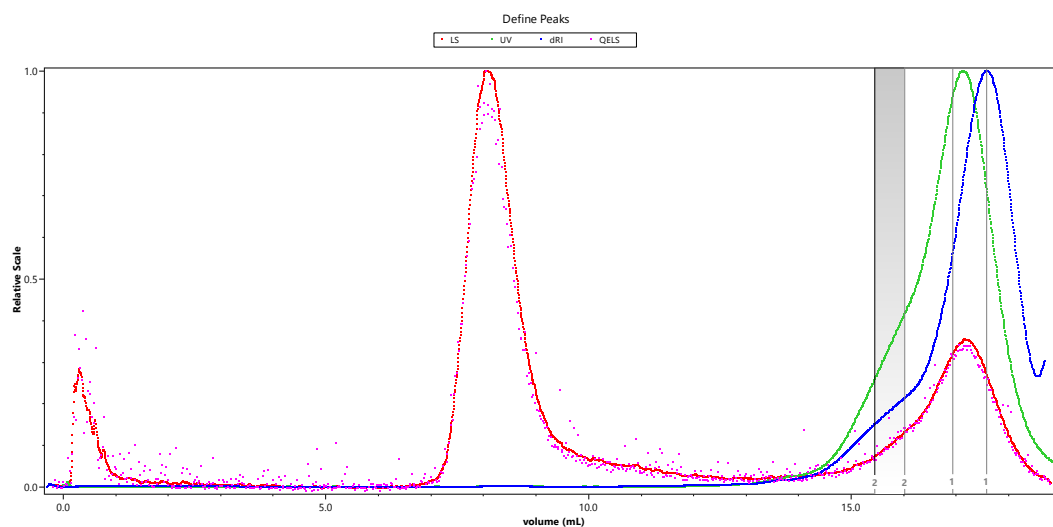
Polydispersity

Mw/Mn	1.002 ($\pm 4.762\%$)
Mz/Mn	1.004 ($\pm 8.356\%$)

rms radius moments (nm)

Rn	16.1 ($\pm 47.5\%$)
Rw	16.3 ($\pm 46.6\%$)
Rz	16.6 ($\pm 45.7\%$)
R(avg)	14.9 ($\pm 5.1\%$)

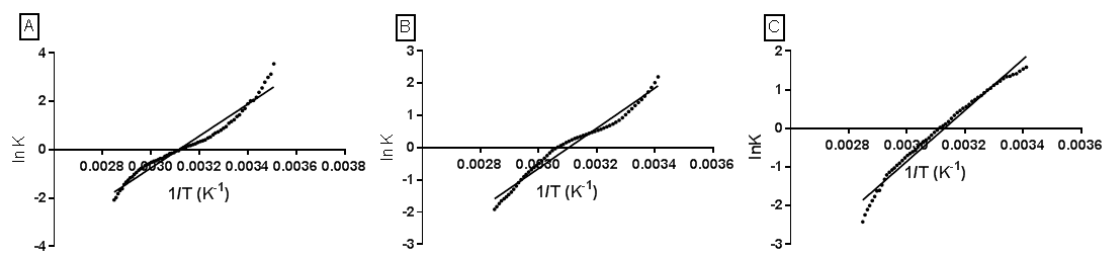
NB00 MALLS Data



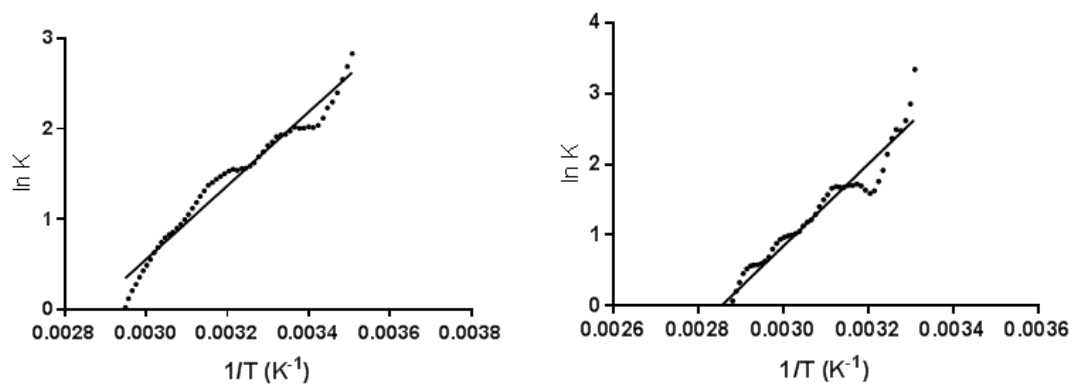
Supplementary Figure 13 MALLS trace for 236 μM NB00, with light scattering marked in red, UV monitoring at 285 nm in green, differential refractometry in blue, and quasi-elastic light scattering traces marked in purple.

Peak Results

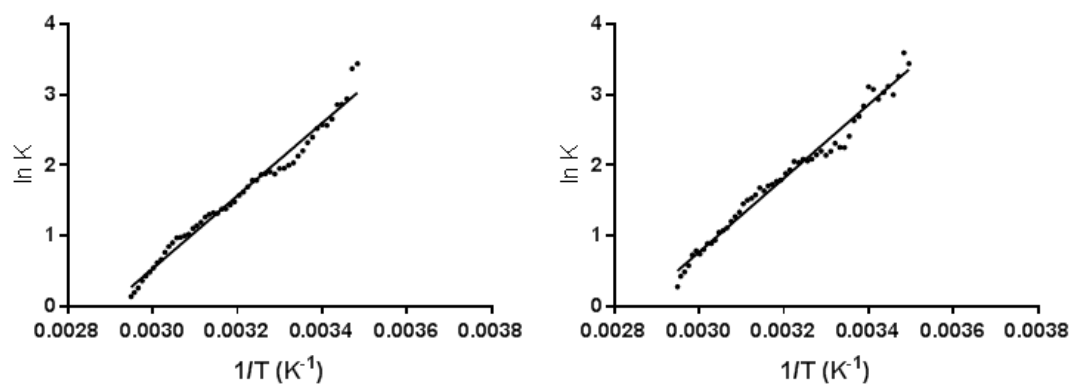
	Peak 1	Peak 2
Hydrodynamic radius (Q) moments (nm)		
Rh(Q)n	68.089 ($\pm 12.185\%$)	180.761 ($\pm 25.039\%$)
Rh(Q)w	66.800 ($\pm 11.432\%$)	179.535 ($\pm 24.604\%$)
Rh(Q)z	65.569 ($\pm 10.627\%$)	178.413 ($\pm 24.144\%$)
Rh(Q)(avg)	1.806 ($\pm 5.264\%$)	1.480 ($\pm 26.625\%$)
Masses		
Calculated Mass (μg)	178.43	34.67
Mass Fraction (%)	83.7	16.3
Molar mass moments (g/mol)		
Mn	5.417×10^3 ($\pm 1.439\%$)	7.680×10^3 ($\pm 3.057\%$)
Mp	3.861×10^3 ($\pm 1.241\%$)	8.698×10^3 ($\pm 2.284\%$)
Mw	5.672×10^3 ($\pm 1.469\%$)	7.727×10^3 ($\pm 2.975\%$)
Mz	5.932×10^3 ($\pm 3.298\%$)	7.773×10^3 ($\pm 6.583\%$)
Mz+1	6.184×10^3 ($\pm 5.112\%$)	7.817×10^3 ($\pm 10.433\%$)
M(avg)	5.214×10^3 ($\pm 0.144\%$)	7.779×10^3 ($\pm 0.305\%$)
Polydispersity		
Mw/Mn	1.047 ($\pm 2.056\%$)	1.006 ($\pm 4.266\%$)
Mz/Mn	1.095 ($\pm 3.598\%$)	1.012 ($\pm 7.258\%$)
rms radius moments (nm)		
Rn	n/a	n/a
Rw	n/a	n/a
Rz	n/a	n/a
R(avg)	n/a	n/a



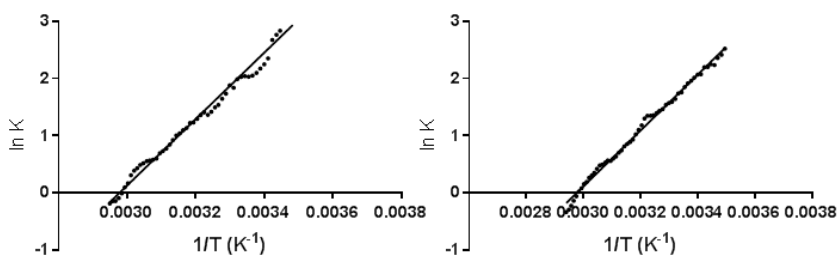
Supplementary Figure 14 Van't Hoff plots for 10uM NB00. A) Apo- NB00 B) 0.3 eq. Ni^{2+} C) 1.0 eq Ni^{2+}



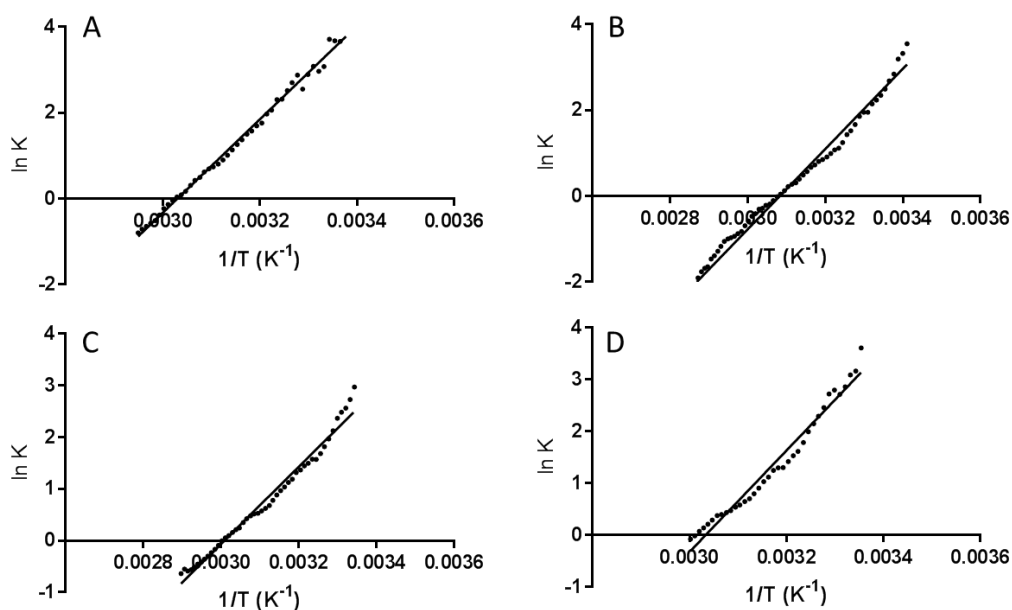
Supplementary Figure 15 Van't Hoff plots for 3uM NB11. A) Apo- NB11 B) 0.3 eq. Ni^{2+}



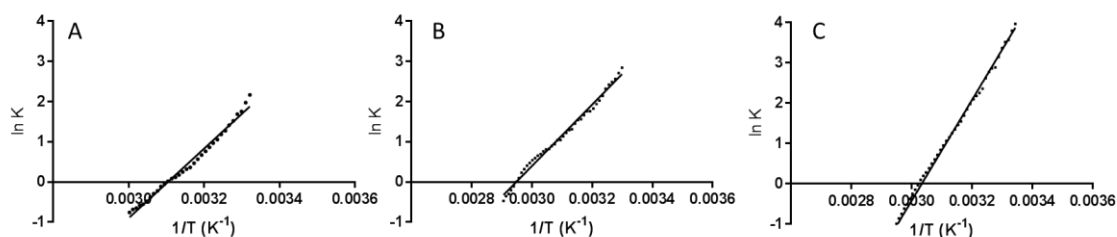
Supplementary Figure 16 Van't Hoff plots for 10uM NB11. A) Apo- NB00 B) 0.3 eq. Ni^{2+}



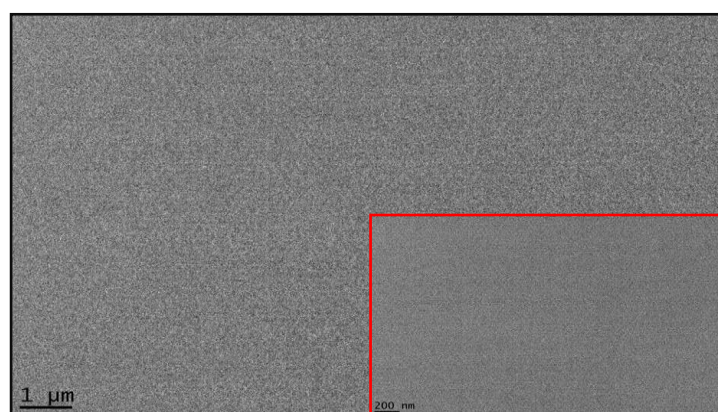
Supplementary Figure 17 Van't Hoff plots for 50uM NB12. A) Apo- NB12 B) 0.3 eq. Ni^{2+}



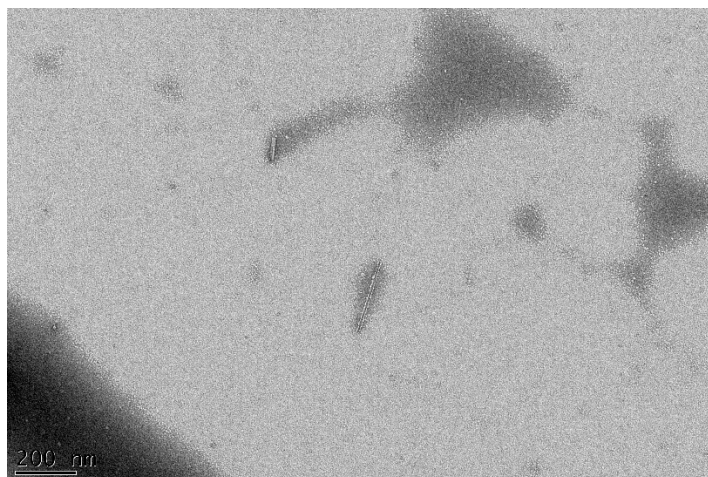
Supplementary Figure 18 Van't Hoff plots for 90uM NB12. A) Apo- NB12 B) 0.3 eq. Ni^{2+} C) 0.6 eq Ni^{2+} D) 1.0 eq Ni^{2+}



Supplementary Figure 19 Van't Hoff plots for 125uM NB12. A) Apo- NB12 B) 0.3 eq. Ni^{2+} C) 1.0 eq Ni^{2+}



Supplementary Figure 20 No fibre formation with fresh 10 μM NB12. Transmission electron micrographs of fresh solution of 10 μM NB12, stained with 1% uranyl acetate. Low-magnification image (scale bars: 1 μm); (inset): high-magnification images (scale bar: 200 nm).



Supplementary Figure 21 Minimal fibres present after addition of 0.3 eq Ni^{2+} to a solution of 10 μM NB12 fibres. Transmission electron micrographs of fresh solution of 0.3 eq Ni^{2+} /10 μM NB12, stained with 1% uranyl acetate. Low-magnification image (scale bars: 1 μm); (inset): high-magnification images (scale bar: 200 nm). Two fibres, lengths 241 & 74 nm, with respective widths of 10.6 and 13.3 nm respectively.